Evasion of the innate apoptotic response by classical swine fever virus N-terminal autoprotease (N^{pro})

Samuel Hardy

Institute for Infection and Immunity

St. George's, University of London

Submitted in accordance with the requirements for the degree of

Doctor of Philosophy

Declaration of Originality

I declare that the work submitted is my own and that I have provided appropriate credit for the work of others who are referenced in the text.

Acknowledgments

Firstly, I would like to thank Dr Julian Seago to whom I am incredibly grateful for the invaluable guidance and supervision he has provided me over the course of my PhD. His enthusiasm and passion kept me motivated throughout. I would also like to thank the other members of my supervisory team, Professor Steve Goodbourn and Dr Ben Jackson. To Steve, not only for his helpful insight but also for encouraging me to utilise CRISPR, a technique which proved to be a genuine turning point in my project. And to Ben, for always being there to answer all the queries and questions I had while in the lab.

I would also like to thank all the fellow students and scientists I have been lucky to befriend during my time here, as Pirbright would not have been as enjoyable without them. To Muni, Muneeb, Roza, Sergio, Ely, Myriam, Mika, Eva, John, Michael, Kitty and everyone in FN05, I wish you all the best.

Finally, I would also like to take this as an opportunity to thank the BBSRC, the Pirbright Institute and SGUL. Without their funding, facilities and support, this PhD would not have been possible.

This thesis is dedicated to my loving parents for their

continued support throughout my studies.

Abstract

Classical swine fever virus (CSFV) is the causative agent of classical swine fever, a notifiable disease of economic importance that causes severe leukopenia, fever and haemorrhagic disease in domesticated pigs and wild boar across the globe. *In vitro* CSFV has been shown to antagonise the induction of type I IFN, partly through a function of its N-terminal protease (N^{pro}) which binds IRF3 and targets it for proteasomal degradation. Additionally, N^{pro} has been shown to antagonise apoptosis triggered by the dsRNA-homolog poly(I:C), however the exact mechanism by which this is achieved has not been fully elucidated.

The ability of N^{pro} to inhibit poly(I:C)-mediated apoptosis was confirmed and in addition N^{pro} was found to antagonise Sendai virus-mediated apoptosis in PK-15 cells. Gene edited PK-15 cell lines were used to show the dsRNA-sensing pattern recognition receptors (PRRs) TLR3 and RIG-I specifically recognise poly(I:C) and SeV respectively, subsequently triggering apoptosis through pathways that converge on IRF3 and culminate in the cleavage of caspase-3. Deletion of IRF3, stable expression of N^{pro} and infection with wild-type CSFV were found to antagonise the mitochondrial relocalisation of Bax, a pro-apoptotic Bcl-2 family protein. Together, these findings show that the putative interaction between N^{pro} and IRF3 is involved not only in its antagonism of type I IFN, but also dsRNA-mediated mitochondrial apoptosis. Elucidation of the mechanism by which N^{pro} antagonises the apoptotic response will help inform the development of novel antivirals and rationally designed, live attenuated vaccines.

Contents

Figures

Tables

Abbreviations

A1	Bcl-2-related protein A1
ABS	Adult bovine serum
ActD	Actinomycin D
ANNOVA	Analysis of variance
APAF1	Apoptotic protease activating factor 1
ATF2	Activating transcription factor 2
ATP	Adenosine triphosphate
Bak	Bcl-2 antagonist or killer
Bax	Bcl-2-associated X protein
Bcl	B-cell lymphoma
Bcl-B	Bcl-2-like protein 10
Bcl-xL	B-cell lymphoma-extra large
BDV	Border disease virus
Bid	BH3 interacting domain death agonist
Bim	Bcl-2 interacting mediator of cell death
BLAST	Basic Local Alignment Search Tool
Bmf	Bcl-2-modifying factor
Bok	Bcl-2 related ovarian killer
BSA	Bovine serum albumin
BVDV	Bovine viral diarrhoea virus
CARD	Caspase activation and recruitment domain
CBP	CREB-binding protein
cFLIP	Cellular FLICE-like inhibitory protein
CHX	Cycloheximide
CI	Confidence interval
Co-IP	Co-immunoprecipitation
CRISPR	Clustered regularly interspaced short palindromic repeats
CSF	Classical swine fever
CSFV	Classical swine fever virus
CTD	Conserved regulatory domain
C-terminal	Carboxy-terminal
DAPI	4',6-diamidino-2-phenylindole
dH_2O	Distilled water
DISC	Death inducing signalling complex
DIVA	Differentiate infected and vaccinated animals

DMEM	Dulbecco's Modified Eagle Medium
DNA	Deoxyribonucleotide acid
dsRNA	Double-stranded ribonucleic acid
EC	European Council
ECMV	Encephalomyocarditis Virus
EDTA	Ethylenediaminetetra acetic acid
EGFP	Enhanced green fluorescent protein
ELISA	Enzyme-linked immunosorbent assay
ER	Endoplasmic reticulum
E^{rns}	Envelope protein RNase secreted
EtOH	Ethanol
EU	European Union
FADD	Fas-associated death domain
FasL	Fas ligand
FasR	Fas receptor
gDNA	Genomic DNA
GFP	Green fluorescent protein
gRNA	Guide RNA
Hrk	Harakiri
hr	hour
HAX-1	HS-1-associated protein-X-1
HCV	Hepatitis C virus
HDR	Homology-directed repair
HEK293T	Human embryonic kidney cell line expressing Simian virus 40 large T antigen
HIV	Human immunodeficiency virus
HRP	Horseradish peroxidase
HSP70	70 kilodalton heat shock proteins
IAP	Inhibitor of apoptosis
IFN	Interferon
IFNAR	Interferon-α/β receptor
IFT	immunofluorescence test
IkBα	Inhibitor of kappa B alpha
IKK	I kappa B kinase
IL	Interleukin
IMS	Intermembrane space
IRES	Internal ribosome entry site
IRF	Interferon regulatory factor
ISG	Interferon stimulated gene

ISRE	Interferon stimulated response element
IU	International units
JAK	Janus activated kinase family
Kb	Kilo base
kDa	Kilo Daltons
km	Kilometres
LamR	Laminin receptor
LB	Lysogeny Broth
LUBAC	Linear ubiquitin chain assembly complex
MAVS	Mitochondrial antiviral signalling
Mcl-1	Myeloid leukaemia cell differentiation protein
MDA5	Melanoma differentiation – associated gene-5
MDBK	Madin–Darby Bovine Kidney cell
mg	Milligram
ml	Millilitre
mM	Millimolar
MOM	Mitochondrial outer membrane
MOMP	Mitochondrial outer membrane permeabilization
mRNA	Messenger ribonucleic acid
MTT	MitoTracker
mtDNA	Mitochondrial DNA
Mx	Myxovirus resistance
MyD88	Myeloid differentiation primary response 88
NEMO	NF-kappa-B essential modulator
NF-kB	Nuclear factor kappa b
ng	Nanogram
NLS	Nuclear localisation signal
nm	Nanometre
nM	Nanomole
Noxa	Phorbol-12-myristate-13-acetate-induced protein 1
N^{pro}	N-terminal autoprotease
NS	Nonstructural
N-terminal	Amino terminal
NTR	Non-translated region
O/N	Overnight
OD	Optical density
OIE	World Organisation for Animal Health (*Office International des Epizooties*)
Oligo	Oligonucleotide

ORF	Open reading frame
PAMP	Pathogen-associated molecular pattern
PBS	Phosphate buffered saline
PCR	Polymerase chain reaction
pDC	plasmacytoid dendritic cell
PK-15	Porcine kidney epithelial cells
PKR	Protein Kinase R
PLA	immunoperoxidase assay
Poly(I:C)	Polyinosinic:polycytidylic acid
PRD	Positive regulatory domain
PRR	Pathogen recognition receptors
PRRSV	Porcine reproductive and respiratory syndrome virus
PtdSer	Phosphatidylserine
Puma	p53 upregulated modulator of apoptosis
Rab	Ras-related protein Rab
RdRp	RNA-dependent RNA polymerase
RE	Restriction enzyme
RIG-I	Retinoic acid - inducible gene I
RIPA	RLR-induced IRF3-mediated pathway of apoptosis
RIPK1	Receptor-interacting serine/threonine-protein kinase 1
RLR	RIG-I like receptors
RNA	Ribonucleic acid
Rnase	Ribonuclease
R/T	Room temperature
rpm	Revolutions per minute
RXT	Ruxolitinib
SD	Standard deviation
SDS-PAGE	Sodium dodecyl sulphate polyacrylamide gel electrophoresis
SeV	Sendai Virus
SK6	Porcine kidney fibroblast cells
Smac	Second mitochondria-derived activator of caspases
ssRNA	Single-stranded ribonucleic acid
STAT	Signal transducers and activators of transcription
SV40	Simian virus 40
tBID	Truncated Bid
TBK1	TANK-binding kinase 1
$TCID_{50}$	Median tissue culture infectious dose
TGEV	Transmissible gastroenteritis virus

TID1	Tumorous imaginal disc 1
TIR	Toll/Interleukin 1 receptor
TLR	Toll like receptor
Tm	Melting temperature
TNF-α	Tumour necrosis factor alpha
TNF-R1	TNF receptor 1
TRADD	TNF-R1-associated DEATH domain protein
TRAF	TNF receptor associated factor
TRAIL	TNF-related apoptosis-inducing ligand
TRIF	Toll/Interleukin-I receptor domain-containing adaptor inducing interferon-β
TYK	Tyrosine kinase
US	United States
UTR	Untranslated region
UV	Ultraviolet
V	Volts
vFLIP	Viral FLICE-like inhibitory protein
VSV	Vesicular stomatitis virus
Y2H	Yeast two-hybrid
Z-VAD(OMe)-FMK	Z-Val-Ala-DL-Asp(OMe)-fluoromethylketone
µg	Microgram
µl	Microlitre
µm	Micrometre
µM	Micromolar

1. Introduction

1.1. Classical swine fever virus (CSFV)

Formerly known as hog cholera virus, the highly contagious and pathogenic classical swine fever virus (CSFV) is responsible for severe haemorrhagic disease in pigs and wild boar (*Sus scrofa*), listed by the World Organisation for Animal Health (OIE) and European Union (EU) as a notifiable disease of economic importance (EC, 1982, OIE, 2019b). Mortality is typically 100% in pigs infected with the most virulent strains, characterised by high fever, leukopenia and petechial haemorrhages, accompanied also by a number of neurological complications (Mittelholzer *et al.*, 2000). Virus spread typically occurs as a consequence of direct contact with infected pigs or their bodily fluids (oronasal and ocular discharge, blood, faeces, urine, semen). Widespread apoptosis and necrosis of uninfected cells has also been observed (Summerfield *et al.*, 2000). An additional finding is the phenomena of persistent infection and immunotolerance in young swine – this can occur as either a direct consequence of vertical transmission across the placenta from mother to foetus, or early post-natal infection (Gottipati *et al.*, 2014, Cabezon *et al.*, 2015, Munoz-Gonzalez *et al.*, 2015).

1.1.1. Epidemiology

1.1.1.1. Geographical distribution

CSFV remains endemic across many parts of the globe in both wild boar and domestic pigs (Arzt *et al.*, 2010). North America has been free from disease for a number of decades, however much of Central and Southern America remain endemically infected while outbreaks, with the exception of Japan, occur frequently across much of Asia (Brown and Bevins, 2018) (figure 1.1).

In 1980, the European Union (EU) launched a new initiative with the aim of eradicating CSFV in member-states. Based primarily on culling as opposed to mass-vaccination, this initiative

proved successful. While the UK last saw an outbreak in 2000, virus has been identified in wild boar populations in parts of Eastern Europe, leading to sporadic outbreaks in Latvia and Lithuania. A particularly severe outbreak occurred in the Netherlands between 1997 and 1998 with loses as high as 2.3 billion US$ (Elber *et al.*, 1999) while in 2009, a smaller outbreak was identified in wild boar of the North Rhine Westphalia region of Germany (Leifer *et al.*, 2010).

1.1.1.2. 2018-2019 Japanese outbreak

More recently in August 2018 (confirmed September 2018), the Gifu prefecture of Japan was struck by an outbreak, the country's first in 26 years. Although these outbreaks have been and are currently being rapidly resolved, new outbreaks are recurring. The OIE have recently reported (18/08/2019) that a total of 1707 domestic pigs have been culled and a total of 68 cases detected in wild boar between July 25th and August 13th (OIE, 2019a). While these outbreaks were initially restricted to Gifu prefecture, cases have been detected in neighbouring provinces and these have primarily occurred in wild boar (figure 1.2). As wild boar are as susceptible to infection as domestic pigs, eradication in CSFV from wild boar populations would be invaluable (Moennig, 2015). Sequence analyses of the 5' UTR, as well as the E2 and NS5B ORFs showed the Japanese isolates belong to subgenotype 2.1 and are closely related to Chinese and Mongolian isolates from 2011-2015 (Nishi *et al.*, 2019, Postel *et al.*, 2019). CFSV remains a global threat to food security, therefore justifying continued research into viral pathogenesis, surveillance and vaccine development.

1.1.1.3. Phylogeny

At present, CSFV is divided into three genotypes and 11 subgenotypes (Postel *et al.*, 2013b). Reflecting the increasing availability of complete CSFV genome sequences deposited to

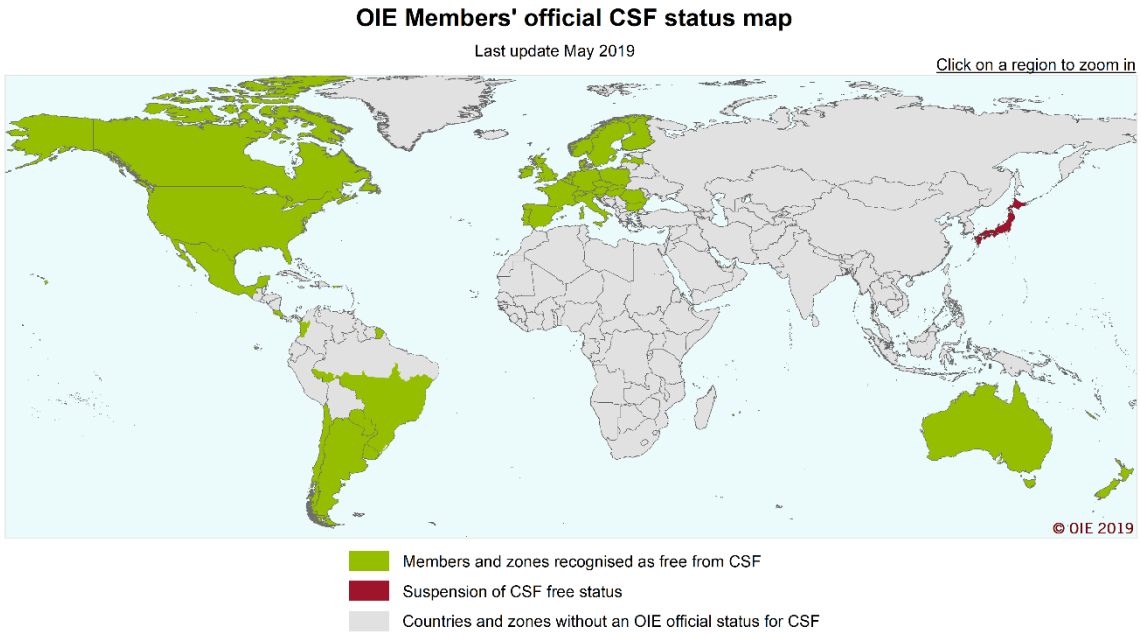

Figure 1.1: Map of OIE member countries and zones (regions of countries) recognised as CSFV-free as of May 2019. (OIE, 2019).

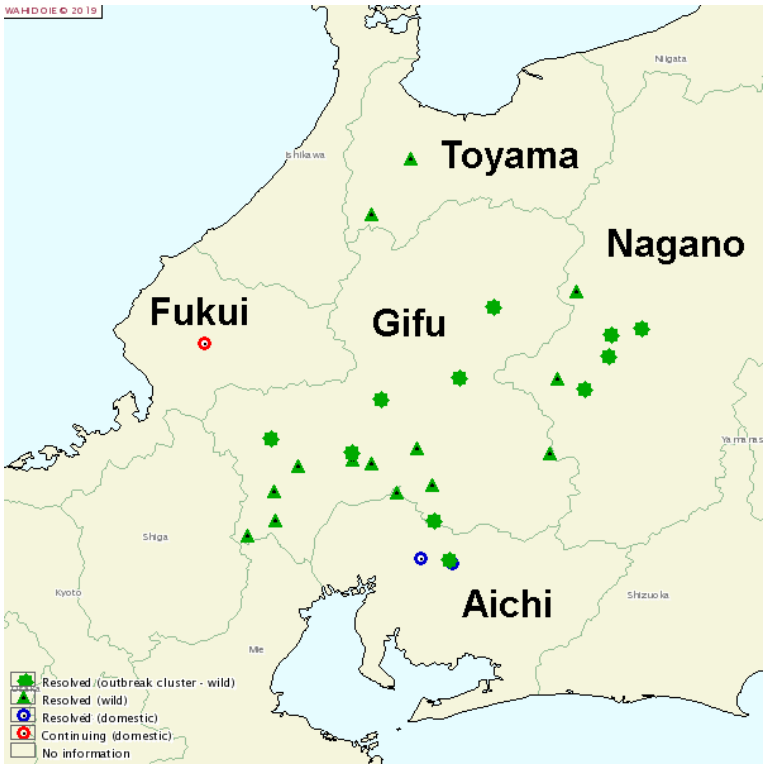

Figure 1.2: Map of current CSFV outbreaks in domestic pig and wild boar populations in Gifu prefecture and surrounding provinces as of August 18th 2019. Resolved wild (green) and domestic cases (blue) and ongoing domestic cases (red) are indicated (adapted from OIE, 2019).

GenBank, our understanding of viral diversity has improved and as such a new genotyping scheme has been proposed – this would instead be comprised of five genotypes and 14

subgenotypes (Rios *et al.*, 2018).

1.1.2. Virus structure

CSFV, along with bovine viral diarrhoea virus (BVDV) and border disease virus (BDV), are all enveloped pestiviruses which belong to the positive-sense single-stranded RNA *Flaviviridae* family of viruses. Members of the *Pestivirus* genus range between 40-60 nm in diameter and possess a genome of approximately 12.3 kb enclosed within a proteinaceous nucleocapsid (Lindenbach *et al.*, 2007) (figure 1.3). The genome of CSFV encodes a single open reading frame (ORF) which is flanked by 5' and 3' untranslated regions (UTRs) and encodes a polyprotein of 3,898 amino acids (Lindenbach *et al.*, 2007) (figure 1.4). The 5' UTR is highly-conserved across the *Pestivirus* genus and has the role of acting as an internal ribosomal entry site (IRES), enabling cap-independent initiation of translation (Rijnbrand *et al.*, 1997). This is in contrast to the majority of host mRNAs which are typically translated as a consequence of a 5' capped structure in a process termed "cap-dependent translation" (Merrick, 2004). Following translation, viral and host proteases process and cleave the polyprotein into 12 mature polypeptides: N^{pro}, C, E^{rns}, E1, E2, p7, NS2, NS3, NS4A, NS4B, NS5A and NS5B (Lindenbach *et al.*, 2007). These proteins encompass a wide range of roles such as cell attachment (E^{rns}, E1, E2), polymerase activity (NS5B) and helicase activity (NS3).

1.1.3. Genome organisation

Genes encoding the four structural proteins (Core, E^{rns}, E1 and E2) are located adjacent to each other in the 5' region of the ORF and are therefore amongst the first viral proteins to be expressed (figure 1.4).

1.1.3.1. N^{pro}

The first protein encoded by the ORF is the N-terminal autoprotease (N^{pro}), a 19 kDa C63 cysteine autoprotease that exhibits co-translational autoproteolytical activity upon itself,

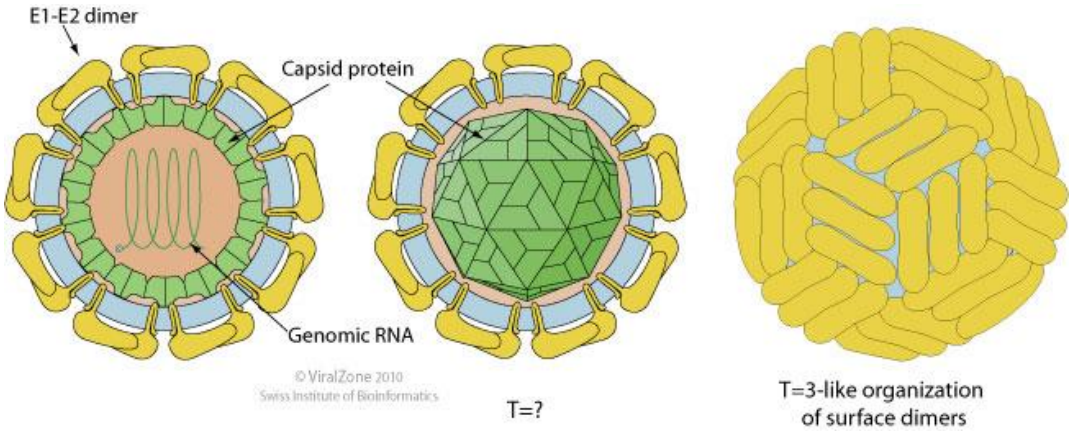

Figure 1.3: Schematic of CSFV virion structure. CSFV virions enveloped, spherical and approximately 40-60 nm in diameter. Positive-sense RNA genome is contained within a nucleocapsid core protein (ViralZone, 2010).

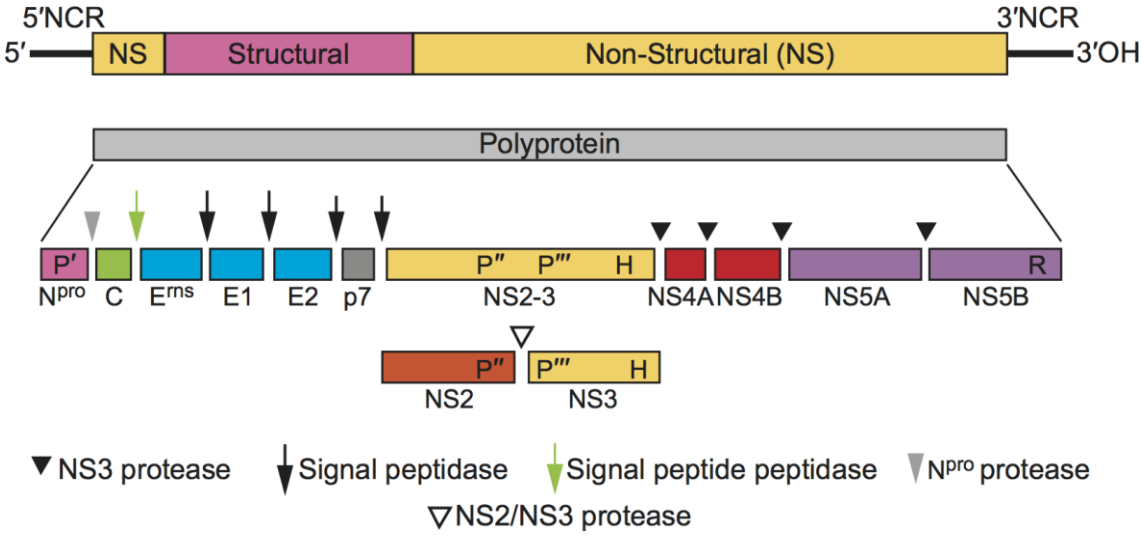

Figure 1.4: Schematic of CSFV genome and polyprotein processing. Positive-sense RNA genome is initially translated as a single polyprotein which then undergoes cleavage by viral and host proteases into 12 mature proteins (ICTV, 2019).

facilitating cleavage from the downstream nucleocapsid Core protein (1.1.3.2) (Wiskerchen *et al.*, 1991, Stark *et al.*, 1993, Rumenapf *et al.*, 1998, Rawlings *et al.*, 2012). Although N^{pro} is dispensable for CSFV replication in the interferon-defective SK6 cell line (Tratschin *et al.*, 1998), deletion has been associated with significant attenuation *in vivo* (Mayer *et al.*, 2004). CSFV N^{pro} has been shown to antagonise *in vitro* induction of double-stranded RNA (dsRNA)-mediated apoptosis (Ruggli *et al.*, 2005, Johns *et al.*, 2010a) and type I IFN (Ruggli *et al.*, 2003, Bauhofer *et al.*, 2005, Ruggli *et al.*, 2005). *In vivo*, antagonism of type I IFN induction by CSFV

N^{pro} was associated with enhanced replication at local sites of infection (Tamura *et al.*, 2014). These functions of N^{pro} are discussed in greater detail in 1.2.4 and 1.3.3.

1.1.3.2. Core

Core protein (Core) encases the viral genome (RNA) to form a proteinaceous viral nucleocapsid, however the exact mechanism by which this is achieved remains to be elucidated. Virions devoid of Core protein were shown to actively integrate complemented Core protein, resulting in improved infectivity of cells pre-treated with IFN (Riedel *et al.*, 2017). Riedel *et al.* suggest the observed phenotype likely corresponds to protection from interferon-stimulated gene (ISG) products such as RNaseL and ISG20, two ISGs that exert ribonuclease and exonuclease activity on viral RNA, respectively (Schoggins, 2019).

1.1.3.3. E^{rns}, E1 and E2

Found on the surface of mature virions, the viral glycoprotein E^{rns} (Thiel *et al.*, 1991, Rümenapf *et al.*, 1993) has been proposed to facilitate initial binding and attachment to host cells through interactions with sugars, heparan sulphate (HS) and laminin (Hulst and Moormann, 1997, Hulst *et al.*, 2001, Chen *et al.*, 2015). This is thought to be important in virus adaption to cell culture (Hulst *et al.*, 2000). In addition to its structural role, infected cells also produce E^{rns} in a soluble, secretable form that has been shown to act as a scavenger receptor for and exert endoribonuclease activity on viral single-stranded RNA (ssRNA), dsRNA (a genome replication intermediate) and its synthetic homolog polyinosinic:polycytidylic acid (poly(I:C)), contributing toward CSFV's antagonism of type I IFN induction (Hausmann *et al.*, 2004, Lussi *et al.*, 2018). With regards to BVDV, a closely related Pestivirus, this mechanism has been proposed to prevent its own pathogen-associated molecular pattern (PAMP) from inadvertently triggering TLR3-mediated induction of type I IFN (Zurcher *et al.*, 2014a, Zurcher *et al.*, 2014b).

Two other glycoproteins, E1 and E2, are located on the surface of the CSFV virion (Thiel *et al.*, 1991, Rümenapf *et al.*, 1993). E2 forms homodimers with itself and heterodimers with E1, the

latter being essential and sufficient for Pestivirus cell entry (Hulst and Moormann, 1997, Wang *et al.*, 2004). The roles of these proteins in mediating attachment and entry into host cells are discussed in greater detail in 1.1.4.1. E2 is the predominant immunogen that elicits a protective humoral response in CSFV-infected pigs (van Zijl *et al.*, 1991, Hulst *et al.*, 1993, Konig *et al.*, 1995, van Rijn *et al.*, 1996).

1.1.3.4. p7

Nonstructural protein p7 is cleaved from E2 by a unique cellular signal peptidase, however this cleavage is incomplete and results in mature E2 and p7 as well as residual E2p7 precursor (Elbers *et al.*, 1996). Recently, it has been proposed that p7 complexes with E2 and NS2 at the ER membrane to modulate virus assembly (Zhao *et al.*, 2017). In addition, p7 was identified as a viroporin, essential for virus replication and virulence in pigs (Gladue *et al.*, 2012). Through a function of its C-terminal transmembrane helix, p7 was observed to form pores in model ER-like membranes in a pH-dependent manner, facilitating the passage of ions (Gladue *et al.*, 2012, Largo *et al.*, 2016). An interaction between p7 and CALMG, a key mediator of cytosolic calcium accumulation, was recently identified (Gladue *et al.*, 2018). These findings are interesting as variations in calcium concentration have been associated with control of cell metabolism, mitosis and apoptosis. Modulation of these responses by a viroporin such as p7 might therefore serve to benefit CSFV infection (Clapham, 2007, Pinton *et al.*, 2008).

1.1.3.5. NS2-3, NS2 and NS3

Due to the endogenous autoprotease activity of NS2, the protein is cleaved from a NS2-3 precursor to yield two mature proteins, NS2 and NS3 – this is made possible through an interaction with the cellular chaperone J-domain protein interacting with viral protein (Jiv90) (Lackner *et al.*, 2006, Isken *et al.*, 2019). Enhancement of NS2-3 processing is a major virulence determinant of cytopathic BVDV strains (Peterhans *et al.*, 2010). Delayed processing of CSFV NS2-3 has also been observed (Lamp *et al.*, 2011) as has cytopathogenicity upon expression of

Jiv90 by a recombinant virus (Gallei *et al.*, 2008), explaining the noncytopathogenic nature of CSFV. Remaining uncleaved as a consequence of depleted Jiv90 (Rinck *et al.*, 2001, Lackner *et al.*, 2005), NS2-3 precursor is required for both CSFV (Moulin *et al.*, 2007) and BVDV virus particle assembly (Agapov *et al.*, 2004).

Once cleaved from its precursor, NS2 is not essential for CSFV replication (Moulin *et al.*, 2007). However, it might serve a regulatory role and facilitate a cellular environment advantageous for viral replication (Tang *et al.*, 2010). NS3 has several functions and is essential for replication: at its C-terminus it exerts autoproteolytic activity, cleaving itself from the remainder of the polyprotein (comprised of NS3, NS4A, NS4B, NS5A and NS5B), while its N-terminal serine protease domain utilises NS4A as a co-factor to bring about subsequent cleavage of the polyprotein to yield its constituent components (Tautz *et al.*, 2000). In addition, NS3 was recently found to interact with tumour necrosis factor receptor-associated factor 6 (TRAF6), an adapter protein of toll-like receptor (TLR) and NF-kB signalling pathways responsible for induction of proinflammatory cytokines (Lv *et al.*, 2017a).

1.1.3.6. NS4A and NS4B

While essential for CSFV replication and particle formation, the only characterised function of NS4A is to act as a co-factor for the NS3 serine protease (Moulin *et al.*, 2007). Also essential for viral replication, the elucidated functions of NS4B are more extensive – NS4B is an NTPase, playing a role in ATP and GTP hydrolysis which are important for membrane trafficking and fusion (Gladue *et al.*, 2011). In addition, the protein appears to antagonise TLR7-mediated responses through a function of a predicted Toll/Interleukin 1 receptor like (TIR-like) binding domain (Fernandez-Sainz *et al.*, 2010).

1.1.3.7. NS5A and NS5B (RdRp)

Nonstructural protein 5A (NS5A) is also essential for replication and has been reported to associate with heat shock protein 70 (HSP70) (Zhang *et al.*, 2015), a protein involved in a

plethora of cellular processes vital to the viral life cycle (Sullivan and Pipas, 2001). Nonstructural protein 5B (NS5B) represents a viral RNA-dependent RNA polymerase (RdRp), responsible for the initiation of RNA synthesis (Steffens *et al.*, 1999). The initiation of replication by NS5B and its regulation by NS5A are discussed in 1.1.4.2.

1.1.4. Virus life cycle

1.1.4.1. Entry

It is the exposed surface glycoproteins of CSFV (E1 and E2) which are primarily responsible for interacting with the host cell plasma membrane and facilitating the process of entry. E1-E2 heterodimers were sufficient for entry of a CSFV-pseudotyped HIV virus into porcine cell lines (Wang *et al.*, 2004) while an earlier study found that when applied exogenously, E2 inhibited infection and cell-to-cell spread of CSFV, suggesting that interactions with specific receptors are responsible (Hulst and Moormann, 1997). While the precise cell-surface receptor for E2 remains undefined, it might be a porcine homolog of bovine CD46, the entry receptor reported for BVDV (Maurer *et al.*, 2004, Krey *et al.*, 2006, El Omari *et al.*, 2013). However, when porcine cell lines were treated with anti-CD46 monoclonal antibody (mAb), infection by field isolates of CSFV was antagonised but not inhibited, suggesting the requirement of additional receptors (Dräger *et al.*, 2015).

Early studies with BVDV suggested that, similarly to Hepatitis C virus (HCV), entry occurs through a clathrin-mediated pathway of endocytosis whereby virions must be primed for low pH prior to fusion (Lecot *et al.*, 2005). In PK-15 cells, uptake of CSFV was later reported to be dynamin and cholesterol-dependent, requiring the action of the Rab5 and Rab7 proteins (Shi *et al.*, 2016). In contrast, a study working with porcine alveolar macrophages found uptake to be caveola-dependent and clathrin-independent, implicating Rab11 in addition to Rab5 and Rab7 (Zhang *et al.*, 2018). Rab proteins belong to a superfamily of monomeric G-proteins that are involved in membrane trafficking and are localised to specific subcellular compartments

(Zhen and Stenmark, 2015). Rab5 and Rab7 are found in early and late endosomes respectively while Rab11 is associated with recycling endosomes and fusion with lysosomes. Therefore, upon uptake via clathrin or caveola-mediated endocytosis, CSFV progresses through early and late endosomes – subsequently, fusion and release of genome occurs either here or in recycling endosomes or lysosomes (Shi *et al.*, 2016, Zhang *et al.*, 2018).

With regards to potential entry receptors, Laminin receptor (LamR) was recently implicated *in vitro*. CSFV co-localised with exogenous LamR and infection was inhibited following its knockdown or pre-treatment with inhibitors or anti-LamR mAbs (Chen *et al.*, 2015). While previously shown to be dispensable for both attachment and entry (Wang *et al.*, 2004), E^{rns} was the only protein of CSFV found to interact with LamR. It is therefore conceivable that by binding to an alternate receptor to that of E2, E^{rns} serves an accessory function in attachment but not cell entry (Chen *et al.*, 2015).

1.1.4.2. Genome replication

Following fusion with endosomal membranes, CSFV virions release their RNA genome into the cytosol. As CSFV contains a positive-sense single-stranded RNA genome, it immediately undergoes translation by ribosomes associated with the rough endoplasmic reticulum (ER). For genome replication to be initiated, a number of non-structural CFSV proteins are required (Risager *et al.*, 2013) however the function of NS5A is most prominent. The viral RdRp NS5B is responsible for the transcription of negative-sense viral RNA from the positive-sense genome, the resulting transcript used as a template for the transcription of new positive-sense RNA (Xiao *et al.*, 2003, Xiao *et al.*, 2004). Together, NS5A and NS5B have the capacity to bind to the 3’ NTR (the site of replication initiation) at two sites, 3’ UTRL-1 and 3’ UTRL-2. Initially NS5A occupies both sites, inhibiting initiation of replication however if NS5B is expressed highly or NS5A expressed lowly, both NS5A and NS5B bind 3’ UTRL-1, initiating replication (Chen et al. 2012, Sheng et al. 2012). Another nonstructural protein, NS3 has been reported to exert

helicase activity on viral RNA, unwinding the secondary structure present at its 3' UTR. Interestingly, studies have found NS5B and NS3 to favour association with negative-sense viral RNA over positive-sense (Xiao *et al.*, 2004, Sheng *et al.*, 2007).

1.1.4.3. Morphogenesis and release

Positive-sense RNA virus replication is membrane-associated and, in the case of HCV, is dependent on the reorganisation of ER membranes (Egger *et al.*, 2002). Little data exists as to whether or not this is the case for CSFV, however BVDV and BDV have been associated with ER rearrangements in bovine embryonic testis cells (Gray and Nettleton, 1987). In contrast, a recent study observed no ER rearrangements in Madin-Darby bovine kidney (MDBK) cells infected with the distantly related Pestivirus Giraffe-1 (Schmeiser *et al.*, 2014).

Maturation of the closely-related BVDV occurs via transport of protein from the ER to the golgi complex as Brefeldin A, an inhibitor of this process, was observed to block virus release but had no effect on assembly or infectivity (Macovei *et al.*, 2006). Data regarding release of progeny CSFV virions is minimal, however Giraffe-1 was observed to leave infected MDBK cells in small exocytotic vesicles following passage through the golgi complex (Schmeiser *et al.*, 2014).

1.1.5. Pathology

1.1.5.1. Transmission

Transmission of CSFV typically occurs oronasally through direct or indirect contact with the urinary, respiratory or alimentary tract excretions of infected individuals or vertically between sow and offspring (Moennig *et al.*, 2003a). Additionally, airborne transmission has also been reported (Roberts, 1995) and uncooked infected pig meat present in feed (swill) also has the capacity to initiate infection in potentially CSFV-free areas (Terpstra, 1988). Indeed, viable virus has been recovered from meat frozen for more than 4 years (Edgar, 1949) and chilled for up to

85 days (Doyle, 1933, Helwig and Keast, 1966), demonstrating the longevity of the virus under a range of conditions.

1.1.5.2. Clinical disease and pathogenesis

CSFV has an incubation period of 7-10 days at which point the virus is actively replicating in lymph nodes and tonsillar tissue (Moennig *et al.*, 2003b). Virulence and clinical outcome are multifactorial, being both age and strain-dependent (Floegel-Niesmann *et al.*, 2003, Moennig *et al.*, 2003b). Infection of piglets less than 12 weeks of age manifests as an acute disease associated with severe leukopenia, fever, haemorrhagic disease and a host of neurological complications (ataxia, convulsions) and death follows 1-3 weeks later. Disease is less acute in older pigs, often resulting in chronic infection, a phenomenon also observed prenatally in piglets infected 50-70 days into gestation (Munoz-Gonzalez *et al.*, 2015). Recovery from acute infection is associated with production of neutralising antibodies against E2 which occur from 13 days post-infection (Tarradas *et al.*, 2014). Chronic and prenatal infection is always lethal and is associated with a failure to generate a neutralising antibody response (Moennig *et al.*, 2003a).

Leukopenia is a key hallmark of CSFV infection, primarily resulting in the depletion of T and B lymphocytes (Summerfield *et al.*, 1998, Summerfield *et al.*, 2006, Summerfield and Ruggli, 2015). Magnitude of leukopenia and speed of onset correlate with strain virulence (Tarradas *et al.*, 2014). Leukocytes are not infected in the early stages of infection; instead this phenomenon is associated with bystander apoptosis caused by high levels of circulating IFN-α (Summerfield *et al.*, 1998, Renson *et al.*, 2010, Tarradas *et al.*, 2014). *In vitro* CSFV antagonises induction of type I IFN in epithelial cells and *in vivo* it antagonises induction in macrophages and cells at the local site of infection (Renson *et al.*, 2010, Tamura *et al.*, 2014). Uninfected pDCs are believed to the primary source of IFN-α (Summerfield *et al.*, 2006), however infected pDCs have also been associated with an induction of this protein (Jamin *et al.*, 2008).

Together, these observations suggest a complex interplay between the virus and the host immune system.

1.1.5.3. Diagnosis

While combinations of analysis of clinical signs and pathology by veterinarians are invaluable (1.1.5.2), ultimately diagnosis is made possible either through indirect (serology) or direct detection (live virus, viral antigen or viral RNA) (Greiser-Wilke *et al.*, 2007). Antibodies are detectable 2-3 weeks post-infection and persist for life. Considered a "gold standard" diagnostic, virus neutralisation tests (VNT) determine the capacity of sera isolated from an individual to neutralise an infection in cell culture (Stear, 2005). While time-consuming and labour-intensive, VNT's do enable discrimination between infections by pestiviruses other than CSFV such as BVDV and BDV. Enzyme-linked immunosorbent assays (ELISAs) are used for the detection of antibodies reactive with CSFV's E2 glycoprotein (Wensvoort *et al.*, 1988, Moser *et al.*, 1996). While high-throughput, these assays can cross-react with antibodies induced by other pestiviruses (Soos *et al.*, 2001, Loeffen, 2005, Muller *et al.*, 2005) and can't be used to accurately identify persistently infected pigs infected *in utero* as maternal-derived antibodies are transferred during gestation (Saubusse *et al.*, 2016). Viral antigen can be directly detected through the inoculation of susceptible cells (PK-15 or SK6) with blood, sera or clarified organ followed by either an indirect immunofluorescence test (IFT) or immunoperoxidase assay (PLA), both of which are also regarded as "gold standard" (Stear, 2005). Considered the most sensitive method of detection, RT-PCR is used routinely in CSFV diagnostics as it has low detection limits and enables earlier detection than with virus isolation (Dewulf *et al.*, 2004, Handel *et al.*, 2004).

1.1.6. Methods of control and prevention

1.1.6.1. Culling and movement restrictions

With regards to methods of control, culling is often the first point of call in any outbreak. Directive 2001/89/EC of the European Council requires that all pigs within a 1 km radius of the CSFV infected farm are culled, however, pre-empting further spread this is often extended to 2 km (Ribbens *et al.*, 2005). Carcases, bedding and feed are also destroyed. This inevitably leads to the death of countless healthy animals and considerable economic losses for farmers in affected areas (Paton and Greiser-Wilke, 2003). Suspension of CSFV-free status by the OIE hinders international trade, providing yet another source of economic loss.

1.1.6.2. Live attenuated vaccines

Live attenuated vaccine usage in EU member-states is legislated by European Council Directive 2001/89/EC (EC, 2001, Postel *et al.*, 2013a). Developed through serial passage in rabbits, the live attenuated and avirulent CSFV C-strain confers rapid immunity (with a few days of vaccination) that appears to persist lifelong (van Oirschot, 2003b, a). At 7 days post-vaccination, sterile immunity is complete (Terpstra *et al.*, 1990, de Smit *et al.*, 2001), however in a recent study it was found to protect the majority of animals from viremia and clinical disease as early as 3 days post-vaccination (Graham *et al.*, 2012). Recently, this rapid onset of protection was associated with upregulation of ISGs linked to the ISG15 pathway (McCarthy *et al.*, 2019). In turn, C-strain is regarded as an effective vaccine for control of outbreaks.

In theory, vaccination against CSFV using C-strain should be straightforward as antigenic sequences are highly conserved due to a low mutation rate (Vanderhallen *et al.*, 1999). Despite this, C-strain vaccines from multiple manufacturers were found to be ineffective against the emergent subgenotype 2.1d CSFV now circulating in China (Luo *et al.*, 2017). In addition, Article 1.9.1 of the OIE Terrestrial Animal Health Code dictates that vaccination of herds with the current generation of live attenuated vaccines must not have taken place in the past 12

months to be granted CSF-free status. This is because pigs vaccinated with C-stain are indistinguishable from those that are infected but subclinical. Failure to differentiate between these two groups of pigs is because they are not Differentiating Infected from Vaccinated Animals (DIVA) vaccines. Therefore, C-strain vaccination is not suitable for routine vaccination in countries seeking to retain or obtain CSF-free status from the OIE.

Over the last decade, work detailing a highly efficacious DIVA vaccine has been published and in 2015 it was finally licensed for usage by the European Medicines Agency (EMA) (Blome *et al.*, 2017). CP7_E2alf (marketed as "Suvaxyn® CSF Marker") is a chimeric live attenuated vaccine based on a BVDV backbone with the E2 coding region replaced by the corresponding sequence of CSFV (Alfort/187) (Koenig *et al.*, 2007). Duration of immunity from a single intramuscular dose has been demonstrated to last for at least 6 months (Gabriel *et al.*, 2012) and has been shown to confer protection against more recent genotypes such as 2.1 and 2.3 (Blome *et al.*, 2014). Due to the attenuated nature of CP7_E2alf, replication following inoculation is limited, however RT-PCR can be used to detect vaccine-specific sequences (Leifer *et al.*, 2009a, Liu *et al.*, 2009) while commercial ELISAs (distributed by Thermofisher and Qiagen) have also been developed to enable detection of anti-CSFV E^{rns} antibodies. However, due to the delayed onset of anti-E^{rns} antibodies these ELISAs are less sensitive than those used for detection of anti-E2 antibodies, thus increasing the likelihood of false negative results (Blome *et al.*, 2012). With regards to the immune responses elicited by the vaccine, following vaccination with CP7_E2alf pre-challenge CSFV-specific IgG1 was found to be less than observed with C-strain vaccination (Renson *et al.*, 2013) while post-challenge CP7_E2alf demonstrated significantly less cytokine induction (e.g. TNF-α, IL-6) (Renson *et al.*, 2014). In addition, full clinical protection is only conferred 1 week post intramuscular and 2 weeks post oral vaccination and the European Medicines Agency (EMA) states that onset of immunity is only after 14 days (Leifer *et al.*, 2009b). During an outbreak, this could prove problematic as

despite the overall efficacy of the vaccine, there would still be a clear time period whereby vaccinated pigs are susceptible to infection.

1.1.6.3. Subunit vaccines

Prior to the development of the live attenuated CP7_E2alf vaccine, subunit vaccines were the only viable DIVA alternative. Two groups have described baculovirus-expressed E2 subunit vaccines that are presently licensed for usage (Lutticken *et al.*, 1998, Moormann *et al.*, 2000). The E2 protein expressed in this system has had its transmembrane domain deleted, resulting in its secretion into the cell culture supernatant, enabling harvest. As with CP7_E2alf, DIVA is made possible through an ELISA that detects anti-CSFV E^{rns} antibody.

However, vaccination-challenge studies seeking to determine efficacy have yielded variable and conflicting results. 14 days post-vaccination, pigs were usually protected when challenged intranasally or orally (Bouma *et al.*, 2000, Uttenthal *et al.*, 2001), however when challenged 13 months post-vaccination, protection was incomplete as 2 out 8 pigs died (de Smit *et al.*, 2001). While single dose vaccination has been found to significantly reduce shedding and viremia (Bouma *et al.*, 2000, Uttenthal *et al.*, 2001), others have reported otherwise (Ziegler and Kaden, 2002). In another study, viremia was detected following challenge as many as 21 days post-vaccination (Uttenthal *et al.*, 2001). The quantity of E2 protein is thought to be a decisive factor and in turn double-vaccinated herds were found to be almost completely protected, however many pigs still developed viremia (Dewulf *et al.*, 2000). Data regarding transmission between unvaccinated and vaccinated pigs following challenge is equally inconclusive and conflicting - reports of transmission occurring up to 21 days post-vaccination are concerning and highlight why C-strain is typically favoured over E2 subunit vaccination during outbreaks (Bouma *et al.*, 2000, Uttenthal *et al.*, 2001).

1.1.6.4. Transgenic pigs

Recently, a group in China developed transgenic pigs that were resistant to CSFV infection (Shimen strain) (Xie *et al.*, 2018). Building on previous studies which explored its efficacy *in vitro* (Xu *et al.*, 2008, Li *et al.*, 2010, Li *et al.*, 2011), Xie *et al.* identified a single shRNA capable of antagonising CSFV infection *in vitro* and subsequently generated knock-in transgenic pigs at the *Rosa26* locus using CRISPR-Cas9 and somatic cell nuclear transfer. Already, this technology has been used to successfully generate transgenic pigs that are resistant to infection with Porcine Reproductive and Respiratory Syndrome virus (PRRSV) (Burkard *et al.*, 2018) and transmissible gastroenteritis virus (TGEV) (Whitworth *et al.*, 2019).

While this development is exciting, genetic manipulation of animals to bring about resistance to specific diseases and infections is not without risk. One danger is that by applying such a selection pressure, CSFV escape mutants might emerge over time rendering transgenic pigs vulnerable to future infections. In addition, opposition to transgenic technologies and food is widespread (Houdebine, 2014), meaning export of pork products to some regions might prove problematic.

1.2. IFN signalling

1.2.1. Sensing of positive-sense RNA viruses

Interferon (IFN) comprise a large family of immunomodulatory proteins which are a key component of the innate immune system. Type I (α, β), type II (γ) and type III (λ) IFN are distinct from one another in their amino acid sequence homology, the cell types they are expressed by and the respective receptors utilised by each in initiating responses (Pestka *et al.*, 2004).

Most mammalian cells sense dsRNA, a viral replicative intermediate of positive-sense RNA viruses such as CSFV, through a series of pattern recognition receptors (PRRs). These receptors

include the endosomal toll-like receptor 3 (TLR3) and two cytoplasmic RNA helicases – retinoic acid-inducible gene I (RIG-I) and melanoma differentiation-associated protein 5 (MDA5) (Randall and Goodbourn, 2008, McNab *et al.*, 2015) (figure 1.5). When activated, pathways downstream of these proteins are responsible for inducing the production and release of pro-inflammatory cytokines such as type I IFN. Cells respond to type I IFN by upregulating a plethora of ISGs, thus activating a key element of the antiviral innate immune system (Franchi *et al.*, 2009, Li *et al.*, 2009, O'Neill *et al.*, 2013). CSFV infection is thought to be sensed by TLR3, MDA5 and RIG-I (Hüsser *et al.*, 2011).

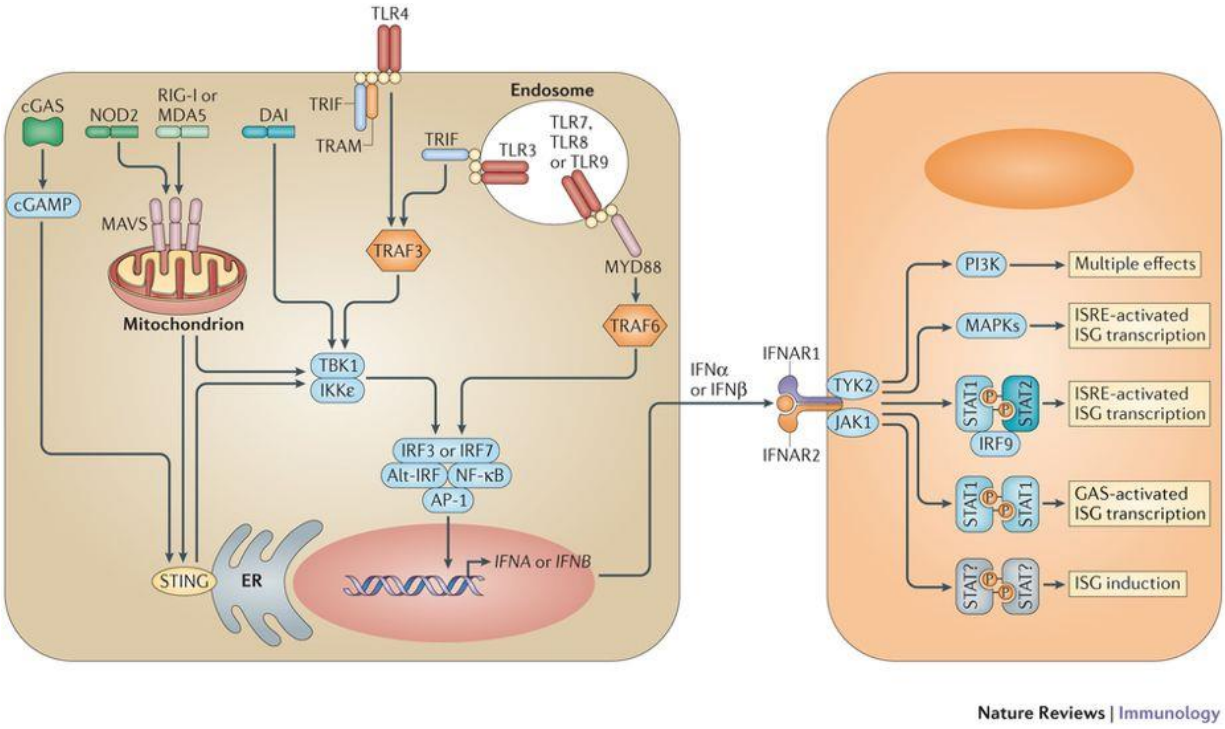

Figure 1.5: Schematic of presently known PRRs and their downstream signalling pathways. Intracellular PRRs such as RIG-I and MDA5 detect cytosolic dsRNA molecules and signal through the mitochondrial adapter protein MAVS to activate IRF3 and NF-kB, transcription factors of type I IFN. Endosomal TLRs detect endocytosed dsRNA or ssRNA and signal through the adapter proteins TRIF or MyD88 and TRAF protein to activate the same transcription factors. Type I IFN is detected by cell surface receptors which upregulate ISGs through the JAK-STAT pathway (EC, 1982, McNab *et al.*, 2015).

1.2.1.1. dsRNA sensing: RIG-I and MDA5

The N-termini of cytosolic PRRs RIG-I and MDA5 both have RNA helicase activity and contain a DExD/H box motif as well as a caspase activation and recruitment domain (CARD), while their C-termini display a conserved regulatory domain (CTD). The CARD domains convey the ability to transduce signals, whilst the CTDs play a role in the recognition of RNA (Yoneyama *et al.*, 2004, Yoneyama and Fujita, 2008). Studies in knockout mice have revealed that these proteins have non-redundant roles by detecting largely distant but also overlapping groups of viruses, indicating differing PAMPs in the induction of host antiviral responses (Kato *et al.*, 2006, Loo *et al.*, 2008). RIG-I is activated by short dsRNA molecules and ssRNA molecules bearing an overhanging 5'-triphospahte (5'-ppp) cap which are both recognised directly by the protein's CTD, while MDA5 is activated by longer dsRNA molecules lacking a cap (Cui *et al.*, 2008). This explains the selectivity of the two proteins and also why some viruses enzymatically remove their cap to prevent recognition by RIG-I (Habjan *et al.*, 2008).

Mitochondrial antiviral-signalling protein (MAVS) is key to the induction of type I IFN by cytosolic dsRNA, facilitating the transduction of signals from RIG-I and MDA5 to the transcription factors IRF3 and NF-kB (Wu and Hur, 2015). RIG-I and MDA5 engage with MAVS via their respective CARD domains, undergoing significant oligomerisation which drives the CARD domains of MAVS to transform into a filament which recruits TRAF2, 3, 5 and 6 (Saha *et al.*, 2006, Paz *et al.*, 2011, Liu *et al.*, 2013) (figure 1.6). It is ultimately the accumulation of TRAF proteins which enables further downstream signal transduction.

There are competing theories with regards to the mechanism by which activated MAVS mediates the activation of IRF3, however the kinases TBK1 and IKKε are a common element of each (Fitzgerald *et al.*, 2003). One theory suggests that upon recruitment of TRAF proteins by MAVS, IKKε and TBK1 are activated which in turn phosphorylate MAVS, facilitating recruitment of IRF3 to MAVS and subsequent phosphorylation of IRF3 by TBK1 (Liu *et al.*, 2015). More

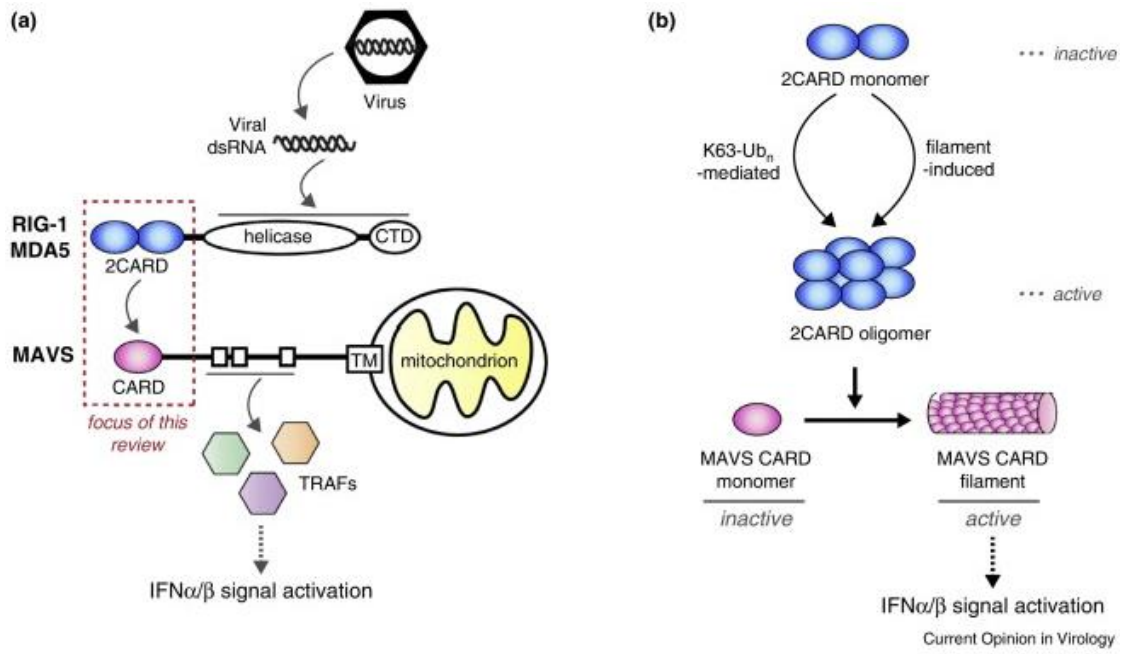

Figure 1.6: Schematic of responses to viral dsRNA by RIG-I, MDA5 and the MAVS adapter protein. Upon activation, RIG-I/MDA5 CARD domains oligomerise with the CARD domain of MAVS, transforming it into a filamentous structure capable of recruiting TRAF proteins and transducing signals required for induction of type I IFN (Wu and Hur, 2015).

recently, Fang *et al.* suggested that MAVS recruits a pre-associated TRAF-IKKε/TBK1 complex which results in the trans-autophosphorylation of each kinase, facilitating phosphorylation of IRF3 (see 1.2.2.1) (Fang *et al.*, 2017). IKKα/β, typically associated with NF-kB signalling, interacts with TBK1 in a process thought to enhance the phosphorylation of IKKε/TBK1 and IRF3 (Fang *et al.*, 2017). In their study, NEMO was key to MAVS-induced activation of IKKα/β and IKKε/TBK1 which is interesting considering the well-characterised roles of NEMO and IKKα/β in NF-kB signalling. Indeed, they observed IKKα/β to directly phosphorylate TBK1 – this was in agreement with previous studies which found NEMO and IKKα/β to be critical for both NF-kB and IRF3/IRF7 signalling (Zhao *et al.*, 2007, Clark *et al.*, 2011), likely explaining these observations.

1.2.1.2. dsRNA sensing: TLR3

Unlike the RIG-I family of receptors which are expressed ubiquitously and detect dsRNA in the cytoplasm of most cell types, TLR3 is predominately expressed in macrophages and dendritic

cells and is strictly endosomal (Takeuchi and Akira, 2008). Internalised dsRNA binds readily to TLR3 after which its cytosolic Toll/IL-1 receptor (TIR) domain recruits TRIF, leading to its oligomerisation and subsequent assembly of a larger signalling complex which cumulates in activation of the NF-kB and IRF3 transcription factors. TLR3 is unique in this respect as it is the only TLR to not utilise the myeloid differentiation primary response 88 (MyD88) adapter protein (Yamamoto *et al.*, 2003), however some elements are common with RIG-I/MDA5-mediated signalling. Initially, TRAF3 and 6 are recruited however each have distinct functions (Hacker *et al.*, 2006, Oganesyan *et al.*, 2006). Both TRAF3 and 6 recruit receptor-interacting serine/threonine-protein kinase 1 (RIPK1), which in turn interacts with and activates the transforming growth factor beta-activated kinase 1 (TAK1) complex, cumulating in the activation and nuclear translocation of NF-kB (see 1.2.2.1). In contrast, TRAF3 alone is sufficient to trigger the recruitment of TBK1 and IKKε in a NEMO-dependent manner (Hacker *et al.*, 2006, Oganesyan *et al.*, 2006). As with RIG-I/MDA5-mediated signalling, this results in the phosphorylation of IRF3, its subsequent dimerization and nuclear translocation.

1.2.1.3. ssRNA sensing: TLR7

Expressed in the endosomes of pDCs, TLR7 is primarily responsible for the sensing of single-stranded RNA (ssRNA) molecules of viral origin (Diebold *et al.*, 2004). Induction of type I IFN by TLR7 requires the adapter protein MyD88 and is responsible for the activation of IRF7, a transcription factor closely related to IRF3 that is constitutively expressed in pDCs (Honda *et al.*, 2004, Kawai *et al.*, 2004). MyD88 achieves this by recruiting IRF7 and TRAF6 to form a complex in the cytosol. It is ultimately the E3 ubiquitin ligase activity of TRAF6 which activates IRF7 through phosphorylation in a TBK1/IKKε-independent manner, resulting in its nuclear relocalisation and induction of IFN-α as well as IFN-β (Kawai *et al.*, 2004).

1.2.2. Activation of type I IFN transcription by IRF3 and IRF7

1.2.2.1. IRF3

Following their activation (discussed in 1.2.1), IRF3 and NF-kB translocate to the nucleus. In the case of IRF3, this is dependent on TBK1/IKKε-mediated phosphorylation of a cluster of C-terminal residues (Ser^{385}, Ser^{386}, Ser^{396}, Ser^{398}, Ser^{402}, Thr^{404}, Ser^{405}) which enables dimerization, binding of CREB binding protein (CBP) and the exposure of a nuclear localisation signal (NLS) (Lin *et al.*, 1998, Servant *et al.*, 2003, Mori *et al.*, 2004, Dragan *et al.*, 2007). Data regarding the importance of phosphorylation at each of these residues is conflicting. It is thought that sequential phosphorylation of site 1 (Ser^{385} and Ser^{386}) and site 2 residues (Ser^{396}, Ser^{398}, Ser^{402}, Thr^{404}, Ser^{405}) takes place, unfolding IRF3 from an autoinhibitory conformation thus enabling dimerization and activation (Lin *et al.*, 1998, Qin *et al.*, 2003, Servant *et al.*, 2003, Bergstroem *et al.*, 2010). However Panne *et al.* suggest phosphorylation at site 2 precedes phosphorylation at site 1 (Panne *et al.*, 2007). In unstimulated cells, NF-kB is retained in the cytosol through an interaction with the inhibitor IkBα (Huxford *et al.*, 1998, Jacobs and Harrison, 1998) which obscures its NLS (Beg *et al.*, 1992). Phosphorylation of IkBα results in its ubiquitination and degradation in a proteasome-dependent manner (Karin and Ben-Neriah, 2000) and exposes the NF-kB NLS, enabling nuclear translocation.

The IFN-β gene promoter contains a series of positive and negative regulatory elements. Upon stimulation, positive regulatory domains (PRD) I, II, III and IV operate together as a virus-inducible enhancer (Kim and Maniatis, 1997) (figure 1.7). PRDI and PRDIII are bound by IRF3 while PRDII and PRDIV are bound by both NF-kB and activated protein-1 (AP-1), a heterodimer of activating transcription factor 2 (ATF2) and c-JUN. Together, these bound proteins form a complex known as the "enhanceosome", driving the further recruitment of general control of amino acid synthesis 5 (GCN5) and CBP (Kim and Maniatis, 1997). In resting cells, the transcriptional start site of the IFN-β gene is obscured by histones in the nucleosome (Agalioti

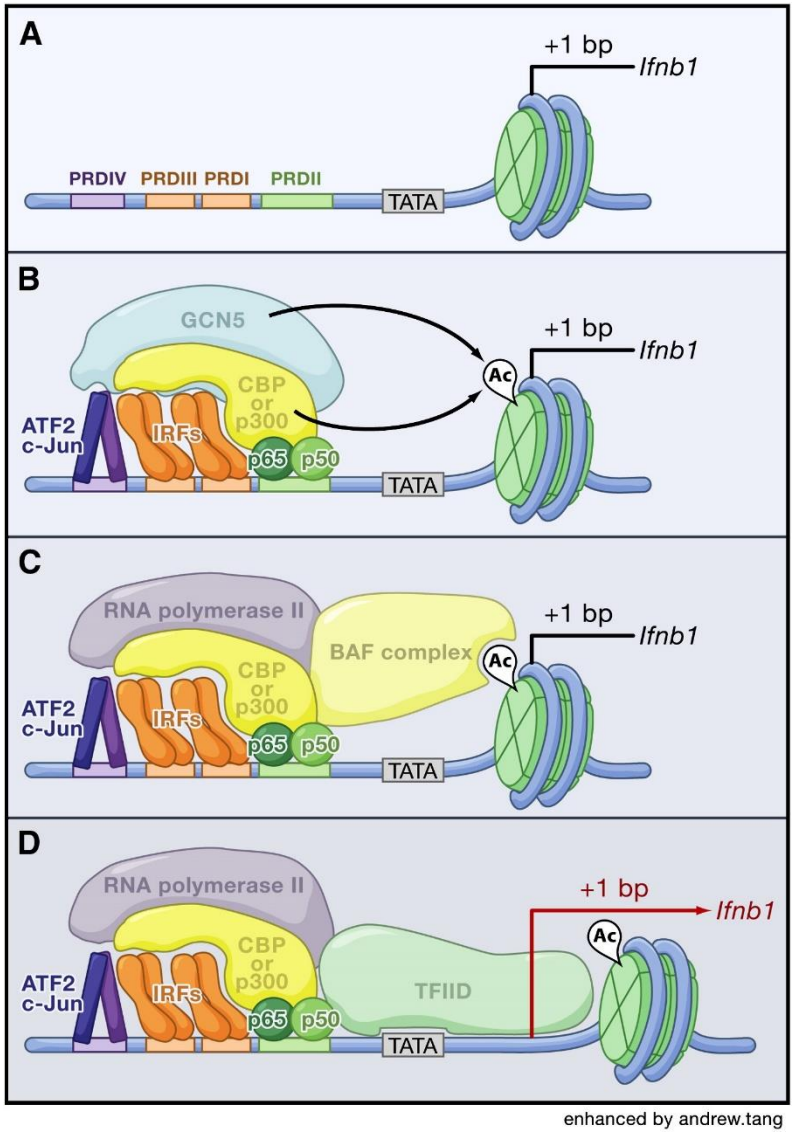

Figure 1.7: Schematic of initiation of IFN-β gene transcription following viral infection. (A) In unstimulated cells, the IFN-β transcription start site is obscured by the nucleosome. (B, C) Engagement by factors including activated IRF3 and IRF7 protein, CBP and NF-kB subunits p65 and p50 forms the "enhancesome", (D) exposing the transcription start site and enabling initiation of IFN-β transcription (Agalioti *et al.*, 2000).

et al., 2000). However, upon stimulation histone acetylation by GCN5 and CBP recruits the Brahma-related gene (BRG)-Brahma (BRM)-associated factor (BAF) complex, displacing the nucleosome. Following exposure of the transcription start site, the transcription factor IID (TFIID) transcription complex is finally recruited, enabling the initiation of IFN-β gene transcription (Agalioti *et al.*, 2000).

1.2.2.2. IRF7

Constitutively expressed in pDCs, the IRF7 transcription factor can substitute for IRF3 and form heterodimers and homodimers which bind to the promoters of IFN-α and IFN-β, activating their transcription. IRF3 has a preference for activation of IFN-β while IRF7 is able to efficiently activate both (Marié *et al.*, 1998, Sato *et al.*, 1998). Importantly, IRF7 is an ISG and is therefore upregulated by type I IFN (discussed in 1.2.3.2), forming a positive-feedback system in non-pDC cell types (Sato *et al.*, 1998, Levy *et al.*, 2002).

1.2.3. Type I IFN-mediated responses

1.2.3.1. JAK-STAT signalling

Upon translation, IFN-α/β (type I IFN) are secreted from the cell and bind to the IFN-α/β receptor (IFNAR) to elicit their antiviral effects. IFNAR is a heterodimer comprised of two subunits, IFNAR1 and IFNAR2 (Novick *et al.*, 1994). In the receptor's resting state, IFNAR1 is bound to tyrosine kinase 2 (TYK2) while IFNAR2 is bound to both Janus kinase 1 (JAK1) and signal transducers and activators of transcription 2 (STAT2) (Stancato *et al.*, 1996). Upon binding of type I IFN, conformational changes occur in the cytosolic tails of IFNAR1 and IFNAR2 which facilitate the activation of TYK2 and JAK1, respectively (Velazquez *et al.*, 1992, Muller *et al.*, 1993). In turn, JAK1 and TYK2 phosphorylate signal transducers and activators of transcription 1 (STAT1) and STAT2, resulting in the formation of an active STAT1-STAT2 active heterodimer (Darnell *et al.*, 1994). Phosphorylation of STAT2 inactivates its nuclear export (Frahm *et al.*, 2006) and STAT1-STAT2 heterdimerisation creates an NLS (Banninger and Reich, 2004). Subsequently, the complex binds to interferon regulatory factor 9 (IRF9), leading to the formation of a heterotrimeric transcription factor termed interferon-stimulated gene factor 3 (ISGF3). Promoters of most ISGs bear an IFN-stimulated response element (ISRE) and it is this element to which ISGF3 binds and enhances transcription (Friedman and Stark, 1985, Porter *et al.*, 1988, Darnell *et al.*, 1994).

1.2.3.2. ISG upregulation

ISGs have a diverse range of functions, however they can generally be split into three groups: antagonists of viral entry, antagonists of replication and antagonists of assembly and egress (Schoggins, 2019). For example the interferon-induced transmembrane (IFITM) family of proteins antagonise virus entry (Bailey *et al.*, 2014) and, in the case of IFITM3, this is achieved by the trafficking of invading virus particles to lysosomes for degradation (Spence *et al.*, 2019). However, ISG15 is more promiscuous and exerts an array of antiviral functions both intracellularly and extracellularly (Dzimianski *et al.*, 2019).

Past studies utilised microarray analysis to identify ISGs and a meta-analysis published in 2011 determined there to be in excess of 450 ISGs induced by type I IFN in a range of cell types from different species (Schoggins *et al.*, 2011). More recently, Shaw *et al.* built on this and found, following treatment with IFN-α, a core set of 62 vertebrate genes to be upregulated in primary fibroblasts from nine mammals (Shaw *et al.*, 2017). In addition to genes classically associated with antiviral responses, genes encoding the PRRs for viral dsRNA (TLR3, MDA5, RIG-I) were found to be particularly conserved in their upregulation as were proteins governing the initial response to type I IFN (STAT1 and STAT2).

1.2.4. Antagonism of IFN induction by CSFV N^{pro}

Early studies on pestiviruses determined that persistent infection of cattle with non-cytopathic strains of BVDV was as a consequence of their inability to mount an effective type I IFN response (Charleston *et al.*, 2001, Schweizer and Peterhans, 2001, Ruggli *et al.*, 2003). This antagonism of the innate type I IFN response is conserved by CSFV. Indeed, type I IFN induction has been shown to be antagonised *in vitro* by the expression of the CSFV N^{pro} protein in multiple IFN-competent cell lines (Ruggli *et al.*, 2005, Seago *et al.*, 2007). Only induction of type I IFN was antagonised and not the JAK-STAT pathway governing response to IFN (Seago *et al.*, 2007).

Importantly, a recombinant N^{pro}-deleted virus (ΔN^{pro} rCSFV) was unable to antagonise type I IFN production, confirming N^{pro} to be the primary source of inhibition during CSFV infection (Ruggli *et al.*, 2003, Bauhofer *et al.*, 2005, Ruggli *et al.*, 2005). While ΔN^{pro} rCSFV is thought to induce type I IFN in response to detection of viral dsRNA by cellular PRRs, levels of dsRNA are unaffected in cells infected with a parental virus (Bauhofer *et al.*, 2005). This indicated that N^{pro}'s ability to antagonise induction of type I IFN is dependent on interactions with host cell proteins.

CSFV and BVDV N^{pro} were shown to have no effect on IRF3 transcription (Hilton *et al.*, 2006, Bauhofer *et al.*, 2007, Chen *et al.*, 2007) or the stability of IRF3 transcripts (Bauhofer *et al.*, 2007). It was subsequently discovered that, through a direct or indirect interaction, CSFV N^{pro} antagonises cellular levels of IRF3 protein by a mechanism dependent on proteasomal degradation (Bauhofer *et al.*, 2007, Seago *et al.*, 2007). Notably, this mechanism is shared with BVDV N^{pro} (Hilton *et al.*, 2006, Seago *et al.*, 2007). It is the polyubiquitination of proteins which targets them to the proteasome for degradation (Zheng and Shabek, 2017). While N^{pro} lacks endogenous ubiquitin ligase activity, required for the polyubiquitination of target protein, it may act as a scaffold to recruit an ubiquitin ligase protein (Bauhofer *et al.*, 2007). Indeed, TRIM56 has been reported to directly interact with BVDV N^{pro} and facilitate the proteasomal degradation of IRF3 (Wang *et al.*, 2011). CSFV N^{pro} has been shown to interact with both monomeric and CBP-bound dimeric IRF, suggesting that the interaction is independent of IRF3 activation and DNA binding (Gottipati *et al.*, 2016).

CSFV N^{pro} contains a novel zinc-binding "TRASH" motif in its C-terminal domain that has been reported to be responsible for its interaction with IRF3 (Ettema *et al.*, 2003, Szymanski *et al.*, 2009). The structure of CSFV N^{pro} showed the TRASH motif contains the key residues Cys^{112}, Cys^{134}, Asp^{136} and Cys^{138}. Zinc-binding is thought to be an essential property of CSFV N^{pro} as

mutation of these residues eliminated its capacity to antagonise the induction of type I IFN *in vitro* (Szymanski *et al.*, 2009).

The significance of the TRASH motif in N^{pro} has been studied *in vivo*. Upon acquisition of a mutation (N136D) which abrogated its interaction with IRF3, N^{pro} was no longer able to antagonise induction of IFN-α while reversion of these mutations recovered this function, enabling enhanced replication at and spread from localised sites of infection (Tamura *et al.*, 2014). An earlier study found mutation of the same residue (Asp^{136}) and an additional residue (Cys^{112}) to only partially attenuate *in vivo* infection with the moderately-virulent Alfort (Ruggli *et al.*, 2009). Despite developing viremia and fever, pigs infected with viruses encoding either N^{pro} mutant displayed antagonised type I IFN, reduced clinical scores and in fact recovered after 12-13 days compared to those infected with parental virus which were euthanised between days 7-11 (Ruggli *et al.*, 2009).

CSFV N^{pro} has also been reported to interact with IRF7 in yeast (Lv *et al.*, 2017b) and pDCs (Fiebach *et al.*, 2011), cells which are typically regarded as "professional" producers of type I IFN (Ning *et al.*, 2011). Type I IFN is partially antagonised in infected pDCs, presumably as a consequence of N^{pro}'s interaction with IRF7 (Fiebach *et al.*, 2011). IRF7 is also partially antagonised by N^{pro} in non-pDC cells, explaining why pDCs are unable to sensitise them (Husser *et al.*, 2012). The high levels of circulating type I IFN detected in CSFV-infected pigs (Jamin *et al.*, 2008) is therefore likely produced by infected and bystander pDCs detecting viral PAMPs in a contact-dependent manner through the pDC-exclusive TLR7 (see 1.2.1.3) (Summerfield, 2012, Python *et al.*, 2013, Summerfield and Ruggli, 2015).

An additional interacting partner of CSFV N^{pro}, IkBα is responsible for the inhibition of NF-kB signalling in unstimulated cells however the relevance of this interaction with respect to CSFV infection has yet to be determined (Doceul *et al.*, 2008).

1.3. Apoptosis

Apoptosis is an orderly programme of cell death employed by multicellular organisms to eliminate damaged, aberrant or infected cells and is an essential component of cell turnover and embryonic development (Nagata, 2018). Early studies defined apoptosis as a morphological state of cells characterised by key hallmarks such as cell shrinking, plasma membrane blebbing and nuclear destruction (karyorrhexis) (Kerr *et al.*, 1972, Saraste and Pulkki, 2000).

Apoptosis of infected cells ultimately serves as yet another mechanism by which the intracellular innate immune system is able to counter viruses at the local site of infection and prevent their wider dissemination within the host (Jorgensen *et al.*, 2017). Leukopenia in CSFV-infected pigs is thought to occur as a consequence of cell death (Sanchez-Cordon *et al.*, 2002, Choi *et al.*, 2004), however these cells rarely contain virus (Summerfield *et al.*, 2000). Taking into account the high titres of virus detected in acutely infected pigs, infected cells resistant to virus-induced apoptosis likely have a role to play in determining the overall clinical outcome (Tamura *et al.*, 2014, Summerfield and Ruggli, 2015).

While various modes of apoptosis exist, they each converge to activate a core set of proteases termed “caspases” (cysteine aspartyl proteases) (Alnemri *et al.*, 1996). By the process of proteolysis, caspases cleave over 1,000 cellular proteins at multiple sites (Crawford *et al.*, 2013), however they do have preferred substrates (Julien *et al.*, 2016). Initiator caspases -2, -8, -9 and -10 transduce apoptotic signals to the executioner caspases -3, -6 and -7 (McIlwain *et al.*, 2013). Shedding light on the biochemical nature of apoptosis, executioner caspase-3 has been shown to cleave substrates resulting in lethal DNA fragmentation (Enari *et al.*, 1998), plasma membrane blebbing (Coleman *et al.*, 2001) and exposure of amine-containing or anionic phospholipids such as phosphatidylserine (PtdSer) (Suzuki *et al.*, 2013, Segawa *et al.*, 2014). Externalised PtdSer acts as a molecular “eat me” signal for disposal by professional

phagocytic cells such as macrophages (Fadok *et al.*, 1992) however failure to initiate this process is associated with pathology and disease (Nagata, 2018).

The intrinsic and extrinsic pathways of apoptosis share many core signalling components and each cumulate in the cleavage of caspase-3 (figure 1.8). As their names suggest, the intrinsic pathway responds to intracellular stimuli and stresses while the extrinsic pathway responds to those of extracellular origin.

1.3.1. Intrinsic pathway

1.3.1.1. Bcl-2 family member proteins and MOMP

Also known as the "mitochondrial pathway", the intrinsic pathway governs cellular responses to a diverse array of stress-related stimuli of intracellular origin such as toxins, hypoxia, infection and radiation-induced damage. Irrespective of the apoptotic stimuli, mitochondrial outer membrane permeabilization (MOMP) is a key hallmark (Tait and Green, 2010). However, this process is tightly regulated by and dependent on the action of Bcl-2 family proteins which are either pro-apoptotic (Bim, Bid, Bad, Puma, Noxa, Hrk, Bmf), anti-apoptotic (Bcl-2, Bcl-xL, Bcl-B, Mcl-1, A1) or effectors (Bax, Bak, Bok) (Czabotar *et al.*, 2014). In response to upstream apoptotic stimuli, pro-apoptotic Bcl-2 family proteins bearing only a single Bcl-2 homology domain (BH3-only) are either upregulated or post-translationally modified (Tait and Green, 2010).

BH3-only "activator" proteins (Bid, Bim, Puma, p53) interact directly with Bax/Bak triggering conformational changes, a prerequisite for initiation of MOMP (Dewson *et al.*, 2008, Gavathiotis *et al.*, 2010, Tait and Green, 2013). In non-apoptotic cells, anti-apoptotic Bcl-2 family proteins (Bcl-2, Bcl-xL, Mcl-1) engage Bax/Bak through their respective BH3 domains, antagonising their activity until overwhelmed by the action of BH3-only "sensitizer" proteins (Chen *et al.*, 2005, Chipuk *et al.*, 2008, Llambi *et al.*, 2011). Interestingly, Bax/Bak

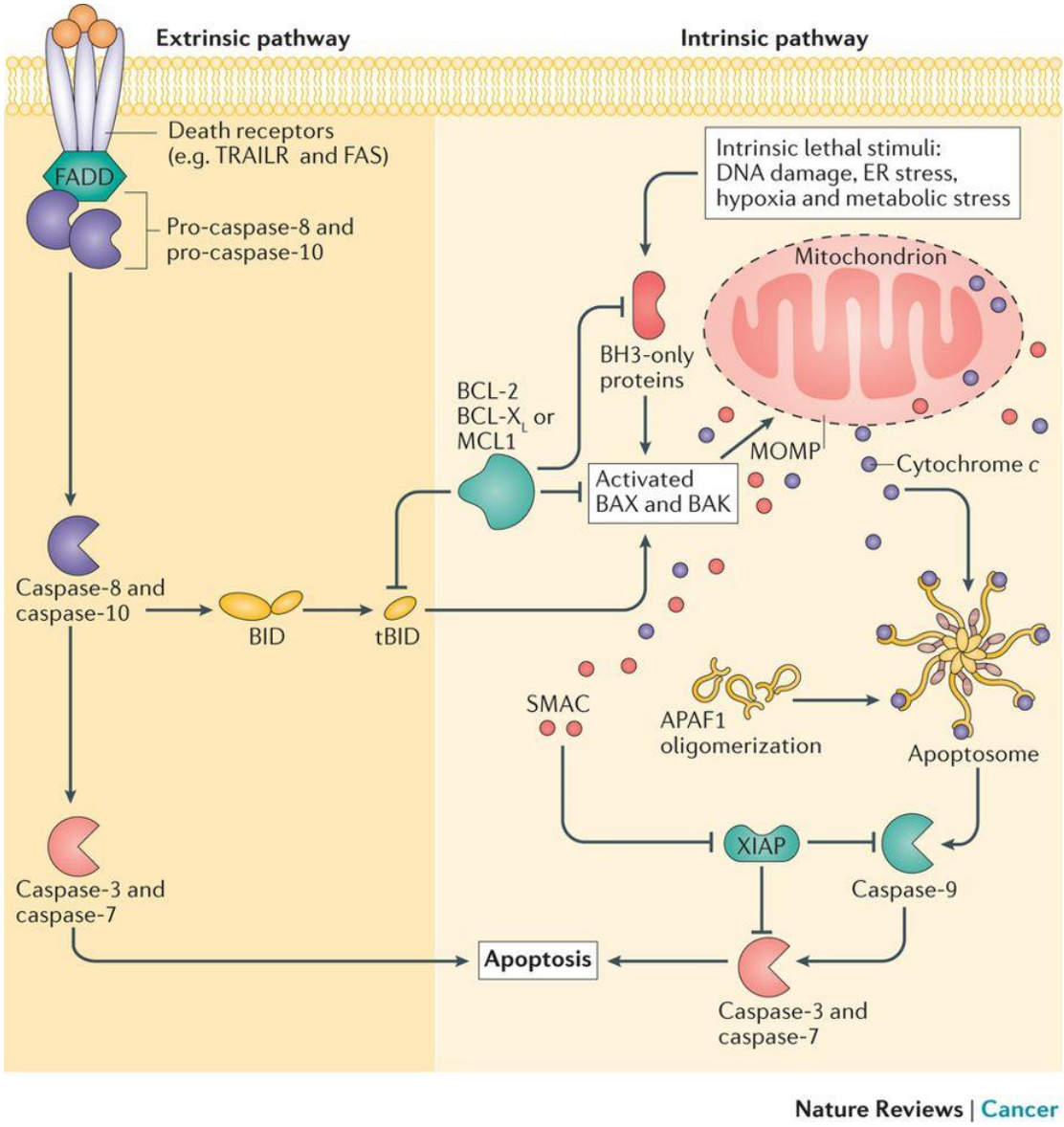

Figure 1.8: Intrinsic and extrinsic pathways of apoptosis converge to initiate apoptosis through the cleavage of executioner caspases (Ichim and Tait, 2016). Intracellular stimuli initiate the intrinsic pathway of apoptosis through modulation of Bcl-2 family member proteins, resulting in mitochondrial outer membrane permeabilization (MOMP) and release of pro-apoptotic mitochondrial intermembrane space (IMS) proteins. Cytochrome c activates Apaf-1 which then activates caspase-9, resulting in activation of caspase-3 via cleavage. Extracellular stimuli initiate the extrinisic pathway of apoptosis and are sensed by cell surface "death receptors". A complex assembles around ligand-bound receptors, resulting in the activation of caspase-8 – this caspase then triggers MOMP through cleavage of Bcl-2 family protein Bid or cleaves caspase-3 directly.

autoactivation has been reported in the absence of known BH3-only activator proteins (Zhang *et al.*, 2016, Jeng *et al.*, 2018).

Recently, there have been significant advances in elucidating the biochemical nature of direct BH3-only protein activation of Bax (Westphal *et al.*, 2014, Cosentino and García-Sáez, 2017, Walensky, 2019). BH3-only proteins initially bind to alpha helices 1 (α1) and 6 (α6) of Bax, exposing α9 which enables insertion into the mitochondrial outer membrane (MOM) (Dengler *et al.*, 2019) (figure 1.9). This exposes the so-called "canonical groove" which facilitates further binding of BH3-only proteins (Dengler *et al.*, 2019). This observation is supported by additional studies which recently found α9 to be sequestered in autoinhibited dimers of cytosolic Bax (Garner *et al.*, 2016, Robin *et al.*, 2018). When exposed, the canonical groove of one Bax monomer interacts with the BH3/α2 domain of another, forming "symmetric" homodimers which undergo homo-oligomerisation (Czabotar *et al.*, 2013, Subburaj *et al.*, 2015) to create pores of variable sizes (Bleicken *et al.*, 2013, Xu *et al.*, 2013). Pores are thought to be either

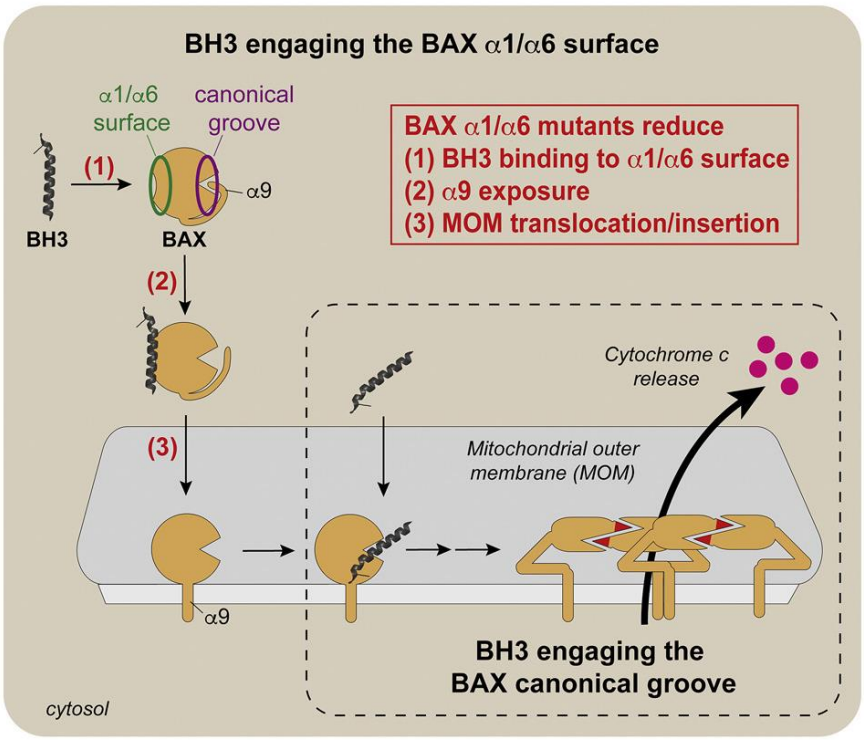

Figure 1.9: Recent model of BH3-mediated direct activation of Bax through sequential engagement of the α1/α6 helices and canonical groove. BH3 domains of BH3-only proteins first engage the α1/α6 surface of BAX, triggering conformational changes which enable insertion of the α9 helice into the MOM. BH3-only proteins bind to the now exposed "canonical groove", further activating Bax and leading to MOMP and Cytochrome c release (Dengler *et al.*, 2019).

lipidic or proteinaceous and serve to initiate MOMP, facilitating release of apoptotic mitochondrial intermembrane space (IMS) proteins (Cosentino and García-Sáez, 2017).

1.3.1.2. The apoptosome

MOMP facilitates the release of proteins from the IMS. Cyotochrome c is a well characterised IMS protein which, upon release, associates with apoptotic protease-activating factor 1 (Apaf-1) to form a wheel-shaped complex termed the "apoptosome" (Riedl and Salvesen, 2007, Yuan and Akey, 2013). The apoptosome is predicted to comprise of 7 Apaf-1 monomers which oligomerise following hydrolysis of ATP nucleotides by their ATPase domains (Kim *et al.*, 2005). Assembly of this complex exposes the N-terminal CARD domains of Apaf-1, facilitating the recruitment and activation of caspase-9 which, in turn, cleaves and activates caspase-3 (Hu *et al.*, 1999, Zou *et al.*, 1999). Interestingly, cleavage of caspase-9 is not a prerequisite for activation (Rodriguez and Lazebnik, 1999, Stennicke *et al.*, 1999). Instead, monomers of caspase-9 are thought to be activated by proximity-induced dimerisation (Boatright *et al.*, 2003, Boatright and Salvesen, 2003, Shi, 2004).

Other IMS proteins released following MOMP include second mitochondria-derived activator of caspase (Smac) and Omi/high temperature requirement A2 (HtrA2) which antagonise the activity of X chromosome-linked IAP (XIAP) (Du *et al.*, 2000, Suzuki *et al.*, 2004), a potent inhibitor of caspase-3, -7 and -9 (Salvesen and Duckett, 2002).

1.3.2. Extrinsic pathway

Also known as the "death receptor-mediated pathway", the extrinsic pathway is directly initiated through a series of transmembrane receptor-mediated interactions involving receptors belonging to the tumour necrosis factor (TNF) family (Walczak, 2013). The cysteine-rich extracellular domains of the TNF family receptors share homology with one-another – in addition, they each possess an intracellular "death domain" to facilitate downstream signal

transduction (Ashkenazi and Dixit, 1998). Death domains function by recruiting death-inducing signalling complexes (DISC) which facilitate the auto-catalytic activation of caspase-8 (Kischkel *et al.*, 1995). The fate of activated caspase-8 is cell and tissue dependent: caspase-8 directly activates caspase-3 in progenitor T-cells while in fibroblasts and hepatocytes caspase-8 triggers MOMP (see 1.3.1.1) through the cleavage of Bid, a BH3-only protein (Peter and Krammer, 1998, Strasser *et al.*, 2009, Walczak, 2013). DISC assembly facilitates the dimerization of caspase-8 monomers, activating it in much the same way that the apoptosome activates caspase-9 (see 1.3.1.2) (Boatright *et al.*, 2003, Oberst *et al.*, 2010).

In the case of the apoptotic inducers Fas ligand (FasL) and tumor necrosis factor (TNF)-related apoptosis-inducing ligand (TRAIL), their respective receptors (FasR and TRAIL-R1/TRAIL-R2) cluster at their intracellular death domains upon ligand binding (Boldin *et al.*, 1996, Walczak *et al.*, 1997, Kischkel *et al.*, 2000, Sprick *et al.*, 2000). The adaptor protein Fas-associated death domain (FADD) assembles with these death domains (Chinnaiyan *et al.*, 1995), leading to the formation of a DISC, recruitment of caspase-8 and its subsequent activation. While primarily responsible for induction of NF-kB signalling, TNF-α and its receptor TNF receptor 1 (TNF-R1) mediate apoptosis in a similar manner to FasL and TRAIL (Walczak, 2013). However, the adapter proteins TNF-R1-associated DEATH domain protein (TRADD) and receptor-interacting protein 1 (RIPK1) are also reported to play a role in DISC formation and caspase-8 activation (Wang *et al.*, 2008, Declercq *et al.*, 2009).

Cellular FLICE-like inhibitory protein (cFLIP) is present in the DISC and exists as two isoforms, $cFLIP_L$ and $cFLIP_S$ which are thought to interfere with necrosis (a caspase-independent mode of cell death) and apoptosis respectively when present at high enough concentrations (Irmler *et al.*, 1997). Both isoforms are upregulated as a consequence of NF-kB signalling, explaining why apoptosis is not the primary output of TNF-α/TNF-R1 signalling (Micheau *et al.*, 2001).

Through its adapter protein TRIF, TRL3 has been reported to recruit a complex termed the "ripoptosome" comprised of RIPK1, FADD and caspase-8 following stimulation of cancer cell lines with poly(I:C) (Feoktistova *et al.*, 2011, Tenev *et al.*, 2011). Expression of members of the inhibitors of apoptosis (IAP) protein family antagonise this pathway as do cFLIP isoforms (Alkurdi *et al.*, 2018), the latter being products of the TLR3-mediated NF-kB signalling.

1.3.3. Antagonism of apoptosis by CSFV N^{pro}

1.3.3.1. What we know so far

An early study in 2001 was the first to demonstrate that infection of macrophages with non-cytopathic BVDV protected them from poly(I:C)-mediated apoptosis (Schweizer and Peterhans, 2001). CSFV was found to share this phenotype (Ruggli *et al.*, 2003), later being attributed to an anti-apoptotic function of N^{pro} (Ruggli *et al.*, 2005, Johns *et al.*, 2010a). The ability of CSFV and BVDV N^{pro} to antagonise type I IFN has been studied extensively and its mechanisms elucidated (discussed in 1.2.4), however the means by which apoptosis is antagonised has yet to be determined. Antagonism of poly(I:C)-mediated caspase-8 and -9 cleavage and tBid activity in CSFV infected cells has been reported (Johns *et al.*, 2010a), however it is uncertain whether this is mediated by N^{pro} or another viral protein. At present, the only published data regarding N^{pro}'s own anti-apoptotic functions confirms an increase in cell survival (Ruggli *et al.*, 2005) and an antagonism of caspase-3 activation (Johns *et al.*, 2010a) upon treatment of porcine cell lines with poly(I:C). Importantly, CSFV N^{pro} was unable to protect CSFV-infected cells from FasL or staurosporine (STS)-mediated apoptosis (Johns *et al.*, 2010a). FasL induces death receptor-mediated apoptosis (see 1.3.2) while STS is thought to induce apoptosis through MOMP and caspase-dependent pathways (Belmokhtar *et al.*, 2001, Zhang *et al.*, 2004, Malsy *et al.*, 2019) and also a caspase-independent pathway (Belmokhtar *et al.*, 2001, Zhang *et al.*, 2004). These observations are significant as they suggest that N^{pro} acts on protein(s)

upstream of the mitochondria to antagonise induction of dsRNA-mediated mitochondrial pathway of apoptosis, independent of death receptor signalling.

CSFV N^{pro} antagonises induction of type I IFN through an interaction with IRF3 that targets it for proteasomal degradation (discussed in 1.2.4). A key question is whether this same interaction is also responsible for the antagonism of apoptosis or whether additional or alternate interactions are required.

1.3.3.2. IRF3

The primary outcome of IRF3 activation is the production of type I IFN and the subsequent upregulation of ISGs (see 1.2.2 and 1.2.3). Porcine genes encoding apoptotic proteins such as caspase-8, Noxa and TRAIL are upregulated by IFN-α (Shaw *et al.*, 2017), suggesting that type I might prove to be pro-apoptotic. However, this is unlikely as the interferon-defective SK6 cell line is still sensitive to poly(I:C)-mediated apoptosis (Ruggli *et al.*, 2005, Johns *et al.*, 2010a).

RNA viruses have been reported to induce an intrinsic pathway of apoptosis termed RLR-induced IRF3-mediated pathway of apoptosis (RIPA) through IRF3-mediated activation of Bax (Chattopadhyay *et al.*, 2010, Chattopadhyay *et al.*, 2011, Chattopadhyay *et al.*, 2016). In Sendai virus (SeV)-infected cells, IRF3 was shown to interact with Bax through a putative BH3-homology domain, facilitating their co-translocation to the mitochondria and Bax's subsequent induction of apoptosis through MOMP (discussed in 1.3.1.1) (Chattopadhyay *et al.*, 2010). Ubiquitination of IRF3 on specific lysine residues was required for induction of this pathway while activation of IRF3's transcriptional activity proved dispensable both *in vitro* and *in vivo* (Chattopadhyay *et al.*, 2016). Induction of RIPA required many of the same components for induction of type I IFN (MAVS, TBK1, TRAF3) but also TRAF2, TRAF6 and the linear ubiquitin chain assembly complex (LUBAC) (Chattopadhyay *et al.*, 2016). RIPA was important in conferring protection against not only SeV but also Vesicular stomatis virus (VSV) and Encephalomyocarditis virus (EMCV), suggesting this pathway might be a more generalised

response to infection with RNA viruses (Chattopadhyay *et al.*, 2011). Indeed, BVDV N^{pro} has been reported to antagonise a sodium arsenate mediated IRF3/Bax-dependent pathway of apoptosis (Jefferson *et al.*, 2014).

1.3.3.3. TID1

In order to further elucidate the functions of N^{pro}, yeast two-hybrid (Y2H) screens were carried out at The Pirbright Institute by Dr Seago. Tumorous imaginal disc 1 (TID1) was identified as a putative binding partner (unpublished work). TID1 has recently been shown to participate in chaperone activities relating to p53-mediated apoptosis as well as maintenance of mitochondrial membrane potential and mitochondrial DNA (mtDNA) integrity (Lu *et al.*, 2006, Ahn *et al.*, 2010, Trinh *et al.*, 2010, Ng *et al.*, 2014). Through a putative BH3 domain p53 directly activates Bax, inducing MOMP (see 1.3.1.1) (Chipuk *et al.*, 2004). TID1 is a member of the DnaJ family of chaperone proteins and exists as two splice variants, both of which are nuclear-encoded mitochondrial matrix proteins which have been reported to act as opposing modulators of apoptosis induced by exogenous stimuli. $hTID1_L$ was shown to increase apoptosis while $hTID1_S$ suppressed it; the pro-apoptotic activity of $hTID1_L$ deriving from a J-domain (Syken *et al.*, 1999). N^{pro} might antagonise p53-mediated apoptosis through this putative interaction as knockdown of TID1 conferred protection against hypoxic and genotoxic stresses (Ahn *et al.*, 2010, Trinh *et al.*, 2010). However, the implications of antagonising p53 during infection with an RNA virus or treatment with a dsRNA ligand such a poly(I:C) remain uncertain.

1.3.3.4. HAX-1

In addition to TID1, HS-1-associated protein X-1 (HAX-1) was also identified as a N^{pro} binding host protein by Y2H analysis (Johns *et al.*, 2010a). Expression of N^{pro} or infection with CSFV redistributed HAX-1 from the mitochondria to perinuclear regions corresponding to the ER. HAX-1 has been associated with promotion of cell survival through regulation of ER calcium ion

activity (Vafiadaki *et al.*, 2009). In addition, ER stress has been associated with HAX-1-dependent apoptosis (Abdelwahid *et al.*, 2016). HAX-1 has also been linked to p53-mediated mitochondrial apoptosis in glioblastoma cell lines (Deng *et al.*, 2017) and cell infected with HCV (Banerjee *et al.*, 2009). Therefore, the implications of N^{pro}'s interaction with HAX-1 and induction of apoptosis remain unclear.

1.4. Project aims

CSFV N^{pro} has been shown to antagonise the induction of dsRNA-mediated apoptosis using poly(I:C), a synthetic homolog of dsRNA (Ruggli *et al.*, 2005, Johns *et al.*, 2010a). As discussed in 1.3.3.1, there is data which suggests a mitochondrial pathway of apoptosis might be antagonised (Johns *et al.*, 2010a). However, these studies did not establish which pathways were responsible for the induction of dsRNA-mediated apoptosis and which interactions between CSFV N^{pro} and cellular proteins were required for this antagonism.

Recent studies have suggested that, upon activation of the same pathways responsible for type I IFN induction, IRF3 mediates a mitochondrial, Bax-dependent pathway of apoptosis independent of its functions as a transcription factor (Chattopadhyay *et al.*, 2010, Chattopadhyay *et al.*, 2011, Chattopadhyay *et al.*, 2016). These studies are interesting when considering the clear proteasome-dependent turnover of IRF3 by N^{pro} (Bauhofer *et al.*, 2007, Seago *et al.*, 2007).

Therefore, this project has two aims: (1) to elucidate the pathways through which dsRNA initiates apoptosis in porcine cell lines susceptible to CSFV and (2) to determine whether turnover of IRF3 by N^{pro} is required for the antagonism of apoptosis or whether alternate interactions are responsible.

1.4.1. Hypothesis

- Turnover of IRF3 by N^{pro} is not only responsible for antagonism of type I IFN but also induction of dsRNA-mediated apoptosis.
- dsRNA-mediated apoptosis in porcine cell lines is dependent on the mitochondria and functions of IRF3 independent of its role as a transcription factor.

1.4.2. Project significance

Apoptosis is an important innate mechanism by which cells counter viruses at local sites of infection, thus preventing wider spread and dissemination within the host (Jorgensen *et al.*, 2017). Indeed, Chattopadhyay *et al.* have demonstrated one means by which viral replication intermediate dsRNA and RNA viruses such as SeV, VSV and EMCV can initiate apoptosis (Chattopadhyay *et al.*, 2010, Chattopadhyay *et al.*, 2011, Chattopadhyay *et al.*, 2016). Viral antagonism of apoptosis is well documented: through confocal and structural studies, African swine fever virus A179L was shown to achieve this by directly binding tBid and Bax (Galindo *et al.*, 2008, Banjara *et al.*, 2017) while viral deletion mutants revealed vFLIP of γ-herpesviruses to inhibit caspase-8's interaction with the DISC (Glykofrydes *et al.*, 2000). This project will further elucidate the mechanism by which dsRNA can initiate apoptosis in porcine cell lines and the mechanisms by which CSFV N^{pro} subverts this innate process.

Persistent infection, immunotolerance and early dissemination of the virus at local sites of infection have been linked to the antagonism of type I IFN induction by CSFV N^{pro} (Tamura *et al.*, 2014). CSFV N^{pro} may further contribute to these phenomena by antagonising the induction of dsRNA-mediated apoptosis (Bensaude *et al.*, 2004, Johns *et al.*, 2010a). Elucidating the mechanism by which N^{pro} antagonises apoptosis may inform the design of future live attenuated vaccines and antivirals for control of outbreaks in typically CSFV-free countries.

2. Materials and methods

2.1. Mammalian cell culture

2.1.1. Cell lines

2.1.1.1. Available within the group

PK-15 (porcine kidney epithelial cells, CCl-33, LGC Promochem), SK6 (porcine kidney fibroblast cells), HEK 293T cells (human embryonic kidney epithelial cells) and HeLa cells (adult human cervical epithelial cells) were available within the group and used as stated. HEK 293T cells (human embryonic kidney cells derived from HEK 293 cells and expressing SV40 large T antigen) were transfected and used to produce 3rd-generation lentivirus as described in 2.12. PK-15 cells were used for the majority of experiments as they have an intact IFN response while SK6 cells, devoid of an IFN response, were used for experiments utilising N^{pro}-deleted CSFV (6.4.1). Also available within the group were three PK-15 cell lines, one expressing N^{pro} (PK-15 N^{pro} 31) and two expressing histidine-tagged N^{pro} (PK-15 His-N^{pro} 23, 61) (Seago *et al.*, 2010). In addition, two PK-15 (PK-15 GFP-11, PK-15 GFP-N^{pro}-4) and two SK6 cell lines (SK6 GFP-1, SK6 GFP-N^{pro}-28) expressing either GFP or GFP-N^{pro} were also available within the group. N^{pro} sequence for these cell lines was derived from CSFV-strain Alfort 187. These cell lines are confirmed to be free from pestivirus.

Henceforth, the N^{pro} protein of CSFV is referred to simply as "N^{pro}" except when referring to the N^{pro} protein of other pestiviruses (BVDV or BDV) or where clarity is beneficial to the point being made.

2.1.1.2. Generated for the project

EGFP and EGFP-N^{pro}-expressing PK-15 cell lines were generated as detailed in 2.12, 2.1.2.4 and 3.4. N^{pro} sequence for these cell lines was derived from CSFV strain Brescia, a highly-virulent

reference strain used extensively in past studies and literature. CRISPR-Cas9 knockout cell lines targeting IRF3, TLR3 and RIG-I were generated as detailed in 2.18.

2.1.2. Cell line propagation

2.1.2.1. Culture media conditions

Unless otherwise stated, all cells were cultured in HEPES-buffered high-glucose DMEM (Dulbecco's Modified Eagle Medium) (Gibco, #32430100) containing GlutaMAX™ (stabilised l-glutamine, in media), 5% (v/v) adult bovine serum (ABS, Selborne Biological Services; Tasmanian origin, tested for BVDV and gamma irradiated), penicillin (50 U/ml)/streptomycin (50 μg/mL) (Gibco, #15140-122); henceforth this is referred to as "complete media". Unless otherwise stated, all cell culture was performed using Greiner CELLSTAR flasks and plates. All incubation steps were performed at 37°C in the presence of 5% CO_2.

2.1.2.2. Passage of cell lines

To maintain continual growth of cell lines, they required passaging once the cell monolayer neared confluency. Media was removed from flasks and the cells washed with an appropriate volume of 1x PBSa (10 ml for a T-75 flask) before the addition of 0.05% trypsin-EDTA (4 ml for a T-75 flask; Gibco, #25300096). Flasks were incubated at 37°C until the majority of cells had rounded up. Flasks were then agitated and cells collected in a suspension after adding an appropriate volume of complete media to neutralise the trypsin-EDTA (5 ml for a T-75 flask). Cells were pelleted by centrifugation at 300 rcf and the supernatant discarded. Pellets were then resuspended in 1 ml of complete media and an appropriate aliquot applied to a new flask containing fresh media.

2.1.2.3. Generation of long-term mammalian cell line stocks

If not required for continued cell culture, individual pellets were instead resuspended in 1-5 ml of storage media comprised of 45% (v/v) ABS, 45% (v/v) complete media and 10% (v/v) DMSO

(Sigma, #276855). 1 ml aliquots were then prepared in sterile cryovials (Sarstedt, #72.377) and frozen at -80°C in Mr. Frosty™ freezing containers (Thermo Scientific, #5100-0001) for long-term storage.

2.1.2.4. Isolation of cell colonies

When generating clonal cell lines (following CRISPR-mediated gene knockout (2.18) or lentivirus transduction (2.12.2)), isolation of single cells was required. Once single cells had multiplied to form visible colonies following removal of selection (puromycin antibiotic), media was aspirated and cells washed with 1x PBS. Sterile 20 µl pipette tips were used to physically pick colonies of cells and resuspend them in 24-well plates containing 500 µl of complete media (10% (w/v) ABS) in each well. As each colony reached confluency they were trypsinised (2.1.2.2), pelleted by centrifugation at 1,000 rcf and stored at -80°C as detailed in 2.1.2.3.

2.2. Viruses

2.2.1. Sendai virus (SeV)

Sendai Virus (SeV), Cantell Strain (ATCC VR-907 Parainfluenza 1), used for induction of apoptosis in PK-15 and SK6 cells, was purchased from Charles River, Wilmington MA, USA (#10100772) at a titre of 2000 HA/ml unless otherwise stated.

2.2.2. CSFV

2.2.2.1. Virus strains

Multiple CSFV strains were available within the group. CSFV strain Alfort/187, referred to henceforth as “Alfort”, was originally obtained from the EU Reference Lab for CSFV (Hannover, Germany). CSFV strain Brescia was originally obtained from the Institute for Animal Science and Health (Lelystad, The Netherlands). Recombinant CSFV with the N^{pro} gene deleted (ΔN^{pro} rCSFV, infectious clone EP#96/2) and a parental recombinant virus (rCSFV, infectious clone

EP#98/2) are derived from CSFV strain Alfort Tübingen and were a kind gift from Prof Dr Gregor Meyers, Friedrich Loeffler Institute (Greifswald, Germany).

rCSFV and ΔN^{pro} rCSFV were grown in SK6 cells which do not induce type I IFN (Ruggli *et al.*, 2003). To infect cells for the purpose of generating frozen stocks, media was removed from 60-70% confluent T-175 cell culture flasks and replaced with 5 ml of serum-free media. 1 ml of the respective virus was applied to the flask and the cells incubated for 1 hour (hr), allowing time for virus attachment and uptake. Virus-containing media was then aspirated and replaced with 25 ml of complete media (5% (v/v) ABS). After a further 72 hr incubation, flasks were subjected to 3x freeze/thaw cycles (-80°C/21°C) to lyse the cells. 5 ml of media was then transferred to a new 60-70% confluent T-175 cell culture flask and the process repeated. Media was centrifuged for 10 minutes at 2,800 rcf/4°C to pellet cell debris after which supernatant containing virus was stored at -80°C in 1 ml aliquots. Sequential infections and freeze-thaw cycles were performed to maximise virus yield. Frozen stocks were recorded on Freezerworks, the institute system for documenting all SAPO3 and SAPO4 viruses.

2.2.2.2. Virus titration

Titration of CSFV stocks was carried out in SK6 cells with all incubation steps performed at 37°C/5% CO_2. Flat bottom 96-well plates were seeded with $1x10^4$ cells/well in complete media and incubated for 18 hr or until 90-100% confluency of the cell monolayer was reached. Media was removed from each well and replaced with 90 µl of serum-free media. 10 µl volumes of virus were applied to the first column of wells for a $1x10^{-1}$ dilution. Virus-containing media was then serially diluted across the remaining columns of wells ($1x10^{-1}$-$1x10^{-10}$) and the cells incubated for 2 hr. Media was removed and replaced with reduced-serum media (2.5% ABS) and the cells incubated for a further 72 hr. After removal of media, cells were transferred to R/T (21°C), washed three times in 1x PBS, fixed for 60 minutes in 4% (v/v) paraformaldehyde in 1x PBS (Santa Cruz Biotechnology, #sc-281692) at R/T, then washed three times in 1x PBS.

Plates were then transferred to 4°C until ready to stain. Henceforth, R/T corresponds to 21°C unless stated otherwise.

The method of staining plates of CSFV-infected cells with anti-E2 mAb largely follows that which is outlined in 2.14.3. Permeabilisation, block and wash steps were performed using 100 µl of the respective reagent per well (see 2.14.3). CSFV was detected using a mouse mAb recognising the E2 glycoprotein of CSFV (APHA, #WH303) and a secondary anti-mouse IgG1 monoclonal antibody (mAb) conjugated to Alexa Fluor 488 (Invitrogen, #A-21121). These antibodies were applied in 100 µl volumes of block solution to each well at concentrations of 1/100 and 1/500 respectively. Finally, 100 µl of 1x PBS was added to each well and then those which were positive for CSFV (wells containing cells showing green fluorescence) were manually scored using a Nikon Eclipse TE300 microscope with a GFP filter. Data was used to calculate the tissue culture infectious dose at which 50% of cells are infected ($TCID_{50}$) and plaque-forming units (pfu) per ml using a spreadsheet employing the Reed-Muench method (Reed and Muench, 1938). Classical plaque assays are not possible with CSFV as it is a non-cytopathic virus.

2.3. Mammalian plasmids

2.3.1. Purchased and externally-sourced

Table 2.1: Purchased and externally sourced plasmids for expression in mammalian cell culture.

Name	Description	Source
pdlMCSpuro-N^{pro}	2nd-gen lentiviral transfer plasmid, encodes CSFV N^{pro} Brescia	Prof. Steve Goodbourn
pLP1	3rd-gen lentiviral packaging plasmid, encodes *gag/pol* gene of HIV-1	Prof. Steve Goodbourn
pLP2	3rd-gen lentiviral packaging plasmid, encodes *rev* gene of HIV-1	Prof. Steve Goodbourn

pLP/VSV-G	3rd-gen lentiviral packaging plasmid, encodes retroviral vesicular stomatitis virus (VSV)-pseudotyped envelope	Prof. Steve Goodbourn
pLMJ1-EGFP	3rd-gen lentiviral transfer plasmid, encodes EGFP	David Sabatini (Addgene plasmid #19319) (Sancak *et al.*, 2008)
pC3-EGFP-hBax	Encodes N-terminal EGFP-tagged human Bax	Richard Youle (Addgene plasmid #19741) (Nechushtan *et al.*, 1999)
pGFP-Cytochrome C	Encodes N-terminal EGFP-tagged human cytochrome c	Douglas Green (Addgene plasmid #41181) (Goldstein *et al.*, 2000)
pCytochrome C-GFP	Encodes C-terminal EGFP-tagged murine cytochrome c	Douglas Green (Addgene plasmid #41182) (Goldstein *et al.*, 2000)
pcDNA3.1	Empty expression plasmid	Invitrogen (available within group)
pX461-poIRF3-g1	Encodes Cas9, GFP and a CRISPR gRNA targeting porcine IRF3	Prof. Steve Goodbourn
pX462-poIRF3-g2	Encodes Cas9, puromycin resistance and a CRISPR gRNA targeting porcine IRF3	Prof. Steve Goodbourn
pX461-poRIG-I-g1	Encodes Cas9, GFP and a CRISPR gRNA targeting porcine RIG-I	Prof. Steve Goodbourn
pX462-poRIG-I-g2	Encodes Cas9, puromycin resistance and a CRISPR gRNA targeting porcine RIG-I	Prof. Steve Goodbourn
pX461-poTLR3-g1	Encodes Cas9, GFP and a CRISPR gRNA targeting porcine TLR3	Prof. Steve Goodbourn
pX462-poTLR3-g2	Encodes Cas9, puromycin resistance and a CRISPR gRNA targeting porcine TLR3	Prof. Steve Goodbourn

2.3.2. Constructed in-house

Table 2.2: Plasmids for expression in mammalian cell culture constructed in-house.

Name	Description
pLMJ1-EGFP-N^{pro}	3rd-gen lentiviral transfer plasmid, encodes EGFP-N^{pro} (CSFV origin)
pC3-EGFP	Expression plasmid, encodes EGFP, prepared from pC3-EGFP-hBax
pcDNA3.1-EGFP-poIRF3-WT	pcDNA3.1 expression plasmid, encodes EGFP-tagged wild-type porcine IRF3 (NP_998935.1)
pcDNA3.1-EGFP-poIRF3-S1	pcDNA3.1 expression plasmid, encodes EGFP-tagged S1 mutant porcine IRF3 (NP_998935.1; S396A and S398A)
pLJM1-FLAG-poIRF3-WT	3rd-gen lentiviral transfer plasmid, encodes N-terminus FLAG-tagged porcine IRF3 (NP_998935.1)
pLJM1-FLAG-poIRF3-S1	3rd-gen lentiviral transfer plasmid, encodes N-terminus FLAG-tagged S1 mutant porcine IRF3 (NP_998935.1; S396A and S398A)

2.4. Plasmid amplification in *Escherichia coli* (*E. coli*)

2.4.1. Transformation of commercial chemically-competent cells

One Shot® TOP10 (ThermoFisher Scientific, #C404006) and NEB® 10-beta (NEB, #C3019H) chemically-competent *E. coli* were transformed, incubated and grown as instructed in the protocols provided by each manufacturer (https://assets.thermofisher.com/TFS-Assets/LSG/manuals/oneshottop10_man.pdf and https://international.neb.com/protocols/0001/01/01/high-efficiency-transformation-protocol-c3019 respectively).

2.4.2. Transformation of chemically-competent cells prepared in-house

On ice, plasmid (typically 50-300 ng) was added to a 50 µl aliquot of *E. coli* JM109 cells which had been produced as described in 2.11. The aliquot was then incubated on ice for 10 minutes (min), heat shocked at 42°C for 45 seconds (sec) and then incubated again on ice for a further 2 min. 250 µl of pre-heated 37°C Super Optimal Broth (S.O.C.; Invitrogen, #15544034) was then added. The cells were incubated at 37°C for 1 hr on an orbital shaker at 200 rpm. Following this, 50-200 µl aliquots were plated onto Lysogeny Broth (LB) agar (in-house) containing ampicillin (100 µg/ml) or kanamycin (50 µg/ml). Plates were incubated for 16-18 hr at 37°C and checked for colonies in the morning, enabling the selection and further amplification of positively transformed bacterial clones.

2.4.3. Generation of stably transformed bacterial stocks

5 ml LB media (in-house) was inoculated with single colonies of *E. coli* (One Shot® TOP10 or JM109) that had previously been confirmed by whole-colony PCR (2.8.2) and/or Sanger sequencing (2.8.3) to contain the desired plasmid. Following an 18 hr incubation on an orbital shaker at 37°C/200 rpm, 1 ml aliquots were taken and used to inoculate 5x 4 ml volumes LB (in-house). After 5 hrs of culture on an orbital shaker at 37°C/200 rpm, 1 ml of glycerol (VWR

International, #24388.26) was added to each culture for a final concentration of 20% (v/v). Cultures were aliquoted into 1 ml volumes and frozen at -80°C. When required, aliquots were thawed at R/T and 10-100 µl of culture added to 5 ml LB media (in-house). Purification of plasmid DNA was performed as detailed in 2.5. All LB used in this procedure was supplemented with ampicillin or kanamycin at final concentrations of 100 µg/ml and 50 µg/ml respectively.

2.5. Purification of plasmid DNA

2.5.1. Miniprep

All plasmid minipreps were performed using overnight (16-18 hr) bacterial cultures (typically 5 ml) and the QIAprep® Spin Miniprep kit (Qiagen, #27104). The manufacturer's instructions were followed (https://www.qiagen.com/gb/resources/resourcedetail?id=ebb38a38-c61c-40a7-910d-9b10d1148022&lang=en), and the recommended additional wash step was carried out. Plasmid DNA was typically eluted in 50 µl volumes of dH_2O.

2.5.2. Quantification

All amplified and purified plasmid DNA was quantified using a NanoDrop® UV spectrophotometer (Thermo Scientific, #ND-1000). The spectrophotometer was blanked using 1 µl of the molecular grade dH_2O (Sigma, #W4502). The sample mount was then wiped clean and 1 µl of plasmid DNA sample subsequently loaded. Final plasmid DNA concentration at an optical density of 260 nm (OD_{260}) was calculated and provided by the accompanying software. Triplicate readings were taken to allow the calculation of average concentration in ng/µl.

2.6. Plasmid manipulation

2.6.1. Restriction digests

Purified plasmid DNA was subject to restriction digestion for both analytical and cloning purposes. All digests were performed using restriction enzyme (RE) sourced from Promega.

Single or double digests were assembled on ice and subsequently incubated over a 2 hr period at 37°C (table 2.3). Digest products were separated on agarose gels containing ethidium bromide (200 ng/ml) as detailed in 2.10 and DNA bands were visualised under ultraviolet light (UV). If required, they were extracted and purified (see 2.10).

Table 2.3: Reagents used for single and double restriction enzyme digests.

Component	Volume for single digest (1 RE, µl)	Volume for double digest (2 REs, µl)
10x buffer (varies)	2	3
10x BSA	2	3
Plasmid DNA	1-4 µg (volume varies)	1-4 µg (volume varies)
RE (varies)	1 unit (1 µl)	2 units (1:1, 2 µl)
dH_2O	X µl to make a total volume of 20	X µl to make a total volume of 30

Note: Bovine serum albumin (BSA) was sourced from Promega (#R3961) and was supplied with each RE.

If performing double digests with REs requiring incompatible buffers (for example, *Hin*dIII/ *Eco*RI or *Not*I/*Bam*HI), sequential digests were performed. DNA from the initial first digest was purified using the DNA Clean & Concentrator-5 kit (Zymo Research, #D4013), following the protocol provided by the manufacturer. Purified DNA was then eluted in 5-10 µl of dH_2O, digested and subjected to a second digest with an alternate RE and its respective buffer.

2.6.2. Ligation

To insert DNA into RE-digested plasmids, ligation was performed. On ice, ligation reactions using T4 DNA ligase (NEB, #M0202) and the supplied buffer were assembled as detailed in table 2.4.

Table 2.4: Reagents used for the ligation of DNA into RE-digested plasmids.

Component	Volume for a single ligation (µl)
10x T4 DNA ligase buffer	2
Vector DNA	50 ng (volume varies)
Insert DNA	(quantity and volume vary)
T4 DNA ligase	1
dH_2O	X µl to make a total volume of 20

Typically, insert DNA was ligated into 50 ng of vector at a ratio of 3:1. To calculate the quantity of insert DNA required (in ng), the following formula was employed:

$$\frac{vector\ (ng)\ \times size\ of\ insert\ (kb)}{size\ of\ vector\ (kb)} \times insert{:}\ vector\ ratio = insert\ (ng)$$

Upon assembly, ligation reactions were gently mixed and incubated for 16-18 hrs at R/T. Chemically competent *E. coli* were then transformed with the resulting ligation products (see 2.4.1 and 2.4.2).

2.7. Transfection of mammalian cell lines with plasmid

2.7.1. Transfection of single plasmids

Unless otherwise stated, $5x10^4$ mammalian cells were seeded onto coverslips or into empty wells of a 24-well plate containing complete media. Cells were then incubated for 18-24 hr until the cell monolayer was 60-80% confluent. Cells were transfected with plasmids using FuGENE® 6 Transfection Reagent (Promega, #E2691) following the manufacturer's protocol (https://www.promega.com/-/media/files/resources/protocols/technical-manuals/101/fugene-6-transfection-reagent-protocol.pdf). Briefly, FuGENE® 6 was added to serum-free media in a sterile 1.5 ml tube. After 5 min incubation at R/T, plasmid was added (typically, 500 ng of plasmid was transfected per well of a 24-well plate) and the tube incubated for a further 30 min at R/T. Media was removed from cells and the FuGENE® 6-plasmid mix applied in a drop-wise manner. Following 4 hr of incubation at 37°C, complete media was applied to the transfected cells (up to 500 µl in a 24-well plate) and incubated for a further 24-48 hr at 37°C to allow time for sufficient protein expression.

2.7.2. Co-transfection of multiple plasmids

To produce 3rd-generation lentivirus and generate CRISPR-Cas9 knockout cell lines, co-transfection of two or more plasmids was required. Information regarding co-transfection can be found in 2.12.1 and 2.18.2.

2.8. Polymerase chain reaction (PCR)

2.8.1. PCR amplification of purified DNA

PCR reaction mixes were prepared on ice. A typical 50 µl mix comprised of 20 µl dH_2O, 25 µl of Q5® High-Fidelity 2X Master Mix (NEB, #M0492S), 1 µl of DNA template (100-250 ng of genomic DNA or 10-50 ng of plasmid DNA) and 4 µl of primers (see 2.20, table 2.12) to give a final concentration of 0.4 µM. PCR reactions were performed using a T100™ Thermal Cycler (Bio-Rad) and the parameters detailed in table 2.5. As per the manufacturer's guidelines, extension times for reactions prepared with Q5® polymerase assumed an amplification rate of 30 seconds/1 kb of sequence.

Table 2.5: Program used to amplify sequence by PCR.

Stage	Procedure	Temperature	Number of cycles
1	Initial denature	95°C, 4 min	1
2	Denature	95°C, 20 sec	30-34
3	Anneal primers	56°C, 20 sec	
4	Extension	72°C, 30 sec	
5	Final extension	72°C, 4 min	1
6		4°C, hold	1

2.8.2. PCR amplification from bacterial colonies

Per colony, each reaction mix was made up to 25 µl using the recipe described in 2.8.1 however ReadyMix™ Taq PCR Reaction Mix (Sigma, #P4600-100RXN) was used instead of Q5® High-Fidelity 2X Master Mix. A small quantity of each colony to be screened was then transferred to and resuspended in the reaction mix using a sterile pipette tip. PCR reactions were run using the program detailed in 2.8.1. As per the manufacturer's guidelines, extension

times for reactions prepared with Taq polymerase assumed an amplification rate of 1 min/1 kb of sequence.

2.8.3. Sanger sequencing

Sequencing of plasmid DNA was carried out by a fluorescent dideoxy chain termination method using the BigDye® Terminator v3.1 Cycle Sequencing Kit (ThermoFisher Scientific, #4337454). Initially, 50-250 ng of PCR product or 250-500 ng of plasmid DNA was prepared in 6.5 µl of molecular-grade DNase and RNase-free dH_2O (Sigma, #W4502-1L) and denatured at 95°C for 2 minutes on a thermocycler before being placed on ice. Additionally, the sequencing mix was prepared on ice – this comprised of 2 µl 5x sequencing buffer (kit), 0.5 µl of big-dye terminator mix (kit) and 1 µl of primer (3.4 pM) (see 2.20, table 2.12). The sequencing mix was then added to the denatured plasmid DNA mix and briefly vortexed before the sequencing reaction was carried out using the program detailed in table 2.6.

Table 2.6: Big-Dye Terminator program used to amplify sequence.

Stage	Temperature	Number of cycles
1	96°C, 2 min	1
2	96°C, 10 sec	25
3	50°C, 10 sec	
4	60°C, 4 min	
5	4°C, hold	1

5 µl of 100 mM EDTA was added to stop the reaction. 100 µl of 100% (v/v) ethanol (EtOH) was then added and tubes centrifuged at 12,000 rcf for 20 min to pellet the DNA precipitate. Supernatant was carefully removed and the resulting pellet washed with 100 µl of 70% (v/v) EtOH and then centrifuged at 12,000 rcf for a further 5 min. Supernatant was removed and the pellet left to dry in a dark microbiological safety cabinet (MBSC) and stored at -20°C until ready for sequencing. The DNA pellet was then resuspended in 20 µl of Hi-Di formamide (Applied Biosystems, #4311320) and Sanger-sequenced on an ABI 3730 DNA Analyser (Applied Biosystems, #3730S) by the Pirbright Institute's in-house sequencing department. Sequence

identity was confirmed using either NCBI's Basic Local Alignment Search Tool (BLAST) (Altschul *et al.*, 1990) or Chromas Lite v2.0.1 (Technelysium Pty Ltd).

2.9. Annealing of oligos for ligation

When a premature termination of a plasmid open reading frame (ORF) was required, oligos bearing tandem repeats of stop codons in alternate reading frames were designed:

```
Top oligo:          5' TGAATCGTAGATACTGA 3'
Bottom oligo:       3' ACTTAGCATCTATGACT 5'
```

Sequence corresponding to the overhangs generated by restriction enzyme digest at the chosen sites of insertion in the destination plasmid (in this case, *Hin*dIII and *Eco*RI) were added to the 5' and 3' termini of each oligo.

```
Top oligo:    5' agcttTGAATCGTAGATACTGAg     3'
Bottom oligo: 3'     aACTTAGCATCTATGACTcttaa 5'
```

Following synthesis, oligos were resuspended in dH_2O to give a concentration of 100 µM and diluted further in dH_2O for a final concentration of 20 µM. 5 µl of each were then mixed with 40 µl of dH_2O. The oligo mix was then incubated at 95°C for 4 minutes in a thermocycler then 70°C for 15 minutes on a heater block. The heater block was then removed from the heating unit and the oligo mix allowed to slowly cool to R/T (~45 min). 1 µl of the annealed oligos were then ligated into the desired destination plasmid (2.6.2).

2.10. DNA gel electrophoresis

6x loading dye (Thermo Scientific, #R1161) was added to aliquots of DNA typically to give a total volume of 24 µl. These samples were then run at 95 V on a Tris/Borate/EDTA (TBE) agarose gel (1% (w/v)) containing ethidium bromide (200 ng/ml; Invitrogen, #15585-011) at R/T in a Mini-Sub® Cell GT tank (BioRad, #329BR019508) before visualisation using a BioRad gel-dock. To determine the estimated size of visualised DNA, 1 kb (NEB, #N0468S) and 100 bp

(NEB, #N0467S) DNA ladders were ran alongside samples on each gel. If required, bands were excised and subjected to further downstream purification using an Illustra GFX PCR DNA and Gel Band Purification Kit (GE Healthcare, #28-9034-70).

2.11. Generation of rubidium-competent *E. coli*

2.11.1. Solutions

Solutions TFB1 and TFB2 were prepared in a fume hood and made up to total volumes of 200 ml and 20 ml respectively.

2.11.1.1. TFB1

- 30 mM potassium acetate
- 100 mM rubidium chloride
- 50 mM calcium chloride
- 15% glycerol (v/v)

2.11.1.2. TFB2

- 10 mM MOPS
- 10 mM rubidium chloride
- 75 mM calcium chloride
- 50 mM manganese chloride
- 15% glycerol (v/v)

2.11.2. Procedure

A -80°C stock of *E. coli* (JM109; *e14*$^{-}$ (McrA^{-}) *recA1 endA1 gyrA96 thi-1 hsdR17* (r_K^- m_K^+) *supE44 relA1 Δ*(*lac-proAB*) [F′ *traD36 proAB lacI*^{q}*ZΔM15*]) was thawed at R/T and a small aliquot streaked onto an agar plate free from antibiotic. Following incubation overnight at 37°C a single colony was picked and added to 20 ml LB; the culture was incubated for 18 hr at 37°C with shaking (200 rpm). 4 ml of the culture was then added to 400 ml of LB and incubated at 37°C with shaking (200 rpm) until the culture had reached an optical density of 550 (OD_{550}).

The 400 ml culture was then transferred to eight 50 ml centrifuge tubes and centrifuged for 5 min at 4°C, 1,000 rcf. The supernatants were discarded, and the pellets were resuspended in

10 ml of cold (4°C) TFB1 and incubated for 5 min at R/T. After incubation, the resuspended pellets were centrifuged for 5 min at 4°C, 1,000 rcf. The supernatants were discarded, and the pellets were each resuspended in 1 ml TFB2; the resuspended cell pellets were then incubated for 15 min on ice, after which 0.5 ml aliquots were prepared with 20% (v/v) glycerol (VWR International, #24388.26) and frozen at -80°C.

2.12. Production of 3rd-generation lentivirus

2.12.1. Production procedure

HEK 293T cells were used for the production of 3rd-generation lentivirus which, upon infection of cell culture, would result in permanent expression of EGFP and EGFP-N^{pro} fusion protein. To do so, cells were transfected with plasmids using TransIT-LT1 Transfection Reagent (Mirus, #MIR2300) following the manufacturer's protocol (https://www.mirusbio.com/assets/protocols/ml001_transit_lt1_transfection_reagent.pdf).

For the generation of lentivirus using a single T-75 culture flask, 200 µl of media (serum and antibiotic-free) was added to two 1.5 ml microcentrifuge tubes. 25 µg of plasmid (2:1:1:1 of pLJM1:pLP1:pLP2:pLP/VSV-G) was then added to one tube and 50 µl of Transit-LTI transfection reagent (MirusBio, #MIR2304) to the other (table 2.7) for a 2:1 ratio of transfection reagent:plasmid. Both tubes were incubated for 5 minutes at R/T after which the plasmid

mixture was gently added to the transfection reagent solution to generate a transfection complex. The complex was briefly vortexed and incubated at R/T for a further 30 minutes, after which additional serum and antibiotic-free media was added to a final volume of 5 ml. Media was removed from HEK 293T cells (at 60-90% confluency) and gently replaced with the 5 ml of transfection complex. After a 4 hr incubation at 37°C, complete media was applied to a final volume of 20 ml. Cells were incubated at 37°C for 72 hr to allow time for lentivirus to be produced and released into the cell culture media.

At 72 hr post-transfection, media was removed using a volumetric pipette and centrifuged at 3,622 rcf for 5 min to pellet any cell debris. Media containing lentivirus was then prepared as 1 ml aliquots which were frozen at -80^{o}C until required.

Table 2.7: Plasmids used for the generation of 3rd-generation lentivirus.

Plasmid	Quantity per transfection (µg)
pLMJ1 (EGFP, EGFP-N^{pro}, FLAG-poIRF3-WT or FLAG-poIRF3-S1)	10
pLP1	5
pLP2	5
pLP/VSV-G	5

2.12.2. Infection of porcine cells with lentivirus

Infections were normally performed in 24-well plates and with cells that were between 30-50% confluent. Prior to infection, media was aspirated and replaced with 500 µl of fresh DMEM (2% (v/v) ABS) containing polybrene at 2 ng/µl. Different volumes (10-200 µl) of virus (untitred) were then applied to the relevant wells and the plates centrifuged at 1,000 rcf for 30 min at R/T. This procedure is referred to as “spinoculation” (O'Doherty *et al.*, 2000).

On the morning following infection, all media in virus and polybrene-containing wells was removed and replaced with 1 ml of fresh DMEM containing 10% (v/v) ABS. Cells were left to grow either for a total of 72 hr or until they had reached 100% confluency, after which they were then either fixed and mounted for visualisation by confocal microscopy (2.13.1) or lysed for Western blot analysis (2.10). For infections carried out on cells in 24-well plates, typically 100 µl of Laemmli lysis buffer was applied to the relevant wells. Collected lysates were then heated at 95°C for 5 min after which they are frozen at -20˚C until required for Western blotting.

For the generation of cell lines stably expressing lentivirus-encoded transgenes, infected cells were incubated with puromycin (3 µg/ml) until large colonies were visible (~1 week) at which point they were isolated, propagated and stored as detailed in 2.1.2.4 and 2.1.2.3.

2.13. Protein analysis

2.13.1. Solutions

2.13.1.1. Laemmli lysis buffer (4x)

- 4% (v/v) SDS
- 10% (v/v) β-mercaptoethanol
- 20% (v/v) glycerol
- 0.004% (w/v) bromophenol blue
- 125 mM Tris HCL (pH 6.8)

The above reagents were prepared in distilled water (dH_2O) to give a 4x stock buffer. 2x buffer was prepared by diluting 50% (v/v) in dH_2O.

2.13.1.2. SDS-PAGE running buffer (10x)

- 250 mM Tris
- 1.92 M Glycine
- 0.1% (w/v) SDS

Diluted 10% (v/v) in distilled dH_2O to give a 1x buffer.

2.13.1.3. Western blot transfer buffer (10x)

- 250 mM Tris
- 1.92 M Glycine

Diluted 10x in dH_2O containing 20% isopropyl alcohol (v/v) to give a 1x buffer.

2.13.1.4. Western blot blocking buffer (1x)

- 5% (w/v) Marvel milk powder
- 0.1% (v/v) Tween-20
- 1x PBS (in-house)

2.13.1.5. Western blot wash buffer (1x)

- 0.1% (v/v) Tween-20
- 1x PBS (in house)

2.13.2. Antibodies

Antibodies for Western blotting were either produced in-house or purchased from Promega, Cell Signalling Technology, Abcam and Santa Cruz Biotechnology and used as detailed in table 2.8.

Table 2.8: Primary and secondary antibody concentrations and conditions of use for the detection of proteins by Western blot analysis.

Protein	Primary antibody	Secondary antibody
CSFV N^{pro}	Rabbit polyclonal anti-N^{pro} DS14 (in-house, ^{11}KTNKQKPMGVEEPVYDATGKPL FGDPS^{37}), 1/3,000 O/N 4°C	Goat polyclonal anti-rabbit IgG (H+L) HRP #W401B (Promega, W4011), 1/5,000 1 hr R/T
CSFV E2	Mouse monoclonal IgG1 anti-E2 WH303 (APHA Scientific, #RAE0826), 1/500 O/N 4°C	Goat polyclonal anti-mouse IgG (H+L) HRP #W402B (Promega, W4021), 1/5,000 1 hr R/T
GFP/EGFP	Rabbit polyclonal anti-GFP (Abcam, #ab290), 1/3,000 O/N 4°C	Goat polyclonal anti-rabbit IgG (H+L) HRP #W401B (Promega, W4011), 1/5,000 1 hr R/T
Cleaved caspase-3	Rabbit monoclonal anti-cleaved caspase-3 Asp175 5A1E (Cell Signalling Technology, #9661), 1/1,000 O/N 4°C	Goat polyclonal anti-rabbit IgG (H+L) HRP #W401B (Promega, W4011), 1/5,000 1 hr R/T
Gamma-tubulin	Mouse monoclonal IgG1 anti-gamma-tubulin GTU-88 (Sigma, #T6557), 1/5,000 1 hr R/T	Goat polyclonal anti-mouse IgG (H+L) HRP #W402B (Promega, W4021), 1/5,000 1 hr R/T
Mx1	Mouse monoclonal IgG1 anti-Mx1 AM39 (Abcam, #ab79609), 1/4,000 O/N 4°C	Goat polyclonal anti-mouse IgG (H+L) HRP #W402B (Promega, W4021), 1/5,000 1 hr R/T
ISG15	Rabbit polyclonal anti-ISG15 H-150 (Santa Cruz Biotechnology, #sc-50366), 1/10,000 O/N 4°C	Goat polyclonal anti-rabbit IgG (H+L) HRP #W401B (Promega, W4011), 1/5,000 1 hr R/T
IRF3	Rabbit polyclonal anti-IRF3 FL-425 (Santa Cruz Biotechnology, #sc-9082), 1/2,000	Goat polyclonal anti-rabbit IgG (H+L) HRP #W401B (Promega, W4011), 1/5,000 1 hr R/T
RIG-I	Mouse monoclonal IgG1 anti-RIG-I D-12 (Santa Cruz Biotechnology, #sc-376845), 1/4,000 O/N 4°C	Goat polyclonal anti-mouse IgG (H+L) HRP #W402B (Promega, W4021), 1/5,000 1 hr R/T
Bax	Rabbit polyclonal anti-Bax (Cell Signalling Technology, #2772), 1/1,000 O/N 4°C	Goat polyclonal anti-rabbit IgG (H+L) HRP #W401B (Promega, W4011), 1/5,000 1 hr R/T

FLAG	Rabbit polyclonal anti-FLAG, DYKDDDDK (Acris, #R1180), 1/2,000 O/N 4^{o}C	Goat polyclonal anti-rabbit IgG (H+L) HRP #W401B (Promega, W4011), 1/5,000 1 hr R/T

Note: Primary and secondary antibodies were applied in 5% milk solution (0.1% Tween-20) and applied to membranes which were incubated either overnight (O/N) at 4°C or for 1 hr at room temperature (R/T) on an orbital shaker.

2.13.3. Sample collection

2x Laemmli lysis buffer (prepared in-house, see 2.13.1.1) was utilised for the collection of all whole cell protein lysate samples comprised of all cellular compartments. Upon addition of buffer to the desired cells, samples were incubated for 5 min at 95°C and frozen at -20°C for storage until ready for analysis by SDS-PAGE and Western blot.

2.13.4. SDS-PAGE

An XCell SureLock™ Mini-Cell Electrophoresis System (Invitrogen, #EI0001) was used for the running of all SDS-PAGE gels. Pre-cast Novex™ 4-20% Tris-Glycine Mini Gels (Invitrogen, #XP04200BOX) were loaded into the system which was then filled with 1x SDS-PAGE running buffer. Assembly of the system was as indicated by the manufacturer. Samples were thawed and incubated for 5 min at 95°C, after which they were loaded into separate wells of a gel in 10-50 µl volumes. 4 µl of full range protein marker (Sigma, #RPN800E) was loaded alongside samples on each gel. Gels were ran at 150-225 V, R/T for approximately 60-90 min or until the dye front had disappeared.

2.13.5. Western blot

A Mini Trans-Blot® Cell system (BioRad, #1703930) was used for the running of all Western blot transfers. The system was assembled and operated as indicated by the manufacturer. Transfers were ran at 200 mA for 70 min. Following transfer, the membrane was removed and placed in Western blot blocking buffer on an orbital shaker for 1 hr at R/T. Fresh blocking buffer, containing primary antibody at the relevant dilution (see 2.13.2, table 2.8), was then

applied and the blot incubated for either 1 hr at R/T or overnight at 4°C with shaking. Following incubation, antibody-containing blocking buffer was aspirated and the membrane washed three times, each time for 15 min at R/T in fresh blocking solution with shaking. Next, secondary antibody (see 2.13.2, table 2.8) diluted in blocking buffer was applied and the blot was incubated for a further 1 hr at R/T with shaking. Membranes were then washed three times with Western blot wash buffer over 45 min and then briefly with 1x PBS (prepared in-house).

Membranes were blotted dry on plain paper and 2 ml of pre-mixed Immobilon™ Western chemiluminescent substrate (Millipore, #WBKLS0500) applied for 1 min. Horseradish peroxidase (HRP) luminescence was detected by exposure onto Medical X-ray blue film (Carestream, #771 1468) in a dark room.

2.14. Confocal microscopy

2.14.1. Mitochondrial labelling

Prior to fixation, single 50 µg vials of MitoTracker™ (MTT) Red CMXRos (Invitrogen, #M7152) or Deep Red FM (Invitrogen, #M22426) were solubilised in DMSO to a 1 mM stock solution. Working solutions of MTT were prepared in complete media pre-heated to 37°C and applied to cells prior to fixation. Cells were incubated at 37°C with 150 nM MTT Red CMXRos for 30 min and with 250 nM MTT Deep Red FM for 45 min.

2.14.2. Coverslip preparation

Growth media was aspirated from the cover slips, after which they were washed twice with 1x PBSa. 4% (v/v) paraformaldehyde in 1x PBS (Santa Cruz Biotechnology, sc-281692) was then applied for 30 min at R/T to fix the cells. Two additional washes with 1x PBSa were subsequently carried out. For nuclear labelling, 1 µg/ml of DAPI was prepared in dH_2O and applied for 15 min at R/T, after which the cover slips were washed twice more in 1x PBSa and

mounted onto glass slides for visualisation using Vectashield (Vector Laboratories, #H-1000) as mounting media and nail varnish to seal them.

2.14.3. Immunofluorescence

Cells prepared on coverslips were fixed according to 2.14.2 and stored overnight at 4°C. They were then washed twice with 1x PBSa and treated with 150 µl of 0.2% (v/v) Triton X-100 (Sigma, #T8787) for 5 min to permeabilise them. After three additional washes in 1x PBSa, coverslips were blocked for 30 min in 10% (v/v) sheep serum (Sigma, #S3772-10ML) or goat serum (Sigma, #G9023-10ML) prepared in 1x PBSa. Primary antibody was then applied at the relevant concentrations stated in table 2.9 and incubated for 30 minutes. Coverslips were subsequently washed five times in 5% (v/v) serum in 1x PBSa, each time for 5 min. The relevant secondary antibody was then applied for 30 min as stated in table 2.9. Coverslips were then treated with 1 µg/ml of DAPI prepared in dH_2O and mounted as described in 2.14.2. All wash steps and incubations with antibody were performed at R/T on a plate shaker (300 rpm).

Table 2.9: Primary and secondary antibody concentrations and conditions of use for the detection of proteins by immunofluorescence/confocal microscopy.

Protein	Primary antibody	Secondary antibody
Cytochrome c	Mouse monoclonal IgG1 anti-cytochrome c 6H2.B4 (BD Biosciences, #556432; rat protein), 1/500	Goat polyclonal anti-mouse IgG1 Alexa Fluor® 488 $^{490}/_{525}$ (Invitrogen, #A-21121), 1/500
Bax	Rabbit polyclonal anti-Bax (Cell Signalling Technology, #2772), 1/200	Goat polyclonal anti-rabbit IgG (H+L) Alexa Fluor® 488 $^{490}/_{525}$ (Invitrogen, #A-11008), 1/500 Goat polyclonal anti-rabbit IgG (H+L) Alexa Fluor® 568 $^{578}/_{603}$ (Invitrogen, #A-11011), 1/500
CSFV E2	Mouse monoclonal IgG1 anti-E2 WH303 (APHA Scientific, #RAE0826), 1/100	Goat polyclonal anti-mouse IgG1 Alexa Fluor® 647 $^{650}/_{665}$ (Invitrogen, #A-21235), 1/500

Note: All antibodies were applied in 5% (v/v) sheep or goat serum (prepared in 1x PBSa) and incubated with coverslips on an orbital shaker (300 rpm) for 30 at R/T. Alexa Fluor dye excitation (nm) / emission (nm) are indicated.

2.14.4. Imaging of prepared slides

Prepared slides of cells were imaged on a Leica TCS SP2 Acousto-Optical Beam Splitter confocal scanning laser microscope at wavelengths appropriate for each Alexa Fluor probe.

2.14.5. Quantification of protein relocalisation

Where specified, protein relocalisation was quantified. Images were initially imported into ImageJ (Schneider *et al.*, 2012) in .tif format and converted to greyscale. Then, the "analyse particles" function was used to automatically determine the total number of nuclei per field of view. For Bax studies, cells demonstrating condensed mitochondrial relocalisation were manually counted and divided by the nuclei count given by ImageJ to give the percent of positive cells; this was repeated for five fields of view for each treatment (n=5). 2-way ANOVA (Graphpad Prism) was used to determine mean, standard deviation (SD) and confidence intervals (CI) for n=5.

2.15. Induction of innate responses in cell lines

2.15.1. Induction of apoptosis with poly(I:C) or SeV

Cells were seeded in either 6, 12 or 24-well plates and grown to a confluency of 70-90%. Cells to be induced were treated with 1-100 µg/ml of poly(I:C) (Sigma, #P1530-25MG) or 2-200 HA/ml SeV (Charles River Laboratories, #10100772) by addition to growth media and incubated for 18-24 hr. In order to collect adherent cells as well as cells in suspension (due to apoptosis), adherent cells were detached by agitation with the blunt end of a pipette tip. Cell suspensions were transferred to 1.5 ml microcentrifuge tubes and centrifuged at 1,000 rcf for 5 min to pellet. Supernatant was removed, and pellets washed once in 100 µl 1x PBS. Following removal of the supernatant, pellets were lysed in 100-200 µl of Laemmli lysis buffer (2.13.1.1) and heated at 95°C for 5 min to denature harvested protein. Cell lysates were frozen at -20°C until ready for Western blot analysis.

2.15.2. Induction of ISG expression with type I IFN

Recombinant porcine IFN-α (RD Systems, #17105-1) was added to media to final concentrations of 10-1,000 IU/ml and incubated with porcine (PK-15, SK6) and human (HEK 293T) cells for 18-24 hr. These conditions were chosen so as to enable sufficient detection of ISGs by Western blot. Following incubation, media was removed and cells washed with an appropriate volume of 1x PBS (500 µl for a 12-well plate). Cells were then lysed directly in 100-200 µl of Laemmli lysis buffer (2.13.1.1) and prepared as in 2.15.1.

2.16. Pharmacological inhibition of cellular processes

The pan caspase inhibiter Z-VAD(OMe)-FMK (Bachem, #N-1560) was prepared as a 20 mM stock solution in DMSO (Sigma, #276855) and applied to cells at a final concentration of 100 µM immediately prior to treatment with either poly(I:C) or SeV (see 2.15.1) where specified. The Janus-kinase (JAK) 1/2 inhibitor Ruxolitinib (RXT; Selleckchem, #INCB018424) was prepared as a 5 mM stock solution in DMSO and applied to cells at a final concentration of 0.5 µM in the same manner as Z-VAD(OMe)-FMK. The proteasome inhibitor MG132 (Sigma, #74790) was prepared as a 10 mg/ml stock solution in DMSO and applied to cells at a final concentration of 25 µM; treated cells were incubated for 18 hr.

2.17. Genomic DNA extraction

All DNA extractions were performed using a DNeasy Blood & Tissue Kit (Qiagen, #69504). Briefly, 1 x 10^5 cells were pelleted at 1,000 rcf for 5 min in a 1.5 ml microcentrifuge tube. Supernatant was removed and the pellets washed in 100 µl of 1x PBS. Pellets were centrifuged again and, following removal of the supernatant, frozen at -20°C until ready for DNA extraction. DNA extraction was then performed as detailed in the "spin column protocol" supplied with the kit (https://www.qiagen.com/gb/resources/resourcedetail?id=6b09dfb8-6319-464d-996c-79e8c7045a50&lang=en) and eluted using the supplied elution buffer.

2.18. CRISPR-Cas9 gene knockout in PK-15 cells

2.18.1. Guide RNA slection (gRNA)

The plasmids detailed in table 2.10 were gifts from Professor Steve Goodbourn, St. George's University of London. To be used in conjugation with a Cas9 nickase mutant, pairs of guide RNAs (gRNAs) with defined offsets from each other were selected using Zhang Lab's "double-nickase" design tool (https://zlab.bio/) which is no longer available. The German Cancer Research Centre (http://www.e-crisp.org/E-CRISP/designcrispr.html) and the Broad Institute (https://portals.broadinstitute.org/gpp/public/analysis-tools/sgrna-design) offer equivalent alternatives.

Table 2.10: Guide RNAs (gRNAs) cloned into pX461 and pX462 CRISPR-Cas9 nickase plasmids.

Knock-out target	gRNA-1 (pX461)	gRNA-2 (pX462)	Offset
IRF3	GCCGCAAGCCGTGCTTCCAA	GGAGGACTTCGGCATCTTCC	+13
TLR3	CTCCATCCAAGGTAGTAAGT	ATTTAACACCATCTCAAAGC	+1
RIG-I	GATGATGGAGATAGAGAGTC	GATGCACTTAAATCTGTCAG	+11

2.18.2. Co-transfection of Cas9n/gRNA plasmids into PK-15 cells

For the co-transfection of each pair of Cas9n/gRNA plasmids, two individual mixes were prepared. The first tube contained 1 µg of each plasmid (2 µg in total) made up to a final volume of 50 µl DMEM (no antibiotic or serum) while the second contained 6 µl of Transit-LTI (MirusBio, #MIR2304) made up to 50 µl in the same media, giving a DNA:transfection reagent ratio of 1:3. Mixes were incubated at R/T for 5 min, after which the plasmid mix was added to the transfection reagent mix and incubated at R/T for a further 30 min.

One hundred µl of transfection mixes (plasmid and transfection reagent) were applied to PK-15 cells (90% confluent) in 12-well plates. Mixes were applied "drop-wise" across the well and the plates rocked gently to ensure equal distribution. An additional 300 µl of media containing no antibiotic or serum was immediately applied to each well. Following 2 hr of incubation at

37°C, 700 µl of complete media was applied to each well. 24 hr post-transfection, media was replaced with reduced-serum media (2.5% (w/v)). 72 hr post-transfection, media was replaced and 3 µg/ml of puromycin was added. Antibiotic selection proceeded for 72 hr, with fresh media containing 3 µg/ml of puromycin being applied after 48 hr. Complete media (10% (w/v) ABS) without puromycin was then applied to the cells. Cells were then incubated until large colonies were visible (~2 weeks) at which point they were isolated, propagated and stored as detailed in 2.1.2.4 and 2.1.2.3.

2.18.3. Screening for knockouts

Post-selection, cells were screened for gene knockout by Sanger sequencing (see 2.8.3). Genomic DNA extracted from cells was subjected to PCR and sequencing as detailed in 2.17, 2.8.1 and 2.8.3. Genomic DNA sequences were aligned using MEGA7 (Mega Software) to identify indels. Where a suitable antibody had been identified (RIG-I and IRF3 only), absence of protein encoded by the target gene was determined by Western blot (see 2.13).

2.19. Yeast two-hybrid screen

The Matchmaker© 3 GAL4-based yeast two-hybrid system (Clontech Laboratories) was used to determine if porcine Bax interacts with either porcine IRF3 or CSFV N^{pro} (discussed in 6.5). Yeast plasmid cloning, yeast transformation and selection by growth on stringent media were performed as detailed in the protocol supplied by the manufacturer (Clontech Laboratories, PR742219; https://www.takarabio.com/assets/documents/User%20Manual/PT3247-1.pdf). Plasmids and the co-transformation combinations utilised are detailed in table 2.11.

Table 2.11: Yeast co-transformations performed using the Matchmaker© 3 GAL4-based yeast two-hybrid system (Clontech Laboratories) and accompanying protocol (Clontech Laboratories, PR742219).

Plasmid co-transformation	pGBKT7 plasmid (DNA binding domain fusion)	pGADT7 (activation domain fusion)
1	CSFV N^{pro}	Porcine IRF3
2	Porcine Bax^{S}	CSFV N^{pro}
3	Porcine Bax^{L}	CSFV N^{pro}
4	Porcine Bax^{S}	Porcine IRF3
5	Porcine Bax^{L}	Porcine IRF3
6	Murine p53	SV40 large T antigen
7	Human lamin C	SV40 large T antigen
8	CSFV N^{pro}	Porcine IkBα
9	Porcine Bax^{S}	EV
10	Porcine Bax^{S}	SV40 large T antigen
11	Porcine Bax^{L}	EV
12	Porcine Bax^{L}	SV40 large T antigen
13	EV	Porcine IRF3
14	Murine p53	Porcine IRF3

Note: The yeast two-hybrid system was used to screen for interactions between CSFV N^{pro}, porcine IRF3 and porcine Bax (long and short isoforms; XM_003127290.5 and XM_013998624.2) (orange). Positive (green) and negative controls (red) were employed. EV indicated where an empty vector has been used. pGBKT7-N^{pro}, pGADT7-IkBα and pGADT7-IRF3 were sourced in-house; pGBKT7-Bax^{L} and pGBKT7-Bax^{S} were prepared for the project using cDNA synthesised by GeneArt (Invitrogen). All other plasmids were supplied by the kit.

Yeast co-transformed with plasmid combinations 1-14 were plated onto double-dropout (DDO) media the amino acids leucine and tryptophan. Those co-transformed with plasmid combinations 1-8 were further plated onto quadruple-dropout (QDO) media additionally lacking the amino acids adenine and histidine. Further details regarding the screen can be found in 6.5.

2.20. Primers

All primers for PCR, cloning or sequencing were sourced either in-house or designed and ordered using Sigma's oligonucleotide (oligo) synthesis service (table 2.12).

Table 2.12: Primers used for PCR, cloning or sequencing throughout the project.

Name	Sequence (5'->3')	PCR and/or cloning	Sequencing
Npro-EcoRI-fw	GCGCGAATTCGGAGTTGAATCATTTTGAACTTTTA	x	
Npro-EcoRI-rev	GCGCGAATTCTTAGCAACTGGTAACCCACAA	x	x
pCMV-fw	CGCAAATGGGCGGTAGGCGTG		x
EGFP-F1_C	TACCTGAGCACCCAGTCCGC		x
EGFP-f1	GGTTTAGTGAACCGTCAGATCC	x	
EGFP-r1	CGTCCATGCCGAGAGTGATC	x	
EGFP-f2	GTGAAGTTCGAGGGCGACAC	x	
Npro-r1	CGGGCCCATGTAGTCCTG	x	
poMDA5 fw.1	CAGTTGTCAGGCACGTTGC	x	
poMDA5 rv.1	CAGCAGTTGGAGACACTCATC	x	
poMDA5 fw.2	GCAAATTGTTCTTCTCTCGAGG	x	x
poMDA5 rv.2	CAACAGTTGCTCCTCCACAC	x	x
poTLR3 fw.2	CTGTTGCCCTTTTGGATACTG	x	x
poTLR3 rev.3	CCATCTTGCCATCAAAAATAGTT	x	x
poTLR3 fw.1	GGTGAAGAGTGAGGAAGGAGG	x	
poTLR3 rev.2	GCATCATGGCTAGTACAGAACG	x	x
poRIG-I fw.2	GCCACTGCAAGGTTTTTGAG	x	x
poRIG-I rev.2	CACCTGGCACAATAAGTACCTG	x	x
poRIG-I rev.1	GGTGCGTGTATTCAGATGGC		x
poIRF3 fw.1	GTACCTGCACTGTGTGATGTGG	x	x
poIRF3 rev.2	CTCTAATATTCCAAGGTCCGC	x	x
poIRF3 fw.3	CCTGGGAGTCCGCCTATATC		x
intEcoRV-poIRF3	CGTAGCGATATCTCAGCTGAACCAGGG	x	
poIRF3-NotI	TGCTTAGCGGCCGCCTAGAAATCCATGTCCTCCACC	x	
BamHI-3frameSTOP-NotI_FW	GATCCTGAATCGTAGATACTGAGC	x	
BamHI-3frameSTOP-NotI_REV	GGCCGCTCAGTATCTACGATTCAG	x	
FW-AgeI-kozak-FLAG-poIRF3	GCTACCGGTGCCACCATGGACTACAAAGACGATGACGACAAGGGAACTCAGAAGCCTCGAATC	x	
RV-poIRF3-EcoRI	GGCTTAGAATTCCTAGAAATCCATGTCCTCCACCAG	x	
KpnI_Kozak_5'EGFP_FW	GCTGGTACCGCCACCATGGTGAGCAAG	x	

3’EGFP_BamHI_5’poIRF3_REV	GGCATGGACGAGCTGTACAAGGGATCCGGAACTCAGAAGCCTCGAATCCTGCCCTGGCTGATATCGTCTG	x	
poIRF3_BamHI_fw	GCAGGATCCGCCACCATGGGAACTCAGAAGCCTCG	x	
poIRF3_NotI_rev	TGCTTAGCGGCCGCCTAGAAATCCATGTCCTCCACC	x	
HindIII-3frameSTOP-EcoRI_FW	AGCTTTGAATCGTAGATACTGAG	x	
HindIII-3frameSTOP-EcoRI_REV	AATTCTCAGTATCTACGATTCAA	x	
SV40polyA_1_REV	GCATCACAAATTTCACAAATAAAGC		x
SV40polyA_2_REV	GTAACCATTATAAGCTGCAATAAACAAG		x
poIRF3_int1_fw	GCTTCCGCATCCCTTGG		x
poIRF3_int2_rev	GTAACTTATCCAGACTGTCTTCGTGG		x
poIRF3_int3_fw	CTGACGGACAGGGGTGTG		x
poIRF3_int4_rev	GACCATCACCAGCCTCTTGAC		x

3. N^{pro} antagonises IFN-independent poly(I:C) and Sendai virus-mediated apoptosis

3.1. Introduction

As discussed in 1.3.3, the N^{pro} protein of CSFV is a documented antagonist of poly(I:C)-mediated apoptosis; however, the mechanism by which this is achieved and the pathways targeted to achieve this have yet to be elucidated (Schweizer and Peterhans, 2001, Ruggli *et al.*, 2003, Ruggli *et al.*, 2005, Johns *et al.*, 2010a, Jefferson *et al.*, 2014). To address this, cell lines available in the group stably expressing N^{pro} with various tags have been assessed for their capacity to antagonise the induction of apoptosis. In addition, a lentivirus expressing fluorescently-tagged N^{pro} has been developed and the role played by IFN in poly(I:C)-mediated apoptosis explored. Henceforth, the N^{pro} protein of CSFV is referred to simply as "N^{pro}" except when referring to BVDV or BDV N^{pro} or where clarity is beneficial to the point being made.

3.2. Stably expressed N^{pro} antagonises poly(I:C) and SeV-mediated apoptosis

3.2.1. His-N^{pro} and N^{pro}

To confirm previous reports of N^{pro}'s ability to antagonise dsRNA-mediated apoptosis, a porcine kidney cell line (PK-15) stably expressing untagged N^{pro} and two expressing His-tagged (6xHis) N^{pro} available within the group (Seago *et al.*, 2007, Johns *et al.*, 2010b, Seago *et al.*, 2010) were analysed. PK-15 His-N^{pro} 23, N^{pro} 31 and His-N^{pro} 61 were grown alongside parental negative control PK-15 cells and whole cell lysates prepared once confluency was reached.

Whole cell lysates were analysed by Western blot using the DS14 rabbit polyclonal antisera against N^{pro} (^{11}KTNKQKPMGVEEPVYDATGKPLFGDPS^{37}) to determine the respective levels of N^{pro} protein in each cell line. Treatment of cells with the proteasome inhibitor MG132 (see 2.16) was not required for the detection and visualisation of His-N^{pro} in the His-N^{pro} 23 cell line which resolved as a single ~19 kDa band, although in agreement with past literature, lysates prepared from cells treated with inhibitor exhibited a comparatively higher expression (figure 3.1, A) (Seago *et al.*, 2010). A band of approximately the same size was also observed for His-N^{pro} 61 following proteasome inhibition, but no clear increase in expression was observed for the N^{pro} 31 cell line due to high background on the blot.

Each N^{pro}-expressing cell line was subsequently assessed for the capacity to antagonise poly(I:C)-mediated apoptosis. As expected, Western blot analysis showed whole cell lysates prepared from PK-15 cells treated with poly(I:C) contained cleaved caspase-3, routinely used as a terminal indicator of apoptosis. In agreement with previous reports, each N^{pro}-expressing cell line exhibited a comparatively reduced level of cleaved caspase-3 following poly(I:C)

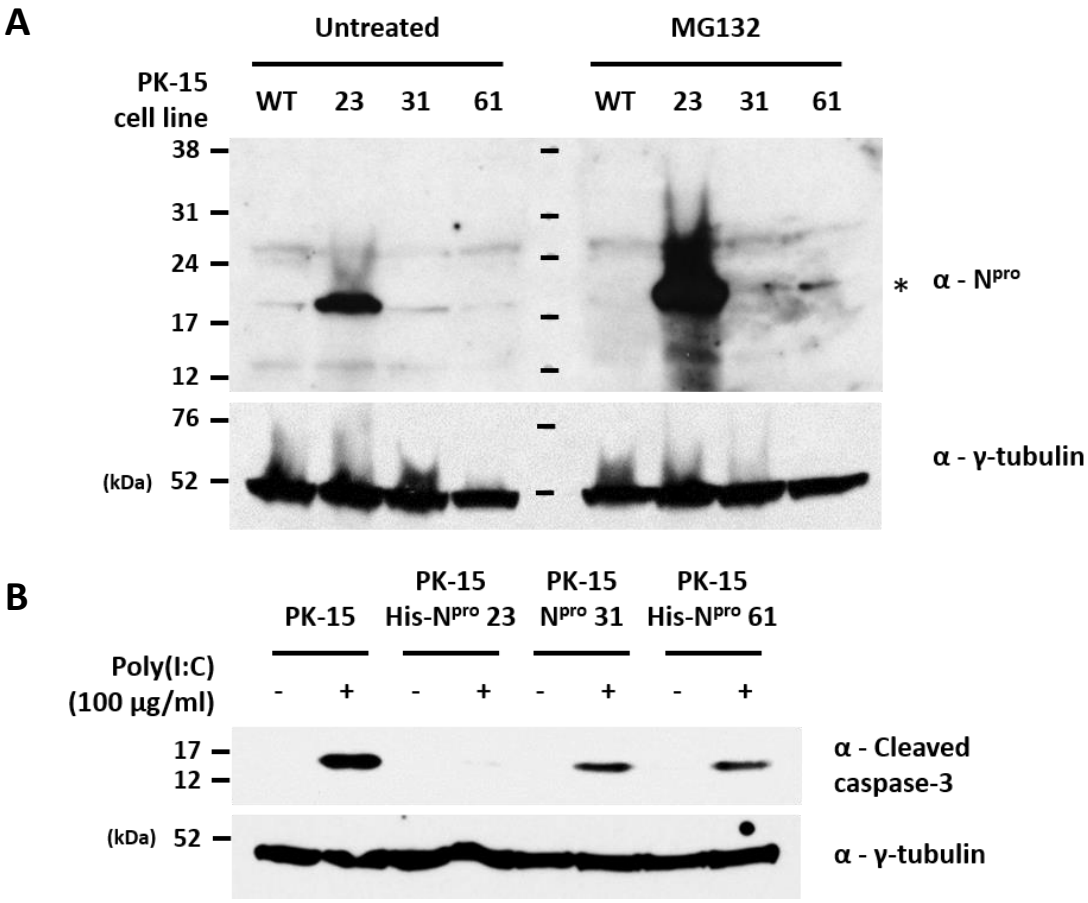

Figure 3.1: Cell lines stably expressing N^{pro} and His-N^{pro} antagonise the induction of poly(I:C)-mediated apoptosis. WT, N^{pro} and His-N^{pro}-expressing PK-15 cells were seeded in 6-well plates and treated with either (A) 25 µM MG132 or (B) 100 µg/ml poly(I:C). 18 hours post-treatment, whole cell lysates were prepared and analysed by Western blot using a polyclonal Ab recognising N^{pro} (*) and a mAb recognising cleaved caspase-3 as indicated. A mAb recognising γ-tubulin was used to determine relative protein concentrations.

treatment, indicating an antagonism of the innate apoptotic response (figure 3.1, B). Out of the three lines treated, His-N^{pro} 23 appeared to antagonise induction of caspase-3 cleavage to the greatest extent. This agreed with figure 3.1, A which revealed the His-N^{pro} 23 line to be a higher expresser of N^{pro} than the N^{pro} 31 and His-N^{pro} 61 cell lines. As expected, all bands corresponding to cleaved caspase-3 ran close to the predicted molecular weight of 17 kDa. Western blot analysis of uncleaved caspase-3 levels would have proved insightful however this was not possible due to the lack of reactvitity with available antibodies.

3.2.2. GFP-N^{pro}

PK-15 and SK6 cell lines stably expressing either GFP or GFP-N^{pro} also available in the group were used for this study. To confirm the expression of GFP or GFP-N^{pro}, Western blots of whole cell lysates were carried out. GFP was detectable without the addition of MG132 in both the PK-15 and SK6 cell lines although the corresponding band was more intense in the presence of inhibitor (figure 3.2). In order to detect GFP-N^{pro} in the PK-15 cell line, treatment with the proteasome inhibitor MG132 was required (figure 3.2). However, proteasome inhibition was not required to detect GFP-N^{pro} in the SK6 cell line (figure 3.2). Both GFP and GFP-N^{pro} migrated at the expected molecular weights of 27 kDa and 46 kDa respectively.

Next, the extent of apoptosis antagonism in these cell lines was examined; as before, whole cell lysates prepared from cell lines treated with poly(I:C) were analysed by Western blot for

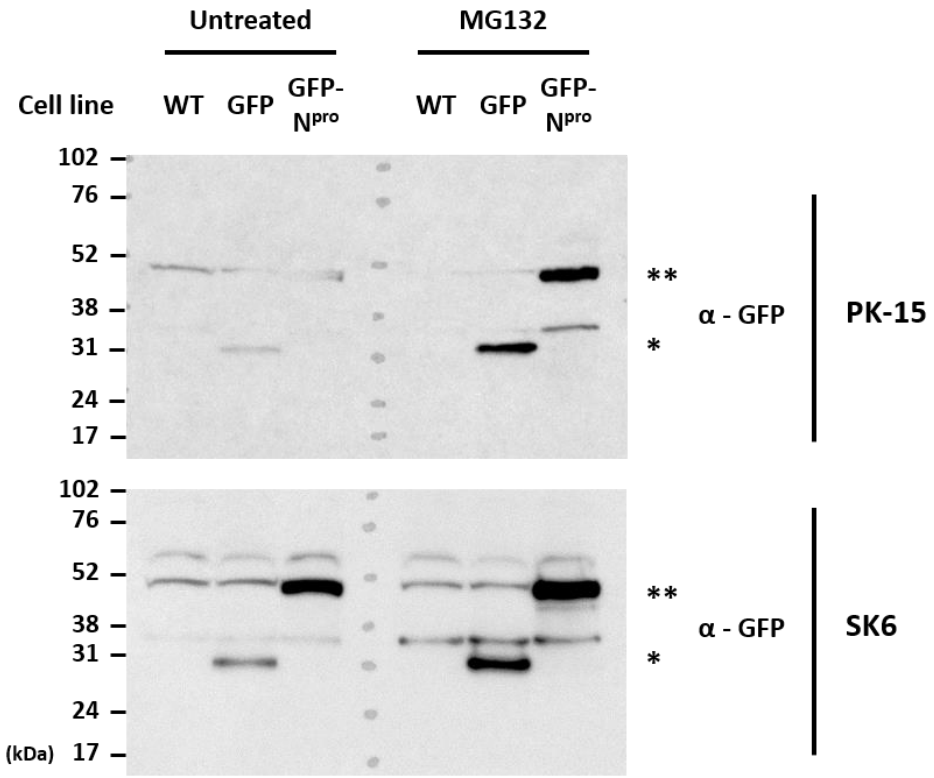

Figure 3.2: Confirmation of GFP and GFP-N^{pro} expression in PK-15 and SK6 stable cell-lines. WT, GFP and GFP-N^{pro}-expressing PK-15 and SK6 cells were seeded in 6-well plates and treated with 25 µM MG132. 18 hours post-treatment, whole cell lysates were prepared and analysed by Western blot using a mAb recognising GFP.

cleaved caspase 3. With regards to the GFP-N^{pro} PK-15 cell line, the level of cleaved caspase-3 was comparatively lower than that observed for the GFP and parental PK-15 control cells (figure 3.3, A). The GFP-N^{pro} SK6 cell line yielded similar findings, exhibiting a markedly reduced level of cleaved caspase-3 in comparison to the respective GFP and parental SK6 control cells (figure 3.3, B). In contrast to the blotted PK-15 lysates, cleaved caspase-3 was detected in all lysate samples prepared from untreated SK6 cells. However, the level of cleaved caspase-3 in lysates prepared from the untreated GFP-N^{pro} SK6 cell line was comparatively lower than that observed for both the GFP and parental SK6 control cells.

Next, to confirm that the expression of GFP-N^{pro} in PK-15 cells could inhibit poly(I:C)-mediated induction of IFN and thus prevent the transcriptional activation of IFN stimulated genes (ISG) such as Mx1, the PK-15 lysate samples were also analysed for the presence of the Mx1 protein. Western blot analysis for Mx1 produced intense bands at 76 kDa for poly(I:C) treated (10 and 100 μg/ml) GFP and parental PK-15 control cells, but no bands were observed for untreated samples (figure 3.3, A). In comparison to the GFP and parental control cells, the level of Mx1 observed in lysates prepared for the poly(I:C) treated GFP-N^{pro} PK-15 cells was markedly reduced, confirming the ability of N^{pro} to inhibit the production of type I IFN. The GFP-N^{pro} SK6 cell line was not assessed for its capacity to antagonise the induction of type I IFN since SK6 cells are defective in their ability to express it (Ruggli *et al.*, 2003).

3.3. Stably expressed N^{pro} antagonises Sendai virus-mediated apoptosis

Since poly(I:C) is widely regarded as an agonist of TLR3-mediated signalling when applied to cell culture media, additional experiments were conducted using Sendai virus (Cantell strain, SeV), a reported agonist of RIG-I-mediated signalling (Strahle *et al.*, 2006, Baum *et al.*, 2010, Kato *et al.*, 2011). A representative N^{pro} cell line (His-N^{pro} 23) and parental PK-15 cells were treated with increasing quantities of SeV and whole cell lysates examined by Western blot for

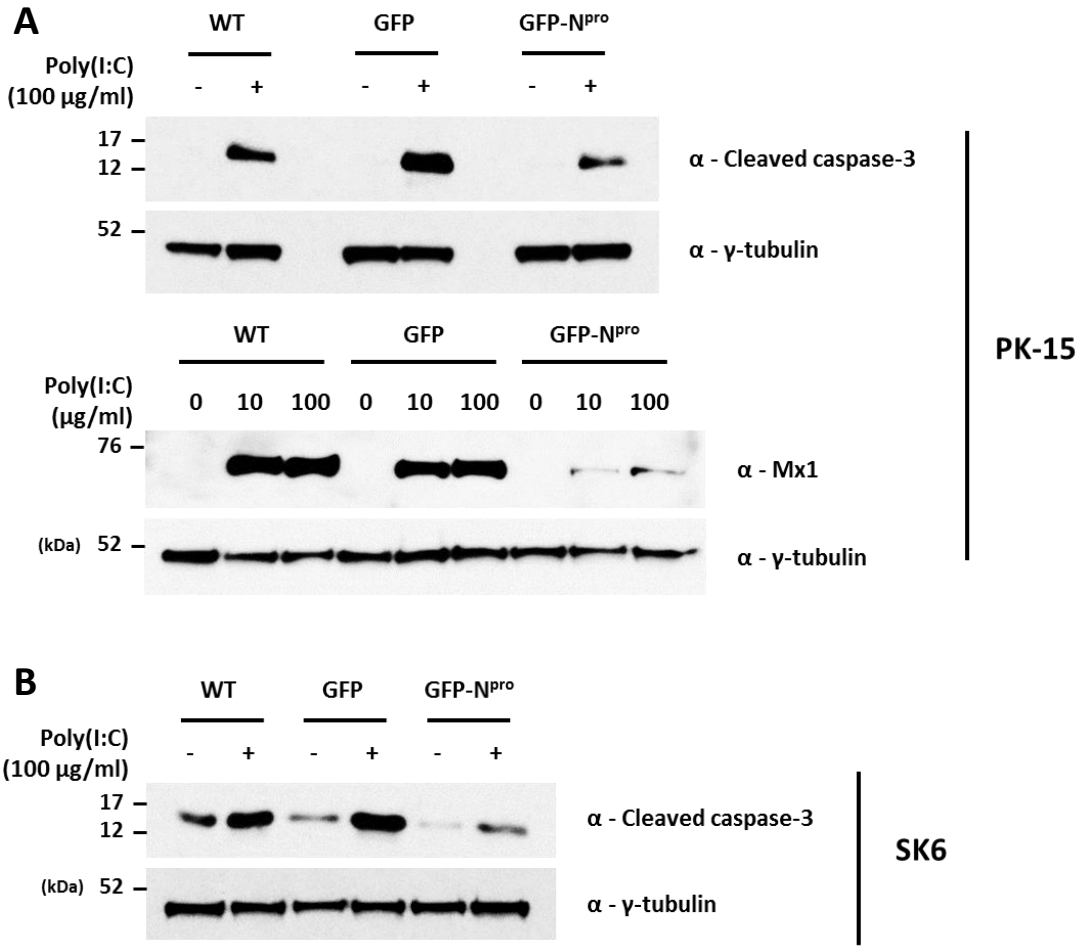

Figure 3.3: Stably-expressed GFP-N^{pro} antagonises the induction of poly(I:C)-mediated apoptosis in PK-15 and SK6 cells and also ISG upregulation in PK-15 cells. WT, GFP and GFP-N^{pro}-expressing (A) PK-15 and (B) SK6 cells were seeded in 6-well plates and treated with poly(I:C) at the indicated concentrations. 18 hours post-treatment, whole cell lysates were prepared and analysed by Western blot using mAbs recognising (A, B) cleaved caspase-3 or (A) Mx1. A mAb recognising γ-tubulin was used to determine relative protein concentrations.

cleaved caspase-3, as well as the ISG products Mx1, ISG15 and RIG-I. Whole cell lysates of poly(I:C)-treated PK-15 cells and the His-N^{pro} 23 cell line were examined alongside as positive and negative controls respectively. Western blot analysis of whole cell lysates confirmed that SeV was able to induce the cleavage of caspase-3 in parental PK-15 cells, but comparatively lower levels were observed for the His-N^{pro} cell line (figure 3.4, B). In agreement with past literature, Mx1, ISG15 and RIG-I were not upregulated following treatment with poly(I:C) in the His-N^{pro} 23 cell line but were in the parental PK-15 cells (figure 3.4, A). At lower quantities (2 HA/ml), SeV treatment induced the expression of Mx1, ISG15 and RIG-I in the control PK-15

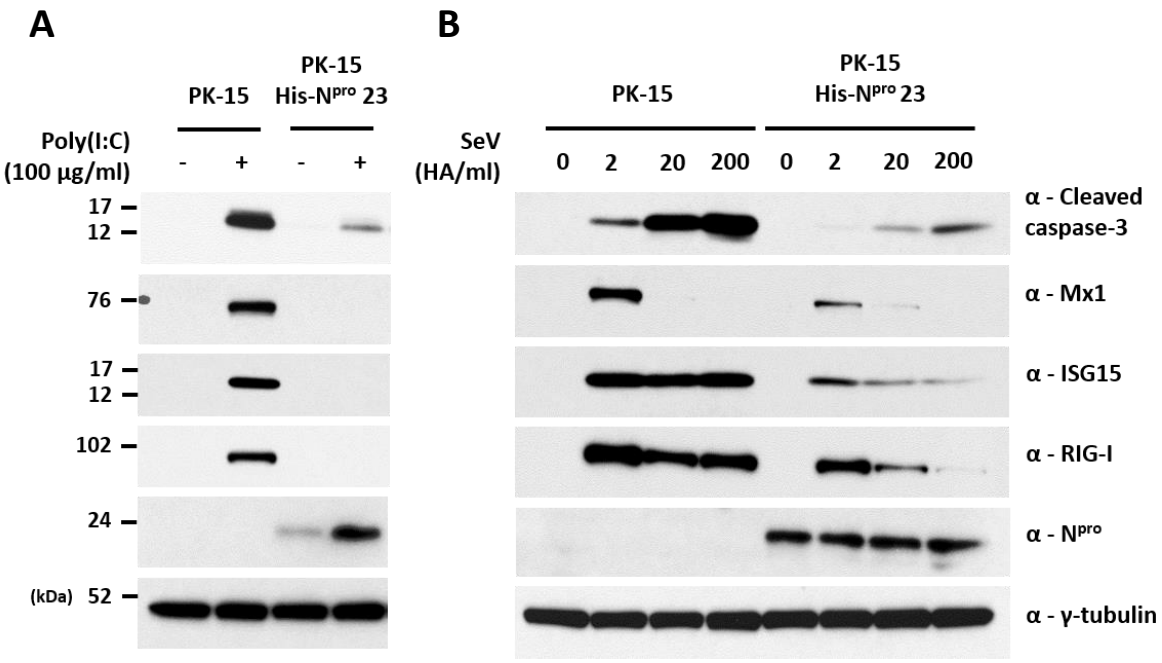

Figure 3.4: N^{pro} antagonises Sendai virus-mediated apoptosis in PK-15 cells. WT and His-N^{pro}-expressing PK-15 cells were seeded in 12-well plates and treated with (A) poly(I:C) or (B) Sendai virus (Cantell strain, SeV) at the indicated concentrations. 18 hours post-treatment, whole cell lysates were prepared and analysed by Western blotting using polyclonal Abs recognising ISG15 or N^{pro} and mAbs recognising cleaved caspase-3, Mx1 or RIG-I as indicated. A mAb recognising γ-tubulin was used to determine relative protein concentrations.

cells and to a comparatively lower level in the His-N^{pro} cell line, demonstrating N^{pro}'s ability to antagonise SeV-induced IFN production (figure 3.4, B). In control PK-15 cells, the level of cleaved caspase-3 showed a positive correlation with the quantity of SeV used, however under the same conditions ISG upregulation exhibited a negative correlation – this can be explained by the presence of the SeV encoded C-protein, a known antagonist of the JAK-STAT pathway that governs the response to type I IFN (Garcin *et al.*, 2002).

3.4. Lentivirus-expressed EGFP-N^{pro} antagonises poly(I:C) and SeV-mediated apoptosis

Having confirmed N^{pro}'s ability to antagonise the induction of poly(I:C)-mediated apoptosis and IFN induction and having also identified N^{pro}'s previously unknown ability to antagonise SeV-mediated apoptosis, a lentiviral system expressing an EGFP-tagged N^{pro} protein was developed to facilitate the study of protein localisation in primary cells and immortalised cell lines. A 3rd-

generation lentiviral expression system was employed instead of the older 2nd-generation system due to the fact that the packaging system is split across two plasmids instead of one, rendering it safer (Dull *et al.*, 1998).

3.4.1. Generation of EGFP-N^{pro}-expressing 3rd-generation lentivirus

PK-15 and SK6 cells were infected with varying volumes (0-200 µl) of collected supernatants prepared from the HEK 293T transfected with EGFP and EGFP-N^{pro}-encoding lentivirus plasmids as detailed in appendix A and 2.12. Whole cell lysates were prepared 72 hours post-infection (hpi) (see 2.13.3) and subsequently subjected to Western blot analysis to confirm the presence of EGFP and EGFP-N^{pro} (see 2.13.4 and 2.13.5). For both the blotted PK-15 and SK6 whole cell lysates, EGFP appeared as a single band of ~33 kDa, which is slightly larger than the predicted MW of 28 kDa, and the intensity of the band increased with an increase in the quantity of lentivirus used to infect the cells (figure 3.5). In both PK-15 and SK6 cell samples, EGFP-N^{pro} resolved as a doublet of bands at both ~47 kDa (figure 3.5, ***) and ~60-65 kDa (figure 3.5, ****), the higher band resolving significantly higher than the predicted MW of 47 kDa. As with the EGFP-encoding lentivirus, band intensity increased with increasing quantities of virus, suggesting that the bands do indeed correspond to EGFP-N^{pro}. In each cell line, the band corresponding to EGFP was of a greater intensity than those corresponding to EGFP-N^{pro}; this is potentially due to the fact that N^{pro} is rapidly turned-over (Seago *et al.*, 2010).

After confirming the expression of the EGFP and EGFP-N^{pro} proteins by Western blot, experiments were conducted to visualise EGFP and EGFP-N^{pro} in PK-15 and SK6 cells by fluorescence confocal microscopy. In EGFP-encoding lentivirus-infected cells, fluorescent protein did not appear to demonstrate any particular sub-cellular localisation and was distributed throughout the cytosol, nucleus and nucleolus (figure 3.6). However, in cells infected with EGFP-N^{pro}-encoding lentivirus, the resulting fluorescent protein adopted a clear localisation to the nucleolus and to a lesser extent, the nucleus and cytoplasm as previously

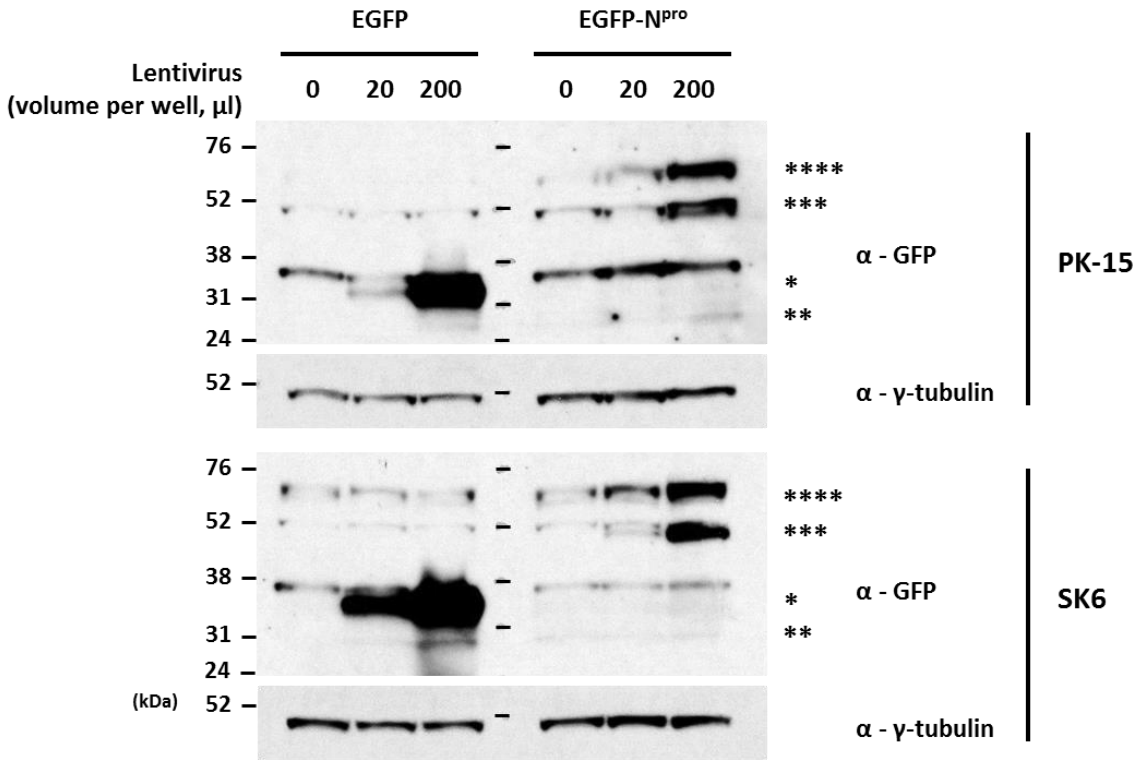

Figure 3.5: EGFP and EGFP-N^{pro} are detectable by Western blot following infection of PK-15 and SK6 cells. PK-16 and SK6 cells were seeded in 24-well plates and infected with increasing crude volumes of 3rd-generation lentivirus encoding EGFP and EGFP-N^{pro} as indicated. 2 µg/ml polybrene was applied to each well after which plates were centrifuged at 1000 rcf for 30 minutes. 72 hours post-infection, whole cell lysates were prepared and analysed by Western blotting using a mAb recognising GFP. A mAb recognising γ-tubulin was used to determine relative protein concentrations. EGFP resolved primarily as a single band (*) with a faint second band also detectable (**) while EGFP-N^{pro} resolved as a doublet (*** and ****).

reported (Doceul *et al.*, 2008, Li *et al.*, 2014). These distinct differences in protein localisation and distribution were visible at both colony level (figure 3.6, A) and single-cell level (figure 3.6, B). In summary, these findings demonstrate the successful generation of a 3rd-generation lentivirus capable of expressing EGFP-N^{pro} fusion protein in infected cells.

In order to confirm EGFP-N^{pro}'s functionality as an antagonist of poly(I:C)-mediated apoptosis, PK-15 cells were infected for 48 hours with fresh aliquots of each respective lentivirus and then treated with poly(I:C) (100 µg/ml) to induce apoptosis (see 2.15.1) and whole cell lysates were subsequently prepared and subjected to Western blot analysis for cleaved caspase-3. As previously observed, EGFP resolved primarily as a single band at ~33 kDa (figure 3.7, *) and

EGFP-N^{pro} as a doublet of ~47 kDa and ~60-65 kDa (figure 3.7, ** and ***). Poly(I:C) treatment induced considerable levels of cleaved caspase-3 in both uninfected and EGFP lentivirus-infected cells. However, no cleaved caspase-3 was observed for the EGFP-N^{pro} lentivirus-infected cells, confirming that EGFP-N^{pro} successfully antagonised the induction of poly(I:C)-mediated apoptosis. As cleaved caspase-3 was undetectable in these samples, it suggests that the lentiviruses used might have been of a higher titre than that used for the infections imaged in figure 3.6. The presence of EGFP-N^{pro} was confirmed not only by Western blot with DS14 but

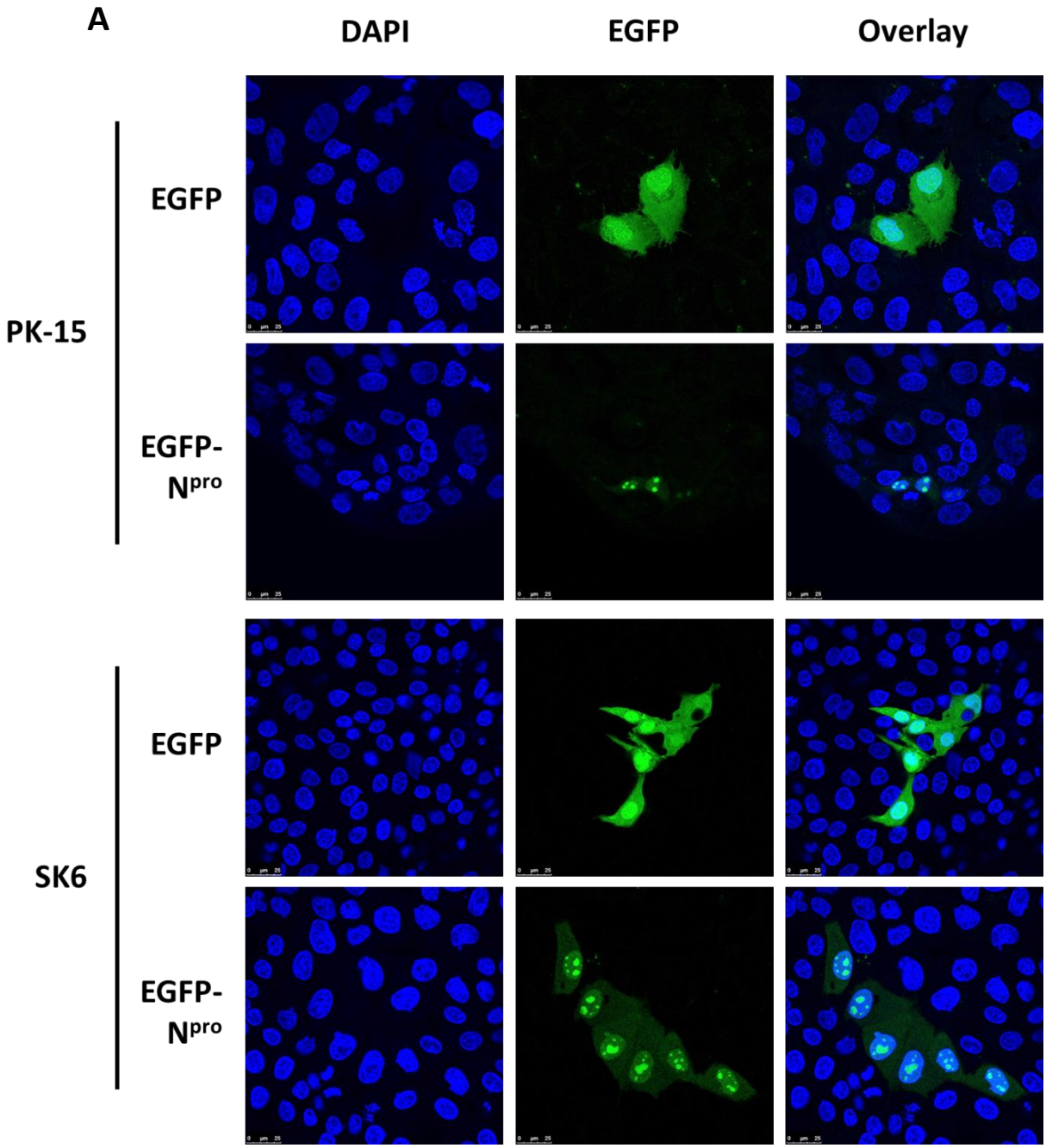

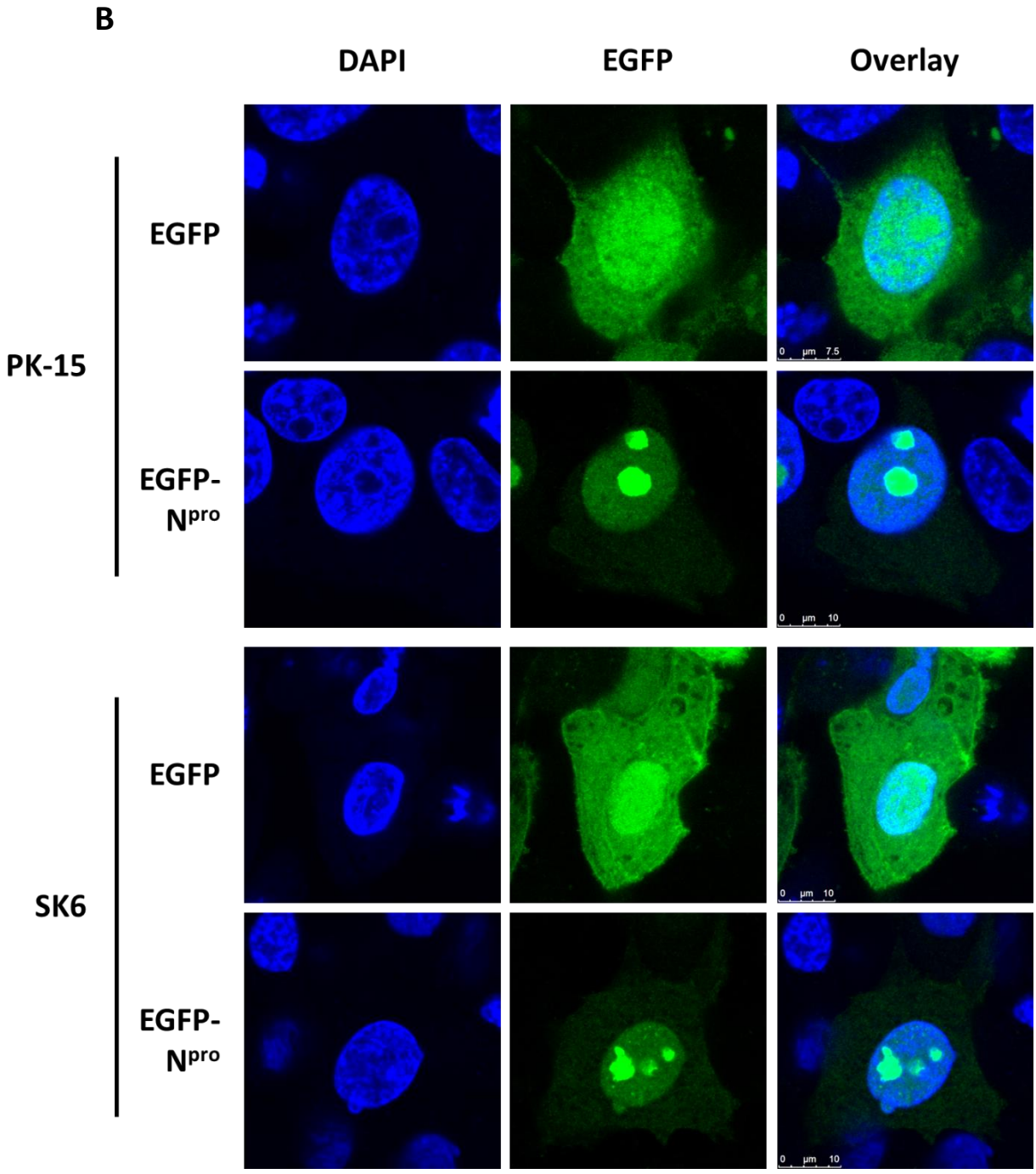

Figure 3.6: Lentivirus-expressed EGFP and EGFP-N^{pro} exhibit distinct localisation within PK-15 and SK6 cells. PK-15 and SK6 cells were infected with 3rd-generation lentiviruses encoding EGFP and EGFP-N^{pro}, fixed 72 hours post-infection and visualised by confocal fluorescent microscopy. (A) Cells were visualised at the colony and (B) single-cell level. Nuclei were stained blue with 1 µg/ml DAPI. As expected, EGFP was distributed throughout each cell while EGFP-N^{pro} was primarily localised to the nucleolus and nucleus.

also an antibody recognising GFP, further confirming the bands' identity – in each case, the larger ~60-65 kDa band was most intense. Interestingly, the EGFP-N^{pro} doublet appeared more

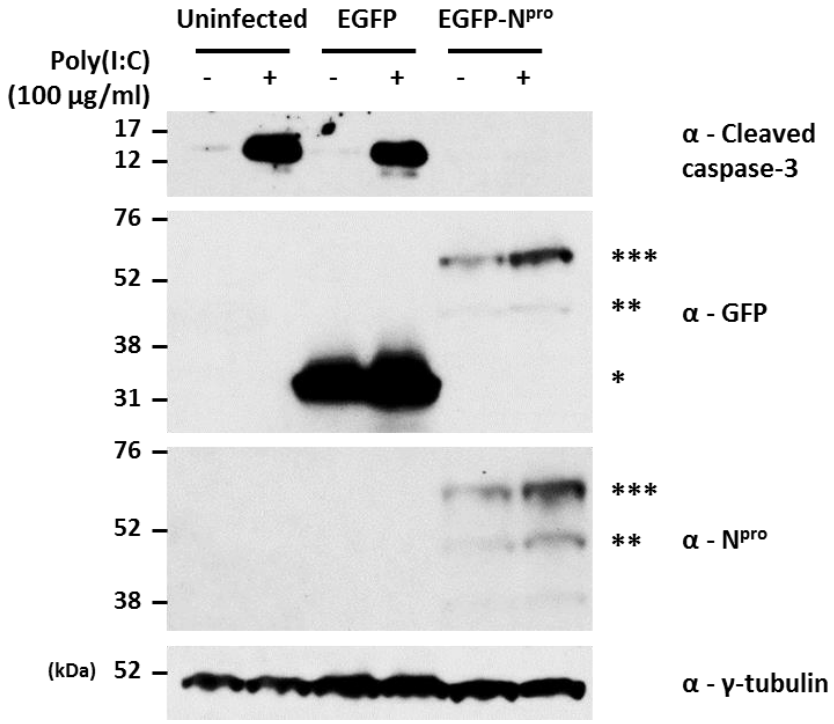

Figure 3.7: Lentivirus-expressed EGFP-N^{pro} antagonises induction of poly(I:C)-mediated apoptosis in PK-15 cells. PK-15 cells were infected with 3rd-generation lentiviruses encoding EGFP and EGFP-N^{pro} for 48 hours and treated with 100 µg/ml poly(I:C). 18 hours post-treatment, whole cell lysates were prepared and analysed by Western blotting using a polyclonal Ab recognising N^{pro} and a mAb recognising GFP. A mAb recognising γ-tubulin was used to determine relative protein concentrations. EGFP resolved as a single band (*) while EGFP-N^{pro} resolved as a doublet (** and ***).

intense following treatment with poly(I:C) which was previously observed in figure 3.4, A.

3.4.2. Establishment of EGFP and EGFP-N^{pro}-expressing PK-15 cell lines by lentivirus transduction

For the purpose of studying these EGFP-N^{pro}-expressing cells further, stably-expressing cell lines were established. Briefly, PK-15 cells were infected with EGFP and EGFP-N^{pro} lentiviruses and at 72 hpi puromycin (3 µg/ml) antibiotic was added for 72 hours. Surviving colonies of cells were then isolated, grown and then either fixed on coverslips for fluorescence confocal microscopy (figure 3.9) or used to prepare whole cell lysates for Western blot analysis (figure 3.8).

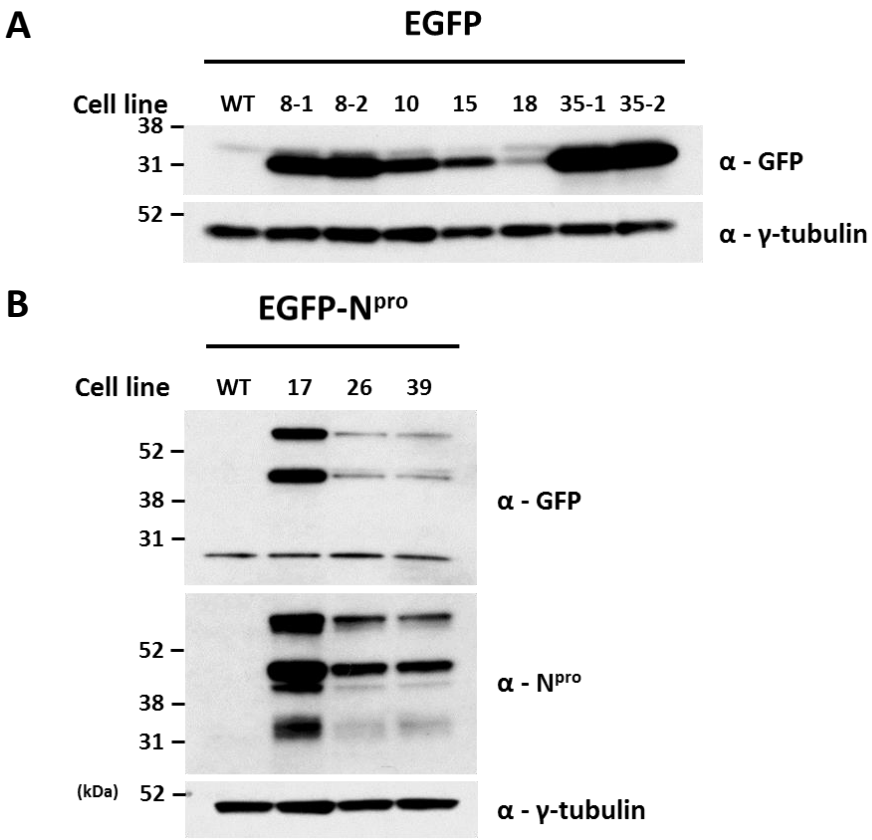

Figure 3.8: Western blot analysis of lentivirus-transduced PK-15 cells identified 7 EGFP and 3 EGFP-N^{pro} stably-expressing cell lines. WT, (A) EGFP and (B) EGFP-N^{pro}-expressing lentivirus-transduced cells were seeded in 12-well plate. Once confluency was reached, whole cell lysates were prepared and analysed by Western blot using a polyclonal Ab recognising N^{pro} and a mAb recognising GFP as indicated. A mAb recognising γ-tubulin was used to determine relative protein concentrations.

Western blot analysis using an antibody recognising GFP identified 7 cell lines that stably expressed EGFP at different levels, as indicated by the varying band intensities. EGFP-35 appeared to be the highest expresser, EGFP-10 an intermediate expresser and EGFP-18 the lowest (figure 3.8, A). With regards to EGFP-N^{pro}, 3 cell lines stably expressing the protein were identified. As previously observed, EGFP-N^{pro} resolved as a doublet at ~47 kDa and ~60-65 kDa with each constituent band of almost equal intensity – these doublets were detected using antibodies reactive against GFP and N^{pro} with the latter revealing a 3rd band running at ~33 kDa (figure 3.8, B). EGFP-N^{pro}-26 and EGFP-N^{pro}-39 were identified to be low expressers and EGFP-N^{pro}-17 a comparably higher expresser. When the EGFP and EGFP-N^{pro} PK-15 cell lines were

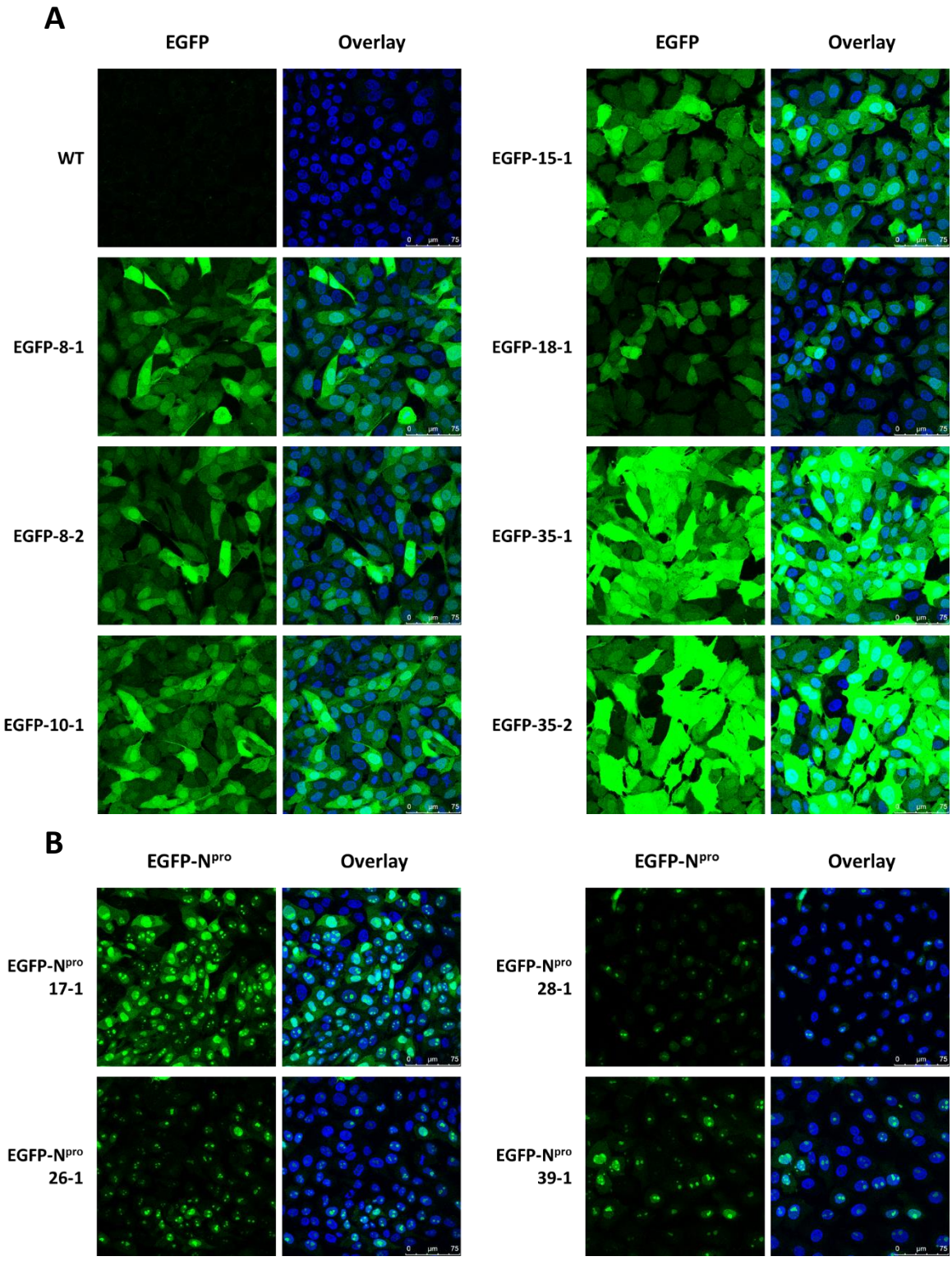

Figure 3.9: Lentivirus-transduced PK-15 cell lines express EGFP and EGFP-N^{pro} to varying degrees. WT, (A) EGFP and (B) EGFP-N^{pro}-expressing cell lines were prepared on coverslips, fixed and visualised by confocal fluorescent microscopy. Nuclei were stained blue with 1 µg/ml DAPI.

analysed by fluorescence confocal microscopy (figure 3.9) the comparative signal intensities of the respective proteins mirrored that seen in Western blots (figure 3.8).

3.4.3. Characterisation of PK-15 cell lines stably expressing EGFP-N^{pro} confirms their ability to antagonise poly(I:C) and Sendai virus-mediated apoptosis

As with each of the N^{pro} (figure 3.1), His-N^{pro} (figure 3.1) and GFP-N^{pro} (figure 3.3) PK-15 cell lines previously screened, established EGFP-N^{pro} cell lines also had to be screened for their capacity to antagonise the induction of poly(I:C) and SeV-mediated apoptosis. Each cell line was treated with 100 µg/ml poly(I:C) or 200 HA/ml SeV for 18 hours, after which whole cell lysates were prepared for analysis by Western blot.

Following treatment with poly(I:C), EGFP-expressing cells displayed pronounced induction of cleaved caspase-3. In comparison, the levels of cleaved caspase-3 were reduced in two EGFP-N^{pro} cell lines (17 and 26, figure 3.10, A) and almost entirely absent from a 3rd (39, figure 3.10, A). This was interesting as despite EGFP-N^{pro} cell line 17 being the highest expresser (figure 3.8, B), it appeared to be the poorest antagonist of poly(I:C)-mediated apoptosis out of the 3 lines screened. This might be due to clonal variation between the cell lines stemming from heterogeneity within the parental population of PK-15 cells. Likewise, EGFP-N^{pro} cell lines 26 and 39 displayed a complete block on the induction of ISG Mx1 induction while low levels of Mx1 were still detectable in the sample corresponding to line 17. However ISG15, another ISG product, was not detected in any of the EGFP-N^{pro} lines screened (figure 3.10, A). In line with previous observations (figure 3.4, A), samples analysed with DS14 revealed levels of EGFP-N^{pro} in each cell line to be increased following induction of poly(I:C)-mediated apoptosis. The same pattern was observed when using an antibody reactive against GFP – levels of EGFP-N^{pro} protein expression increased while EGFP expression levels remained unchanged.

As with poly(I:C) treatment, SeV triggered significant induction of cleaved caspase-3 in the EGFP-expressing cell line, induction which was almost entirely antagonised by EGFP-N^{pro} cell line 39 and partially by lines 17 and 26 (figure 3.10, B). This pattern in caspase-3 cleavage

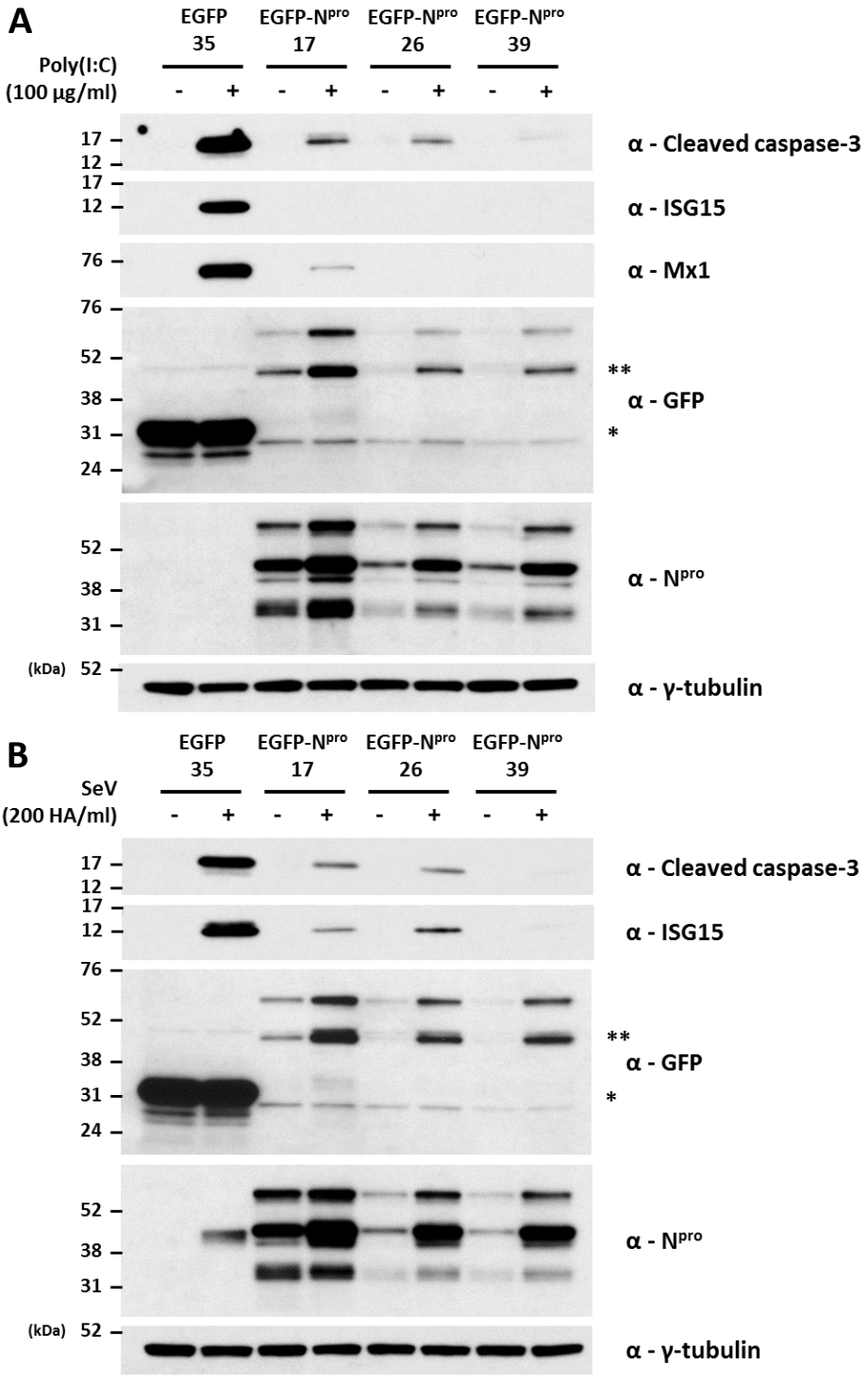

Figure 3.10: PK-15 cell lines stably expressing EGFP-N^{pro} antagonise poly(I:C) and Sendai virus-mediated apoptosis. EGFP and EGFP-N^{pro}-expressing PK-15 cell lines were seeded in 12-well plates and treated with (A) 100 µg/ml poly(I:C) or (B) 200 HA/ml SeV (Cantell strain). 18 hours post-treatment, whole cell lysates were prepared and analysed by Western blotting using polyclonal Abs recognising ISG15 or N^{pro} and mAbs recognising cleaved caspase-3, Mx1 or GFP as indicated. A mAb recognising γ-tubulin was used to determine relative protein concentrations.

mirrored what was seen following poly(I:C) treatment (figure 3.10, A). ISG15 upregulation was also absent from EGFP-N^{pro} cell line 39, however it was detectable in lines 17 and 26 at low

levels. In addition, blotting with GFP and N^{pro}-reactive antibodies revealed the same upregulation of EGFP-N^{pro} that was observed following poly(I:C) treatment.

Taken together, these results show that *in vitro* EGFP-tagged N^{pro} localises correctly in porcine cell lines and displays the two key hallmarks of N^{pro}'s immunomodulatory activity, namely antagonism of dsRNA-mediated apoptosis (using poly(I:C) and SeV as apoptotic inducers) and type I IFN induction.

3.5. Poly(I:C)-mediated apoptosis is amplified by type I IFN

N^{pro}'s interaction with IRF3 and the subsequent proteasomal degradation of IRF3 are both well documented in past literature (Bauhofer *et al.*, 2007, Seago *et al.*, 2007). A series of experiments were therefore conducted to explore whether N^{pro}'s ability to antagonise apoptosis stems from this interaction and the resulting antagonism of IFN induction and ISG upregulation.

3.5.1. JAK-STAT inhibitor treatment significantly reduces poly(I:C) but not SeV-mediated apoptosis

The pharmacological inhibitor ruxolitinib (RXT) has been shown to effectively block the JAK-STAT pathway that mediates response to type I IFN (referred to hereafter as "the type I IFN signalling response") (Mesa, 2010). Prior to using RXT to determine the role of IFN in poly(I:C) and SeV-mediated apoptosis, a useable working concentration first had to be established – a concentration high enough to sufficiently block ISG upregulation but not so high that it triggers unintended cytotoxic effects (Szymanska *et al.*, 2015). Therefore, PK-15 cells were treated with 0.5 μM or 4 μM RXT, or DMSO as a negative control, and then subsequently treated with either poly(I:C) (100 μg/ml) or porcine IFN-α (1000 IU/ml) to induce ISG upregulation. 18 hours post-treatment (hpt), whole cell lysates were prepared and analysed for the presence of Mx1

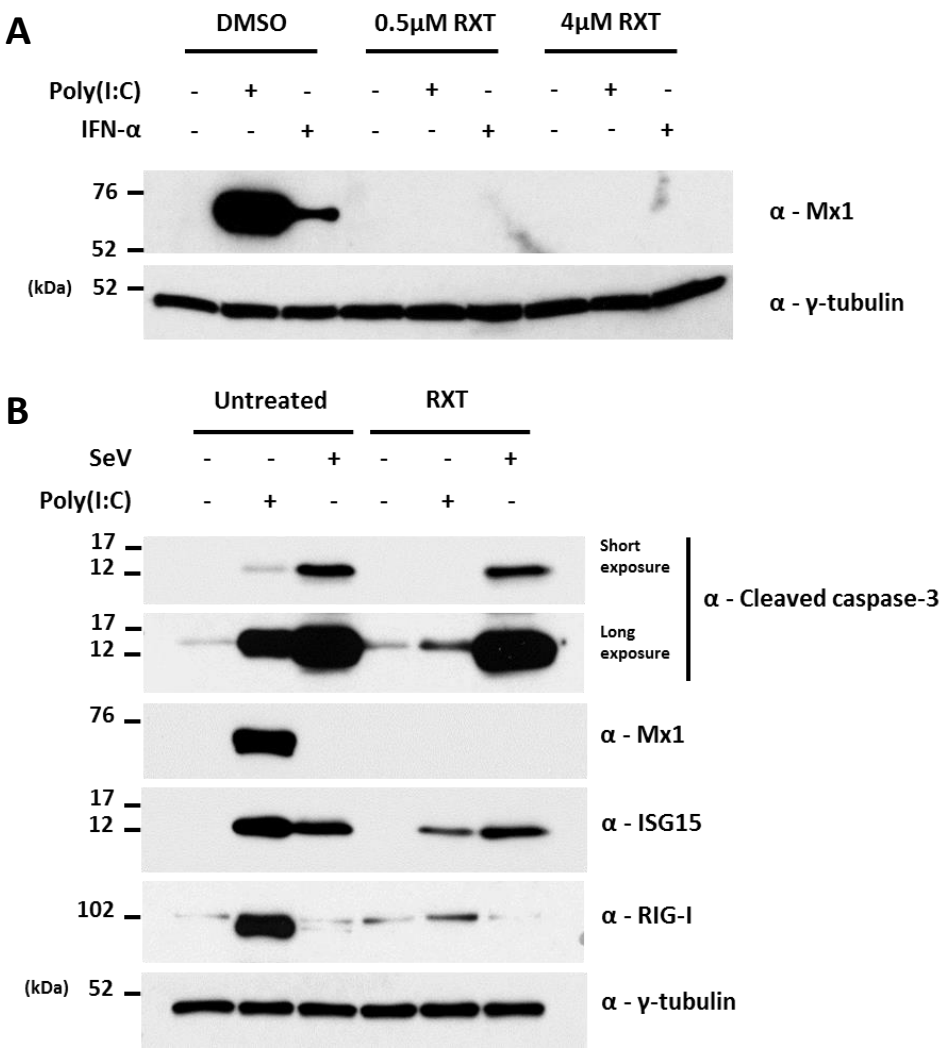

Figure 3.11: JAK-STAT inhibitor Ruxolitinib antagonises poly(I:C)-mediated apoptosis but not SeV-mediated apoptosis. (A) PK-15 cells were seeded in 12-well plates and treated either with DMSO or JAK-STAT inhibitor Ruxolitinib (RXT) at the indicated concentrations. 18 hours post-treatment, whole cell lysates were prepared and analysed by Western blot using a mAb recognising Mx1. A mAb recognising γ-tubulin was used to determine relative protein concentrations. (B) PK-15 cells were seeded in 12-well plates and treated with poly(I:C) or SeV in the presence or absence of 0.5 µM RXT. 18 hours post-treatment, whole cell lysates were prepared and analysed by Western blot as in (A) using a polyclonal Ab recognising ISG15 and additional mAbs recognising cleaved-caspase-3 or RIG-I as indicated.

by Western blot. The lower concentration of RXT tested, 0.5 µM was sufficient to entierly block Mx1 upregulation in response to both poly(I:C) and IFN-α treatment (figure 3.11, A).

PK-15 cells were subsequently treated with either poly(I:C) or SeV in the presence of 0.5 µM RXT (figure 3.11, B) and whole cell lysates were then analysed by Western blot for cleaved caspase-3. Interestingly, a large reduction in cleaved caspase-3 was observed in comparison to

cells treated with poly(I:C) in the absence of RXT (figure 3.11, B). However, the levels of cleaved caspase-3 in cells treated with SeV were unaffected by the presence of RXT. To confim RXT treatment had efficiently blocked the type I IFN signalling response following poly(I:C) treatment, the sample lysates were then analysed for Mx1, ISG15 and RIG-I; as expected, the upregulation of Mx1 and RIG-I was inhibited in the presence of RXT, while ISG15 upregulation was only partially antagonised since IRF3 can likely bind directly to its promoter (Grandvaux *et al.*, 2002, Ashley *et al.*, 2019). SK6 cells were not treated with RXT as they are defective in their ability to produce IFN (Ruggli *et al.*, 2003).

3.5.2. Type I IFN amplifies poly(I:C)-mediated apoptosis

In order to further elucidate the impact that IFN has on poly(I:C)-mediated apoptosis, PK-15 and SK6 cells were treated with poly(I:C) in the presence of increasing quantities of porcine IFN-α (0, 100, 1000 IU/ml). For both the PK-15 and SK6 treated cells, subsequent Western blot analyses revealed a positive correlation between the quantity of IFN-α used and the observed level of cleaved caspase-3 (figure 3.12). The increase in cleaved caspase-3 was most pronounced with SK6 cells, a cell line known to be incapable of producing endogenous IFN (Ruggli *et al.*, 2003). Importantly, IFN-α treatment alone was incapable of inducing caspase-3 cleavage.

3.5.3. Type I IFN only partially restores sensitivity of N^{pro}-expressing cells to poly(I:C)-mediated apoptosis

If type I IFN alone were responsible for the observed apoptosis, a restoration of cleaved caspase-3 would be expected in N^{pro}-expressing cells treated with both poly(I:C) and IFN. This is due to the fact that N^{pro} and CSFV infection antagonise levels of IRF3, thus inhibiting production of IFN-β (La Rocca *et al.*, 2005, Ruggli *et al.*, 2005, Bauhofer *et al.*, 2007, Seago *et al.*, 2007).

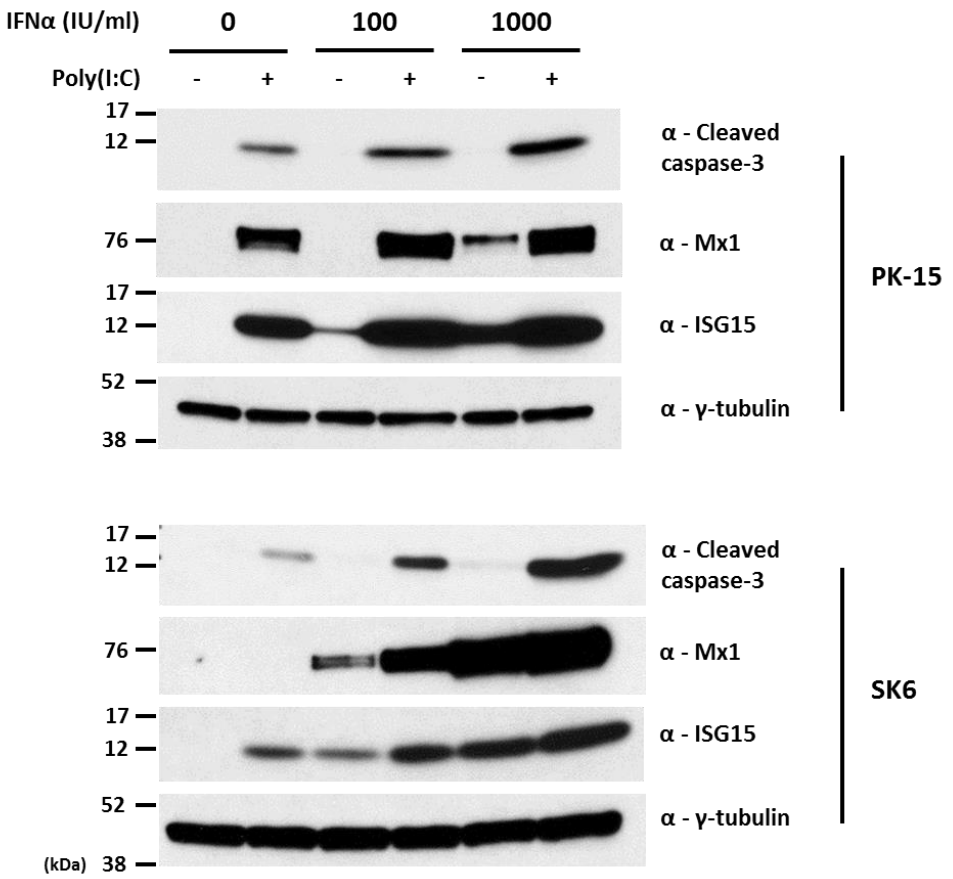

Figure 3.12: IFN-α amplifies poly(I:C)-mediated apoptosis but does trigger comparable levels of apoptosis in the absence of poly(I:C). PK-15 (top) and SK6 (bottom) cells were seeded in 12-well plates and treated with increasing concentrations of porcine IFN-α in the presence or absence of poly(I:C). 18 hours post-treatment, whole cell lysates were prepared and analysed by Western blot using a polyclonal Ab recognising ISG15 and mAbs recognising cleaved caspase-3 or Mx1 as indicated. A mAb recognising γ-tubulin was used to determine relative protein concentrations.

A His-N^{pro}-expressing PK-15 cell line (23) and parental PK-15 control cells were treated with poly(I:C) (100 µg/ml) in the presence or absence of porcine IFN-α (1000 IU/ml) and 18 hpt whole cell lysates were analysed by Western blot for cleaved caspase-3. As previously observed, poly(I:C) treatment of N^{pro} expressing cells induced lower levels of cleaved caspase-3 compared to treated PK-15 control cells (figure 3.13). When the N^{pro}-expressing PK-15 cell line received both poly(I:C) and IFN-α treatment, the level of cleaved caspase-3 increased, however, a much lower level of cleaved caspase-3 was still observed compared with PK-15 control cells treated with poly(I:C) alone (figure 3.13). Subsequent Western blot analyses did

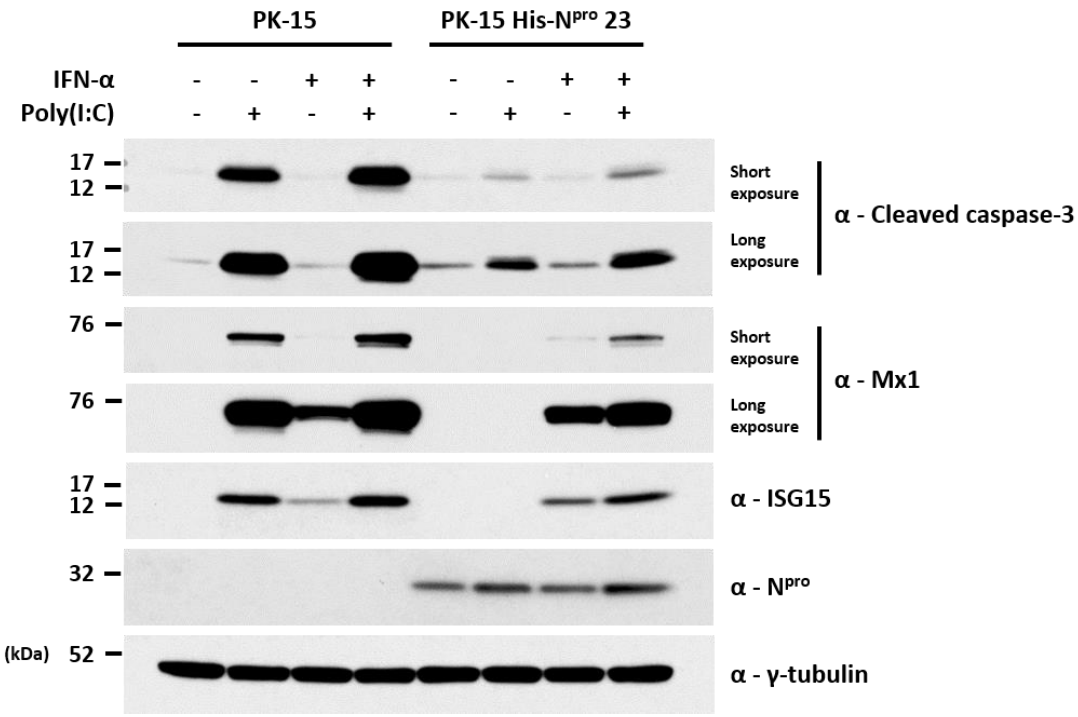

Figure 3.13: IFN-α treatment partially restores sensitivity of N^{pro}-expressing cells to poly(I:C)-mediated apoptosis. WT and His-N^{pro}-expressing PK-15 cells were seeded in 12-well plates and treated with 100 µg/ml poly(I:C) in the presence or absence of 1000 IU/ml porcine IFN-α. 18 hours post-treatment, whole cell lysates were prepared and analysed by Western blot using polyclonal Abs recognising ISG15 or N^{pro} and mAbs recognising cleaved caspase-3 or Mx1 as indicated. A mAb recognising γ-tubulin was used to determine relative protein concentrations.

not detect Mx1 and ISG15 expression by N^{pro}-expressing cells following poly(I:C) treatment, but did following combined poly(I:C)/IFN-α treatment. Additionally, while N^{pro} expression increased following poly(I:C) treatment, IFN-α treatment did not appear to have any effect on N^{pro} expression.

3.6. Discussion

The N^{pro} protein of CSFV and BVDV has been documented to antagonise poly(I:C)-mediated apoptosis by numerous groups, however the mechanism by which this occurs has not yet been determined (Schweizer and Peterhans, 2001, Ruggli *et al.*, 2003, Ruggli *et al.*, 2005, Johns *et al.*, 2010a, Jefferson *et al.*, 2014). Initially, a number of cell lines stably-expressing either untagged or tagged (His and GFP) N^{pro} available within the group were assessed for their capacity to antagonise poly(I:C)-mediated apoptosis – in turn, each was found to antagonise the process, confirming previous reports. While screening these cell lines, N^{pro} was unexpectedly found to antagonise SeV-mediated apoptosis, something which has not been reported in the literature. This was particularly interesting since to date the only experiments studying the ability of N^{pro} to antagonise apoptosis have utilised poly(I:C) applied to cell culture media – a treatment thought to trigger TLR3-mediated signalling (Alexopoulou *et al.*, 2001, Salaun *et al.*, 2006). SeV copy-back defective interfering (cbDI) RNA is widely reported to be an agonist of the RIG-I signalling pathway (Strahle *et al.*, 2006, Baum *et al.*, 2010, Kato *et al.*, 2011), suggesting that N^{pro} is capable of targeting pro-apoptotic signalling triggered by multiple pathways. In the present work, cleaved caspase-3 was employed as a terminal indicator of apoptosis. However, additional readouts could have also been employed such as annexin V-positive cell populations which can be identified via fluorescence-activated cell sorting (FACS) and also live cell imaging to confirm cell rounding and detachment at multiple timepoints post-treatment.

Lentivirus has a number of benefits – namely, the ability to infect a wide range of cells types including primary cells, and also the ability to permanently transduce cultured cells more efficiently than other techniques such as transfection and electroporation. By generating a lentivirus capable of transducing porcine cells with an expression cassette encoding EGFP-N^{pro}, it should now be possible to perform localisation studies on N^{pro} and also to study the effects

of N^{pro} expression in primary cells. Lentivirus-expressed EGFP-N^{pro} localises correctly in transduced cells (figure 3.6), which is in agreement with past literature (Doceul *et al.*, 2008, Li *et al.*, 2014), and still retains the ability to antagonise dsRNA-mediated apoptosis and IFN induction (figures 3.7 and 3.10), confirming its viability and usefulness for performing such studies. Unexpectidly, lentivirus-expressed EGFP-N^{pro} was observed to resolve as a triplet of bands with the 47 kDa middle band resolving at the fusion protein's predicted molecular MW (figures 3.8 and 3.10). The higher band might represent modified forms of the protein while the smallest band might correspond to cleavage products. While these observations might indicate potential limitations of lentiviral expression of EGFP-N^{pro}, they do not appear to have affected the protein's capacity to antagonise induction of poly(I:C) and SeV-mediated apoptosis.

Prior to the current work, it was not known whether the apoptosis antagonised by N^{pro} occurred in an IFN-dependent or IFN-independent manner. Since N^{pro} targets IRF3 for proteasomal degradation it was tempting to suggest that the source of this antagonism is the absence of IFN. Pharmacological inhibition of the JAK-STAT pathway using RXT and subsequent treatment of cells with porcine IFN-α revealed the apoptosis mediated by poly(I:C), but not SeV, to be amplified while IFN-α alone appeared to cause no detectable caspase-3 cleavage. Upon activation, caspase-3 targets many proteins for cleavage, however ISGs are themselves not reported to be targeted, explaining why addition of IFN to cells treated with an apoptotic agonist such as poly(I:C) appears to have an effect. Ultimately, the type I IFN signalling response is required for the upregulation of a diverse range of ISGs, a number of which are pro-apoptotic. In light of this, it is likely that components of the TLR3 signalling pathway (but not the RIG-I-dependent pathway) are upregulated by type I IFN, thus explaining the observed amplification of caspase-3 cleavage. Shaw *et al.* reported upregulation of TLR3, caspase-8, Noxa and TRAIL expression in *ex vivo* porcine skin fibroblast cultures following IFN treatment (Shaw *et al.*, 2017), while Renson *et al.* found elements of the Fas and TRAIL signalling

pathways to be upregulated in uninfected bystander peripheral blood mononuclear cells (PBMC) during *in vivo* infection with a related Pestivirus, BVDV (Renson *et al.*, 2010). To test this theory, poly(I:C)-treated N^{pro}-expressing cells were additionally treated with IFN-α and this treatment did marginally recover induction of caspase-3 cleavage, suggesting N^{pro}'s anti-apoptotic potential does not rest entirely in its ability to antagonise transcriptional upregulation of IFN. Direct amplification of poly(I:C)-mediated apoptosis by IFN-α has been previously described (Kaiser *et al.*, 2004), however the capacity of type I IFN to modulate the innate apoptotic response likely varies depending on tissue and cell type. SeV encodes C-protein, an antagonist of STAT1 phosphorylation, which likely explains the apparent absence of ISG upregulation or subsequent effect from the RXT treatment (Garcin *et al.*, 2002).

Together, these experiments have further confirmed N^{pro}'s anti-apoptotic potential in cell culture whilst also providing insight into additional pathways of apoptosis that might also be antagonised. Furthermore, tools have been developed which will allow present and future studies to explore the functions and localisation of N^{pro} not only in established cell lines but also primary cells too. The following chapters detail the elucidation of the pathways of apoptosis antagonised by N^{pro} and further explore the pivotal role played by IRF3.

4. Targeted CRISPR knockout of innate immune and apoptotic genes to identify pathways antagonised by N^{pro}

4.1. Introduction

When stably expressed in cell-culture, N^{pro} antagonises the induction of apoptosis triggered by two agonists, poly(I:C) and Sendai virus. In order to elucidate the mechanism used by N^{pro} to antagonise the induction of apoptosis, it was first necessary to identify the cell signalling pathways through which these two agonists act in a cell line susceptible and relevant to CSFV infection. The PK-15 porcine kidney cell line was selected as it is routinely used for research on CSFV and has functional type I IFN and apoptotic responses. To functionally characterise the two agonist pathways in PK-15 cells, methods were identified that could be used to reduce the expression of target genes; these included methodologies for knocking-down or knocking-out target gene expression.

Both shRNA and siRNA-knockdown utilise the mammalian cell's own RNAi machinery (Argo-2, Dicer) to cleave target mRNA sequences at the RNA-induced silencing complex (RISC). While the ability to deliver shRNA by a viral vector such as lentivirus confers some improvement to cell delivery, overall knock-down efficiency can be limited by protein half-life and there is the chance of off-target binding and induction of innate responses such as IFN (Bridge *et al.*, 2003).

Clustered regularly interspaced short palindromic repeats (CRISPR), identified in numerous species of bacteria, comprise an adaptive immune system that confers protection against invading DNA viruses (bacteriophage) (Mojica *et al.*, 2005, Barrangou *et al.*, 2007). This system was later adapted and developed to allow the editing of eukaryotic genomes, enabling the manipulation and deletion of entire genes (Cong *et al.*, 2013, Ran *et al.*, 2013b). Briefly, Cas9

nuclease protein (commonly of *Streptococcus pyogenes*) associated with short sequences of "guide RNA" (gRNA) binds to corresponding segments of genomic DNA upstream of an NGG protospacer-adjacent motif (PAM), enabling the formation of Cas9-mediated double-stranded breaks (DSBs). DSBs are subsequently repaired by one of two mechanisms. One of these, non-homologous end-joining (NHEJ), is an error-prone process during which insertion or deletions (termed indels) form – these can result in frameshift mutations and total gene knockout by introduction of a premature stop codon. Another mechanism is homology-directed repair (HDR), a process which relies upon Rad51 proteins which direct genomic recombination with an exogenous template. Since wild-type Cas9 only relies upon a single PAM site and target sequence in order to introduce DSBs, off-target binding and activity is possible when there is homology elsewhere in the genome. Further to this, studies have demonstrated that Cas9 can tolerate multiple mismatches between gRNA and target sequence (Fu *et al.*, 2013, Hsu *et al.*, 2013). In response, the D10A mutant of Cas9 was developed (Cas9n). In its native form, Cas9 has two independent single-stranded nicking activities and the D10A change inactivates one of these, converting the enzyme into one with single-stranded nicking activity. By targeting two independent "nicking" nuclease molecules to two closely linked sites on opposite strands using a pair of gRNAs the resulting nicks are close enough as to effectively generate a double-stranded break which is repaired by HDR (Cong *et al.*, 2013, Ran *et al.*, 2013a). Unopposed gRNA single-stranded nicks in genomic DNA are repaired with very high efficiency, meaning that off-target effects are minimal. This iteration of CRISPR is thought to improve specificity by up to 1000-fold (Dianov and Hübscher, 2013). Indels introduced during the repair of cut sequence can introduce frameshift mutations and therefore premature stop codons. Upon translation, this brings about nonsense-mediated decay of the remaining transcript, effectively "knocking out" the protein encoded by the target gene (Popp and Maquat, 2016).

This system has clear advantages over siRNA and shRNA knockdown, in effect enabling the complete elimination of target proteins as opposed to simply reducing their levels of

expression. In turn, this allows clearer conclusions to be drawn when using resulting cell lines experimentally. Therefore, double-nickase CRISPR was chosen as the method to be used in the elucidation of poly(I:C) and Sendai virus-mediated pathways of apoptosis antagonised by N^{pro}.

4.2. Guide RNA (gRNA) target selection and design

As discussed in 1.3.3.2, the same pathways that are responsible for the induction of IFN in response to dsRNA have also been implicated in the induction of apoptosis in response to agonists of dsRNA signalling such as poly(I:C) and Sendai virus. TLR3 and RIG-I were therefore selected as targets for CRISPR knockout due to their established roles in the sensing of intracellular and extracellular dsRNA (discussed in 1.2.1.1 and 1.2.1.2). IRF3 transduces upstream signalling from TLR3 and RIG-I and was also chosen for knockout. Suitable target sequences were identified in coding exons of each target gene using an online service hosted by Zhang Lab (http://crispr.mit.edu/) which, at the time of writing, was no longer available (figure 4.1, A). When possible, target sequences were chosen that disrupted the coding sequence of genes in early codons - this was done to reduce the possibility of generating truncated gene products with wild type or aberrant functions. Suitable target sequences were identified in the first coding exons of TLR3 and IRF3 however the 10th coding exon of RIG-I was the first to contain suitable sequences. These target guide sequences were subsequently cloned into the Cas9n plasmid vectors pX461 and pX462, which encode the green fluorescent protein (GFP) and puromycin resistance markers respectively (see 2.18.1, table 2.10 and table 2.1). The resulting plasmids were then transfected into wild-type PK-15 cells and individual cell lines were selected for screening as detailed in 2.18.2 and 2.1.2.4 (figure 4.1, B).

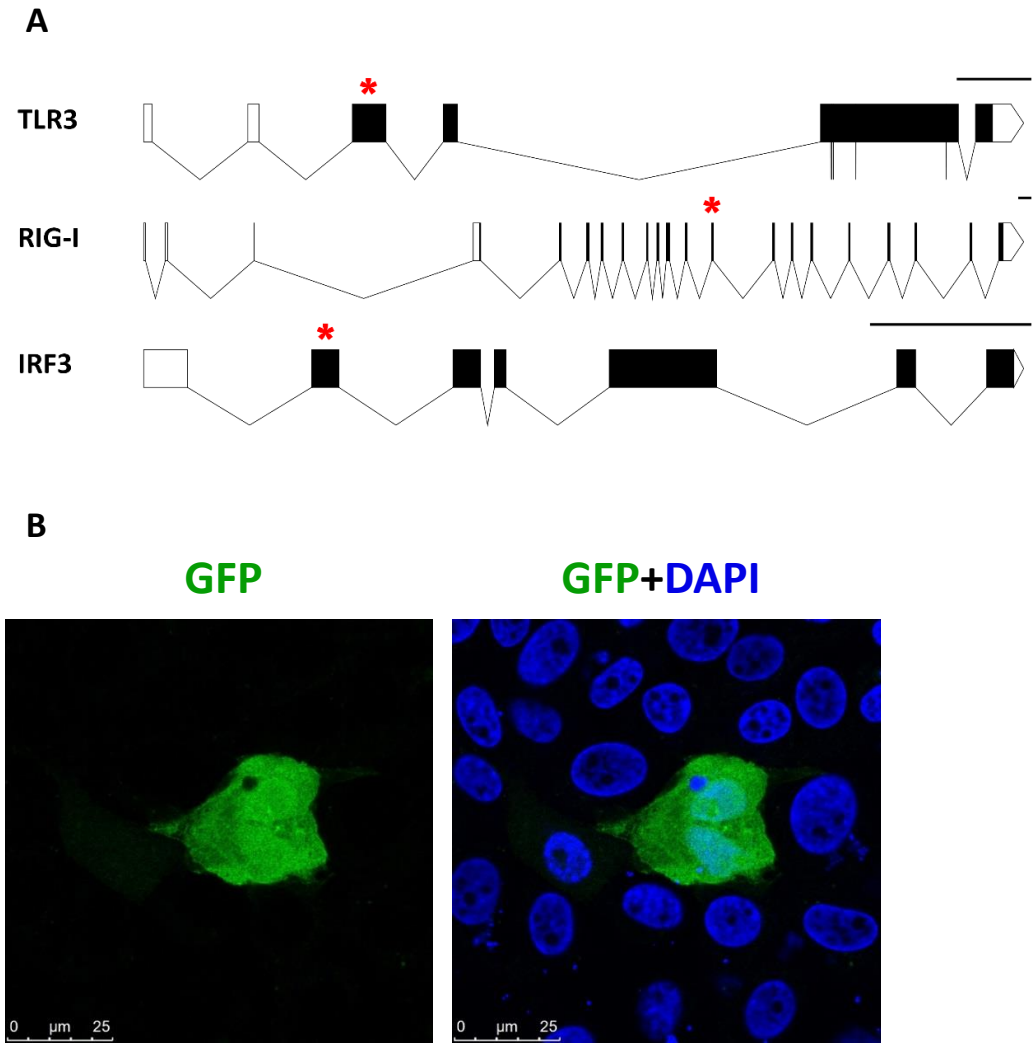

Figure 4.1: Generation of CRISPR-Cas9 knockout PK-15 cell lines. (A) Introns, coding exons and 5'/3' UTRs for each target gene were identified using Ensembl's transcript-display (http://www.ensembl.org/Sus_scrofa/Info/Index) and formatted using Nikhil Bhatla's Exon-Intron Graphic Maker tool (http://wormweb.org/exonintron). Clear shapes correspond to UTRs and filled shapes correspond to coding exons. * (red) indicates coding exons targeted by gRNA pairs; introns/exons are to scale. Scale bars represent 1000 bp. (B) Representative confocal images of wild-type PK-15 cells co-transfected with gRNA-encoding plasmids pX461 (GFP) and pX462 (puromycin) prior to antibiotic selection.

4.3. Generation of TLR3 knockout cell lines

4.3.1. Identification of TLR3 knockout cell lines by Western blot

Prior to the screening of isolated colonies of possible TLR3 knockout PK-15 cells, an antibody reactive against porcine TLR3 first had to be identified. However, screening of multiple antibodies yielded none that were reactive.

4.3.2. Identification of TLR3 knockout cell lines by PCR and Sanger sequencing

TLR3 colonies were selected for genomic DNA (gDNA) extraction, PCR amplification and Sanger sequencing. In the absence of Western blot data that would have indicated putative knockouts, a larger selection of colonies were selected for screening by this approach.

To confirm the TLR3 gene had been targeted, gDNA was extracted from non-edited PK-15 and edited cell lines as detailed in 2.17. One of two pairs of primers were used to amplify a region of the TLR3 gene (~1 kb) within the first exon that contained both gRNA target sites; primer pair one (poTLR3 fw.2, poTLR3 rev.3; table 2.12) was used to amplify gDNA extracted from edited cell lines 2, 4, 8, 9 and primer pair two (poTLR3 fw.1, poTLR3 rev.2; table 2.12) for edited cell lines 3, 6, 10, 11. Both sets of primers were used to amplify gDNA extracted from non-edited PK-15 cells. A modified version of the PCR program detailed in 2.8.1 was used: reactions were denatured at 95°C for 30s, annealed at 57°C for 30 seconds and extended at 72°C for 50 seconds for a total of 30 cycles. Each reaction was analysed by agarose gel electrophoresis as detailed in 2.10 (figure 4.2). A single band close to the expected size of the PCR product (1 kb) was observed for the non-edited PK-15 cells (positive control). In contrast, single marginally smaller bands were observed for cell lines 3, 4, 8 and 9, suggesting the presence of small indels. The band corresponding to cell line 6 ran considerably higher (1.5kb) than that observed for non-edited PK-15 cells, indicative of a large insertion within or between

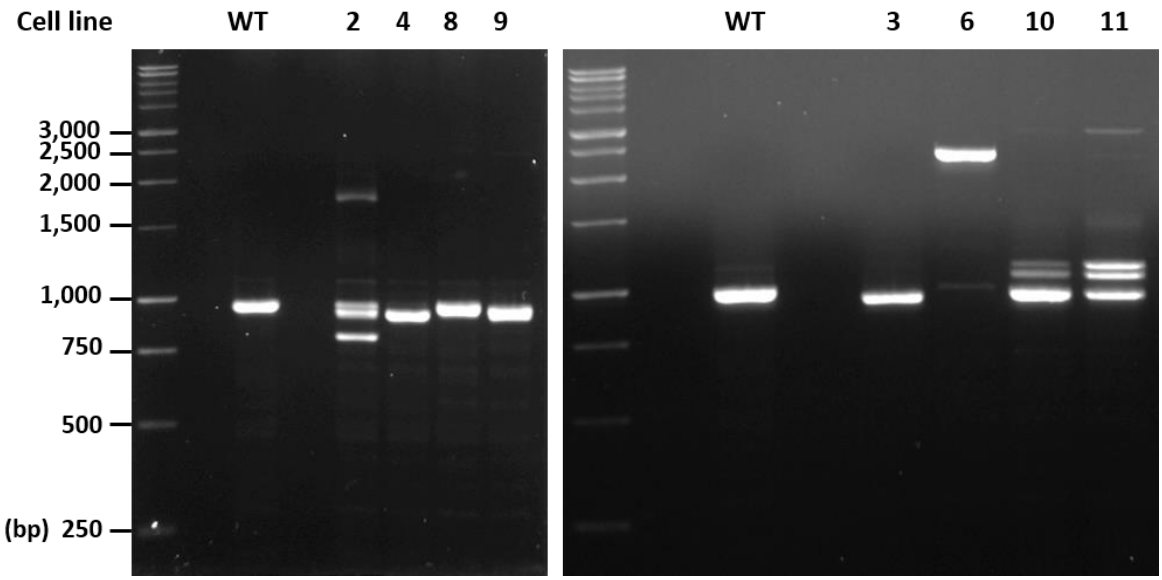

Figure 4.2: PCR amplification of TLR3 gene edited cell lines reveals putative indels. gDNA was extracted from non-edited PK-15 cells and PK-15 cell lines (2, 3, 4, 6, 8, 9, 10 and 11) gene edited for TLR3. One of two primer pairs was then used to amplify a region (~1 kb) of the TLR3 gene that contained both gRNA target sites. Primer pair one (poTLR3 fw.2, poTLR3 rev.3; table 2.12) was used to amplify gDNA extracted from edited cell lines 2, 4, 8, 9 (left) and primer pair two (poTLR3 fw.1, poTLR3 rev.2; table 2.12) for edited cell lines 3, 6, 10, 11 (right). PCR products were analysed by agarose gel electrophoresis. 1 kb DNA ladder values are indicated in bp.

the gRNA target sites. Cell lines 2, 10 and 11 gave multiple bands of considerable but varied intensity, suggesting indel heterozygosity.

Bands from the lanes corresponding to cell lines 3, 4 and 6 were subsequently gel-purified and sequenced as detailed in 2.10 and 2.8.3 using a selection of primers (poTLR3 fw.2, poTLR3 rev.2, poTLR3 rev.3; table 2.12) in order to obtain full coverage across the gRNA target sites. In order to maximise the quantity of template present in each sequencing reaction, additional gel-purified band (6 µl) was added in place of the dH_2O that would normally be added when sequencing plasmid DNA. Chromatogram data from each reaction was analysed in Chromas Lite software and the respective FASTA sequences aligned with each other and a reference genomic porcine TLR3 sequence (NC_010457.5:46966262-46977774) using MEGA7 software. The resulting alignments were then reformatted using EMBL's MView software (http://www.ebi.ac.uk/Tools/msa/mview/; figure 4.3) (Brown *et al.*, 1998). Aligned sequences from cell lines 3 and 4 each contained indels of 32 bp and 34 bp respectively. Both indels had

extended upstream of the first target sequence (figure 4.3). As expected, the WT sequence aligned fully with the chosen reference sequence.

When aligned with the same reference sequence, it was discovered that the roughly 1.5 kb insert present in cell line 6 was inserted at the 5' guide gRNA target site and is comprised of 3 discrete sets of sequence. Using NCBI BLAST software (https://blast.ncbi.nlm.nih.gov/Blast.cgi) (Altschul *et al.*, 1990), 1,276 bp of insert sequence was identified as partial Cas9n sequence from either the pX461 (Addgene plasmid #48140 pSpCas9n(BB)-2A-GFP) or pX462 vector (Addgene plasmid #62987 pSpCas9n(BB)-2A-Puro) that had presumably been inserted by recombination (figure 4.4). The remaining 30 bp sequence not aligning with vector was analysed by BLAST software, identifying a 22 bp duplicated and recombined TLR3 sequence from a segment downstream of the 3' gRNA target site; BLAST was unable to determine the identity or origin of the remaining 8 bp sequence.

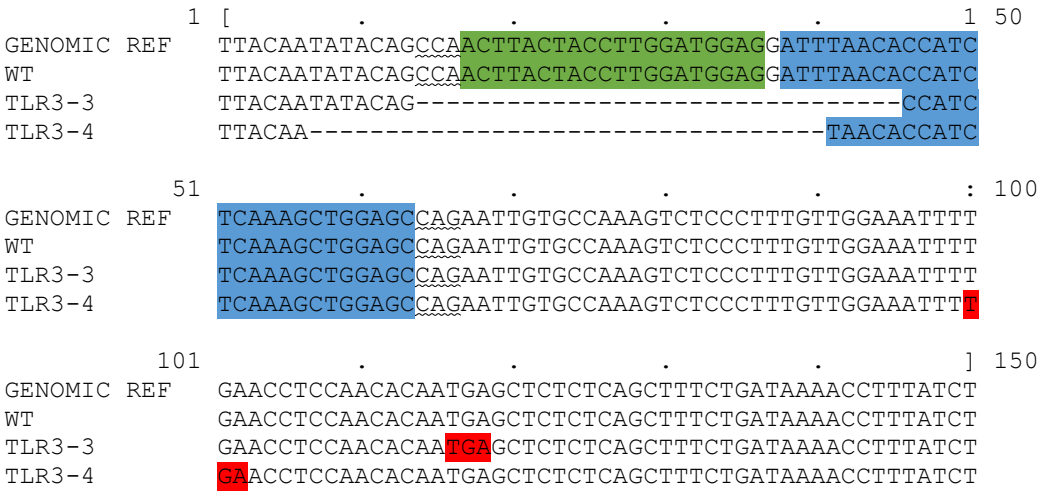

Figure 4.3: Alignment of nucleotide sequences determined for TLR3 gene edited cell lines 3 and 4 reveals indels within the first coding exon. TLR3 sequences obtained using gDNA extracted from non-edited PK-15 cells (WT) and PK-15 cell lines (3 and 4) gene edited for TLR3 were aligned with the gDNA sequence for porcine TLR3 (NC_010457.5:46966262-46977774) using MEGA7 software. Small indels of 32 bp and 34 bp were identified in the sequences determined for cell lines 3 and 4 respectively. PAM sites (waves, underlined) and the sequence of the first (green) and second (blue) gRNA targets are indicated as are premature stop codons (red).

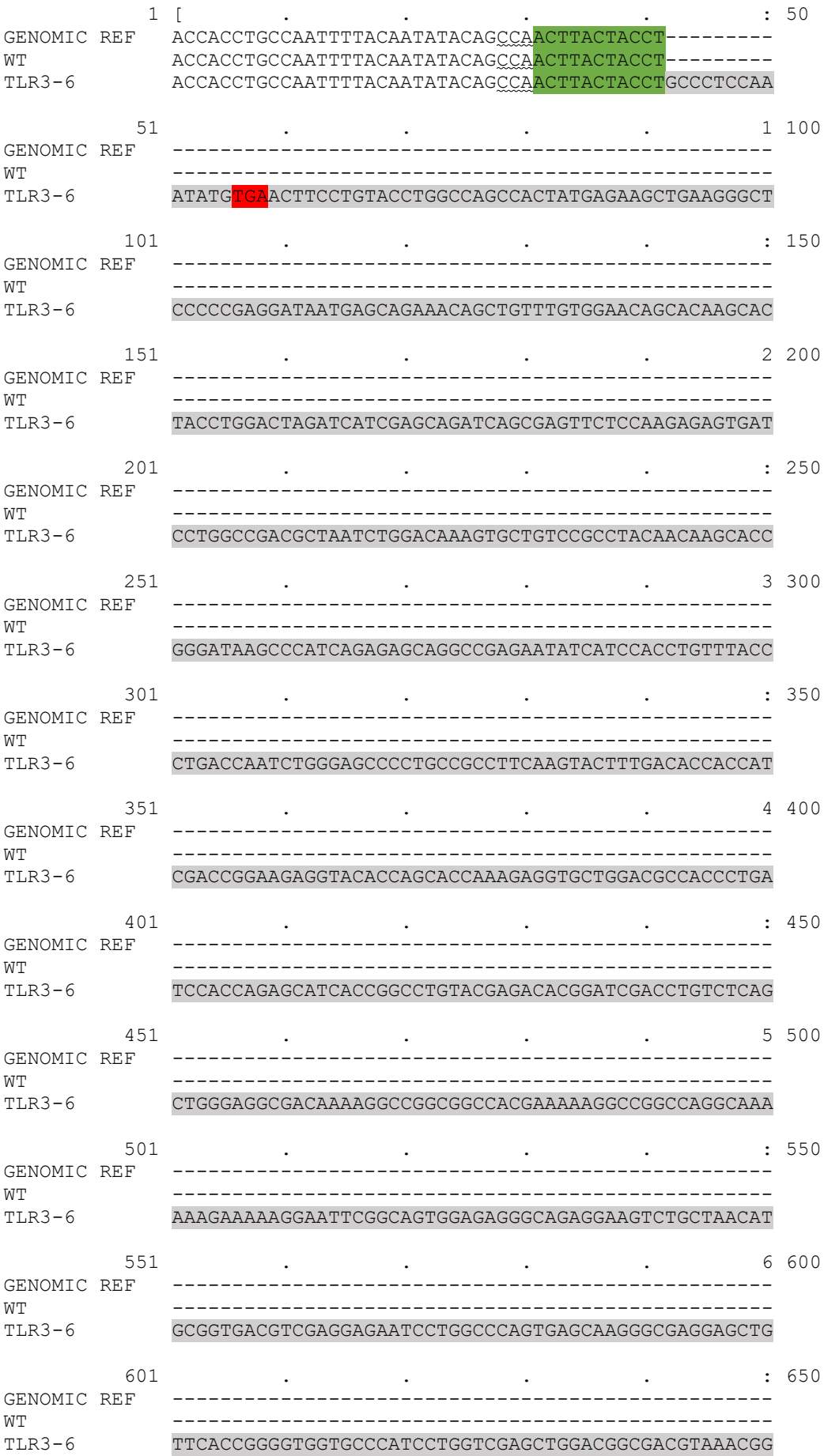
1 [. . . . : 50
GENOMIC REF ACCACCTGCCAATTTTACAATATACAGCCAACTTACTACCT---------
WT ACCACCTGCCAATTTTACAATATACAGCCAACTTACTACCT---------
TLR3-6 ACCACCTGCCAATTTTACAATATACAGCCAACTTACTACCTGCCCTCCAA
51 . . . . 1 100
GENOMIC REF ---------
WT ---------
TLR3-6 ATATGTGAACTTCCTGTACCTGGCCAGCCACTATGAGAAGCTGAAGGGCT
101 . . . . : 150
GENOMIC REF ---------
WT ---------
TLR3-6 CCCCCGAGGATAATGAGCAGAAACAGCTGTTTGTGGAACAGCACAAGCAC
151 . . . . 2 200
GENOMIC REF ---------
WT ---------
TLR3-6 TACCTGGACTAGATCATCGAGCAGATCAGCGAGTTCTCCAAGAGAGTGAT
201 . . . . : 250
GENOMIC REF ---------
WT ---------
TLR3-6 CCTGGCCGACGCTAATCTGGACAAAGTGCTGTCCGCCTACAACAAGCACC
251 . . . . 3 300
GENOMIC REF ---------
WT ---------
TLR3-6 GGGATAAGCCCATCAGAGAGCAGGCCGAGAATATCATCCACCTGTTTACC
301 . . . . : 350
GENOMIC REF ---------
WT ---------
TLR3-6 CTGACCAATCTGGGAGCCCCTGCCGCCTTCAAGTACTTTGACACCACCAT
351 . . . . 4 400
GENOMIC REF ---------
WT ---------
TLR3-6 CGACCGGAAGAGGTACACCAGCACCAAAGAGGTGCTGGACGCCACCCTGA
401 . . . . : 450
GENOMIC REF ---------
WT ---------
TLR3-6 TCCACCAGAGCATCACCGGCCTGTACGAGACACGGATCGACCTGTCTCAG
451 . . . . 5 500
GENOMIC REF ---------
WT ---------
TLR3-6 CTGGGAGGCGACAAAAGGCCGGCGGCCACGAAAAAGGCCGGCCAGGCAAA
501 . . . . : 550
GENOMIC REF ---------
WT ---------
TLR3-6 AAAGAAAAAGGAATTCGGCAGTGGAGAGGGCAGAGGAAGTCTGCTAACAT
551 . . . . 6 600
GENOMIC REF ---------
WT ---------
TLR3-6 GCGGTGACGTCGAGGAGAATCCTGGCCCAGTGAGCAAGGGCGAGGAGCTG
601 . . . . : 650
GENOMIC REF ---------
WT ---------
TLR3-6 TTCACCGGGGTGGTGCCCATCCTGGTCGAGCTGGACGGCGACGTAAACGG

```
          651         .         .         .         7 700
GENOMIC REF   --------------------------------------------------
WT            --------------------------------------------------
TLR3-6        CCACAAGTTCAGCGTGTCCGGCGAGGGCGAGGGCGATGCCACCTACGGCA

          701         .         .         .         : 750
GENOMIC REF   --------------------------------------------------
WT            --------------------------------------------------
TLR3-6        AGCTGACCCTGAAGTTCATCTGCACCACCGGCAAGCTGCCCGTGCCCTGG

          751         .         .         .         8 800
GENOMIC REF   --------------------------------------------------
WT            --------------------------------------------------
TLR3-6        CCCACCCTCGTGACCACCCTGACCTACGGCGTGCAGTGCTTCAGCCGCTA

          801         .         .         .         : 850
GENOMIC REF   --------------------------------------------------
WT            --------------------------------------------------
TLR3-6        CCCCGACCACATGAAGCAGCACGACTTCTTCAAGTCCGCCATGCCCGAAG

          851         .         .         .         9 900
GENOMIC REF   --------------------------------------------------
WT            --------------------------------------------------
TLR3-6        GCTACGTCCAGGAGCGCACCATCTTCTTCAAGGACGACGGCAACTACAAG

          901         .         .         .         : 950
GENOMIC REF   --------------------------------------------------
WT            --------------------------------------------------
TLR3-6        ACCCGCGCCGAGGTGAAGTTCGAGGGCGACACCCTGGTGAACCGCATCGA

          951         .         .         .         0 1000
GENOMIC REF   --------------------------------------------------
WT            --------------------------------------------------
Tlr3-6        GCTGAAGGGCATCGACTTCAAGGAGGACGGCAACATCCTGGGGCACAAGC

         1001         .         .         .         : 1050
GENOMIC REF   --------------------------------------------------
WT            --------------------------------------------------
TLR3-6        TGGAGTACAACTACAACAGCCACAACGTCTATATCATGGCCGACAAGCAG

         1051         .         .         .         1 1100
GENOMIC REF   --------------------------------------------------
WT            --------------------------------------------------
TLR3-6        AAGAACGGCATCAAGGTGAACTTCAAGATCCGCCACAACATCGAGGACGG

         1101         .         .         .         : 1150
GENOMIC REF   --------------------------------------------------
WT            --------------------------------------------------
TLR3-6        CAGCGTGCAGCTCGCCGACCACTACCAGCAGAACACCCCCATCGGCGACG

         1151         .         .         .         2 1200
GENOMIC REF   --------------------------------------------------
WT            --------------------------------------------------
TLR3-6        GCCCCGTGCTGCTGCCCGACAACCACTACCTGAGCACCCAGTCCGCCCTG

         1201         .         .         .         : 1250
GENOMIC REF   --------------------------------------------------
WT            --------------------------------------------------
TLR3-6        AGCAAAGACCCCAACGAGAAGCGCGATCACATGGTCCTGCTGGAGTTCGT
```

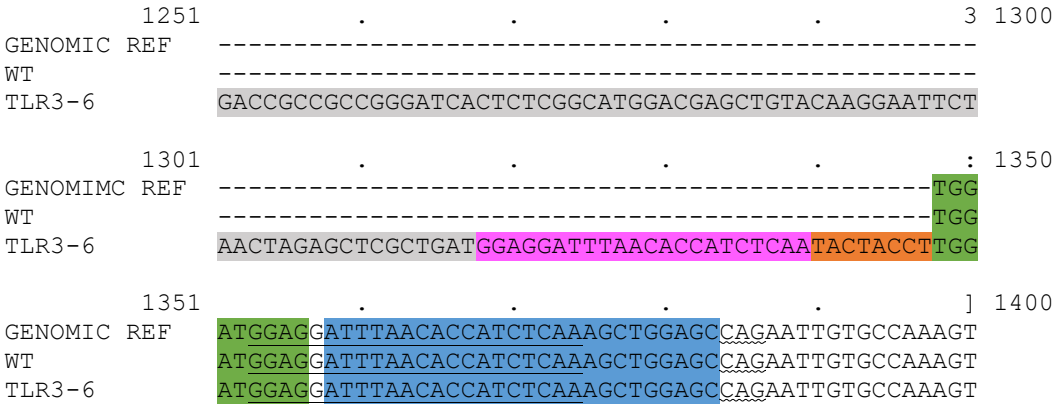

Figure 4.4: Alignment of nucleotide sequence determined for TLR3 gene edited cell line 6 reveals a large insertion within the first coding exon. Sequences obtained from cell line 6 were also aligned with a reference sequence for porcine TLR3 (NC_010457.5:46966262-46977774) in MEGA7. A large insertion was identified upstream of the second gRNA target site (blue) and within the first (green) which aligned with TLR3 sequence (pink and underlined) and sequence from either the px461 or px462 Cas9n vector (grey); the identity of an 8 bp segment of the insert was not determined (orange). PAM sites (waves, underlined) and a premature stop codon (red) are indicated.

A

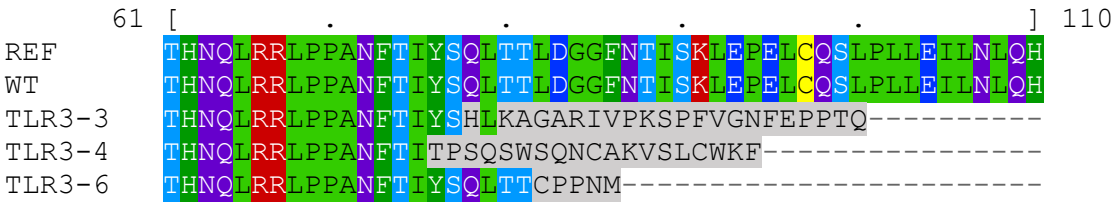

B

Cell line	Amino acid residue count	Predicted molecular weight (kDa)
TLR3-3	99	11.32
TLR3-4	92	10.78
TLR3-6	85	9.83

Figure 4.5: Amino acid alignment reveals TLR3 gene edited cell lines 3, 4 and 6 contain premature stop codons. (A) The TLR3 sequences shown in Figures *** and *** were translated and then aligned with reference TLR3 sequence (NP_001090913.1) using MEGA7 software. Truncated protein products were identified for all the TLR3 gene edited cell lines (3, 4 and 6). Colours relate to the physiochemical properties of each amino acid while grey indicates inserted or non-homologous sequence. (B) Bioinformatics.org's protein molecular weight prediction tool was used to predict the molecular weights of the translated sequences.

The gDNA sequences from TLR3 cell lines 3, 4 and 6 were then translated using ExPASy's Translate tool software (https://web.expasy.org/translate/) and aligned using MEGA7 software with a reference amino acid sequence for porcine TLR3 (NP_001090913.1) (figure 4.5, A). As premature stop codons were introduced in each instance (figures 4.3 and 4.4, red), translated sequences were truncated and the remaining sequences were predicted to generate proteins of ~10 kDa, considerably smaller than predicted molecular weight of TLR3 (104 kDa) (figure 4.5, B).

4.4. Generation of RIG-I knockout cell lines

4.4.1. Identification of RIG-I knockout cell lines by Western blot

As with the TLR3 knockout cells, an antibody reactive against porcine RIG-I first had to be identified in order to screen lysates from each colony by Western blot for presence or absence of the protein. Whole cell lysates from IFN-α-treated PK-15 cells were used to screen a sample of sc-376845 mAb (Santa Cruz) for its ability to detect endogenous porcine RIG-I by Western blot; lysates from IFN-α-treated HEK 293T cells were employed as a positive control. In the lanes corresponding to PK-15 cells, a single band was at detected at ~100 kDa following IFN-α treatment. This is close to the 108 kDa predicted by the ExPASy molecular weight prediction software (figure 4.6), however, a band of the same size was also observed for the HEK 293T cells. Additional bands, both larger (~115-120 kDa) and smaller (52 kDa), were present for the HEK 293T cells but were considerably weaker in intensity than the ~100 kDa band. RIG-I (encoded by the DDX58 gene) is known to be an ISG and is therefore upregulated in response to IFN – indeed, Shaw *et al.* observed a 7.8 $\log_2$ fold change in expression (Shaw *et al.*, 2017). Therefore, the ~100 kDa band that appears to increase in intensity following treatment was presumed to correspond to RIG-I. The additional bands detected in the lanes corresponding to HEK 293T lysates are possibly truncated or modified forms of the protein or are nonspecific.

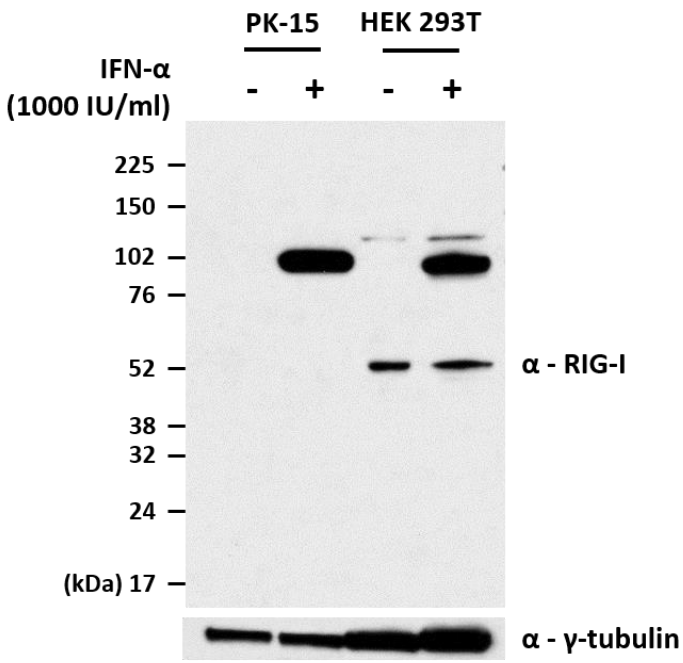

Figure 4.6: Identification of an antibody for detection of porcine RIG-I by Western blot. WT PK-15 and HEK 293T cells were treated with 1000 IU/ml IFN-α for 18 hours and whole cell lysates harvested and analysed by Western blot using a mAb (Santa Cruz, #sc-376845) that recognises human RIG-I; sc376845 was used at 1/200. A mAb recognising γ-tubulin (Sigma, #T6557) was used to determine relative protein concentrations.

Fresh whole cell lysates were prepared from IFN-α-treated putative RIG-I knockout cell lines and analysed by Western blot alongside control lysates prepared from treated and untreated wild-type PK-15 cells (figure 4.7). As with the initial screening of sc-376845, the band thought to correspond to porcine RIG-I ran as previously observed, however on this occasion a faint band was visible above it in the lane corresponding to untreated, unstimulated wild-type PK-15 cells. In each lane corresponding to a candidate RIG-I knockout cell line, the intense band presumed to correspond to RIG-I was no longer detectable, although faint bands were observed for cell lines 15 and 17. Lower bands were visible in the lanes corresponding to cell lines 10 and 14; these bands possibly correspond to truncated RIG-I proteins whereby coding sequence had been cut and edited but not knocked out of frame. Consequently, cell lines 3, 6 and 10 were selected for further screening.

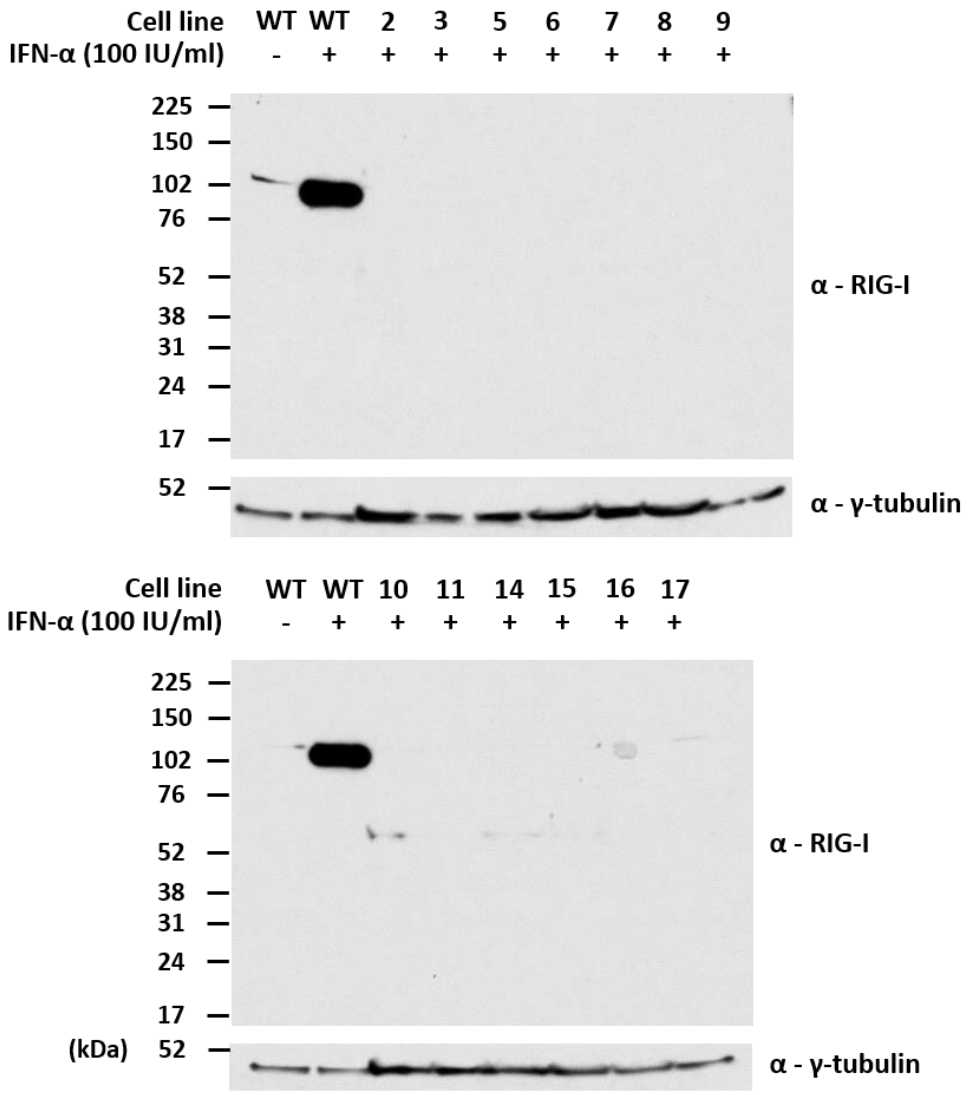

Figure 4.7: Identification of putative RIG-I knockout cell lines by Western blot. PK-15 cells (WT) and putative RIG-I knockout PK-15 cell lines (2, 3, 5, 6, 7, 8, 9, 10, 11, 14, 15, 16, 17) were seeded in 12-well plates and treated with IFN-α at the indicated concentration. 18 hours post-treatment, whole cell lysates were prepared and analysed by Western blotting using a mAb recognising RIG-I (Santa Cruz, #sc-376845) as indicated. A mAb recognising γ-tubulin (Sigma, #T6557) was used to determine relative protein concentrations. Cell lines 3, 6 and 10 were selected for further screening.

4.4.2. Identification of RIG-I knockout cell lines by PCR and Sanger sequencing

Putative RIG-I knockout cell lines selected for further screening were subjected to genomic DNA extraction, PCR amplification of porcine RIG-I and Sanger sequencing as detailed in 2.17, 2.8.1 and 2.8.3. DNA extracted from non-edited PK-15 cells was used as a positive control.

Briefly, upon extraction a single-pair of primers (poRIG-I fw.2, poRIG-I rev.2; table 2.12) were used to amplify a 750 bp fragment encompassing both gRNA target sites within the 10th coding exon of porcine RIG-I using the PCR program detailed in 4.3.2. Analysis of the amplification products by agarose gel electrophoresis revealed a single band of the expected size (750 bp) in the control PK-15 lane (figure 4.8). Comparatively larger bands were observed for cell line 2 (~850 bp) and cell line 3 (~2,000 bp), suggesting large insertions between or close to the gRNA target sites (figure 4.8). Cell lines 6 and 10 exhibited bands of similar size to the control PK-15 cells. Unexpectedly, no bands were detected from sequence amplified from cell lines 5 and 14, suggesting large deletions had occurred, potentially destroying the target PCR primer sites. Since a single intense PCR product was observed for each sample, deletions and insertions were likely homozygous.

The single bands from each lane corresponding to cell lines 3, 6 and 10 were subsequently gel-purified and sequenced alongside non-edited PK-15 sequence extracted from the same gel as detailed in 2.10 and 2.8.3. A number of primers (poRIG-I fw.2, poRIG-I rev.1, poRIG-I rev.2;

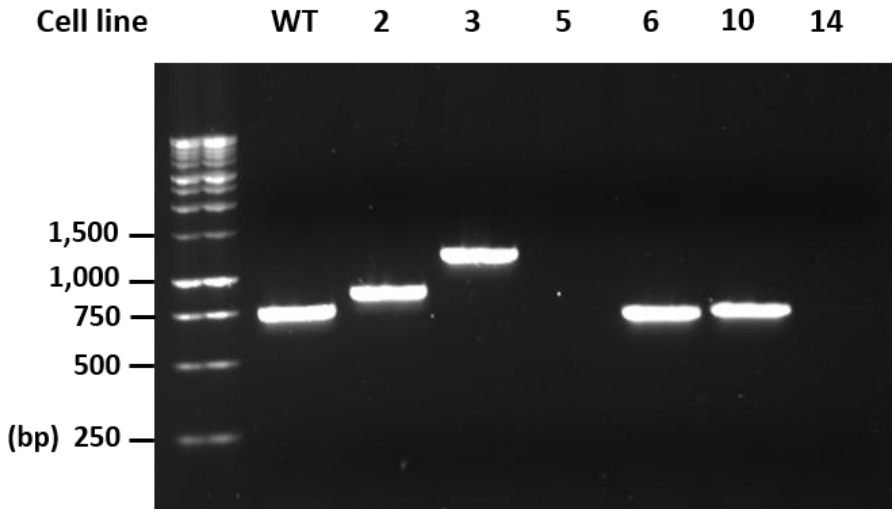

Figure 4.8: PCR amplification of RIG-I gene edited PK-15 cell lines reveals putative indels. gDNA was extracted from non-edited PK-15 cells (WT) and PK-15 cell lines (lines 2, 3, 5, 6, 10 and 14) gene edited for RIG-I. PCR primers (poRIG-I fw.2, poRIG-I rev.2; table 2.12) were then used to amplify a region (750 bp) containing both gRNA target sites within the RIG-I gene. PCR products were analysed by agarose gel electrophoresis. 1 kb DNA ladder values correspond to length in bp.

table 2.12) were utilised in order to obtain full coverage of the sequence within and flanking each gRNA target site. Obtained sequences were then aligned with a reference porcine RIG-I gDNA sequence (NC_010452.4:33891720-33976151) using MEGA7 software.

Deletions of 24 bp and 3 bp were identified in the RIG-I cell line 6 and 10 sequences respectively. The RIG-I cell line 6 indel spanned both gRNA target sites while the RIG-I cell line 10 indel is within the 5' gRNA target site (figure 4.9). Since both of these deletions are multiples of three, the respective coding sequences should remain in-frame and therefore the remainder of the transcript should be translated in its entirety. Alignment of the RIG-I sequence determined for cell line 3 revealed the presence of a large insert of 456 bp adjacent to and immediately upstream of the 5' gRNA target site (figure 4.10). Sequence analysis using BLAST software revealed the majority of inserted sequence (452 bp) to be a reverse-complemented portion of the ampicillin resistance gene (AmpR) from either the px461 or px462 Cas9n vector. However, it was not possible to determine the origin or identity of the remaining 4 bp (figure 4.10, orange). In addition to this insert a 17 bp insertion was also identified, spanning from the 5' gRNA target site into the 3' site (figure 4.10, grey) followed by a 10 bp deletion (figure 4.10). The 17 bp insertion corresponded to sequence from the AmpR gene of the expression vector. Upon translation using ExPASy it was noted that a premature stop codon (TAA) had been introduced, leaving an ORF of only 16 bp of the AmpR gene (figure 32, red). Overall, these indels are in agreement with the alterations in band sizes seen in figure 4.8.

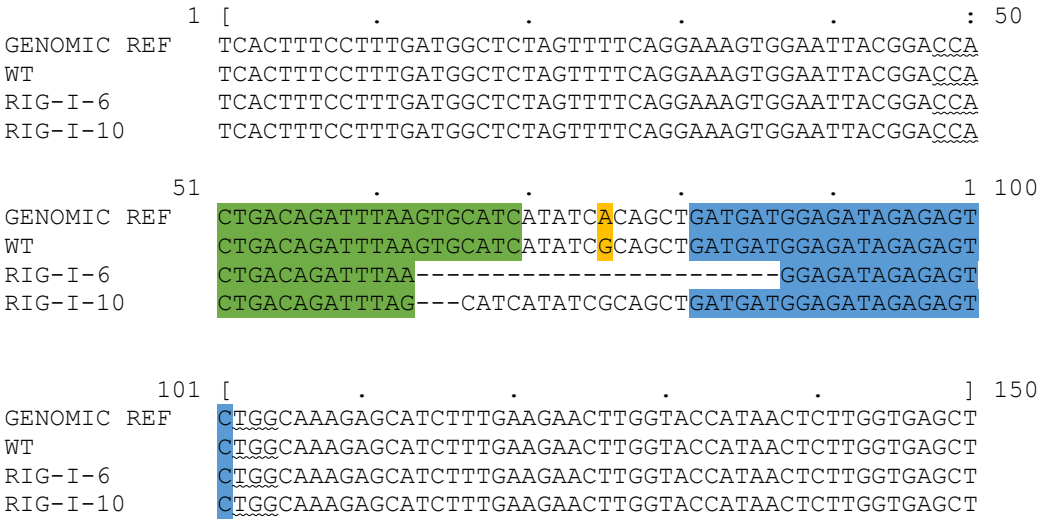

Figure 4.9: Alignment of nucleotide sequence determined for RIG-I gene edited cell lines 6 and 10 reveals indels within the 10th coding exon. Sequenced PCR products spanning the gRNA sites within the 10th coding exon of RIG-I were aligned with each other and a reference sequence (NC_010452.4:33891720-33976151) for porcine RIG-I using MEGA7 software. Small deletions of 24 bp and 3 bp were identified in the sequences determined for cell lines 6 and 10 respectively. A single synonymous mutation was identified in the non-edited PK-15 (WT) sequence (yellow). PAM sites (waves, underlined) and the sequence of the first (green) and second (blue) gRNA targets are indicated.

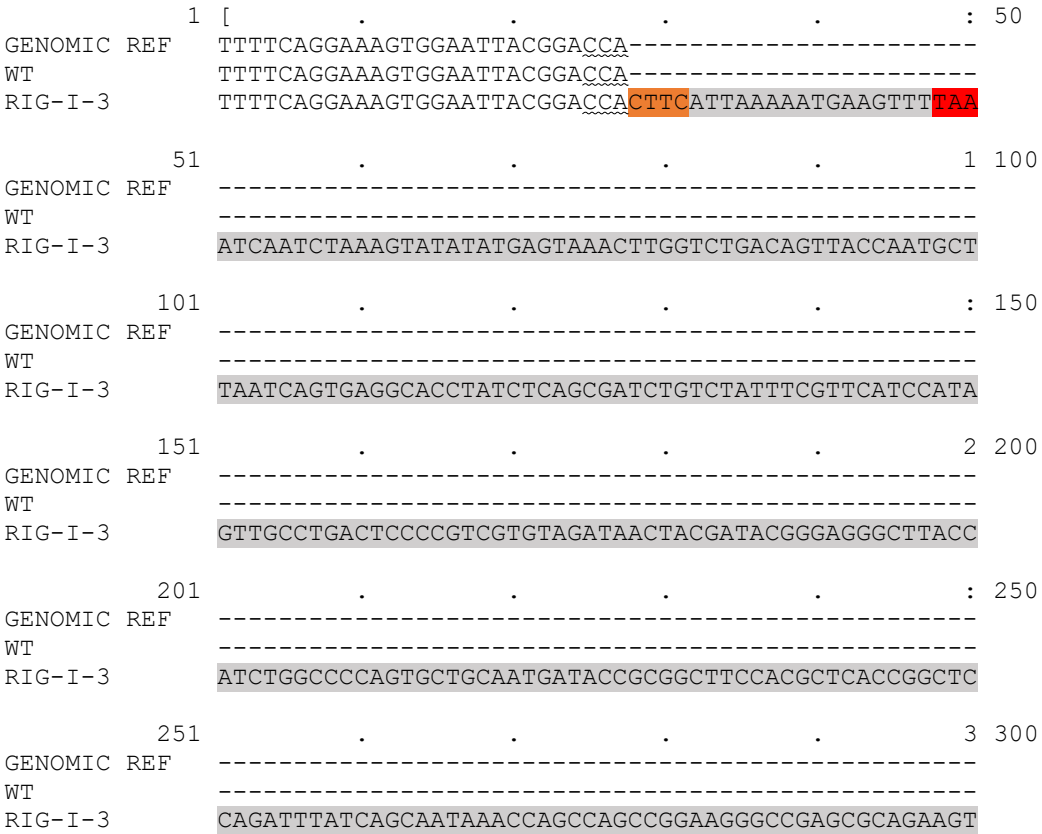

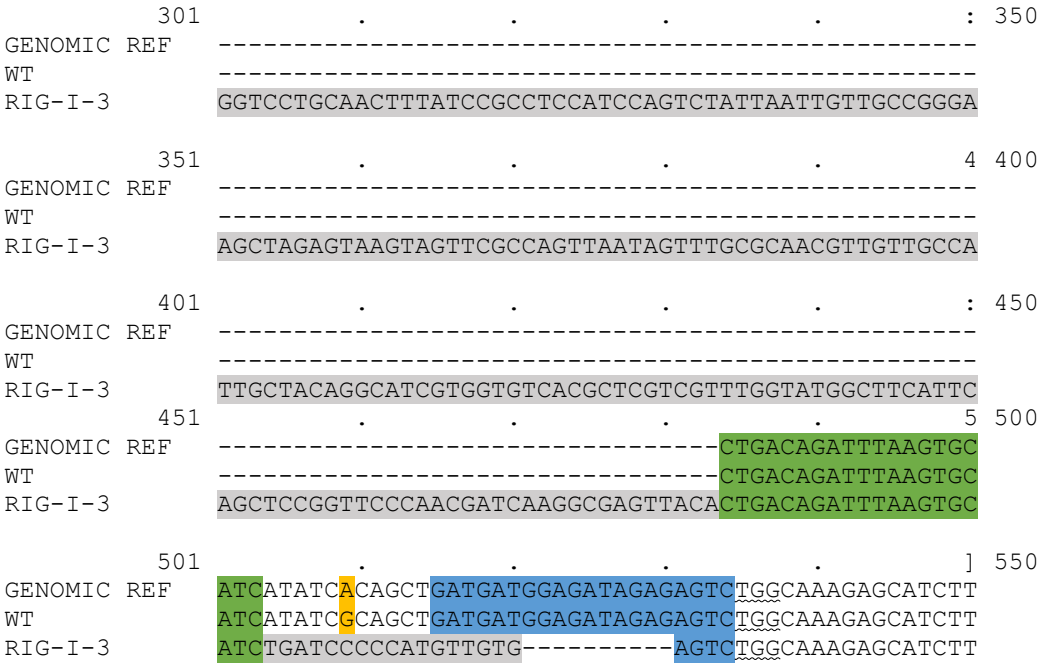

Figure 4.10: Alignment of nucleotide sequence determined for RIG-I gene edited cell line 3 reveals a large insertion and a small deletion within the 10th coding exon. Sequences determined for cell line 3 and unedited PK-15 cells (WT) were aligned with gDNA reference sequence (NC_010452.4:33891720-33976151) for porcine RIG-I using MEGA7 software. A large insertion (456 bp, grey) was identified adjacent to and immediately upstream of the first (green) and second gRNA target sites (blue). An additional insertion (17 bp, grey) was identified between each gRNA target site, followed by a short 10 bp deletion. A single synonymous mutation was identified in the WT sequence (yellow). PAM sites (waves, underlined) and a premature stop codon (red) are indicated.

Nucleotide sequences from RIG-I cell lines 3, 6 and 10 were subsequently translated as detailed in 4.3.2, the resulting amino acid sequences aligned against a reference sequence for porcine RIG-I (NP_998969.2) (figure 4.11, A). A premature stop codon only appears to have been introduced in the cell line featuring a large insertion, cell line 3, hence why transcript translation does not terminate prematurely with cell lines 6 and 10. The RIG-I sequence of cell line 3 aligned partially with the reference gDNA RIG-I sequence, after which the large 456 bp insertion resulted in a further 6 nucleotides of ORF followed by a premature stop codon. The resulting truncated RIG-I protein had a predicted MW of 53.72 kDa (figure 4.11, B). With regards to RIG-I cell lines 6 and 10, since no frameshift was introduced by either indel a premature stop codon was not introduced however there were slight differences in the

A

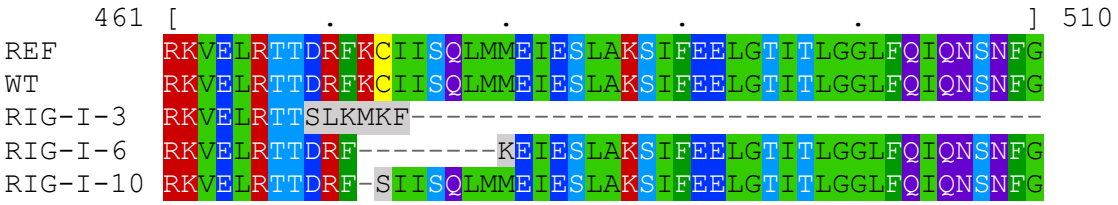

B

Cell line	Amino acid residue count	Predicted molecular weight (kDa)
RIG-I-3	473	53.72
RIG-I-6	935	106.98
RIG-I-10	942	107.78

Figure 4.11: Aligned translated sequence from the RIG-I gene of cell line 3 but not cell lines 6 or 10 indicates premature termination of each transcript and formation of truncated protein. (A) Translated genomic sequence from cell lines 3, 6 and 10 were aligned using MEGA7. Colours relate to the physiochemical properties of each amino acid while grey indicates inserted or non-homologous sequence. (B) Bioinformatics.org's protein molecular weight prediction tool was used to predict the molecular weights of the translated sequences.

resulting sequence (figure 4.11, B, grey). These proteins are predicted to be 106.98 kD and 107.78 kDa respectively (figure 4.11, B).

4.5. Generation of IRF3 knockout cell lines

4.5.1. Identification of IRF3 knockout cell lines by PCR and Sanger sequencing

Due to the poor specificity of the available anti-IRF3 antibody, potential IRF3 knockout cell lines were first screened by PCR and Sanger sequencing as detailed previously (4.3.2 and 4.4.2).

Briefly, following gDNA extraction a single pair of primers (poIRF3 fw.1, poIRF3 rev.2; table 2.12) were used to amplify an 803 bp fragment spanning the gRNA target sites within the first coding exon of porcine IRF3 in WT and candidate knockout cell lines using the PCR program

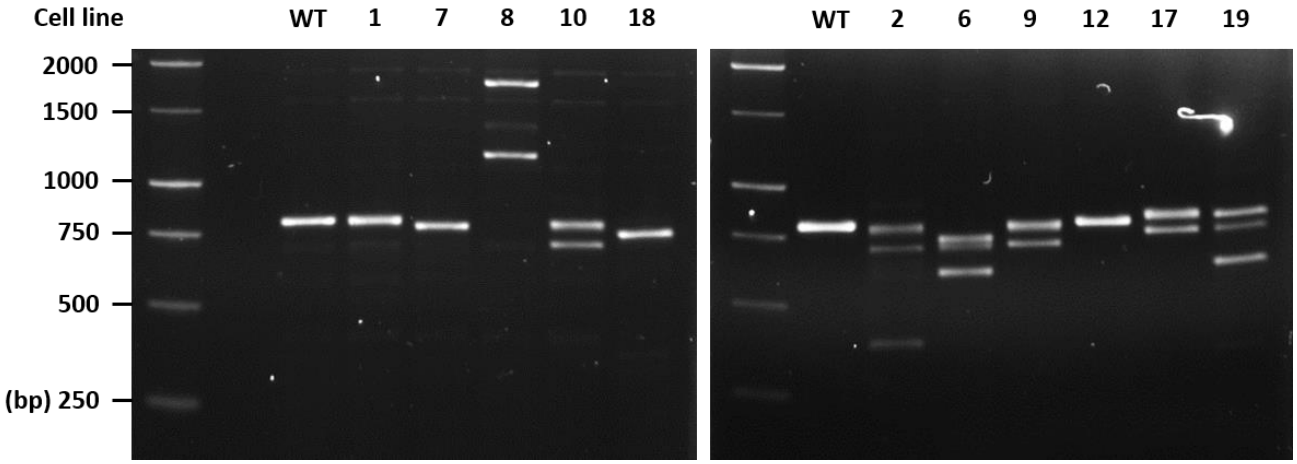

Figure 4.12: PCR amplification of wild-type and IRF3 knockout cell line genomic sequence reveals likely indels and insertions. 803 bp fragments spanning both gRNA target sites within the IRF3 gene were PCR amplified using DNA extracted from WT and IRF3 cell lines 1, 2, 6, 7, 8, 10, 12, 17, 18 and 19 using poIRF3 fw.1/poIRF3 rev.2 forward and reverse primers. Products were ran on a 1% agarose gel and individual bands selected for DNA extraction and Sanger sequencing. G5711 1 kb DNA ladder values correspond to sequence length in bp.

detailed in 4.3.2. PCR products were subsequently analysed by agarose gel electrophoresis; a band of the expected size (803 bp) was observed for the wild-type cell line, while candidate knockout cell lines yielded bands of varying sizes (figure 4.12). Lines 7, 12 and 18 were selected for sequencing and Western blot analyses, as they each exhibited a single PCR product suggesting putative edits were homozygous. PCR products for cells lines 7 and 18 ran comparatively lower than the wild-type band suggesting the introduction of deletions. The PCR product for cell line 12 ran at a comparable size to the wild type band, but the presence of a small deletion or insertion was possible. PCR products from the remaining cell lines ran as multiple bands suggesting they were either heterozygous or were mixed, non-clonal pools of cells.

The remainder of the PCR products for cell lines 7, 12 and 18 were then run on fresh gels, gel extracted and Sanger sequenced using a range of primers (poIRF3 fw.3, poIRF3 rev.1, poIRF3 rev.2; table 2.12); their nucleotide sequences were then aligned against a genomic reference

(NC_010448.4:c54706079-54701733) using MEGA software and respective deletions of 13, 28 and 61 bp were identified (figure 4.13).

Since each deletion was not a multiple of three, it was concluded that frameshifts in the coding sequence had been introduced. However, upon translation it was noted that no premature stop codon had been introduced in the first coding exon. In the absence of genomic sequence from the second coding exon, missing sequence was introduced using a cDNA sequence available on NCBI (NM_213770.1) and new translations were performed. Assuming that the pre-mRNA of each was spliced correctly, transcripts from cell lines 7, 12 and 18 were predicted to terminate prematurely at a newly introduced stop codon (TGA) 86 nt into the second coding exon (figure 4.14, A, red). The IRF3 genes of cell lines 7, 12 and 18 were predicted to encode 74, 79 and 63 amino acid proteins, with molecular weights of 11.79, 11.70 and 10.64 kDa respectively (figures 4.14, B and C).

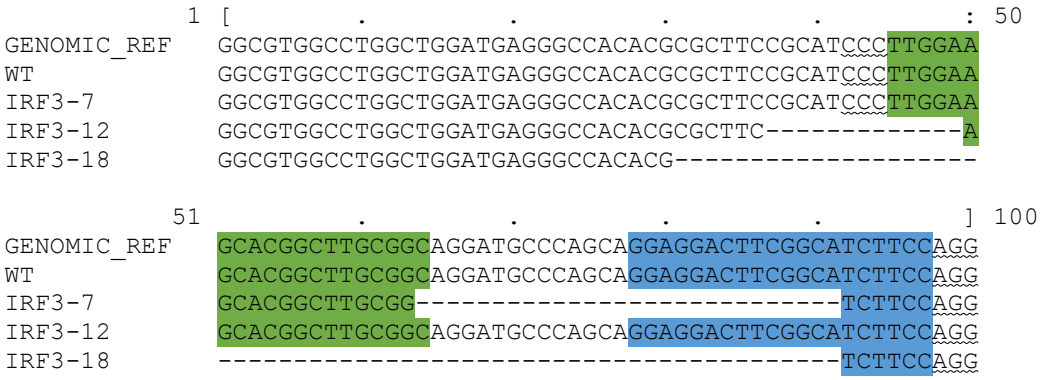

Figure 4.13: Alignment of nucleotide sequences determined for IRF3 gene edited cell lines 7, 12 and 18 reveals indels within the first coding exon. Sequenced PCR products spanning both gRNA target sites were aligned with each other and a reference sequence for porcine IRF3 in MEGA7. 13 bp, 28 bp and 61 bp were identified in the sequence determined for cell lines 7, 12 and 18 respectively. PAM sites (waves, underlined) and the sequence of the first (green) and second (blue) gRNA targets are indicated.

A

GCCTGGGCCGAGGCCAGTGGTGCCTACACTCCTGGGAAGGATAAGCCCGACCTGCCCACCTGGA
AGAGGAATTTCCGGTCTGCCCTGAACCGGAAAGAAGCATTGCGTTTAGCAGAGGACCACAGCAA
GGACCCCCACGACCCACACAAGATCTATGAGTTTGTGACCTCAG

B

C

Cell line	Amino acid residue count	Predicted molecular weight (kDa)
IRF3-7	74	11.79
IRF3-12	79	11.70
IRF3-18	63	10.64

Figure 4.14: IRF3 genes of cell lines 7, 12 and 18 are predicted to contain premature termination codons and encode truncated proteins. (A) Available cDNA (NM_213770.1) of the 2nd coding exon of IRF3 was used to identify the introduction of a premature stop codon in the IRF3 ORF of cell lines 7, 12 and 18. (B) Translated genomic sequence from cell lines 7, 12 and 18 was aligned using MEGA7 software; colours relate to the physiochemical properties of each amino acid while grey indicates inserted or non-homologous sequence. (C) Bioinformatics.org software was used to predict the molecular weights of IRF3 proteins encoded by cell lines 7, 12 and 18.

4.5.2. Identification of IRF3 knockout cell lines by Western blot

In order to confirm the absence of full length IRF3 protein in cell lines 7, 12 and 18, untreated whole cell lysates were analysed by Western blot using a rabbit polyclonal Ab (FL-425, Santa Cruz) recognising IRF3. A band running close to the predicted molecular weight of 47 kDa was detected in whole cell lysate prepared from wild-type PK-15 cells, but no bands were observed for the putative IRF3 knockout cell lines 7, 12 and 18.

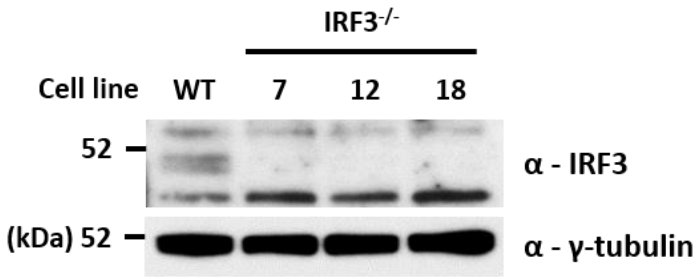

Figure 4.15: Confirmation of IRF3 absence in candidate knockout cell lines by Western blot. Lysates from unstimulated WT and candidate IRF3 knockout cell lines were subject to Western blot analysis to identify cell lines producing no IRF3 protein; 1/3000 sc-9082 (Santa Cruz) and 1/5000 T6557 (Sigma) were used to detect IRF3 and the loading-control γ-tubulin respectively. A band corresponding to IRF3 (predicted: 47 kDa) was not detected in samples from any of the IRF3 candidate knockout cell lines screened. RPN800E ladder values correspond to protein molecular weight in kDa.

4.6. Discussion

TLR3, RIG-I and IRF3 knockout PK-15 cell lines have been successfully generated in triplicate. While not discussed any further, MDA5 knockout PK-15 cell lines were also generated (appendix B). In order to achieve this, the first coding exon of each was targeted, introducing frameshifts and stop codons through indels which are predicted to result in premature termination of transcripts. However, depending on where the stop codon has been introduced, a sizeable portion of protein might still be produced – this was most notable for RIG-I as the 10th coding exon was targeted. Therefore, it was important to consider whether these residual, truncated proteins were likely to retain any physiological functions.

With regards to TLR3, truncated proteins of approximately 10 kDa were predicted. The leucine-rich repeating (LRR) ectodomains required for dsRNA-binding, homodimerisation and activation were almost entirely absent from each of these truncated proteins; out of a total of 23 LRRs present in TLR3, the truncated proteins each contained only LRR 1 (AA 52-75) in its entirety and only portions of LRR 2 (AA 76-99) (Bell *et al.*, 2003). The cytoplasmic Toll IL-1 receptor (TIR) homology domain required for recruitment of the adaptor protein TRIF required for downstream signal transduction was also absent (Alexopoulou *et al.*, 2001). It was therefore inconcievable that these small 10 kDa proteins would have any physiological functions.

As the 10th coding exon of RIG-I was targeted, only partial truncation of the protein was expected. Two cell lines (6 and 10) were devoid of a frameshift and RIG-I proteins present in these were predicted to be approximately 107 kD and 108 kDa respectively while in a third line (3) the truncated RIG-I comprised of 468 amino acids was expected to be 53.72 kDa. Porcine RIG-I is a 927 amino acid protein and therefore cell line 3 will still be producing a significant portion of it the protein. The N-terminus of the sequence is comprised of two CARD domains (1-92; 100-186) and a helicase domain (250-429). As with MDA5, these CARD domains are

responsible for downstream signal transduction via MAVS while the helicase domain and carboxy terminal domain (CTD) are both thought to be required for interaction with RNA molecules. Truncation of the human RIG-I CTD from nucleotide position 797 has been shown to have little effect on IFN-β promoter activity when analysed by luciferase assay following stimulation with poly(I:C), however more extensive truncations lacking the pincer domain and the C-terminus of the helicase domain (1-744 and 1-734 respectively) have been shown to render the protein constitutively active in the absence of any ligand (Louber *et al.*, 2015). A naturally-occurring truncated frameshift variant of human RIG-I (1-229) terminating after its CARD domains was also found to be constitutively active (Pothlichet *et al.*, 2009, Shigemoto *et al.*, 2009). In the absence of functional characterisation of the RIG-I cell line 3, however, it was not possible to determine whether or not the translated protein will be constitutively active or functional. With regards to RIG-I lines 6 and 10, only short indels bringing about deletions of AA 460-470 and AA 460 were identified respectively. Downstream of these deletions, a combination of substitutions in the C-terminus of the helicase domain of human RIG-I (K508A, Q511A, V514A and K518A) were found by others to abolish recognition of poly(I:C) and $^{5'ppp}$dsRNA in multiple cell types (Louber *et al.*, 2015). However as with RIG-I cell line 3, it was not possible to determine whether these proteins would be constitutively active or functional upon translation without proper characterisation.

With regards to IRF3, it seemed unlikely that any of the truncated proteins (ranging from 10-12 kDa) would have a physiological role. Dimerisation and subsequent activation of IRF3's transcriptional functions relies upon phosphorylation at a pair of phosphoacceptor sites clustered at the C-terminus of IRF3. The first of these sites is comprised of Ser^{385} and Ser^{386} while the second site spans a cluster of serine and threonine amino acids from AA 396-405 (Lin *et al.*, 1998, Yoneyama *et al.*, 1998, Servant *et al.*, 2003). A putative IRF3-mediated pathway of apoptosis, RIPA is thought to rely upon linear polyubiquitination at lysine residues 105, 193, 313 and 315 (Chattopadhyay *et al.*, 2016). Each truncated protein terminates prematurely in

the N-terminal DNA-binding domain which would normally be comprised of 120 residues – in the absence of the other IRF3 domains which facilitate dimerization, activation and induction of apoptosis, it seemed likely these truncated proteins would be non-functional.

Using these cell lines in triplicate, it was possible to elucidate the cell signalling pathways of apoptosis targeted by N^{pro} – this is addressed in chapter 5.

5. Identification of dsRNA-sensing pathways antagonised by N^{pro} using targeted CRISPR-knockout cell lines

5.1. Introduction

It was hypothesised that the functional characterisation of poly(I:C) and SeV-induced apoptosis in PK-15 cells would help inform the mechanism by which N^{pro} mediates its inhibition. Poly(I:C) and SeV have been shown to be recognised by specific PRRs, namely TLR3 (Alexopoulou *et al.*, 2001) and RIG-I (Strahle *et al.*, 2006, Baum *et al.*, 2010). Both TLR3 and RIG-I transduce signals through IRF3, inducing type I IFN and the upregulation of a number of genes in a diverse range of cells (Schafer *et al.*, 1998, Yoneyama *et al.*, 1998, Takeuchi and Akira, 2010). In chapter 3 type I IFN treatment was shown not to induce apoptosis in PK-15 cells but could amplify poly(I:C)-mediated apoptosis. This chapter investigates whether poly(I:C) and SeV are recognised by TLR3 and RIG-I respectively in PK-15 cells, and if specific components of the signalling cascade upstream of IFN production are responsible for the induction of apoptosis. Indeed, recent work by others suggests that IRF3 may play an additional role in the induction of dsRNA-mediated apoptosis in mice and HT1080 cells, a human cell line (Chattopadhyay *et al.*, 2010, Chattopadhyay *et al.*, 2011, Chattopadhyay *et al.*, 2016). Having generated, screened and validated a suite of CRISPR-Cas9 knockout cell lines targeting TLR3, RIG-I and IRF3 in triplicate (chapter 4), this chapter documents their subsequent use to functionally characterise the apoptotic response of PK-15 cells to poly(I:C) and SeV (Cantell strain) treatments.

5.2. Functional characterisation of PK-15 TLR3$^{-/-}$ cell lines

5.2.1. TLR3 is required for poly(I:C)-mediated apoptosis

Based on published literature, poly(I:C)-mediated apoptosis in PK-15 cells was expected to act through the PRR TLR3. To confirm this, TLR3$^{-/-}$ cells (described in chapter 4) were screened in triplicate by Western blot analysis (see 2.13) for their capacity to respond to extracellular poly(I:C) (100 μg/ml for 18 hr) in the presence or absence of the JAK-STAT inhibitor RXT (0.5μM).

As previously observed, extracellular poly(I:C) triggered caspase-3 cleavage in WT PK-15 cells and this was either reduced significantly or eliminated in cells additionally treated with RXT (figure 5.1). Confirming the efficacy of RXT, the ISG Mx1 was undetectable in any of the samples harvested from inhibitor-treated cells. However, no cleaved caspase-3 was detected in any of the screened TLR3$^{-/-}$ cell lines and, irrespective of RXT presence, nor was Mx1. Low levels of cleaved caspase-3 were detected in unstimulated samples however levels did not increase in samples from TLR$^{-/-}$ following extracellular treatment with poly(I:C). In turn, these results confirm that TLR3 is a sensor and mediator of extracellular poly(I:C)-mediated apoptosis in PK-15 cells.

5.2.2. TLR3 has no role in SeV-mediated apoptosis

To establish whether TLR3 has any role in the sensing of intracellular dsRNA in PK-15 cells, the same cell lines were treated with SeV (200 HA/ml), a reported agonist of RIG-I signalling (Strahle *et al.*, 2006, Baum *et al.*, 2010). Whole cell lysates were again harvested and subjected to Western blot analysis. Caspase-3 cleavage was clearly detectable at equal levels in WT cells and each of the TLR3$^{-/-}$ cell lines screened (figure 5.2). Concurrently, ISG15 appeared to be upregulated in each cell line to levels comparable to the respective samples from WT cells. Therefore, it is clear that deletion of TLR3 has no observable effect on cellular capacity to respond to intracellular agonists of dsRNA-mediated signalling such as SeV.

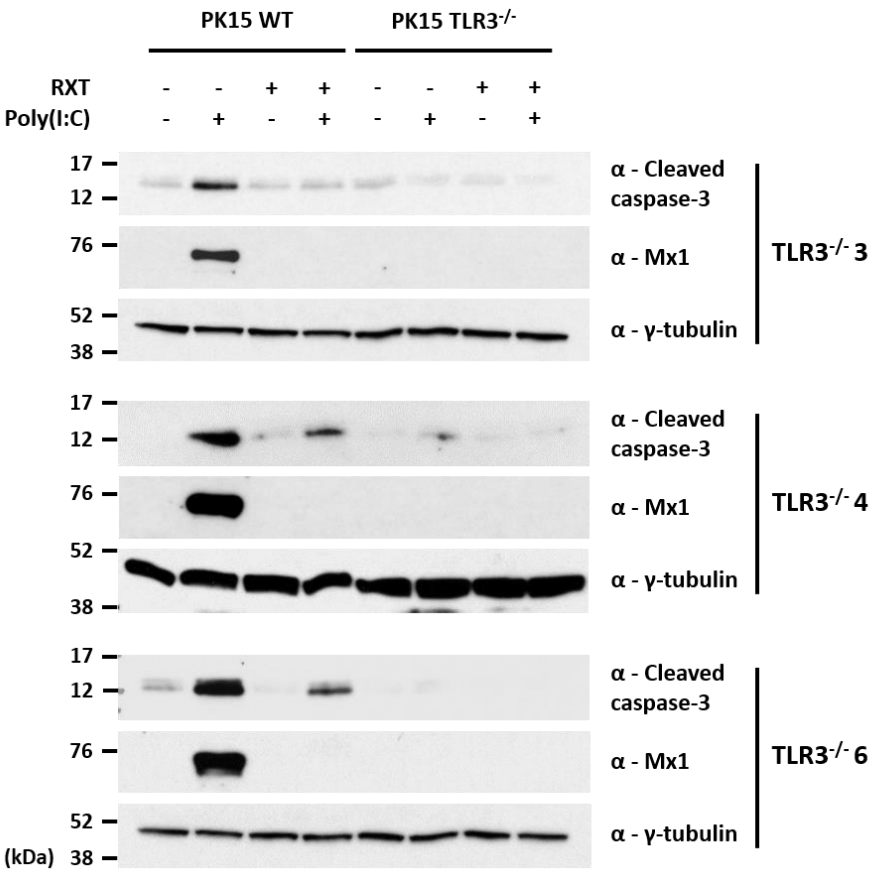

Figure 5.1: TLR3 is required for induction of extracellular poly(I:C)-mediated apoptosis in PK-15 cells. WT and three CRISPR-Cas9 knockout TLR3$^{-/-}$ PK-15 cell lines were seeded in 12-well plates and treated with 100 µg/ml poly(I:C) in the presence or absence of RXT. 18 hours post-treatment, whole cell lysates were prepared and analysed by Western blot using mAbs recognising cleaved caspase-3 and Mx1. A mAb recognising γ-tubulin was used to determine relative protein concentrations.

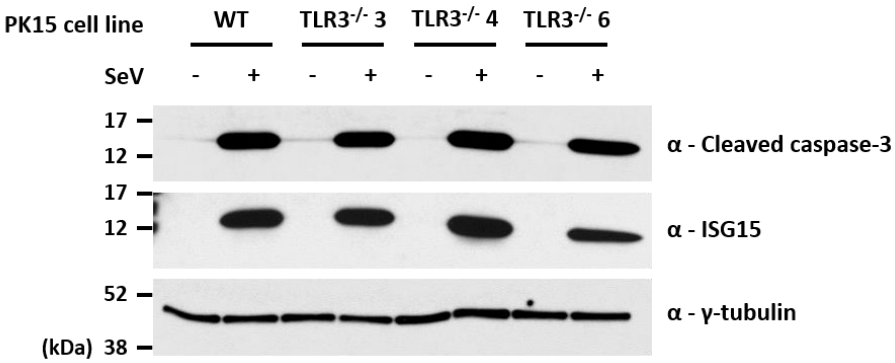

Figure 5.2: TLR3 is not required for induction of SeV-mediated apoptosis in PK-15 cells. WT and three CRISPR-Cas9 knockout TLR3$^{-/-}$ PK-15 cell lines were seeded in 12-well plates and treated with 200 HA/ml SeV. 18 hours post-treatment, whole cell lysates were prepared and analysed by Western blot using a polyclonal Ab recognising ISG15 and a mAb recognising cleaved caspase-3. A mAb recognising γ-tubulin was used to determine relative protein concentrations.

5.3. Functional characterisation of PK-15 RIG-I$^{-/-}$ cell lines

5.3.1. RIG-I is required for SeV-mediated apoptosis

As with the TLR3$^{-/-}$ PK-15 cell lines, RIG-I$^{-/-}$ cell lines generated in chapter 4 were also screened for their capacity to respond to dsRNA agonists. SeV is reported to be recognised by the RIG-I PRR (Strahle *et al.*, 2006, Baum *et al.*, 2010), so the RIG-I$^{-/-}$ cell lines were screened and characterised using SeV. WT and RIG-I$^{-/-}$ PK-15 cells were treated with SeV (200 HA/ml) for 18 hr) after which whole cell lysates were harvested and subjected to Western blot analysis (figure 5.3).

All but one of the RIG-I$^{-/-}$ cell lines screened (RIG-I$^{-/-}$ 10) displayed a complete absence of caspase-3 cleavage following SeV treatment, a finding which was mirrored by the absence of ISG15 upregulation (figure 5.3). Samples from RIG-I$^{-/-}$ 10 displayed low levels of caspase-3 cleavage and ISG15 following SeV treatment. As expected, treatment with RXT did not alter the observed induction of caspase-3 cleavage or ISG15 upregulation, confirming that SeV-induced apoptosis acts independently of IFN induction and response. Interestingly, while RXT did antagonise SeV-mediated upregulation of RIG-I in WT cells, induction of caspase-3 cleavage was unaffected.

5.3.2. RIG-I has no role in poly(I:C)-mediated apoptosis

To further confirm the role and specificity of RIG-I in SeV-mediated apoptotic signalling, RIG-I$^{-/-}$ cells were treated extracellularly with poly(I:C) (100 µg/ml for 18 hr) and whole cell lysates harvested for analysis by Western blot. Poly(I:C)-mediated caspase-3 cleavage was unchanged in RIG-I$^{-/-}$ cell line 3 compared to the WT sample but was marginally increased in RIG-I$^{-/-}$ cell lines 6 and 10 (figure 5.4), however the γ-tubulin loading control confirms this is likely attributable to protein loading discrepancies. It is therefore clear that deletion of RIG-I from

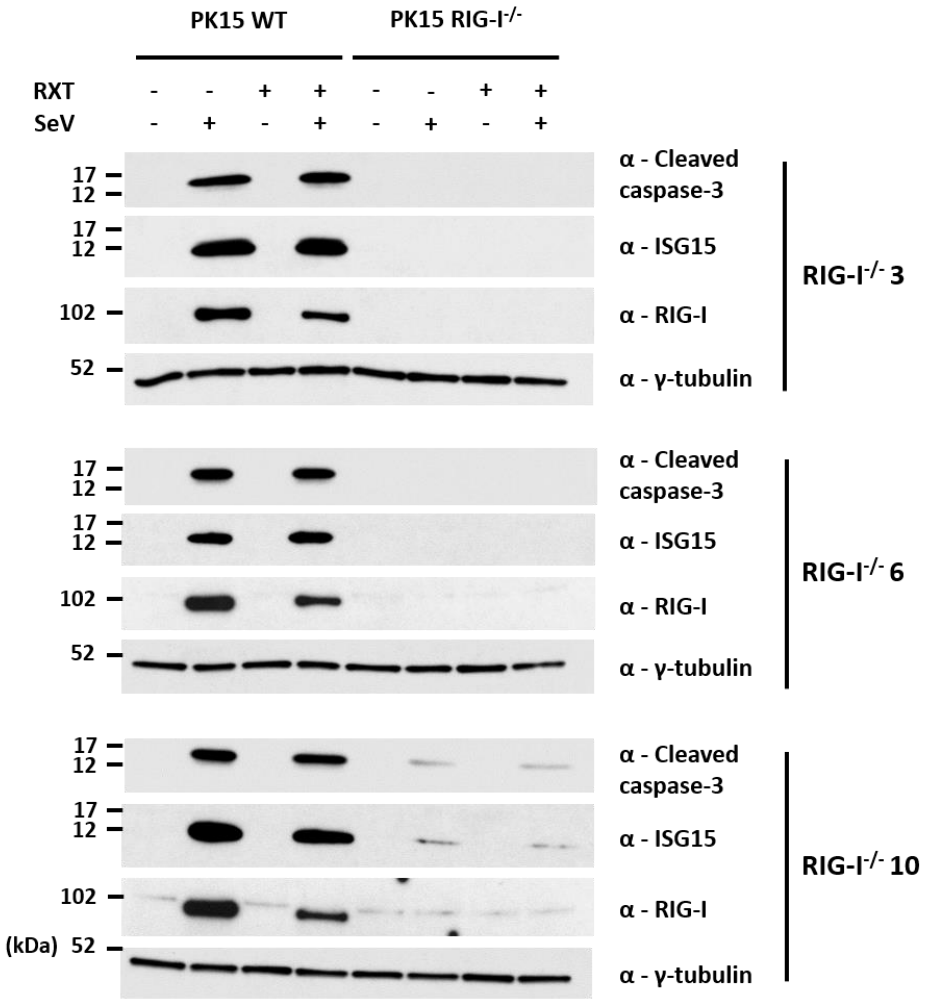

Figure 5.3: RIG-I is required for induction of SeV-mediated apoptosis in PK-15 cells. WT and three CRISPR-Cas9 knockout RIG-I$^{-/-}$ PK-15 cell lines were seeded in 12-well plates and treated with 200 HA/ml SeV in the presence or absence of RXT. 18 hours post-treatment, whole cell lysates were prepared and analysed by Western blot using a polyclonal Ab recognising ISG15 and mAbs recognising cleaved caspase-3 and RIG-I. A mAb recognising γ-tubulin was used to determine relative protein concentrations.

PK-15 cells has no effect on their capacity to initiate pro-apoptotic signalling in response to extracellular poly(I:C) treatment. The presence of low-level RIG-I expression in RIG-I$^{-/-}$ 10 was not unexpected as CRISPR-Cas9 gene editing had not introduced a frameshift in the genome of this cell line; this was discussed in 4.4 and 4.6.

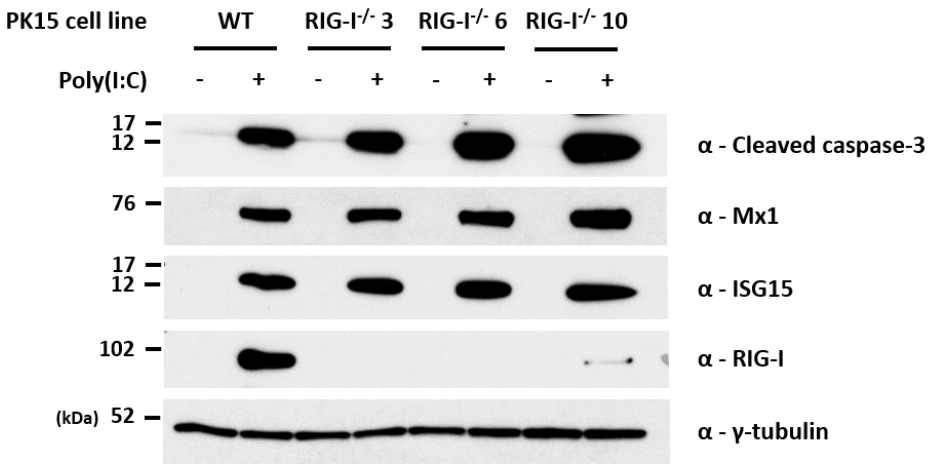

Figure 5.4: RIG-I is not required for induction of extracellular poly(I:C)-mediated apoptosis in PK-15 cells. WT and three CRISPR-Cas9 knockout RIG-I$^{-/-}$ PK-15 cell lines were seeded in 12-well plates and treated with 100 µg/ml poly(I:C). 18 hours post-treatment, whole cell lysates were harvested and analysed by Western blot using a polyclonal Ab recognising ISG15 and mAbs recognising cleaved caspase-3, Mx1 and RIG-I. A mAb recognising γ-tubulin was used to determine relative protein concentrations.

5.4. Functional characterisation of PK-15 IRF3$^{-/-}$ cell lines

5.4.1. IRF3 is essential for poly(I:C) and SeV-mediated apoptosis

Since IRF3 is known to coordinate signal transduction downstream of RIG-I and TLR3 activation, it was important to determine the capacity of IRF3$^{-/-}$ PK-15 cells to respond to poly(I:C) and SeV, confirmed agonists of TLR3 and RIG-I-mediated pro-apoptotic signalling in PK-15 cells. IRF3$^{-/-}$ cell lines were prepared in triplicate and treated extracellularly with either poly(I:C) (100 µg/ml) or SeV (200 HA/ml) for 18 hr and visualised using a recently acquired light microscope capable of imaging live cells. Both treatments triggered significant levels of cell rounding and detachment of WT PK-15 cells, indicative of cell death and apoptosis (figure 5.5). However, this phenotype was entirely absent from the poly(I:C)-treated well, and clearly reduced in the SeV-treated well of IRF3$^{-/-}$ cells when compared to treated WT cells.

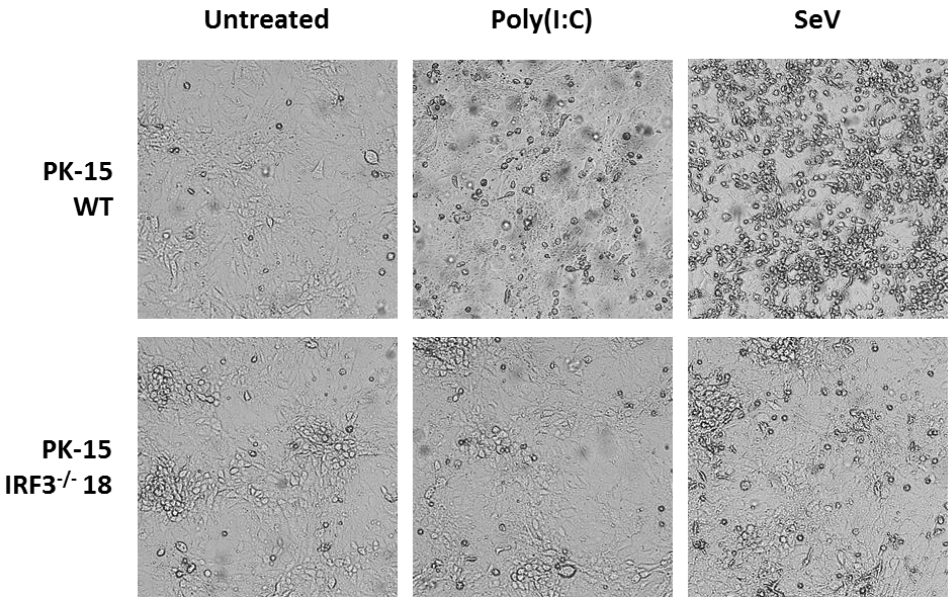

Figure 5.5: Deletion of IRF3 protects PK-15 cells from poly(I:C) and SeV-mediated cell death. WT and a representative CRISPR-Cas9 knockout IRF3$^{-/-}$ PK-15 cell line (line 18) were seeded in 12-well plates and treated with poly(I:C) and SeV. 18 hours post-treatment, wells of cells were visualised and imaged.

Having collected images of each well, the treatments were repeated in the presence and absence of RXT and whole cell lysates subsequently harvested and analysed by Western blot. When IRF3$^{-/-}$ cell lines were treated extracellularly with poly(I:C), caspase-3 cleavage initially appeared absent, however on longer film exposures a low level of cleaved caspase-3 was observed in samples from untreated IRF3$^{-/-}$ cells (figure 5.6). RXT reduced poly(I:C)-mediated caspase-3 cleavage in WT control cells, but it did not appear to have any noticeable, consistent effect on the induction of caspase-3 cleavage in any of IRF3$^{-/-}$ cell lines. IRF3$^{-/-}$ 7 displayed a marginal increase in poly(I:C)-mediated caspase-3 cleavage, IRF3$^{-/-}$18 decreased while IRF3$^{-/-}$ 12 remained unchanged – these slight variations in band intensity are likely attributable to differences in total protein loading. Interestingly, despite the presence of low levels of cleaved caspase-3 in each of the untreated IRF3$^{-/-}$ cell lines, there was no detectable upregulation of two ISGs, Mx1 and ISG15.

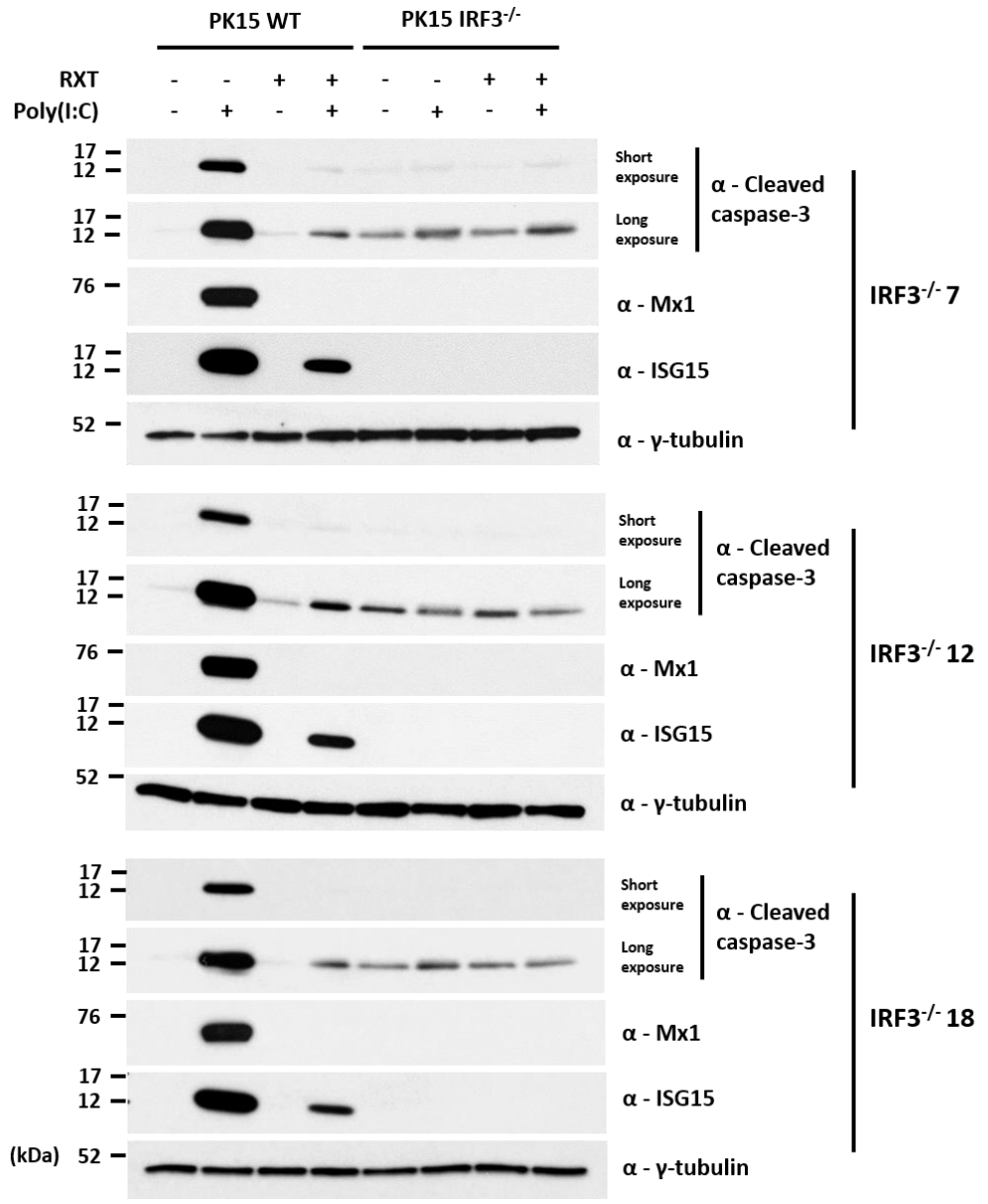

Figure 5.6: IRF3 is essential for induction of extracellular poly(I:C)-mediated apoptosis in PK-15 cells. WT and three CRISPR-Cas9 knockout IRF3$^{-/-}$ PK-15 cell lines were seeded in 12-well plates and treated with 100 µg/ml poly(I:C) in the presence or absence of RXT. 18 hours post-treatment, whole cell lysates were prepared and analysed by Western blot with a polyclonal Ab recognising ISG15 and mAbs recognising cleaved caspase-3 and Mx1. A mAb recognising γ-tubulin was used to determine relative protein concentrations.

Subsequently, these same IRF3$^{-/-}$ cell lines were treated with SeV. Compared to WT controls, SeV-mediated caspase-3 cleavage was greatly reduced in each of the IRF3$^{-/-}$ cell lines tested (figure 5.7); only on longer exposures was a low level of cleaved caspase-3 detected. Unlike poly(I:C)-treated IRF3$^{-/-}$ cells, ISG15 was marginally upregulated following SeV treatment,

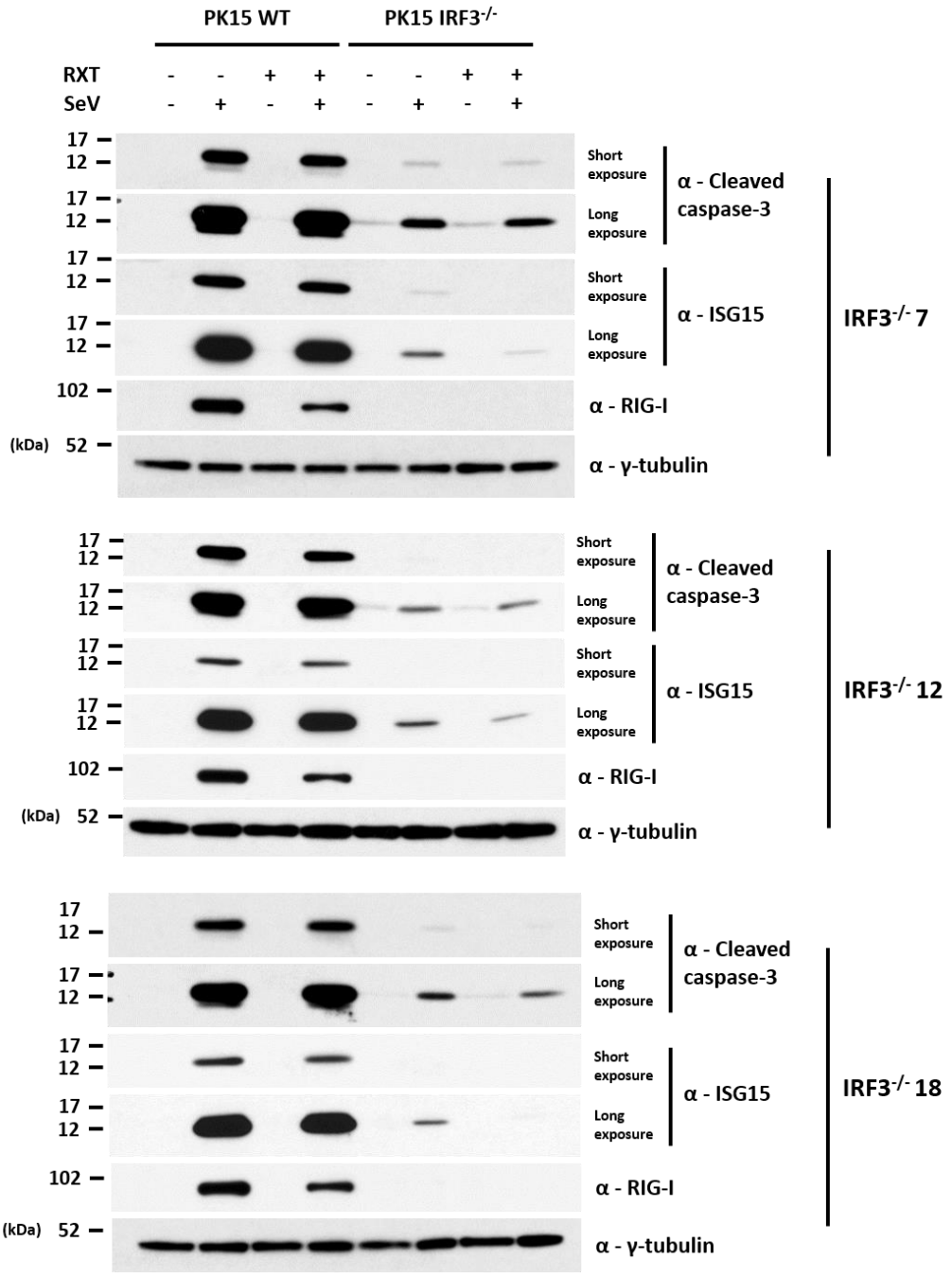

Figure 5.7: IRF3 is essential for induction of extracellular SeV-mediated apoptosis in PK-15 cells. WT and three CRISPR-Cas9 knockout IRF3$^{-/-}$ PK-15 cell lines were seeded in 12-well plates and treated with 200 HA/ml SeV in the presence or absence of RXT. 18 hours post-treatment, whole cell lysates were prepared and analysed by Western blot using a polyclonal Ab recognising ISG15 and mAbs recognising cleaved caspase-3, Mx1 and RIG-I. A mAb recognising γ-tubulin was used to determine relative protein concentrations.

however the levels of upregulation were greatly reduced compared to WT controls. RXT did not appear to have any effect on caspase-3 cleavage in the IRF3$^{-/-}$ cells, while a partial

reduction in ISG15 upregulation was observed but only on longer exposures.

Together, these findings suggest that IRF3 is largely indispensable for the induction of poly(I:C) and SeV-mediated apoptosis in PK-15 cells.

5.4.2. Deletion of IRF3 has no significant effect on the response to type I IFN

In order to confirm that in PK-15 cells IRF3 is responsible only for the induction of type I IFN and not the response (mediated by the JAK-STAT pathway), WT PK-15 cells and a representative IRF3$^{-/-}$ cell line was treated with increasing concentrations of porcine IFN-α for 18 hr (see 2.15.2). As detailed in 2.13, whole cell lysates were prepared and subjected to Western blot analysis (figure 5.8).

Mx1 upregulation was detectable in WT and IRF3$^{-/-}$ samples from 100 IU/ml IFN-α while ISG15 was detected with as little as 10 IU/ml (figure 5.8). Despite the clear induction of both ISGs in each of the cell lines tested a small reduction in the upregulation of each was noted in the IRF3$^{-/-}$ cell line.

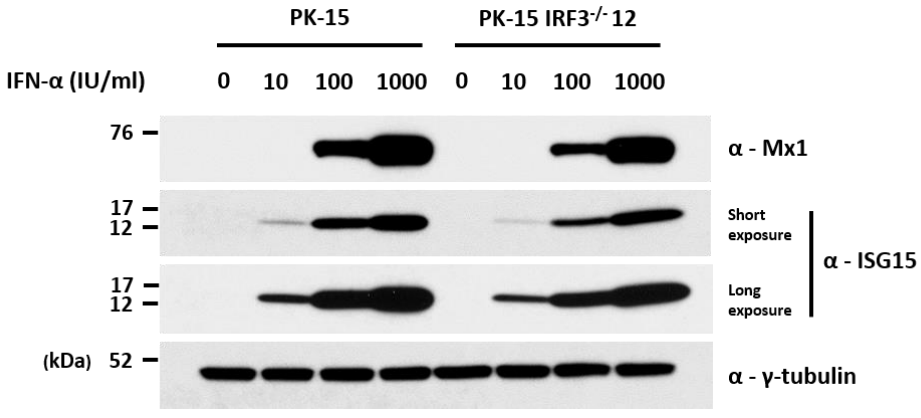

Figure 5.8: Deletion of IRF3 has no significant effect on the response to type I IFN. WT and IRF3$^{-/-}$ 12 PK-15 cell lines were seeded in 12-well plates and treated with 0-1000 IU/ml porcine IFN-α. 18 hpt, whole cell lysates were prepared and analysed by Western blot using a polyclonal Ab recognising ISG15 and a mAb recognising Mx1. A mAb recognising γ-tubulin was used to determine relative protein concentrations.

5.5. Discussion

By utilising a suite of CRISPR-Cas9 knockout cell lines, it has been possible to fully elucidate the initial pathways through which poly(I:C) and SeV mediate apoptosis in PK-15 cells, an endothelial porcine kidney cell line relevant to CSFV infection. The dsRNA-sensing PRRs RIG-I and TLR3 were found to be essential for SeV and poly(I:C)-mediated apoptosis respectively, while IRF3, typically associated with IFN upregulation, was required for coordinating the apoptotic response to each. Since N^{pro} has been shown to antagonise poly(I:C) and SeV-mediated apoptosis, it can therefore be concluded that it likely does so by targeting RIG-I/IRF3 and TLR3/IRF3 signalling pathways.

5.5.1. TLR3

The endosomal PRR TLR3 has been widely reported as a sensor of extracellular dsRNA and thus the protein's essential role in mediating apoptosis (capsase-3 cleavage) in response to poly(I:C) applied to cell culture was not entirely unexpected (Alexopoulou *et al.*, 2001, Salaun *et al.*, 2006). In the present work, aside from the basal levels detected, cleaved caspase-3 was absent from $TLR3^{-/-}$ PK-15 cells following poly(I:C) treatment. In addition, ISG upregulation was not detected as indicated by the absence of Mx1 from treated cells. Following treatment with SeV, a putative RIG-I agonist, the role of TLR3 as a sensor of poly(I:C) and extracellular dsRNA in PK-15 cells was further validated since induction of caspase-3 cleavage occurred equally across all WT and $TLR3^{-/-}$ cell lines screened. In turn, this confirmed that in PK-15 cells TLR3 is solely responsible for the induction of extracellular poly(I:C)-mediated apoptosis. This allows us to conclude that N^{pro} antagonises TLR3-mediated apoptotic responses.

The role of TLR3 during viral infections is complex, controversial and thought to be redundant in some cells and tissues possibly due to compensation from other innate pathways (Chattopadhyay and Sen, 2014). It is tempting to suggest that TLR3 serves to induce innate responses such as type I IFN and apoptosis following endocytosis of extracellular dsRNA of viral

or host origin released from neighbouring cells that have succumbed to the effects of infection (Vercammen *et al.*, 2008, Perales-Linares and Navas-Martin, 2013) and that CSFV N^{pro} is, in turn, able to antagonise these responses. However, *in vitro* CSFV is a largely non-cytopathic virus and the cytopathic effect observed *in vivo* occurs primarily in uninfected bystander cells due to cytokines such as IFN-α secreted by pDCs and TNF-α, IL-6 and IL-1β by macrophages (Summerfield and Ruggli, 2015). However Hüsser *et al*. observed significantly reduced induction of IFN-β following knockdown of TLR3 and infection with an N^{pro}-deleted virus, supporting the idea of TLR3 having a protective (albeit antagonised) role during CFSV infection (Hüsser *et al.*, 2011). In light of this discovery, they suggested that CSFV viral dsRNAs might activate TLR3 signalling following uptake into endosomes during autophagy as observed by Lee *et al*. who explored this same process but in the context of pDCs and TLR7-mediated detection of viral infections (Lee *et al.*, 2007). Indeed, *in vitro* autophagy has been shown to be active in CSFV-infected porcine cells (Pei *et al.*, 2014, Luo *et al.*, 2018). Therefore, by acting on TLR3 directly or on a downstream protein, *in vivo* N^{pro} is possibly able to antagonise TLR3-mediated apoptosis triggered in response to endocytosed dsRNA molecules released from neighbouring dead cells or as a consequence of autophagy following infection and intracellular production of dsRNA molecules.

Despite its usefulness as an intracellular agonist of IRF3 activity through its copy-back defective interfering (cbDI) RNA (Strahle *et al.*, 2006, Baum *et al.*, 2010, Kato *et al.*, 2011), SeV is a virus which ultimately encodes a range of proteins, some of which have immunomodulatory functions. One such protein is C protein, a known antagonist of the JAK-STAT pathway that governs the response to type I IFN (Garcin *et al.*, 2002). Because of IFN's importance in amplifying poly(I:C)-mediated apoptosis, it was important to identify an intracellular agonist of the same pathways likely mediated by SeV but lacking any capacity to antagonise the IFN response. This would help not only to validate the specificity of poly(I:C) as a TLR3 agonist but also to identify a suitable agonist for the validation of RIG-$I^{-/-}$ PK-15 cells.

Transfected poly(I:C) has been previously used to study intracellular dsRNA-mediated responses in a number of cell types, with shorter sequences found to trigger RIG-I-mediated responses and longer sequences MDA5-mediated responses (Kato *et al.*, 2006, Kato *et al.*, 2008). However, upon transfection, no clear induction of cleaved caspase-3 and only limited upregulation of the ISG Mx1 were detected in TLR3$^{-/-}$ cells compared to WT PK-15 cells (appendix C). Therefore, it was concluded that transfection of poly(I:C) using the present method was not a suitable means of validating or characterising intracellular responses to dsRNA in each of the knockout cell lines studied (RIG-I, TLR3, IRF3). Due to its ability to mediate completely TLR3-independent apoptosis in PK-15 cells (figure 5.2), SeV was therefore selected as the most suitable agonist of intracellular dsRNA-mediated responses to continue screening and characterising the remaining knockout cell lines (RIG-I and IRF3).

5.5.2. RIG-I

As previously detailed, SeV is widely reported to be an agonist of RIG-I-mediated responses including apoptosis and thus RIG-I's apparent requirement for SeV-mediated apoptotic responses in PK-15 cells was expected and in agreement with past literature (Yoneyama *et al.*, 2004, Chattopadhyay *et al.*, 2010, Chattopadhyay *et al.*, 2011). In the present work, cleaved caspase-3 and ISG15 upregulation each appeared to be absent from RIG-I$^{-/-}$ PK-15 cells following SeV treatment with only minimal levels of each detected in one of the lines (RIG-I$^{-/-}$ 10) and this was due to the incomplete knockout of the RIG-I gene in that particular line. RIG-I knockout was found to have no observable effect on extracellular poly(I:C)-mediated apoptosis (when applied to cell culture media), further validating RIG-I's role as a sensor of only intracellular dsRNA. In turn, this confirmed that in PK-15 cells RIG-I is solely responsible for the induction of SeV-mediated apoptosis. These results show that N^{pro} antagonises RIG-I-mediated apoptotic responses.

The role of RIG-I during viral infection of mammalian cells is well established: cytosolic sensing of short dsRNA molecules and those bearing 5'-triphosphates (5'ppp) serves to potently induce type I IFN following infection of a range of tissues with a diverse collection of viruses (Yoneyama *et al.*, 2004). In some cases, activation of RIG-I has been associated with the induction of apoptosis, most notably by SeV (Chattopadhyay *et al.*, 2010, Chattopadhyay *et al.*, 2011) which has been used in this work to characterise the role of porcine RIG-I. With regards to CSFV and N^{pro}, limited literature is available however as with TLR3, Hüsser *et al*. found IFN-β induction to be reduced in PK-15 cells following knockdown of RIG-I and infection with an N^{pro}-deleted virus (Hüsser *et al.*, 2011). Therefore, by acting on RIG-I directly or on a downstream protein, *in vivo* N^{pro} is likely able to antagonise RIG-I-mediated apoptosis triggered by cytosolic, intracellular dsRNA molecules during CSFV infection.

5.5.3. IRF3

IRF3's role as a master regulator of intracellular innate responses is well established, transducing upstream signals from PRRs such as TLR3, RIG-I and MDA5 in its capacity as a transcription factor for type I IFN (Schafer *et al.*, 1998, Yoneyama *et al.*, 1998, Takeuchi and Akira, 2010). However, its role as a mediator of apoptotic responses following stimulation of these upstream pathways is unclear and less well defined. In the present work, cleaved caspase-3 and ISGs were almost undetectable in $IRF3^{-/-}$ PK-15 cells following treatment with poly(I:C) and SeV, respective agonists of TLR3 and RIG-I-mediated apoptosis. In turn, this confirmed that in PK-15 cells IRF3 is largely indispensable for the induction of apoptosis mediated by each agonist. This enables us to conclude that the apoptosis antagonised by N^{pro} is mediated via pathways that converge on IRF3 to bring about caspase-3 cleavage. N^{pro}'s antagonism of type I IFN induction is well characterised and occurs via an interaction with IRF3 that brings about its proteasomal degradation (Bauhofer *et al.*, 2007, Seago *et al.*, 2007). Due to IRF3's apparently pivotal role in coordinating RIG-I and TLR3-mediated apoptosis, it is

therefore conceivable that this same interaction is responsible for N^{pro}'s antagonism of apoptosis.

Low levels of cleaved caspase-3 and ISG detected in SeV-treated $IRF3^{-/-}$ cells on longer Western blot exposures suggests another apoptotic pathway may be triggered however IRF3 still appears to be the primary route through which RIG-I-mediated apoptotic signals are transduced. PKR may be responsible for the residual apoptosis detected in this instance (Takeuchi *et al.*, 2008).

Chattopadhyay *et al*. have demonstrated that IRF3 undergoes ubiquitination and interacts with Bcl-2 family member Bax to bring about mitochondrial apoptosis following activation of RIG-I signalling by SeV (Chattopadhyay *et al.*, 2010, Chattopadhyay *et al.*, 2011, Chattopadhyay *et al.*, 2016) and others have observed STING to mediate a similar Bax-dependent pathway of apoptosis through an interaction with IRF3 following ER stress (Petrasek *et al.*, 2013, Qiao *et al.*, 2018). Together, these findings provide potential explanations for the observed reliance on IRF3 as a mediator of apoptosis in PK-15 cells. By targeting IRF3, N^{pro} can antagonise both TLR3 and RIG-I-mediated apoptotic responses, suggesting that during *in vivo* CSFV infection there is scope for the pro-apoptotic activity of dsRNA molecules of both intracellular and extracellular origin to be antagonised. Indeed, the pro-apoptotic function of IRF3 has been shown to exert antiviral activity – *in vivo*, a mutant of murine IRF3 unable to promote IFN transcription (S388A, S390A) was still able to protect mice from infection with SeV Strain 52 and Cantell, both of which are deadly in $IRF3^{-/-}$ mice (Chattopadhyay *et al.*, 2016). The role of IRF3 in the putative Bax-mediated pathway of apoptosis in PK-15 cells is further explored in the following chapter (chapter 6).

Aside from the putative IRF3-Bax pathway of apoptosis potentially triggered following TLR3 and RIG-I stimulation, it is possible that IRF3's apoptotic activity in PK-15 cells arises from an upregulation of pro-apoptotic genes. In chapter 3, pharmacological inhibition of the JAK-STAT

pathway using RXT and subsequent treatment of cells with porcine IFN-α revealed the apoptosis mediated by poly(I:C), but not SeV, to be amplified however IFN-α alone appeared to cause no detectable caspase-3 cleavage. Shaw *et al.* reported upregulation of TLR3, caspase-8, Noxa and TRAIL expression in *ex vivo* porcine skin fibroblast cultures following IFN treatment (Shaw *et al.*, 2017). Despite its antagonism of the type I IFN signalling response, SeV is still capable of upregulating the levels of IFN-independent ISGs such as ISG15 (see figures 5.2, 5.3 and 5.7). If porcine IRF3 is indeed able to bind directly to the promoters of ISGs such as Noxa and TRAIL, it is conceivable that these proteins are the means by which IRF3 exerts its pro-apoptotic activity. Noxa has been implicated in virus-mediated apoptosis and its upregulation has been found to occur in both an IFN-dependent (Eitz Ferrer *et al.*, 2011) and independent (Knowlton *et al.*, 2012) manner. Likewise, TRAIL displays similar activity and can be upregulated in an IFN-independent manner likely by the direct binding of IRF3 to the ISRE of its promoter (Kirshner *et al.*, 2005). In order to further explore IFN-independent pro-apoptotic transcriptional functions of IRF3, a mutant was constructed with the intention of it to be devoid of transcriptional activity – this is discussed in 6.6 and appendix D.

Future studies should therefore seek to identify specific agonists of alternate sensors of dsRNA MDA5 (appendix B) and PKR in PK-15 cells. In doing so, it should be possible to determine the extent to which each are responsible for mediating apoptotic responses and also the capacity for them to be antagonised by N^{pro}. These studies would be insightful since they may reveal IRF3-independent pathways of apoptosis also antagonised by N^{pro}. It would also be insightful to delete these same genes in SK6 cells, another porcine cell line, and to also knock down their expression in primary porcine cells. Doing so would further validate this chapter's key findings and reaffirm the importance of these genes and their respective proteins in the induction of dsRNA-mediated apoptosis.

5.5.4. Conclusions

In addition to triggering signalling cascades that cumulate in the induction of type I IFN, it was unclear prior to the completion of these experiments as to whether the PRRs TLR3 and RIG-I were responsible for the induction of apoptosis. Since TLR3 and RIG-I-mediated signalling converge on IRF3 in their induction of type I IFN, and in light of recent literature exploring the role of IRF3 (Chattopadhyay *et al.*, 2010, Chattopadhyay *et al.*, 2011, Chattopadhyay *et al.*, 2016), it was hypothesised that stimulation of each pathway with specific agonists would trigger apoptosis. Stimulation of TLR3 and RIG-I with poly(I:C) and SeV respectively triggered not only induction of type I IFN but also apoptosis in a manner that was ultimately dependent on the presence of IRF3 – the significance of this being N^{pro}'s well-characterised antagonism of IRF3 through interaction and proteasomal degradation (Bauhofer *et al.*, 2007, Seago *et al.*, 2007). In turn, these experiments have deepened our understanding of the nature of N^{pro}'s antagonism of dsRNA-mediated apoptosis. In chapter 3 it was established that type I IFN amplifies poly(I:C)-mediated apoptosis however IFN alone was incapable of triggering comparable levels of apoptosis to what is achieved with poly(I:C) alone. What remained unclear, however, is the means by which IRF3 exerts its pro-apoptotic activity if not in an entirely IFN and transcriptional manner. This question is addressed in the following chapter, chapter 6.

6. N^{pro} antagonises an IRF3-dependent mitochondrial pathway of apoptosis

6.1. Introduction

The results presented in chapter 3 show N^{pro}'s ability to antagonise both poly(I:C) and SeV-mediated apoptosis and demonstrate the ability of type I IFN to amplify poly(I:C)-mediated apoptotic responses. The results presented in chapters 4 and 5 describe how CRISPR-Cas9 knockout technology was used to show TLR3 and RIG-I are essential in mediating poly(I:C) and SeV-mediated apoptotic responses, respectively. The inability of cells that had been gene edited for IRF3 to mediate poly(I:C) and SeV-induced apoptosis confirmed that both of these pathways utilise signalling cascades that converge on IRF3. What remained to be established however was the nature of IRF3's role in apoptosis. Firstly, it remained to be determined whether IRF3 mediates a mitochondrial or non-mitochondrial pathway of apoptosis. And secondly, whether IRF3 mediates apoptosis directly or by upregulating the expression of apoptotic proteins. It was hypothesised that the elucidation of IRF3's role in poly(I:C) and SeV-mediated apoptosis would provide valuable insight into the pathways antagonised by N^{pro} in order to achieve its immunomodulatory functions.

6.2. N^{pro} antagonises IRF3-dependent mitochondrial relocalisation of Bax

CSFV has previously been shown to antagonise poly(I:C)-mediated mitochondrial release of cytochrome c and caspase-9 cleavage (Johns *et al.*, 2010a). Furthermore, N^{pro}'s ability to target IRF3 for ubiquitin-dependent proteasomal degradation has been well documented. More recently, IRF3 has been reported to play a role in a transcription-independent pathway of apoptosis that reportedly relies upon an interaction with the pro-apoptotic protein Bax and its subsequent translocation to the mitochondrial outer membrane (Chattopadhyay *et al.*, 2010, Chattopadhyay *et al.*, 2011, Chattopadhyay *et al.*, 2016). Therefore, experiments were conducted in order to investigate whether Bax can relocalise to the mitochondrial membrane following the induction of apoptosis in the presence of N^{pro} and in the absence of IRF3.

6.2.1. Poly(I:C) and SeV trigger mitochondrial relocalisation of Bax

Experiments using PK-15 cells and immunofluorescence confocal microscopy were performed in order to confirm the relocalisation of endogenous Bax to the mitochondria following exposure to the respective TLR3 and RIG-I agonists, poly(I:C) and SeV. PK-15 cells were treated with each agonist for 18 hr in the absence or presence of Z-VAD(OMe)-FMK (100 µM; Bachem), an inhibitor of the downstream effector caspases, in order to maximise the number of cells for visualisation by immunofluorescence. Treated cells were then stained with MitoTracker Red CMXRos for 30 min after which they were fixed and subjected to immunofluorescent staining to detect Bax.

In both poly(I:C) and SeV treated PK-15 cells Bax was undetectable prior to treatment (figure 6.1, A), in agreement with past work studying the phenomena by subcellular fractionation (Chattopadhyay et al. 2010, Chattopadhyay et al. 2011, Chattopadhyay et al. 2016) and immunofluorescence confocal microscopy (Murphy *et al.*, 2000). However, following treatment with either poly(I:C) or SeV Bax was detectable in a significant portion of cells, more

so with SeV than poly(I:C) (figure 6.1, A). Upon closer inspection, Bax signal appeared as distinct, condensed puncta that co-localised with the mitochondrial membrane, but did not appear to have been internalised (figure 6.1, B). The observed puncta appeared to be adjacent to the mitochondria, potentially associated with the mitochondrial membrane. In PK-15 cells that had been treated with either agonist the mitochondria exhibited a condensed morphology characteristic of apoptosis. In comparison, the mitochondria of untreated cells retained a more elongated morphology, typical of mitochondria in non-apoptotic cells. These data indicated that poly(I:C) and SeV trigger a mitochondrial pathway of apoptosis characterised by relocalisation of Bax to the mitochondria.

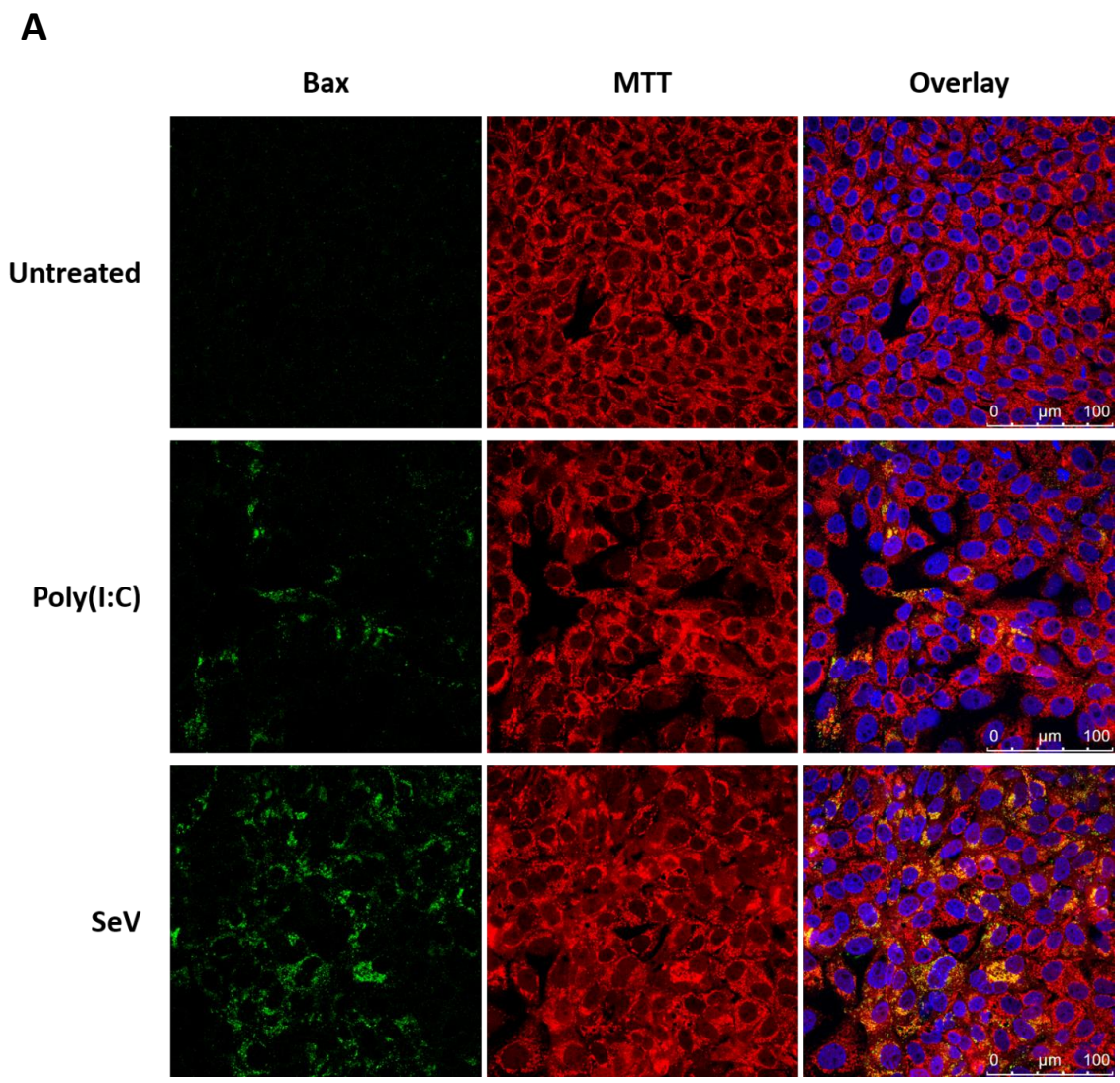

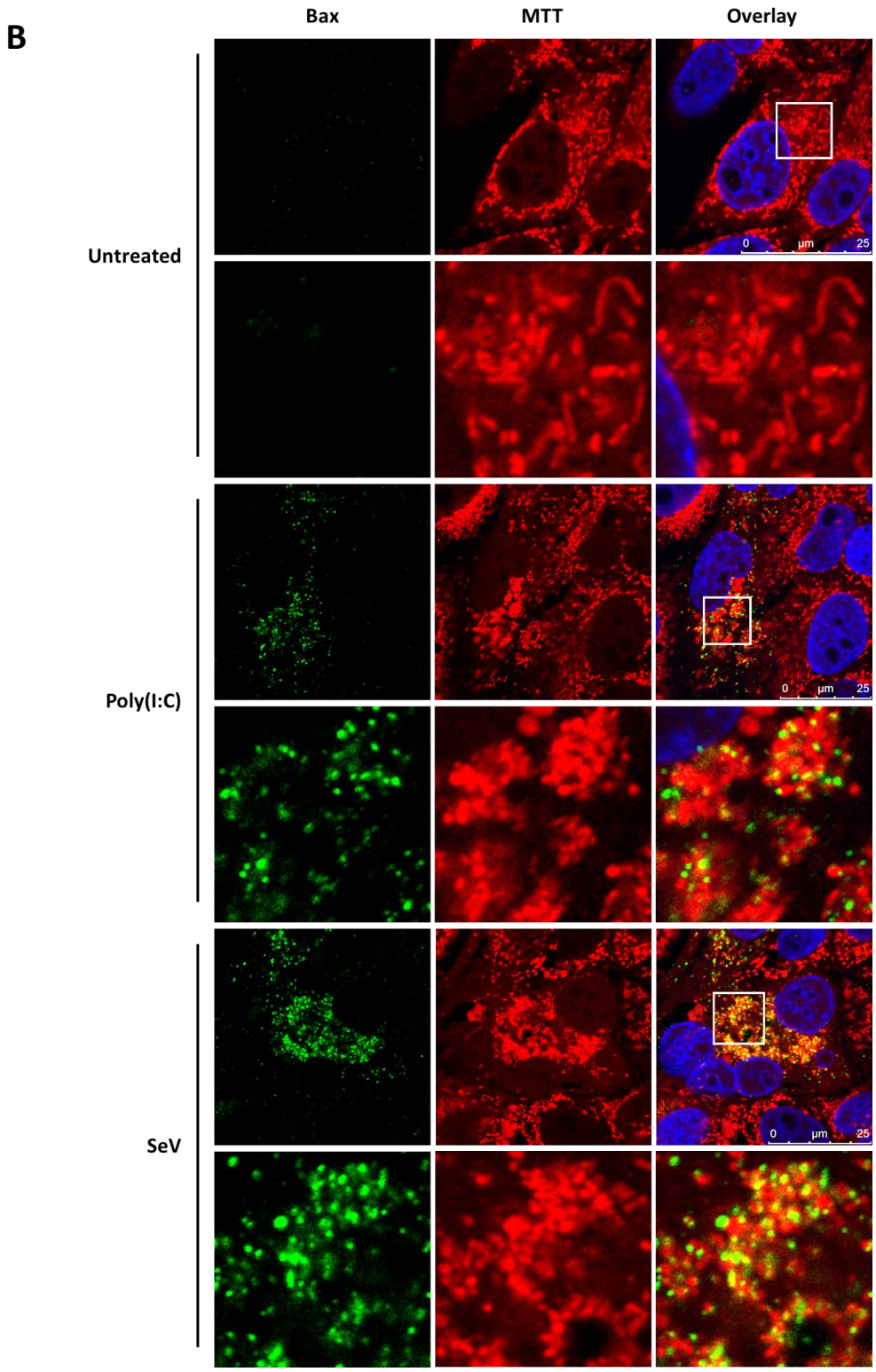

Figure 6.1: Bax relocalises to the mitochondrial membrane as distinct puncta in PK-15 cells following treatment with poly(I:C) and SeV. PK-15 cells were seeded onto coverslips in 24-well plates and treated with 100 µg/ml poly(I:C) or 200 HA/ml SeV in the presence of 100 µM caspase inhibitor Z-VAD(OMe)-FMK (Bachem). 18 hours post-treatment, cells were treated with MitoTracker (MTT) Red CMXRos (red) for a further 30 min and fixed with 4% paraformaldehyde. Fixed cells were analysed by immunofluorescence using a polyclonal Ab recognising Bax which was co-stained with Alexa Fluor 488 IgG H+L (green). Nuclei are stained blue with DAPI. Cells were first visualised at a lower magnification (A) and then at the single-cell level (B); white boxes indicate cropped fields of view.

6.2.2. Deletion of IRF3 antagonises poly(I:C) and SeV-mediated mitochondrial relocalisation of Bax

As stated previously, IRF3 has been implicated as a key mediator of a mitochondrial pathway of apoptosis termed RIPA, entirely independent of its transcriptional functions. This pathway has been studied in both human and murine cells but not porcine cells. IRF3 has already been shown to be essential for poly(I:C) and SeV-mediated apoptosis as indicated by the absence of cleaved caspase-3 in IRF3$^{-/-}$ cells treated with each apoptotic agonist. In order to determine if IRF3 mediates apoptosis using the RIPA pathway in porcine cells, WT and triplicate IRF3$^{-/-}$ PK-15 cell lines were prepared on coverslips and treated with either poly(I:C) (100 μg/ml) or SeV (200 HA/ml) and Z-VAD(OMe)-FMK. While a large proportion of WT PK-15 cells displayed mitochondrial relocalisation following SeV treatment, there was a complete absence in one IRF3$^{-/-}$ cell line (line 18) and an almost complete absence in the other two tested (lines 7 and 12) (figure 6.2). In addition, no relocalisation was detected in any of the IRF3$^{-/-}$ cell lines following treatment with poly(I:C). Indeed, these data indicated a requirement for IRF3 in facilitating poly(I:C) and SeV-mediated mitochondrial relocalisation of Bax.

6.2.3. Stably-expressed N^{pro} antagonises poly(I:C) and SeV-mediated mitochondrial relocalisation of Bax

Having shown a positive correlation between the presence of IRF3, relocalisation of Bax and the induction of poly(I:C) or SeV induced apoptosis, N^{pro}'s capacity to antagonise Bax relocalisation was next investigated. In knowing that N^{pro} targets IRF3 for proteasomal degradation, it was hypothesised that expression of N^{pro} – either stably in cell culture or through infection with CSFV – would also antagonise the mitochondrial relocalisation of Bax following treatment of cells with poly(I:C) or SeV.

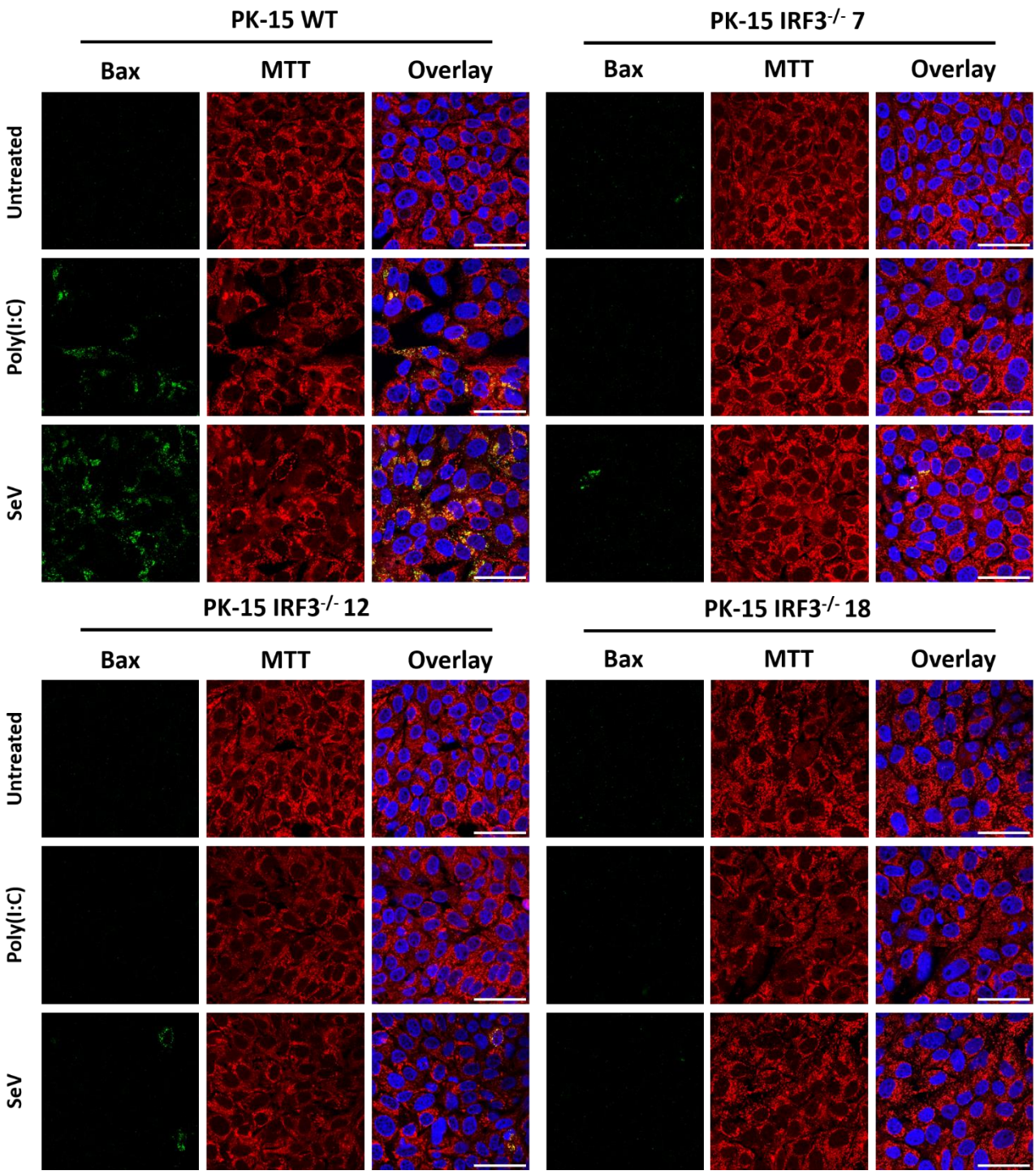

Figure 6.2: Deletion of IRF3 antagonises poly(I:C) and SeV-mediated mitochondrial relocalisation of Bax. WT and IRF3$^{-/-}$ PK-15 cells were seeded onto coverslips in 24-well plates and treated with 100 µg/ml poly(I:C) or 200 HA/ml SeV in the presence of 100 µM caspase inhibitor Z-VAD(OMe)-FMK. 18 hours post-treatment, cells were treated with MitoTracker (MTT) Red CMXRos for a further 30 min and fixed with 4% paraformaldehyde. Fixed cells were analysed by immunofluorescence using a polyclonal Ab recognising Bax which was co-stained with Alexa Fluor 488 IgG H+L (green). Nuclei are stained blue with DAPI. Scale bars represent 45 µM

WT PK-15 cells were prepared on coverslips alongside His-N^{pro} 23 PK-15 cells and subsequently treated with Z-VAD(OMe)-FMK and either agonist. While poly(I:C) was still applied at 100 µg/ml, SeV was applied at 20 HA/ml as well as the original 200 HA/ml so that any antagonism of Bax relocalisation by N^{pro} could be more readily detected. Upon visualisation of stained cells by immunofluorescence confocal microscopy (figure 6.3), a large portion of poly(I:C) and SeV-treated WT cells displayed Bax relocalisation. In comparison, Bax relocalisation was entirely absent from His-N^{pro} 23 cells treated with poly(I:C) and 20 HA/ml SeV (figure 6.3). Treatment with 200 HA/ml SeV did not trigger a noticeably higher proportion of cells to display Bax

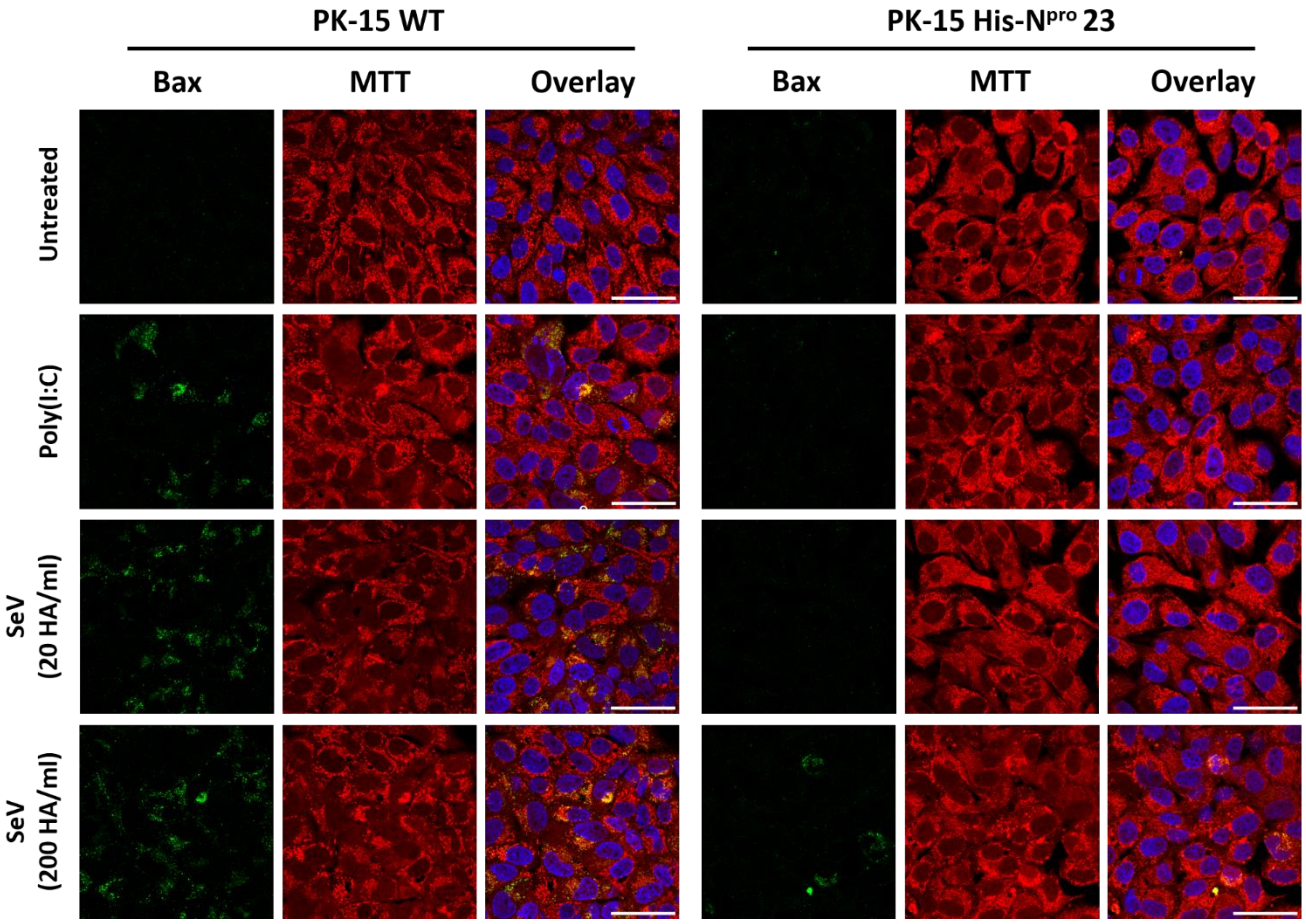

Figure 6.3: Stably-expressed His-N^{pro} antagonises poly(I:C) and SeV-mediated mitochondrial relocalisation of Bax. WT and His-N^{pro} 23 PK-15 cells were seeded onto coverslips in 24-well plates and treated with 100 µg/ml poly(I:C) or 200 HA/ml SeV in the presence of 100 µM caspase inhibitor Z-VAD(OMe)-FMK. 18 hours post-treatment, cells were treated with MitoTracker (MTT) Red CMXRos (red) for a further 30 min and fixed with 4% paraformaldehyde. Fixed cells were analysed by immunofluorescence using a polyclonal Ab recognising Bax which was co-stained with Alexa Fluor 488 IgG H+L (green). Nuclei are stained blue with DAPI. Scale bars represent 45 µM

relocalisation, however Bax relocalisation was detectable but markedly less than that observed in WT cells. Together, these observations suggested that N^{pro} is able to antagonise poly(I:C) and SeV-mediated mitochondrial relocalisation of Bax.

In order to further confirm N^{pro}'s antagonism of Bax relocalisation, EGFP-10 and EGFP-N^{pro}-17 PK-15 cell lines were treated as previously detailed; in this experiment an alternative mitochondrial label (MitoTracker Deep Red FM) was used that excites at the longer wavelength of 644 nm. As these cell lines express EGFP and an EGFP-tagged protein, a secondary antibody with a conjugated fluorophore different to EGFP's excitation wavelength of 488 nm had to be utilised – therefore, Bax was co-stained with Alexa Fluor 568. Upon visualisation by immunofluorescence confocal microscopy, Bax relocalisation was clearly detectable in the EGFP-10 cell line (figure 6.4, false-coloured as cyan), however relocalisation was almost undetectable in the EGFP-N^{pro}-17 cell line. In addition to confirming N^{pro}'s ability to antagonise mitochondrial relocalisation of Bax, it also confirmed that N^{pro} is able to achieve this even when tagged with EGFP (33 kDa), a considerably larger tag than His (1 kDa). Interestingly, EGFP and to a lesser extend EGFP-N^{pro} signal was observed to increase following treatment with SeV (figure 6.4), a phenomenon which was previously observed in 3.4.3 while screening the cell lines by Western blot to determine their capacity to antagonise induction of apoptosis (figure 3.10). While the apparent increase in EGFP signal intensity does not coincide with an increase in EGFP protein levels (figure 3.10), interactions with or modifications by proteins associated with apoptosis might be responsible. N^{pro} is actively turned-over in a proteasome-dependent manner (Seago et al., 2010), therefore the apparent increase in EGFP-N^{pro} protein levels when assessed by confocal microscopy (figure 6.4) and Western blot (figure 3.10) might be attributed to a potential stabilising interaction with a cellular protein. EGFP and EGFP-N^{pro} cell lines were not treated with poly(I:C) due to the reduced sensitivity of Alexa Fluor 568 secondary antibody in detecting Bax labelled with primary antibody. This was not an issue,

however, since poly(I:C) and SeV had already been shown to trigger convergent, IRF3-dependent pathways of apoptosis in PK-15 cells.

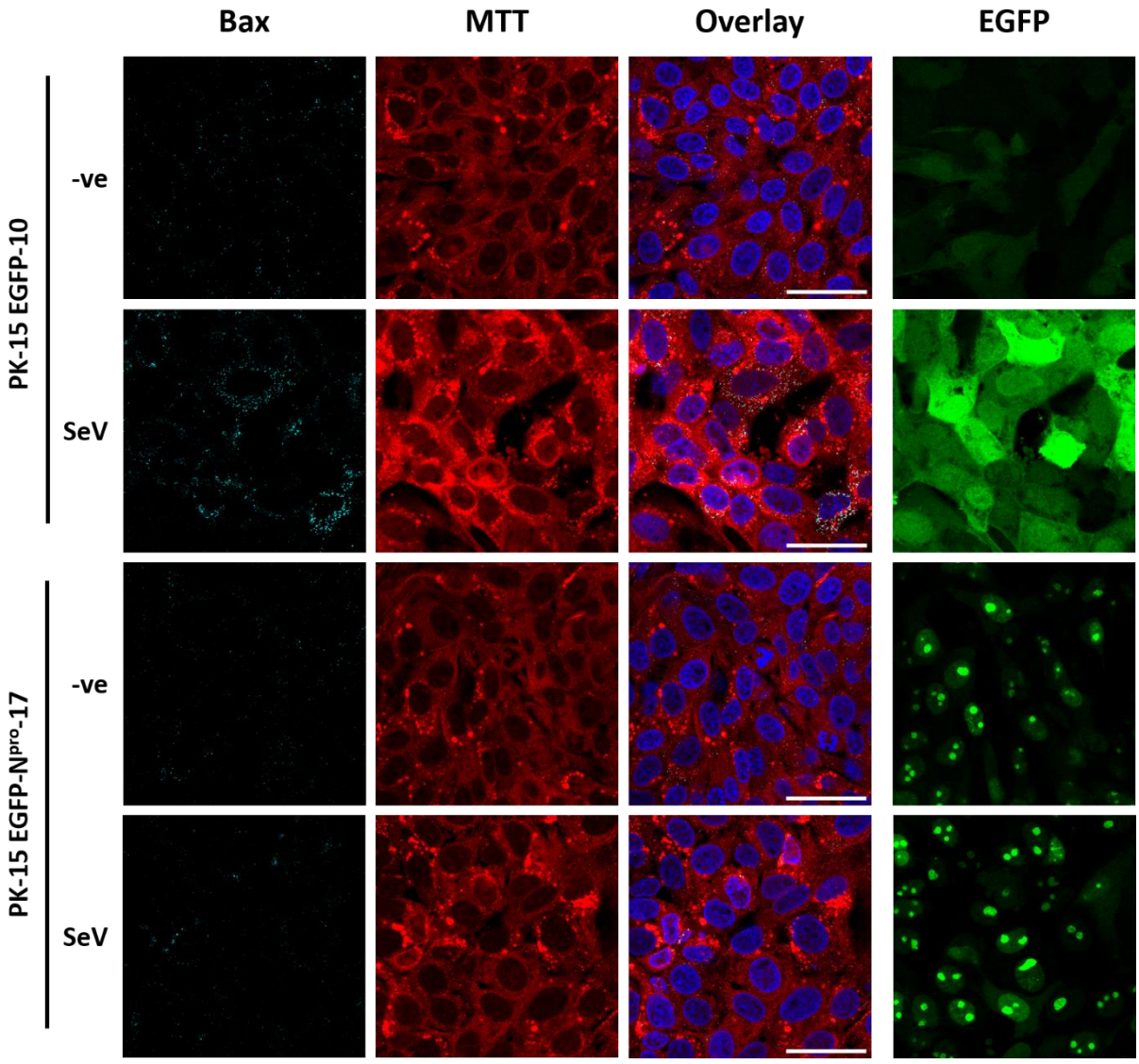

Figure 6.4: Stably-expressed EGFP-N^{pro} antagonises SeV-mediated mitochondrial relocalisation of Bax. EGFP-10 and EGFP-N^{pro}-17 PK-15 cells were seeded onto coverslips in 24-well plates and treated with 20 HA/ml SeV in the presence of 100 µM caspase inhibitor Z-VAD(OMe)-FMK. 18 hours post-treatment, cells were treated with MitoTracker (MTT) Deep Red FM (red) for a further 30 min and fixed with 4% paraformaldehyde. Fixed cells were analysed by immunofluorescence using a polyclonal Ab recognising Bax which was co-stained with Alexa Fluor 568 IgG H+L (cyan). Nuclei are stained blue with DAPI. EGFP channels were not included in the merged overlay images for ease of visualising mitochondrial relocalisation of Bax. Scale bars represent 45 µM

6.2.4. Poly(I:C) triggers mitochondrial relocalisation of EGFP-hBax in both WT and IRF3$^{-/-}$ PK-15 cells

While visualisation of endogenous Bax relocalisation proved to be an effective and insightful way of exploring IRF3's role in apoptosis and elucidating the mechanism of N^{pro}'s antagonism of it, a mammalian expression vector encoding an EGFP-tagged human Bax was initially employed. This was due to its extensive use in past and recent literature (Nechushtan *et al.*, 1999, Kale *et al.*, 2018, Rudd and Devaraj, 2018, Ader *et al.*, 2019) and the relative ease of visualising a fluorescently-tagged protein compared to the difficulty in identifying antibodies suitable for immunofluorescence that are reactive with porcine protein.

Briefly, WT and IRF3$^{-/-}$ 18 PK-15 cells were transfected with pEGFP-C3-hBax (Addgene plasmid #19741), incubated for 24 hr to allow time for exogenous protein expression to occur and then treated with Z-VAD(OMe)-FMK and poly(I:C) for either 10 or 18 hr prior to incubation with MitoTracker Red CMXRos and fixation. Poly(I:C) treatments were staggered in order that cells were fixed at the same time-point. Due to the poor transfection efficiency of PK-15 cells, images collected were of representative single-cells as opposed to wider fields of view that would have encompassed a larger number of cells.

Upon visualisation by confocal microscopy, EGFP-hBax was observed to be distributed diffusely in the cytosol and nucleus (figure 6.5, A and B) however upon closer inspection some protein was localised around the mitochondria in a uniform manner (figure 6.5, C). At 10 hpt with poly(I:C), EGFP-hBax had lost its nuclear and cytosolic distribution in WT cells and was now localised almost exclusively with the mitochondria. Unlike untreated cells, EGFP-hBax now appeared as condensed puncta possibly co-localised with the mitochondrial membrane however it did not appear to have been internalised. By 18 hpt, EGFP-hBax signal had considerably increased and instead of appearing as condensed puncta the protein now

presented as a single homogenous mass within transfected cells as did the mitochondria (figure 6.5, C).

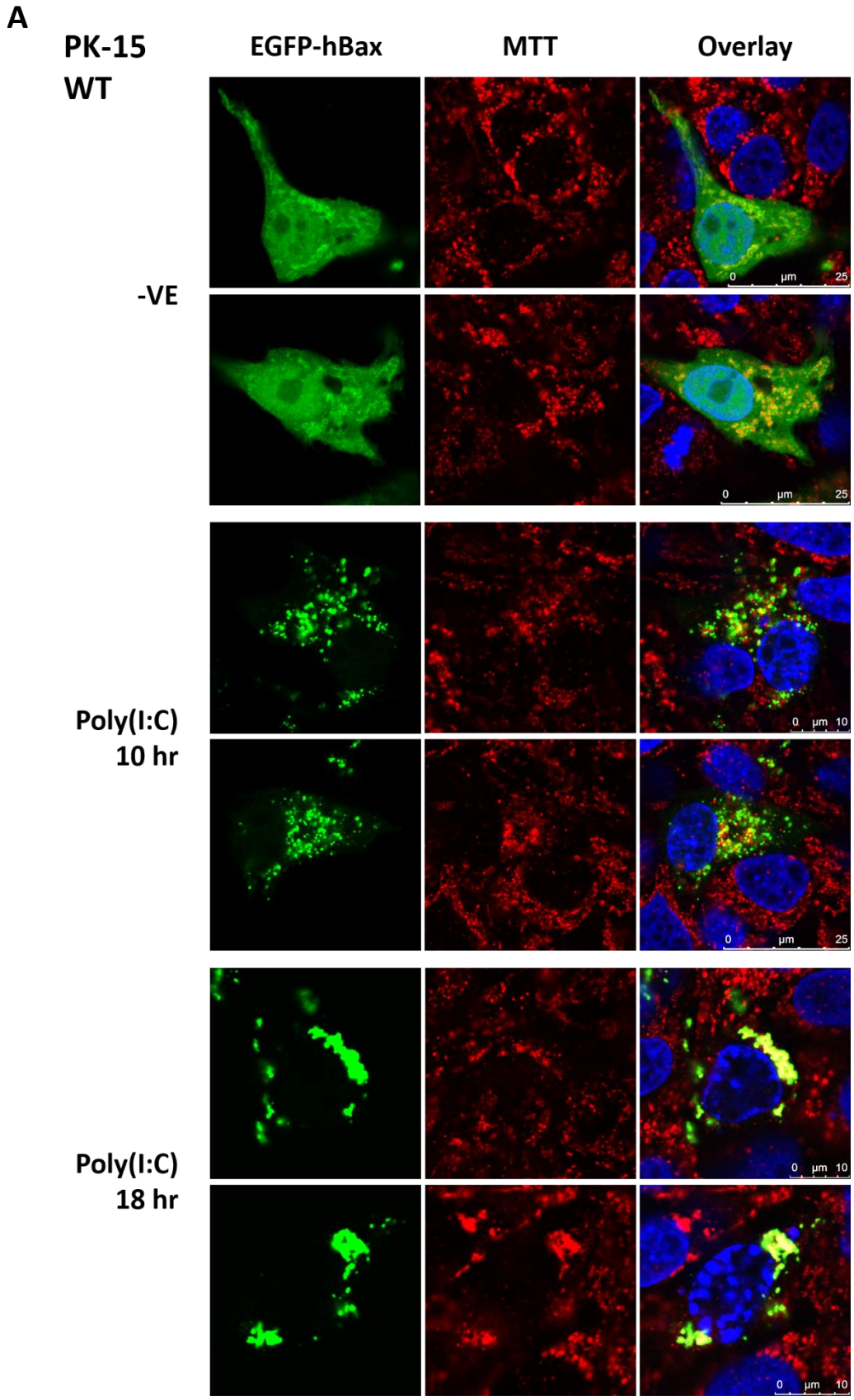

B

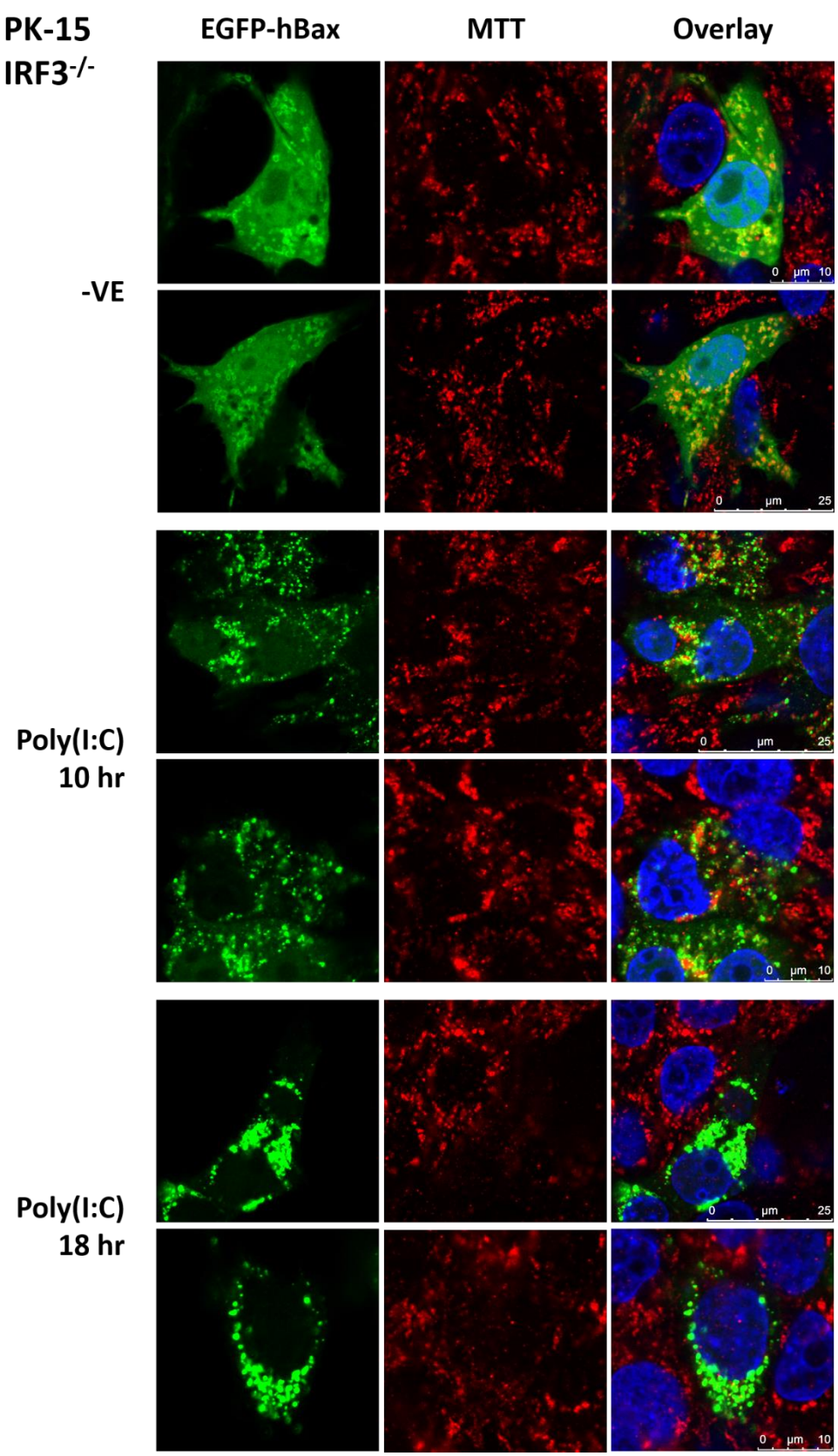
PK-15
IRF3-/-
EGFP-hBax
MTT
Overlay
-VE
Poly(I:C)
10 hr
Poly(I:C)
18 hr
0 µm 10
0 µm 25

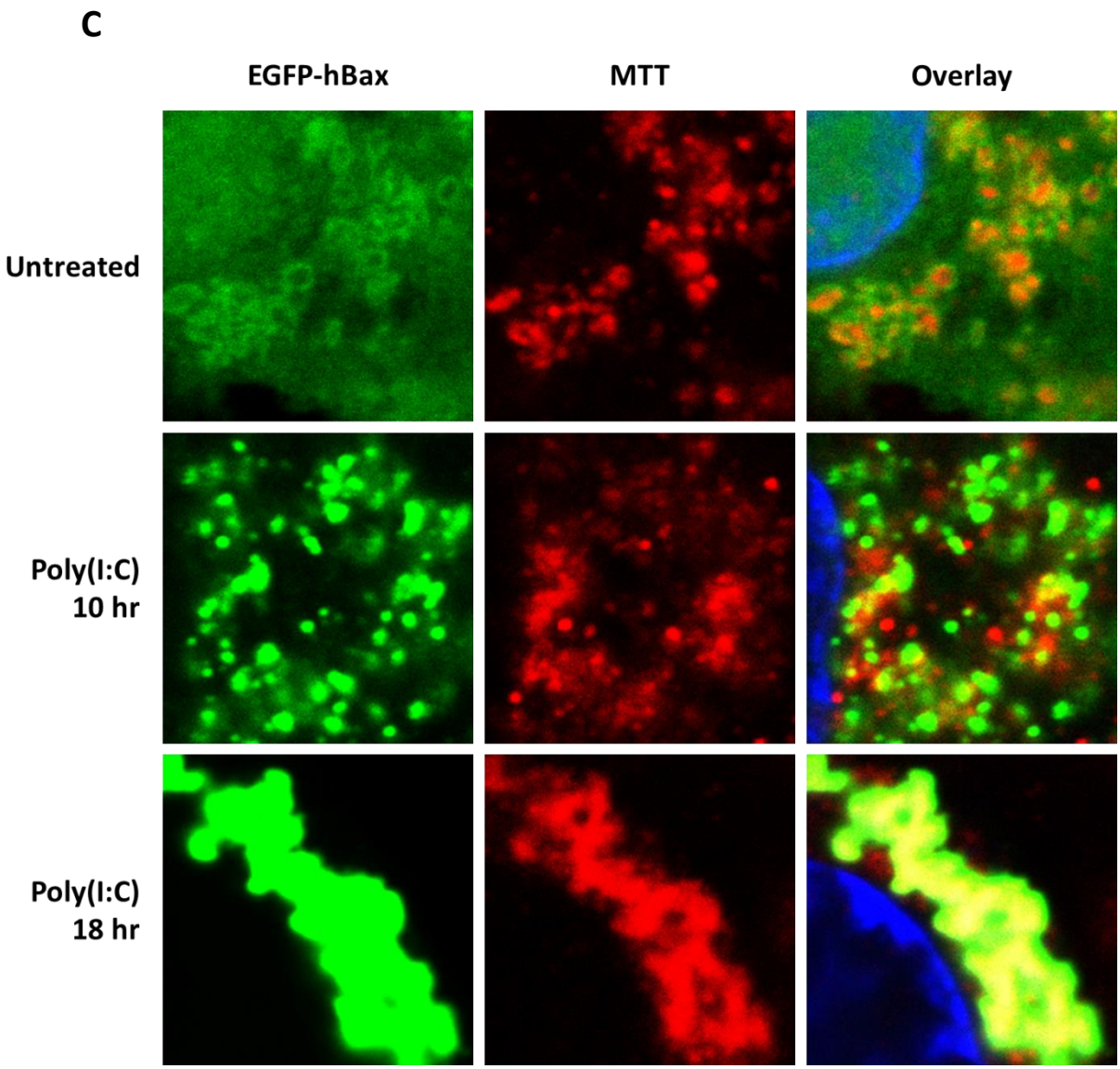

Figure 6.5: Transfected EGFP-hBax relocalises to the mitochondria in poly(I:C)-treated WT and IRF3$^{-/-}$ PK-15 cells. (A, C) WT and (B) IRF3$^{-/-}$ 18 PK-15 cells were seeded onto coverslips in 24-well plates and transfected with pEGFP-C3-hBax (Addgene plasmid #19741). 24 hours post-transfection, cells were treated with poly(I:C) for a further 10 or 18 hours in the presence of 100 µM caspase inhibitor Z-VAD(OMe)-FMK. Cells were treated with MitoTracker (MTT) Red CMXRos (red) for a further 30 min and fixed with 4% paraformaldehyde. Fixed cells were then analysed by confocal microscopy; images of WT cells (A) were cropped and enlarged (C) for clearer visualisation of protein localisation. Nuclei are stained blue with DAPI.

At this time-point, due to the condensed nature of the EGFP-hBax and MitoTracker signals, it was not possible to determine whether hBax was still associated with the mitochondrial membrane or whether it had now been internalised. In transfected IRF3$^{-/-}$ cells, EGFP-hBax had an identical distribution as in WT cells however at 10 hpt there was potentially more protein

retained in the cytosol and nucleus and by 24 hpt the homogenous, intense distribution of mitochondrial and EGFP-hBax signal observed in WT cells was not present – condensed puncta were still identifiable (figure 6.5, A and B).

6.2.5. Transfection of WT and IRF3$^{-/-}$ PK-15 cells with EGFP-hBax does not induce or amplify caspase-3 cleavage

Because of the discrepancy between IRF3's reported role in directing Bax to the mitochondria (Chattopadhyay *et al.*, 2010) and the data presented in 6.2.4 (figure 6.5) which suggests that EGFP-tagged Bax can still relocalise even in the absence of IRF3, the apoptotic potential of transfected Bax was investigated. An experiment was subsequently performed in order to determine whether EGFP-hBax could restore the sensitivity of IRF3$^{-/-}$ PK-15 cells to poly(I:C)-mediated apoptosis and whether it could amplify the apoptosis observed in WT PK-15 cells.

WT and IRF3$^{-/-}$ PK-15 cells were prepared in 24-well plates, transfected with pC3-EGFP-hBax and pC3-EGFP (a control plasmid prepared in-house[1]) and treated with poly(I:C) for 18 hr in the absence of Z-VAD(OMe)-FMK. Whole-cell lysates were then analysed by Western blot for the presence of cleaved caspase-3, Bax and EGFP. Cleaved caspase-3 was detected at equal levels in poly(I:C)-treated WT cells overexpressing EGFP and EGFP-hBax, however it remained completely undetectable in the IRF3$^{-/-}$ cells, irrespective of EGFP-hBax overexpression (figure 6.6). Interestingly, while EGFP-hBax was easily detected using an antibody that recognises endogenous Bax protein (figure 6.6, **) it was undetectable using an antibody that recognises EGFP (figure 6.6, ****). In turn, these observations suggested that EGFP-hBax is by itself not pro-apoptotic in PK-15 cells but failed to explain why or how EGFP-hBax was able to relocalise to the mitochondria even in the absence of IRF3.

[1] Two oligos bearing internal stop codons (HindIII-3frameSTOP-EcoRI_FW, HindIII-3frameSTOP-EcoRI_REV; table 2.20) were annealed (see 2.9) and ligated into pC3-EGFP-hBax following *Hin*dIII/*Eco*RI digest of insert and vector.

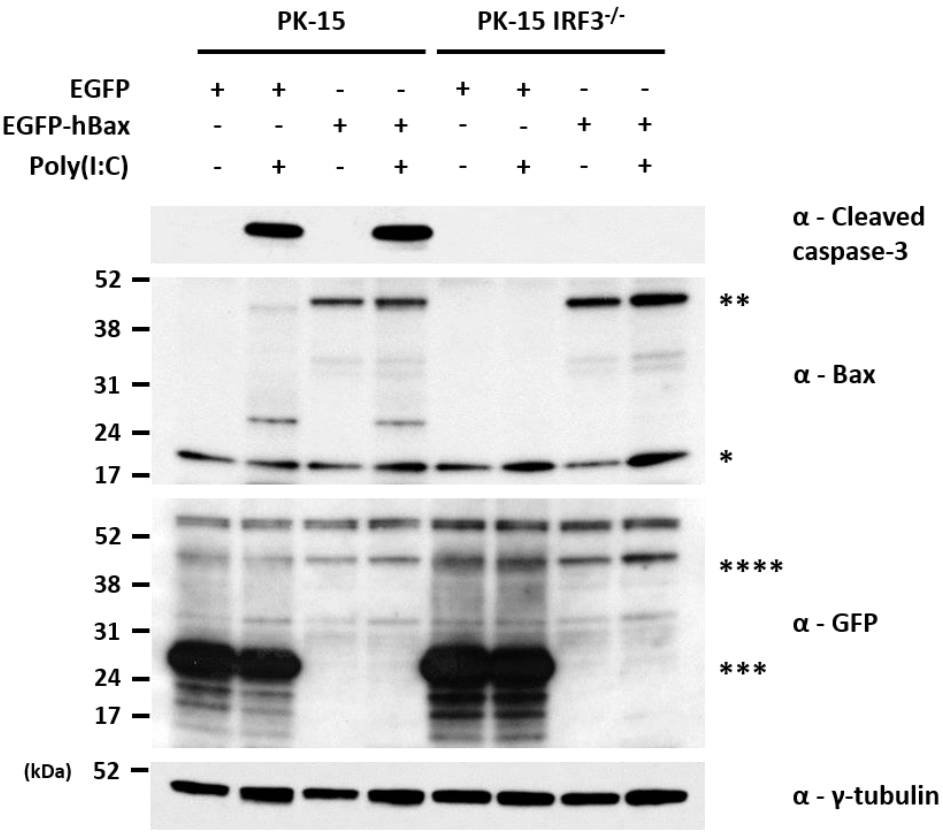

Figure 6.6: Transfection of WT and IRF3$^{-/-}$ PK-15 cells with EGFP-hBax does not induce or amplify caspase-3 cleavage. WT and IRF3$^{-/-}$ 18 PK-15 cells were prepared in 24-well plates and transfected with either pC3-EGFP-hBax (Addgene plasmid #19741) or pC3-EGFP (in-house). 24 hours post-transfection, cells were treated with poly(I:C) for a further 18 hours. Whole cell lysates were prepared and analysed by Western blotting using polyclonal Abs recognising cleaved caspase-3 or Bax and a mAb recognising GFP. A mAb recognising γ-tubulin was used to determine relative protein concentrations. Bax (*) and EGFP-hBax (**) resolved as single bands with the Bax polyclonal; EGFP resolved as a single band (***) while EGFP-hBax was undetectable at the expected position (****) with the GFP monoclonal Ab.

6.3. Bax does not appear to be an ISG and loss of relocalisation is independent of expression levels

While the nature of Bax's role in IRF3-mediated apoptosis has been reported for murine and human cells, it remains to be determined for PK-15 cells – a porcine cell line in which an IRF3-mediated pathway of apoptosis is antagonised by CSFV N^{pro}. In 6.2.5 (figure 6.6) it was established that overexpression of Bax was not pro-apoptotic. One key, remaining question to be addressed was whether Bax is an ISG and whether its levels of expression have a role in its ability to relocalise to the mitochondria in PK-15 cells.

6.3.1. Poly(I:C) but not SeV-mediated mitochondrial relocalisation of Bax protein is antagonised by inhibition of the type I IFN signalling response

In order to determine whether mitochondrial relocalisation of Bax is dependent on an intact ISG response, WT PK-15 cells were treated with Z-VAD(OMe)-FMK and either porcine IFN-α, poly(I:C) or SeV in the presence or absence of RXT, a janus kinase inhibitor that prevents ISG expression mediated by the type I IFN signalling response (stimulation of the JAK-STAT pathway). At 18 hpt, poly(I:C) and SeV triggered significant levels of Bax relocalisation, but IFN-

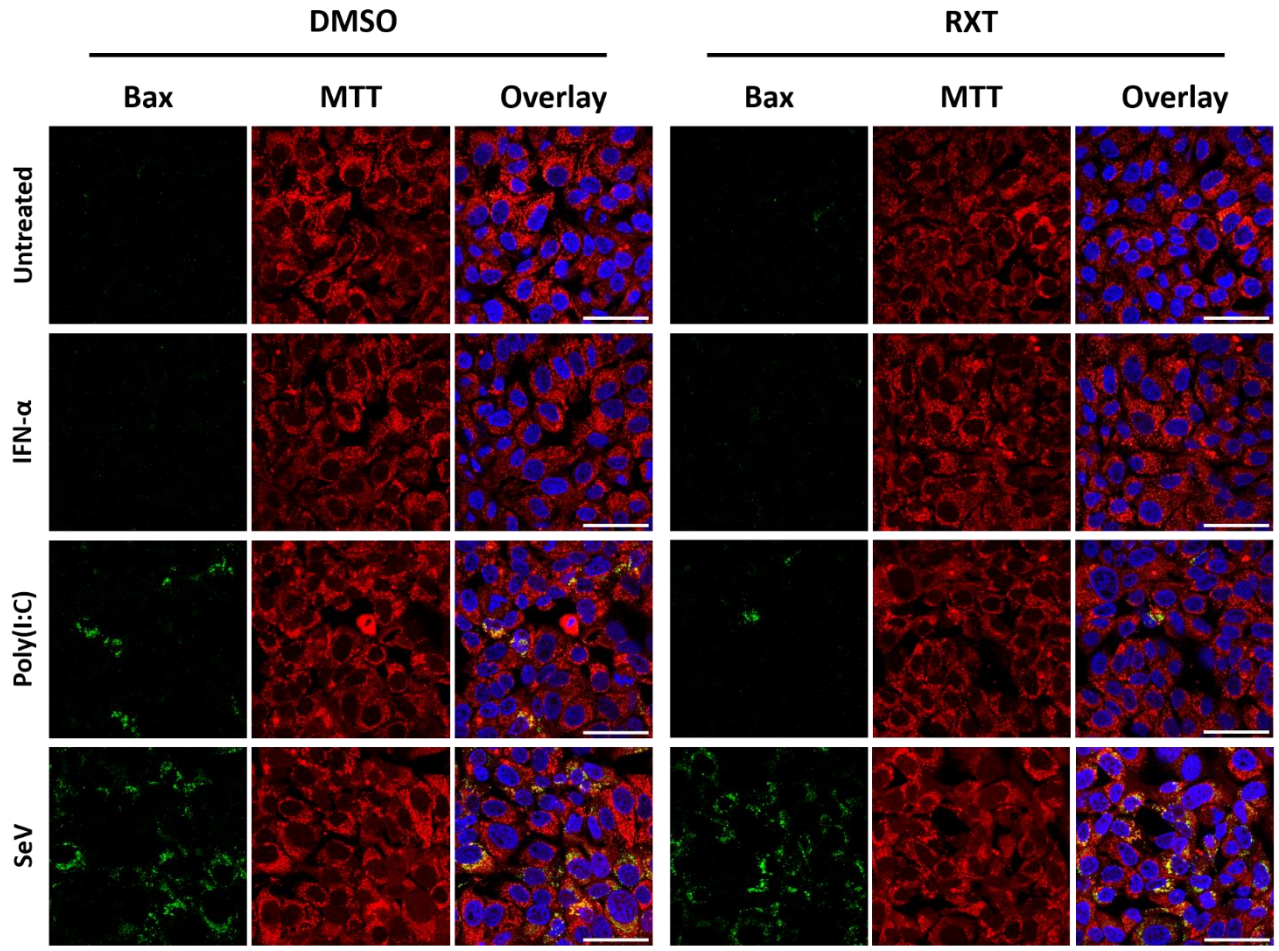

Figure 6.7: Poly(I:C) but not SeV-mediated mitochondrial relocalisation of Bax protein is antagonised by inhibition of the type I IFN signalling response. WT PK-15 cells were seeded onto coverslips in 24-well plates treated with 100 µM Z-VAD(OMe)-FMK and either 1000 IU/ml porcine IFN-α, 100 µg/ml poly(I:C) or 200 HA/ml SeV in the presence of DMSO or 0.5 µm RXT. 18 hours post-treatment, cells were treated with MitoTracker (MTT) Red CMXRos (red) for a further 30 min and fixed with 4% paraformaldehyde. Fixed cells were analysed by immunofluorescence using a polyclonal Ab recognising Bax which was co-stained with Alexa Fluor 488 IgG H+L (green). Nuclei are stained blue with DAPI. Scale bars represent 45 µM

α did not appear to trigger any (figure 6.7). However, when treated with RXT, poly(I:C)-mediated mitochondrial relocalisation of Bax was heavily antaognised while SeV-mediated relocalisation remained entirely unaffected. This showed that poly(I:C) stimulation of the JAK-STAT signalling pathway enhances the relocalisation of Bax in PK-15 cells. SeV stimulation of the JAK-STAT signalling pathway was not expected to have an effect as it encodes C-protein, a known antagonist of Janus kinase (JAK) 1/2 (Garcin *et al.*, 2002).

6.3.2. Bax protein expression levels are unaffected by inhibition of the type I IFN signalling response

In knowledge of the newfound role of the type I IFN signalling response in enabling poly(I:C)-mediated mitochondrial relocalisation of Bax, it was important to determine whether the reason for this phenomenon was because of an upregulation of Bax protein. WT PK-15 cells were treated with either porcine IFN-α, poly(I:C) or SeV in the absence of Z-VAD(OMe)-FMK and whole-cell lysates were then analysed by Western blot for the presence of Bax, cleaved-caspase-3 and the ISGs Mx1 and ISG15. ISG expression was analysed in order to confirm successful antagonism of the type I IFN signalling response.

Levels of Bax protein expression appeared to be relatively consistent, both in the presence of each agonist (IFN-α, poly(I:C) and SeV) and RXT (figure 6.8). In agreement with previous observations, cleaved caspase-3 production was reduced following poly(I:C) but not SeV treatment in the presence of RXT. This indicated that upregulation of Bax expression is not a prerequisite for the induction of IRF3 and Bax-mediated apoptosis and further confirmed that the type I IFN signalling response (stimulation of the JAK-STAT pathway) upregulates poly(I:C)-mediated apoptosis.

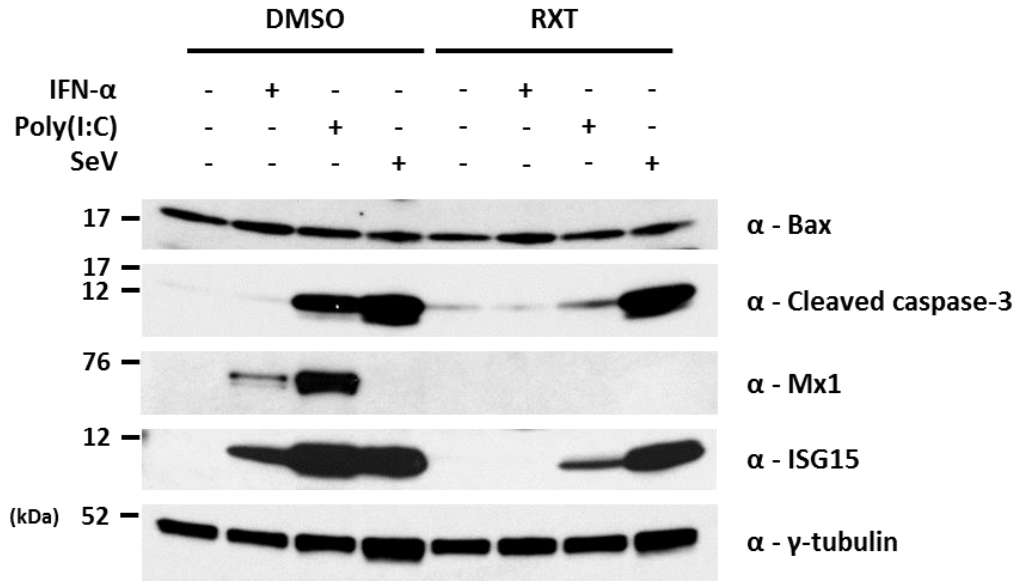

Figure 6.8: Bax protein expression levels are unaffected by inhibition of the type I IFN signalling response. WT PK-15 cells were prepared in 12-well plates and treated with either 1000 IU/ml porcine IFN-α, 100 µg/ml poly(I:C) or 200 HA/ml SeV in the presence of DMSO or 0.5 µm RXT. Whole cell lysates were prepared and analysed by Western blotting using polyclonal Abs recognising Bax, cleaved caspase-3 or ISG15 and a mAb recognising Mx1. A mAb recognising γ-tubulin was used to determine relative protein concentrations.

6.3.3. Bax protein expression levels remain unchanged in the absence of IRF3

It had been established that poly(I:C) and SeV-mediated mitochondrial relocalisation of Bax is dependent on IRF3 (6.2.2, figure 6.2) and antagonised by stable expression of N^{pro} (6.2.3, figures 6.3 and 6.4). In addition, the type I IFN signalling response had been shown to be responsible for amplification of poly(I:C)-mediated Bax relocalisation (6.3.1, figure 6.7). Next, experiments were conducted to determine if the levels of Bax expression change in the absence of IRF3. Whole cell lysates prepared from WT and a representative $IRF3^{-/-}$ PK-15 cell line (line 18) were analysed by Western blot for the presence of Bax. While cleaved caspase-3 was absent from poly(I:C)-treated $IRF3^{-/-}$ cells, levels of Bax protein expression were indistinguishable from those observed in WT cells (figure 6.9).

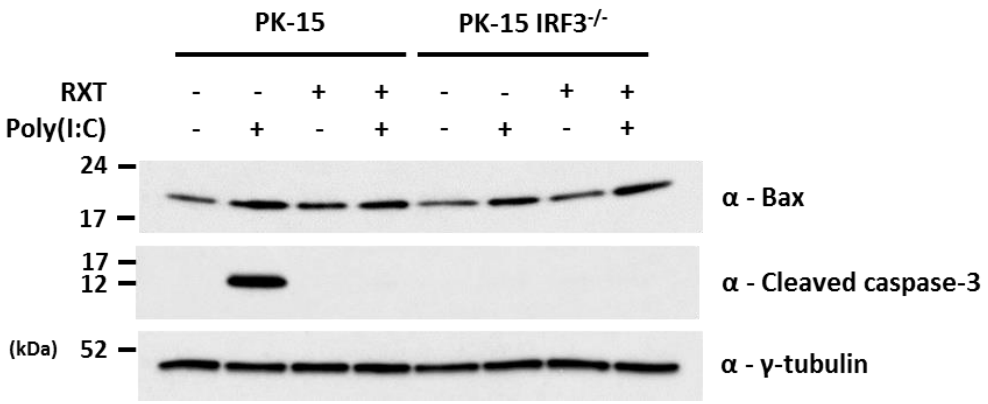

Figure 6.9: Bax protein expression levels are unaffected by the absence of IRF3. Whole cell lysates from poly(I:C) and RXT-treated WT and IRF3$^{-/-}$ PK-15 previously analysed in 5.4.1 (figure 5.6) were analysed by Western blotting using a polyclonal Ab recognising Bax. Cleaved caspase-3 and γ-tubulin data has been duplicated from figure 5.6.

6.3.4. Bax protein expression levels remain unchanged in the presence of N^{pro}

While N^{pro} targets IRF3 for proteasomal degradation, deletion of IRF3 was not observed to have any effect on levels of Bax protein expression. One remaining possibility is that N^{pro} may antagonise apoptosis by modulating and antagonising levels of Bax. To that end, N^{pro}-expressing cell lines were assessed to determine whether N^{pro} has the capacity to antagonise Bax expression.

Initially, a representative N^{pro}-expressing PK-15 cell line, His-N^{pro} 23, was used to assess the expression level of Bax due to its previously observed strong antagonism of poly(I:C) and SeV-mediated apoptosis. WT and His-N^{pro} 23 PK-15 cells were treated with either poly(I:C) or SeV at two different concentrations (20 HA/ml and 200 HA/ml). 18 hpt, whole cell lysates were prepared and analysed by Western blot for the presence of Bax, cleaved-caspase 3 and N^{pro}. Bax protein expression levels appeared to remain relatively consistent with each treatment across each cell line (figure 6.10). Despite N^{pro}'s clear antagonism of both poly(I:C) and SeV-mediated apoptosis, as noted by the antagonism of cleaved caspase-3 induction, there was no

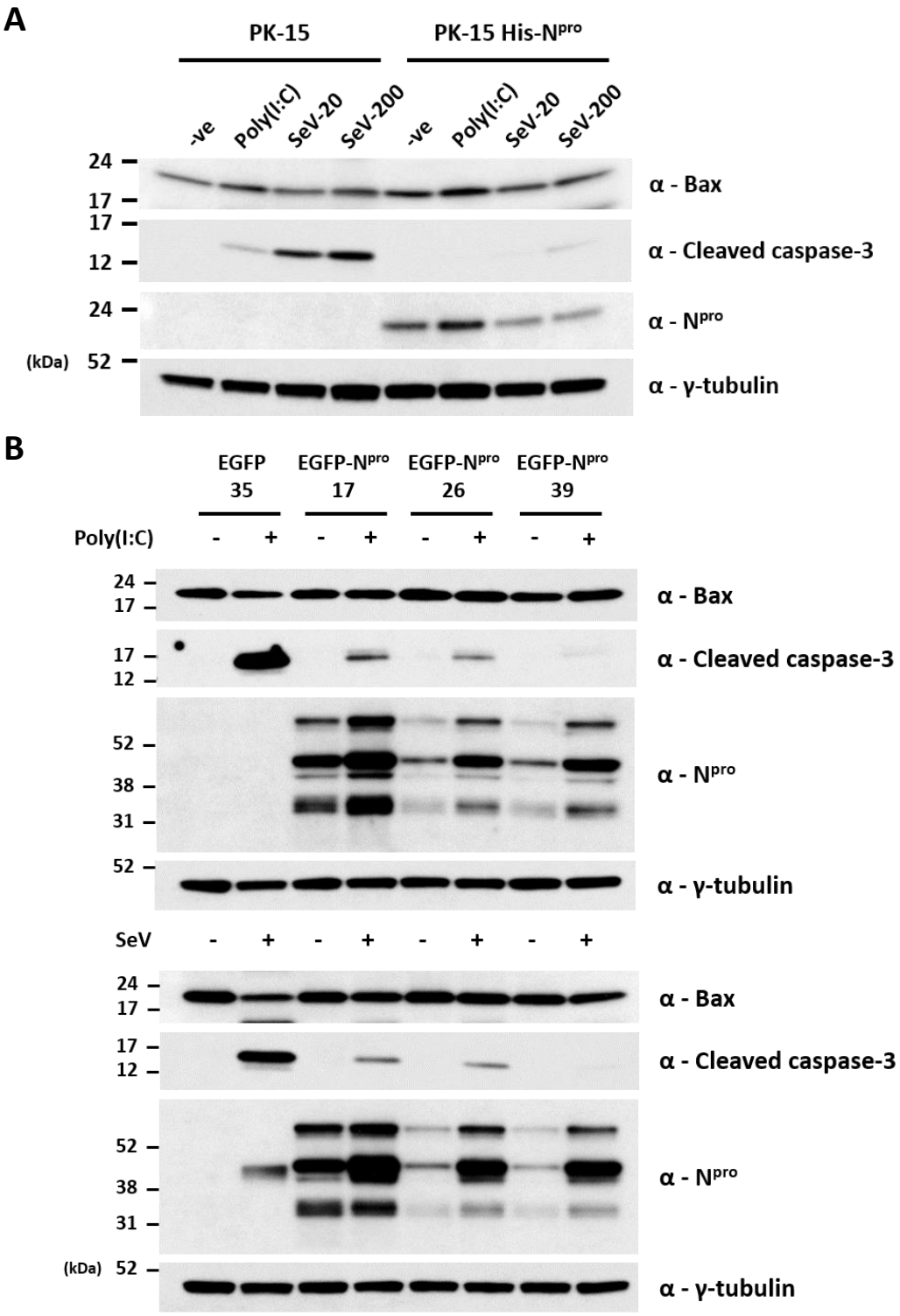

Figure 6.10: Bax protein expression levels remain unchanged in the presence of N^{pro}. (A) WT and His-N^{pro} 23 PK-15 cells were prepared in 12-well plates and treated with either 100 µg/ml poly(I:C) or SeV (20 or 200 HA/ml). Whole cell lysates were prepared and analysed by Western blotting using polyclonal Abs recognising Bax, cleaved caspase-3 or N^{pro}. A mAb recognising γ-tubulin was used to determine relative protein concentrations. (B) Whole cell lysates from poly(I:C) (top) and SeV-treated (bottom) EGFP and EGFP-N^{pro} PK-15 cell lines previously analysed by Western blot in 3.4.3 (figure 3.10) were re-analysed using a polyclonal Ab recognising Bax. Cleaved caspase-3, N^{pro} and γ-tubulin data has been duplicated from figure 3.10.

detectable antagonism of Bax protein expression levels. In line with previous observations,

notable increases in N^{pro} expression were noted following treatment with poly(I:C) but not SeV (figure 6.10, A).

To further confirm N^{pro}'s inability to antagonise Bax protein expression, whole cell lysates from three poly(I:C) or SeV-treated EGFP-N^{pro} cell lines were also analysed for the presence of Bax. As observed with the His-N^{pro} 23 cell line (figure 6.10, A), levels of Bax remained consistent across each of the EGFP-N^{pro} cell lines analysed despite a clear antagonism of both poly(I:C) and SeV-mediated apoptosis in each (figure 6.10, B).

6.4. CSFV antagonises pro-apoptotic IRF3/Bax activity

6.4.1. Wild-type and N^{pro}-deleted recombinant CSFV (rCSFV) strains antagonise poly(I:C)-mediated Bax relocalisation and caspase-3 cleavage while only wild-type rCSFV is able to partially antagonise SeV-mediated Bax relocalisation and caspase-3 cleavage

In order to demonstrate that CSFV mirrors N^{pro}'s antagonism of not only poly(I:C) and SeV-mediated caspase-3 cleavage but also mitochondrial relocalisation of Bax, infections of SK6 cells were performed. SK6 cells were prepared in 24-well plates and infected (MOI 0.2) with WT or N^{pro}-deleted (ΔN^{pro}) recombinant CSFV Alfort (rCSFV) and then treated with each agonist prior to analysis by immunofluorescence microscopy (figure 6.11, A and B) and Western blot (figure 6.11, C). SK6 cells, which do not produce IFN but do undergo apoptosis following poly(I:C) treatment, were used for these experiments due to the inability of ΔN^{pro} rCSFV to efficiently replicate in PK-15 cells which have an intact IFN response.

When analysed by immunofluorescence microscopy, SK6 cells that were infected with rCSFV prior to poly(I:C) treatment displayed no visible Bax relocalisation ($p<.001$), while those infected with ΔN^{pro} rCSFV displayed reduced levels of relocalisation in comparison to the uninfected cells ($p=.001$). However, when treated with SeV, only a partial reduction in Bax relocalisation was observed with rCSFV while none was observed with ΔN^{pro} rCSFV (figure 6.11,

A and B). Significance was determined by calculating the proportion of cells displaying Bax relocalisation as detailed in 2.14.5. Subsequent Western blot analyses confirmed that rCSFV inhibited the production of cleaved caspase-3 and ISG15 upregulation following poly(I:C) treatment, but could only partially inhibit cleaved caspase-3 production following SeV treatment (figure 6.11, C). ΔN^{pro} rCSFV also inhibited the production of cleaved caspase-3 and ISG15 upregulation following poly(I:C) treatment, but did not antagonise either following SeV

A

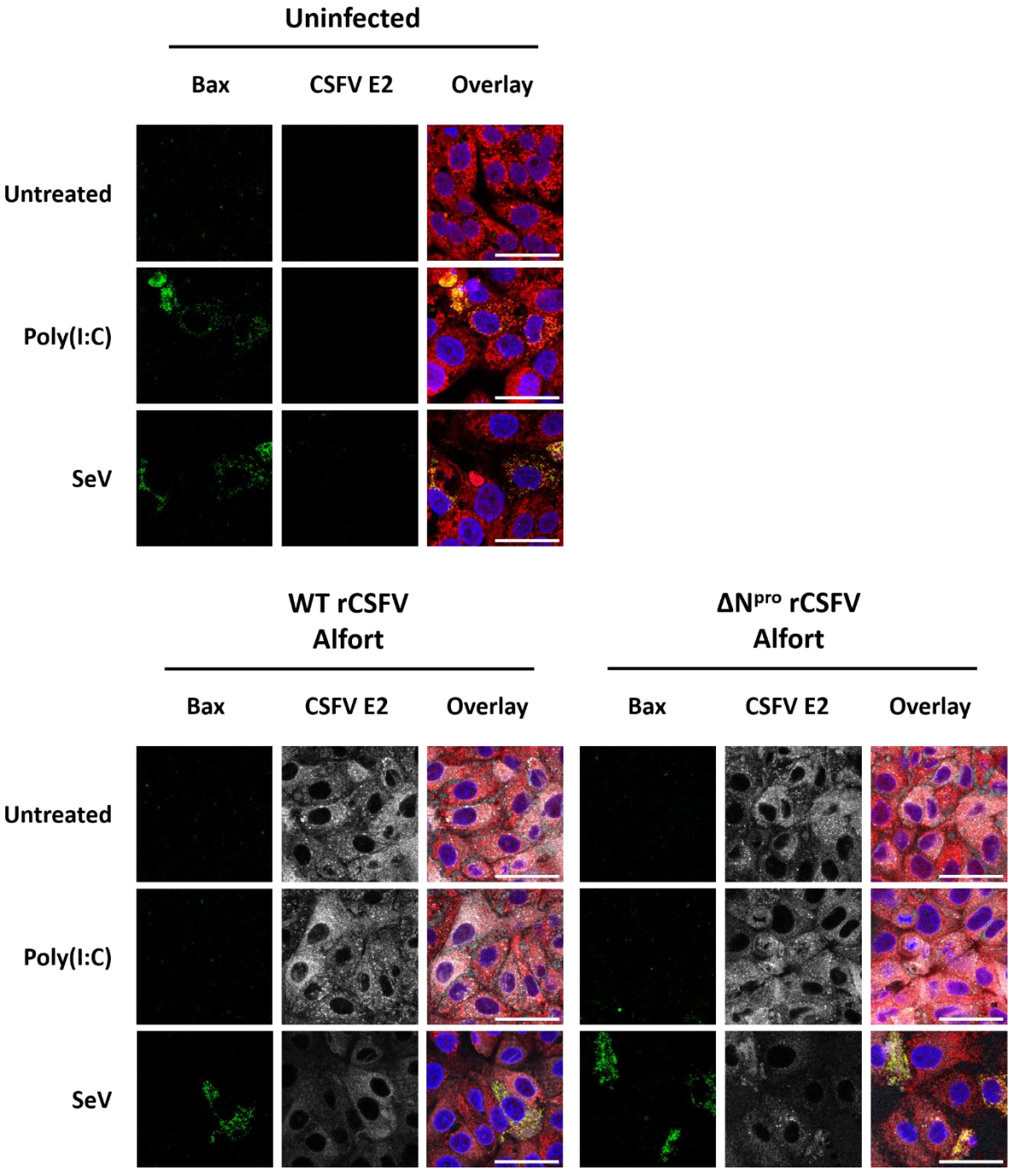

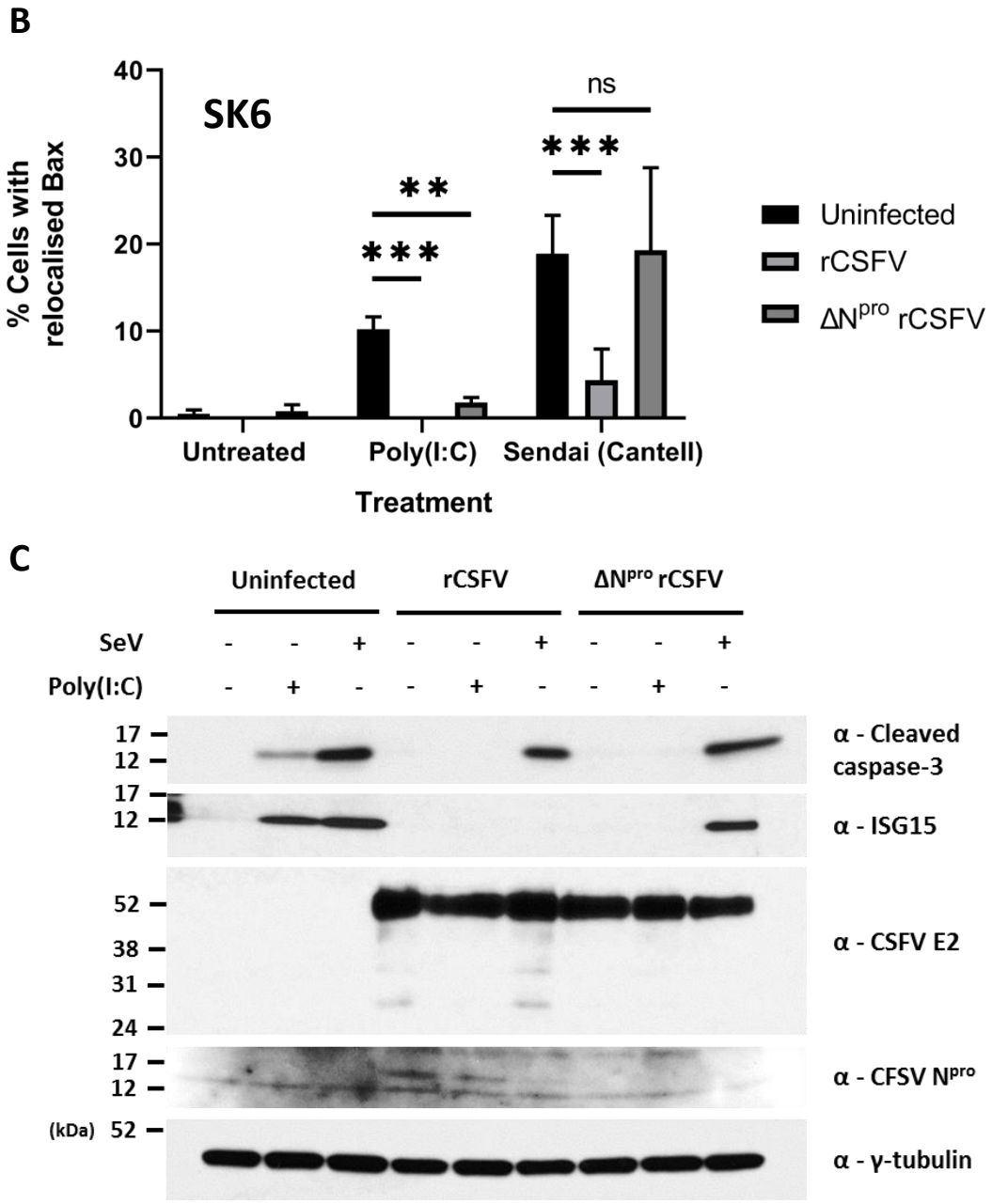

Figure 6.11: Wild-type and N^{pro}-deleted recombinant CSFV (rCSFV) strains antagonise poly(I:C)-mediated Bax relocalisation and caspase-3 cleavage while only wild-type rCSFV is able to partially antagonise SeV-mediated Bax relocalisation and caspase-3 cleavage. (A) SK6 cells were infected (MOI of 0.2) with WT or ΔN^{pro} rCSFV Alfort for 72 hr and then treated with poly(I:C) or SeV as indicated. 18 hours post-treatment, cells were treated with MitoTracker (red) and analysed by immunofluorescence microscopy using a polyclonal Ab recognising Bax (green) and a mAb recognising CSFV E2 (grey). Nuclei are stained blue with DAPI. (B) The percentage of cells displaying Bax relocalisation following each treatment was then quantified; ns: not significant, **: p<.01, ***: p<.001. (C) In parallel, whole cell lysates from replicate samples were analysed by Western blot using polyclonal Abs recognising ISG15 or N^{pro} and mAbs recognising cleaved caspase-3, or CSFV E2. A mAb recognising γ-tubulin was used to determine relative protein concentrations.

treatment. Comparison of the respective levels of structural E2 glycoprotein expressed following either infection confirmed the viruses had replicated to equivalent levels, however,

the low levels of N^{pro} expressed by rCSFV indicated a low level of virus replication (figure 6.11, C).

It was therefore hypothesised that the inability of rCSFV to completely inhibit Bax localisation and effectively inhibit caspase-3 cleavage following SeV treatment was due to inefficient virus replication and consequently low levels of N^{pro} expression. To address this, additional experiments were performed in which rCSFV alongside two wild-type CSFV strains (Alfort and Brescia) were also used to infect SK6 and PK-15 cells prior to SeV treatment.

6.4.2. Wild-type CSFV Alfort and Brescia strains antagonise SeV-mediated caspase-3 cleavage and mitochondrial Bax relocalisation in PK-15 and SK6 cells

PK-15 and SK6 cells were infected (MOI 0.2) with either rCSFV, CSFV Alfort or Brescia strains and subsequently treated with SeV. Fixed cells were then subjected to immunofluorescence analysis (figure 6.12, A and B). Following treatment with SeV, rCSFV, CSFV Alfort and CSFV Brescia-infected PK-15 cells each demonstrated reduced Bax relocalisation ($p=.021$, $p<.001$, $p<.001$) in comparison to non-infected PK-15, however, the reduction was most significant with the two non-recombinant Alfort and Brescia strains. Antagonism of Bax relocalisation in SeV treated SK6 cells appeared comparable, irrespective of infecting CSFV strain ($p<.001$, $p<.001$, $p<.001$).

To determine whether the reduction in SeV-mediated Bax relocalisation in CSFV Alfort and Brescia infected PK-15 and SK6 cells corresponded to reduced levels of caspase-3 cleavage, replicate lysates were subjected to Western blot analysis. Infection of PK-15 cells with CSFV Alfort and Brescia was associated with a greater reduction in caspase-3 cleavage than that observed in rCSFV-infected cells while in infected SK6 cells the reduction was comparable, irrespective of infecting CSFV strain (figure 6.12, C). Levels of N^{pro} expression were noticeably higher in cells infected with the non-recombinant CSFV Alfort and Brescia strains in

comparison to that observed for rCSFV. In summary, these results confirmed that CSFV is indeed capable of antagonising SeV-mediated mitochondrial Bax relocalisation and cleavage of caspase-3 in multiple porcine kidney endothelial cell lines.

6.5. Yeast two-hybrid screen confirms IRF3/N^{pro} interaction but not IRF3/Bax or N^{pro}/Bax interactions

6.5.1. Conservation of a putative BH3-homology domain suggests possible interaction between porcine IRF3 and Bax

An *in vitro* interaction between human IRF3 and Bax has been reported (Chattopadhyay *et al.*, 2010, Chattopadhyay *et al.*, 2011) and IRF3$^{-/-}$ mice have been developed in which this IRF3/Bax-mediated pathway of apoptosis no longer exists, suggesting the interaction also has significance *in vivo* (Chattopadhyay *et al.*, 2016).

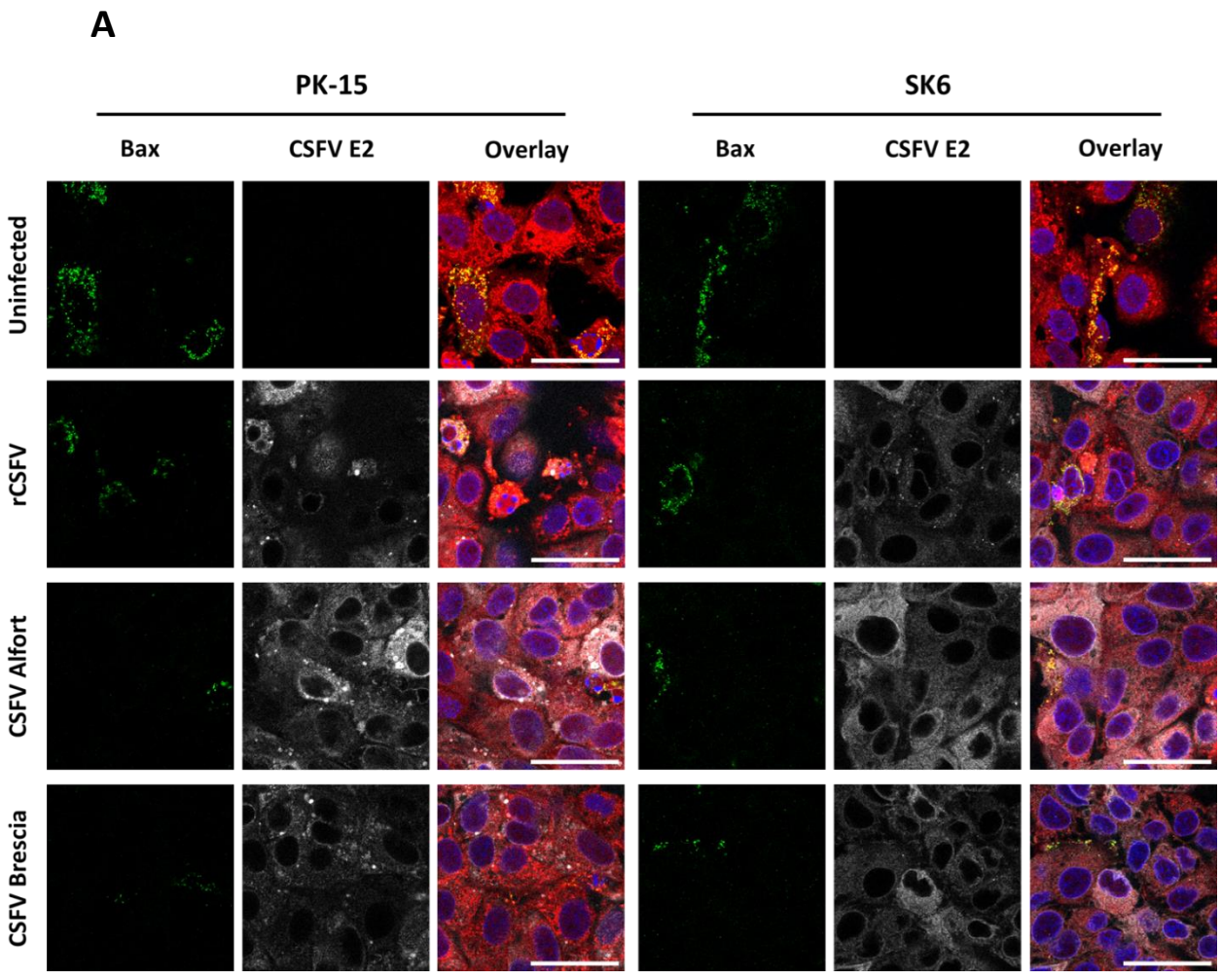

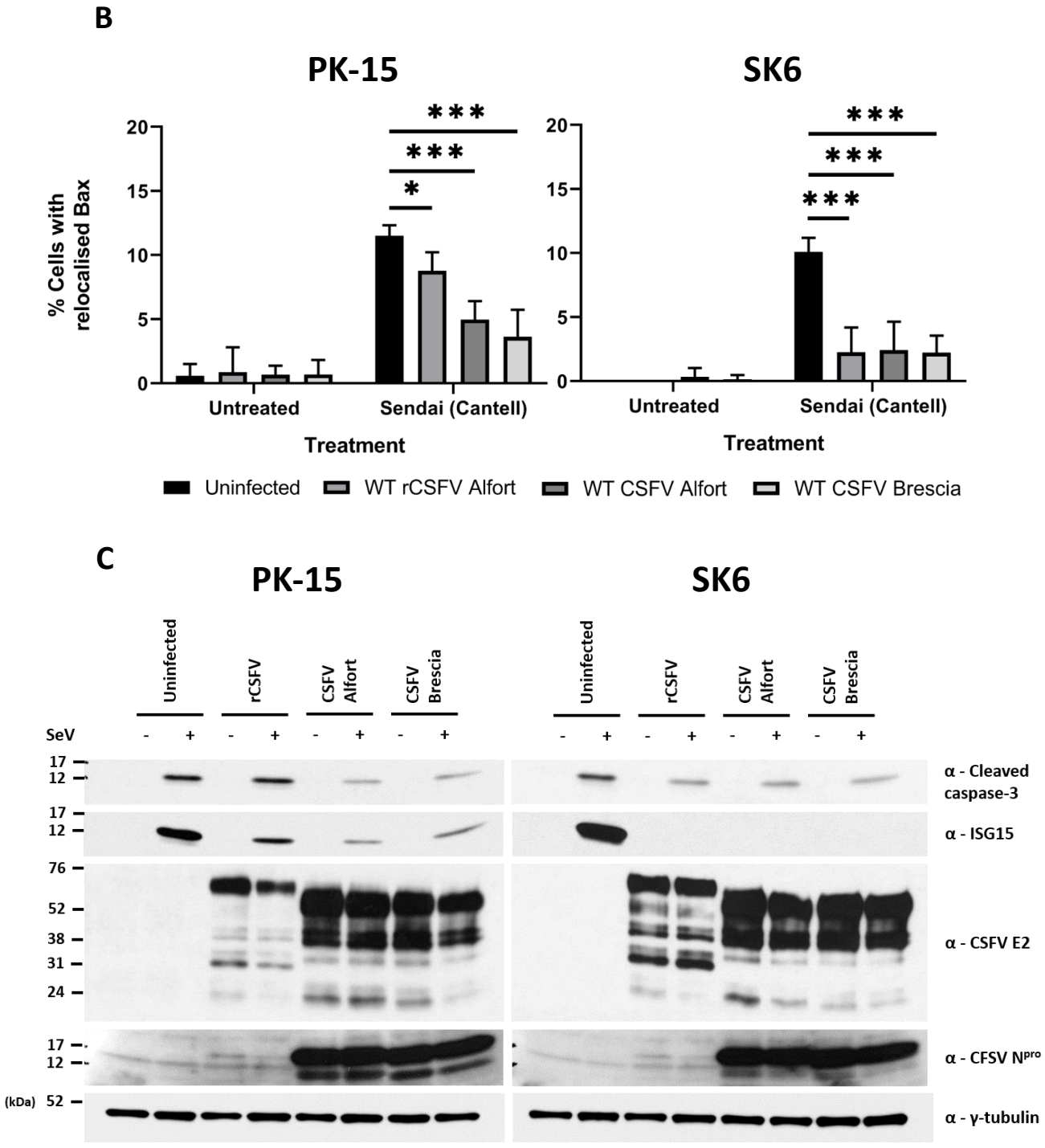

Figure 6.12: Wild-type CSFV Alfort and Brescia strains antagonise SeV-mediated caspase-3 cleavage and mitochondrial Bax relocalisation in PK15 and SK6 cells. (A) WT PK-15 and SK6 cells were infected (MOI of 0.2) with rCSFV Alfort, CSFV Alfort or CSFV Brescia for 72 hr and then treated with SeV. 18 hours post-treatment, cells were treated with MitoTracker (red) and analysed by immunofluorescence staining using a polyclonal Ab recognising Bax (green) and a mAb recognising CSFV E2 (grey). Nuclei are stained blue with DAPI. (B) The percentage of cells displaying Bax relocalisation following each treatment was then quantified; ns: not significant, *: p<0.05, **: p<.01, ***: p<.001. (C) In parallel, whole cell lysates from replicate samples were analysed by Western blot using polyclonal Abs recognising ISG15 or N^{pro} and mAbs recognising cleaved caspase-3 or CSFV E2. A mAb recognising γ-tubulin was used to determine relative protein concentrations.

Indeed, they confirmed a putative BH3-only domain in human IRF3 to be required for its interaction with Bax. Subsequent alignments with known porcine homologs of human BH3-only proteins and a human consensus sequence (Day *et al.*, 2008) were performed and indicated the same domain might also be present in porcine IRF3 (figure 6.13). While only 2 residues appear to be conserved at the residue level (Leu^{370} and Asp^{375}), they have each been implicated in facilitating interactions with other Bcl2-family proteins (Hinds and Day, 2005). Despite lacking conservation, other residues of porcine IRF3 (Val^{366}, Leu^{373}, Ala^{377} and Arg^{377}) appear to share the same biochemical properties as their BH3-only protein counterparts.

To determine whether porcine IRF3 and Bax interact and whether CSFV N^{pro} has any capacity to act directly on Bax, a yeast two-hybrid screen was performed. Identification of interactions between these proteins would shed light on their respective roles in poly(I:C) and SeV-mediated apoptosis. The yeast two-hybrid system has been used extensively within the group to explore and elucidate protein-protein interactions which is why it was chosen over immunoprecipitation (IP) and immunofluorescence microscopy co-localisation. The Clontech Matchmaker© 3 GAL4-based yeast two-hybrid system enables the screening of interactions

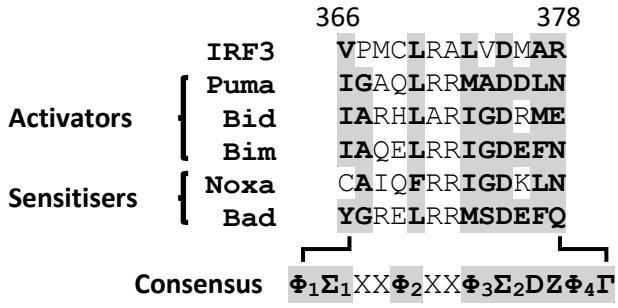

Figure 6.13: Porcine IRF3 shares homology with "activator" and "sensitiser" BH3-only proteins and also a human consensus sequence, suggesting the existence of a putative BH3 domain. Porcine IRF3 (NP_001184051.1), Puma (XP_013853986.2), Bid (NP_001025706.1), Noxa (NP_999312.2) and Bad (XP_020938542.1) protein sequences were aligned in MEGA, revealing conservation of residues with similar biochemical properties. Key consensus residues that define the human BH3 domain are highlighted grey; Φ_1–Φ_4 represent hydrophobic residues (Φ_2 is usually a conserved leucine), Σ_1 and Σ_2 are small residues (G, A, S), Z is usually an acidic residue, D is a conserved aspartate, Γ is a hydrophilic residue (N, H, D or Y) and X is any residue (Day *et al.*, 2008).

between two proteins by employing cDNA sequences encoding proteins of interest fused to either the GAL4 DNA binding domain (DNA-BD) or GAL4 activation domain (AD) (Fields and Song, 1989, Chien *et al.*, 1991). When these fusion proteins interact, the DNA-BD and AD are brought into close proximity enabling the transcription of reporter proteins which either facilitate growth on restrictive media or hydrolyse chromogenic substrates. Ultimately, only yeast containing plasmids encoding interacting proteins will be able to survive under the most stringent media selection. Positive and negative controls are included to confirm both the functionality of the system and to determine whether any components have the capacity to self-activate (table 6.1).

Table 6.1: Positive and negative control vectors were employed in order to confirm system functionality, identify self-activation and also non-specific interactions.

Vector	Type	Control
pGADT7-IkBα	+	Human IkBα interacts with CSFV N^{pro} (Doceul *et al.*, 2008)
pGADT7-T	+	T interacts with 53 (Iwabuchi *et al.*, 1993, Li and Fields, 1993)
pGBKT7-53	+	53 interacts with T (Iwabuchi *et al.*, 1993, Li and Fields, 1993)
pGBKT7-LAM	-	LAM does not interact with T (Bartel *et al.*, 1993, Ye and Worman, 1995)
pGADT7	-	Empty vector
pGBKT7	-	Empty vector

Note: Acronyms: SV40 large T antigen (T), murine p53 (53), human lamin C (LAM). + and - indicate positive and negative controls respectively.

6.5.2. Cloning of Bax yeast two-hybrid vectors

Briefly, cDNA sequences encoding full-length porcine Bax (Bax^L, XM_003127290.5) and a predicted truncated isoform utilising a putative downstream start codon (Bax^S, XM_013998624.2) were each synthesised in the pMA-RQ vector (GeneArt). To generate pGBKT7-Bax vectors, cDNA (600 bp and 500bp, respectively) encoding Bax^L and Bax^S proteins were gel-purified and ligated into *Nde*I/*Sma*I-digested pGBKT7 plasmid.

6.5.3. Screen for potential interactions between IRF3, $Bax^{L/S}$ and N^{pro}

Yeast were prepared and co-transformed with the vector combinations outlined in table 2.11 and figure 6.15 as detailed in 2.19. Transformed yeast were initially plated onto double dropout (DDO) media deficient in leucine (Leu) and tryptophan (Trp) – this enabled the isolation of yeast cells which had received both plasmids since they encoded Leu and Trp biosynthesis genes which are otherwise absent from the cells (figure 6.16, A, top). A lawn of white colonies were observed for yeast co-transformed with N^{pro}+IRF3 as well as the positive controls N^{pro}+IkBα (Doceul *et al.*, 2008) and T+53 (Iwabuchi *et al.*, 1993, Li and Fields, 1993). However only a handful of orange colonies were observed for any of the yeast co-transformed with a plasmid encoding either Bax isoform. Negative control T+LAM yeast displayed significantly more growth on DDO media than yeast co-transformed with $Bax^{L/S}$ vectors, however observed colonies were the same pigmentation.

Yeast were then restreaked from the DDO plates onto quadruple dropout (QDO) media lacking adenine (Ade) and histidine (His) in addition to Leu and Trp in order to isolate cells in which an interaction had occurred. White colonies were again detected for yeast co-transformed with N^{pro}+IRF3 and the positive controls N^{pro}+IkBα and T+53, indicating interactions between the

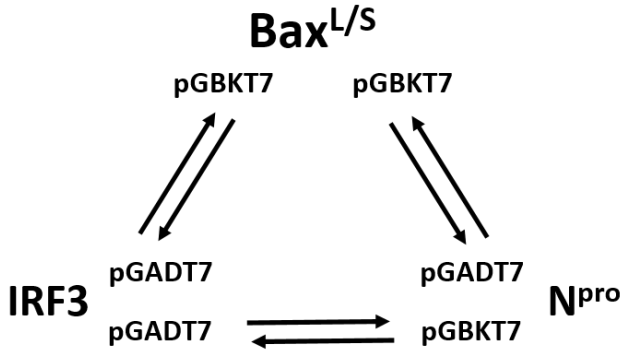

Figure 6.15: Vector cloning for yeast two-hybrid screen of porcine Bax, porcine IRF3 and N^{pro} (CSFV Alfort). (A) Bax^{L} and Bax^{S} ($Bax^{L/S}$) cDNA sequences were extracted from NdeI/SmaI-digested plasmids for ligation into NdeI/SmaI-digested pGBKT7 GAL4 DNA-BD yeast vector. (B) Interactions between $Bax^{L/S}$+IRF3, IRF3+N^{pro} and also N^{pro}+$Bax^{L/S}$ were screened for using the yeast two-hybrid system.

respective proteins. However, unlike on DDO media lacking only Leu and Trp, no orange colonies were observed on QDO media for any of the yeast transformed with a plasmid encoding Bax. As an additional control and to identify self-activation/non-specific interactions, yeast were co-transformed with $Bax^{L/S}$ vector and pGADT7 empty vector; on DDO media the resulting colonies were orange and few in number and this remained unchanged when cells were co-transformed with $Bax^{L/S}$ vector and pGADT7-T (figure 6.16, A, bottom). In contrast, co-transformation of IRF3 and either empty pGBKT7 or pGBKT7-53 (negative controls for IRF-3-N^{pro} interaction) produced many orange colonies on DDO media.

6.5.4. Isolation of potential $Bax^{L/S}$ colonies

Colonies from yeast co-transformed with IRF3+$Bax^{L/S}$ and N^{pro}+$Bax^{L/S}$ on DDO media were re-streaked onto fresh DDO media (figure 6.16, B) and subsequently QDO media alongside single colonies of positive-control N^{pro}+IRF3, N^{pro}+IkBα and T+53 yeast and negative-control T+LAM yeast. However, no colony growth was observed while each positive control (N^{pro}+IRF3, N^{pro}+IkBα and T+53) displayed significant growth. In summary, these data confirm the putative interaction between CSFV N^{pro} and porcine IRF3 but failed to identify whether there are interactions between either isoform of porcine Bax and CSFV N^{pro} or porcine IRF3.

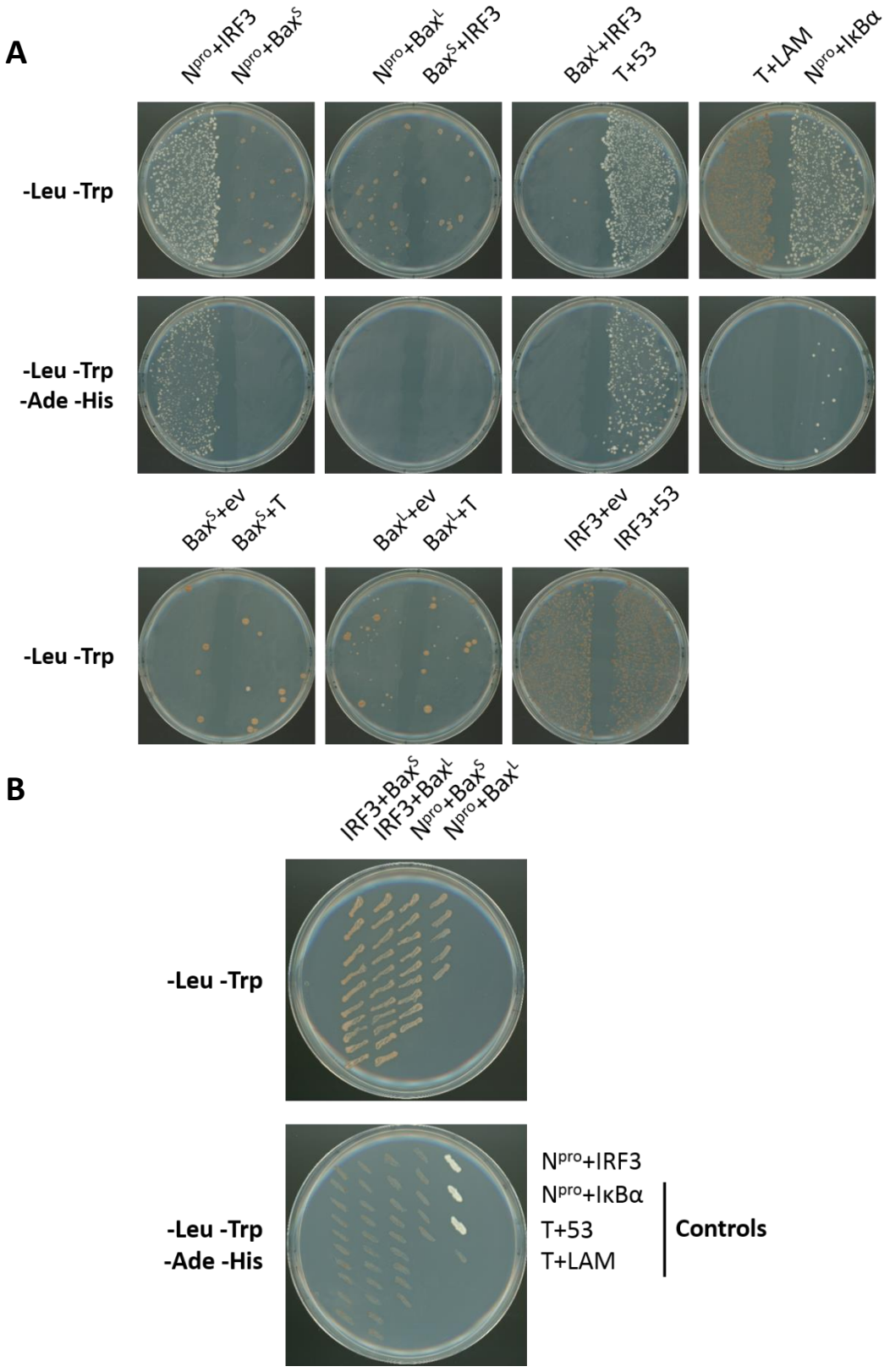

Figure 6.16 Yeast two-hybrid screen confirms interaction between N^{pro} and porcine IRF3 but not $Bax^{L/S}$ and N^{pro} or porcine IRF3. (A) Yeast were co-transformed with the indicated vectors and plated onto double dropout (DDO) media deficient in Leu and Trp or quadruple dropout (QDO) media deficient in Leu, Trp, Ade and His. Usage of an empty vector control is indicated with ev. (B) Individual colonies of yeast co-transformed with IRF3+$Bax^{L/S}$, N^{pro}+$Bax^{L/S}$, N^{pro}+IRF3, the positive controls N^{pro}+IkBα and T+53 and also the negative control T+LAM.

6.6. Generation of porcine IRF3 mutant to investigate IFN and transcriptional upregulation-independent IRF3-mediated apoptosis

According to recent work by Chattopadhyay *et al*., IRF3 has a directly pro-apoptotic function that is entirely separate from its ability to upregulate the transcription of a host of genes including that which encodes IFN-β, a type I IFN (Chattopadhyay *et al.*, 2010, Chattopadhyay *et al.*, 2011, Chattopadhyay *et al.*, 2016). As discussed in 1.3.3.2, they demonstrated *in vivo* that a murine IRF3 S1 mutant containing two serine mutations (Ser^{388} and Ser^{390} to Ala) was unable to mediate gene upregulation but retained its ability to trigger apoptosis following challenge with SeV (Strain 52). These residues have been identified as having a potentially essential role in IRF3's interaction with CREB-binding protein (CBP), a prerequisite for IRF3's binding to gene promoters (Lin *et al.*, 1998, Servant *et al.*, 2003, Chen *et al.*, 2008). In 6.5, a yeast two-hybrid screen was performed however it failed to identify an interaction between porcine IRF3 and porcine Bax. In a renewed attempt to determine whether porcine IRF3 retains the apoptotic functions of its murine counterpart, a porcine IRF3 construct bearing the same serine residue mutation was generated with the intention of investigating its ability to restore poly(I:C) and SeV-mediated apoptosis in the absence of ISG upregulation.

6.6.1. IRF3 phosphorylation sites are conserved

In order to establish whether the serine residues in question are conserved, sequence alignments of human (NP_001562.1), murine (XP_006541058.1) and porcine IRF3 (NP_998935.1) were performed using MEGA7 (Mega Software). IRF3 has two phosphorylation sites at its c-terminus termed sites 1 and 2 (figure 6.17, A) each comprised of serine or threonine residues. The alignment showed that Ser^{396} and Ser^{398}, the site 2 residues mutated in murine IRF3 by Chattopadhyay *et al*., were conserved in porcine IRF3 as well as every other

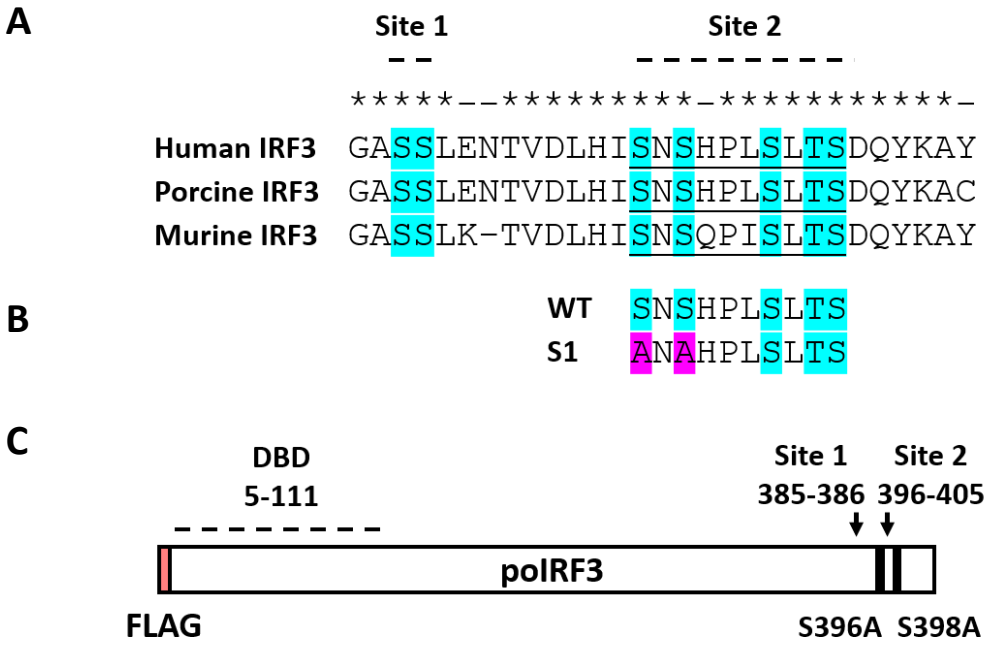

Figure 6.17: Conserved serine residues implicated in IRF3's transcriptional activity were mutated and cloned into the lentiviral plasmid pLJM1 as EGFP FLAG-tagged fusions. (A) Alignments of human, porcine and murine IRF3 protein sequences were performed in MEGA7 (Mega Software) to confirm conservation of residues implicated in IRF3's transcriptional activity. Conserved (*) and non-conserved residues (-) are indicated as is the DNA binding domain (DBD) of IRF3. Mutations were designed in porcine IRF3 (B) which were subsequently cloned into the lentiviral plasmid pLJM1 to generate N-terminal FLAG-tagged WT and S1 mutant poIRF3 fusions (C).

serine and threonine residue at each of the two sites. Therefore, a porcine S1 mutant of IRF3 (poIRF3^{S1}) was prepared (figure 6.17, B and C).

6.6.2. Generation of pcDNA3.1 plasmids expressing EGFP-tagged WT or S1 mutant porcine IRF3

Initially, EGFP-tagged poIRF3^{WT} and poIRF3^{S1} fusions were prepared in the mammalian expression vector pcDNA3.1 as outlined in appendix D. WT and S1 mutant IRF3 expressed successfully in PK-15 and SK6 cells and their cytosolic, non-nuclear distribution was correct, however the overall rate of transfection of these plasmids in PK-15 cells was very poor (data not shown). Therefore, the decision was made to instead express each construct via 3rd-generation lentivirus.

6.6.3. Production of 3rd-generation lentiviruses expressing FLAG-tagged WT or S1 mutant porcine IRF3

To enable expression of poIRF3^{WT} and poIRF3^{S1} via lentivirus, each sequence was first subcloned into the lentiviral transfer plasmid, pLJM1. The FLAG tag (DYKDDDDK) was chosen instead of EGFP due to its vastly reduced size. Briefly, poIRF3^{WT} and poIRF3^{S1} were PCR amplified with a forward primer containing an *Age*I restriction site, Kozak sequence, start codon and FLAG tag cDNA and a reverse primer containing an *Eco*RI restriction site (FW-AgeI-kozak-FLAG-poIRF3, RV-poIRF3-EcoRI; table 2.20). The resulting PCR products were ligated into *Age*I/*Eco*RI-digested pLJM1 to generate pLJM1-FLAG-poIRF3-W1 and pLJM1-FLAG-poIRF3-S1. 3rd-generation lentiviruses expressing FLAG-tagged poIRF3^{WT} or poIRF3^{S1} were subsequently generated using the procedure outlined in 2.12.1.

IRF3$^{-/-}$ PK-15 cell lines (7 and 18) were then infected with each lentivirus and enriched as pools of transduced cells using puromycin selection (see 2.12.2). To confirm expression of FLAG-tagged poIRF3^{WT} and poIRF3^{S1}, whole cell lysates were prepared from these cells. Whole cell lysates were also prepared from uninfected wild-type and IRF3$^{-/-}$ PK-15 cells as negative controls. When analysed by Western blot, bands of the expected size (48 kDa) and of identical intensity were detected for each of the cell lines infected with lentiviruses encoding either IRF3 fusion protein (figure 6.18).

Due to time constrains however, it was not possible to study the functionality of either IRF3 fusion protein or to determine whether the S1 mutant has the capacity to restore sensitivity to poly(I:C) and SeV-mediated apoptosis in IRF3$^{-/-}$ PK-15 cells.

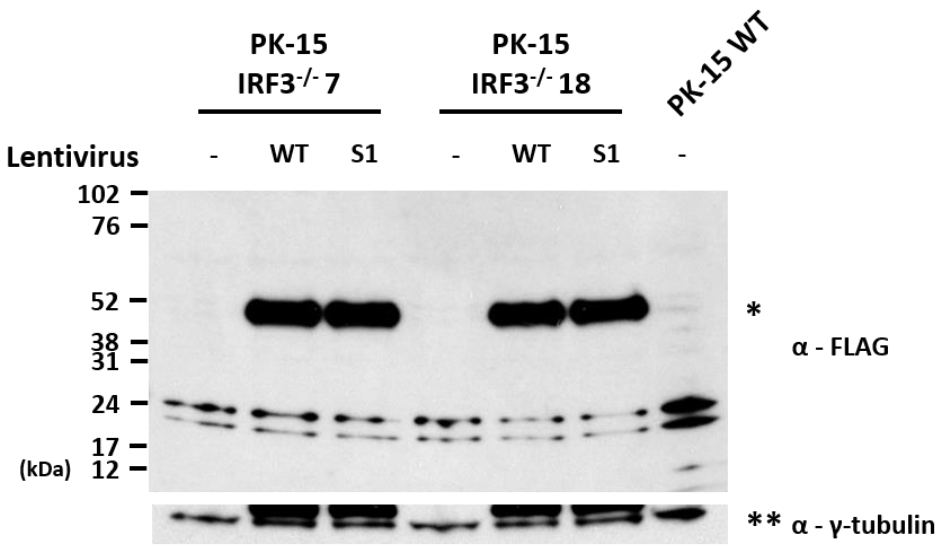

Figure 6.18: FLAG-tagged WT and S1 mutant porcine IRF3 resolve at their predicted sizes when analysed by Western blot. IRF3$^{-/-}$ PK-15 cell lines (7 and 18) infected with lentivirus encoding FLAG-tagged WT and S1 mutant porcine IRF3 were prepared in 12-well plates. Following 18 hrs of incubation, whole cell lysates were prepared and analysed alongside a sample from uninfected wild-type PK-15 cells by Western blotting using a mAb recognising the FLAG epitope. A mAb recognising γ-tubulin was used to determine relative protein concentrations. FLAG (*) and γ-tubulin (**) are indicated.

6.7. Discussion

IRF3 is a master regulator of the transcription of the IFN-β gene as well as a host of other proteins with innate antiviral functions (Randall and Goodbourn, 2008). Through an interaction, the N^{pro} protein of CSFV brings about the proteasomal degradation of IRF3, eliminating this response (Bauhofer *et al.*, 2007, Seago *et al.*, 2007). The importance of IRF3 in coordinating the induction of pro-apoptotic TLR3 and RIG-I mediated responses was shown in chapter 5. IRF3 has been implicated in the induction of a dsRNA-mediated IRF3/Bax dependent pathway of apoptosis termed RIPA (RLR-induced IRF3 mediated Pathway of Apoptosis) that also cumulates in cleavage of caspase-3 and cell death (Chattopadhyay *et al.*, 2010, Chattopadhyay *et al.*, 2011, Chattopadhyay *et al.*, 2016). Importantly, the authors showed that this pathway had no requirement for new transcriptional upregulation of genes (Chattopadhyay *et al.*, 2010) and instead relied upon linear polyubiquitiniation of IRF3 at specific lysine residues as opposed to phosphorylation (Chattopadhyay *et al.*, 2016). Considering N^{pro}'s well-documented ability to antagonise levels of IRF3 in CSFV-infected cells and those which stably express N^{pro}, it was important to determine the exact mechanism by which IRF3 mediates apoptotic responses in porcine cells and whether RIPA is a conserved pathway in cells which are susceptible to CSFV infection.

6.7.1. IRF3/Bax-mediated apoptosis

This putative IRF3/Bax-mediated pathway was found to be not only active in porcine kidney endothelial cells (as indicated by the absence of endogenous Bax relocalisation in $IRF3^{-/-}$ cells) but also heavily antagonised by both stable expression of N^{pro} and infection with CSFV as seen by the absence of, or significant reduction in, mitochondrial relocalisation of endogenous Bax and associated cleavage of caspase-3. In the present work, Bax staining appeared as distinct puncta associated with the mitochondria following treatment with poly(I:C) and SeV, likely corresponding to oligomeric pores comprised of Bax and possibly Bak homodimers. These

oligomeric homodimers have been reported to facilitate mitochondrial outer membrane permeabilization (MOMP) and release of apoptotic proteins such as cytochrome c and Smac (Zhou and Chang, 2008, Zhang *et al.*, 2017). As discussed in 1.3.1.1, BH3-only Bcl2-homology proteins such as Bid and Bim bind to Bax and Bak, promoting their oligomerisation at the mitochondrial outer membrane (MOM) (Wang *et al.*, 1996, Harada *et al.*, 2004, Shamas-Din *et al.*, 2011). Chattopadhyay *et al.* identified a putative BH3-only domain near the c-terminus of IRF3 (Chattopadhyay *et al.*, 2010), a domain which also appears to be relatively conserved in porcine IRF3 (figure 6.13). Conformational changes that occur following activation of IRF3 may expose its putative BH3 domain of IRF3 and facilitate its interaction with Bax (Chattopadhyay *et al.*, 2010) as might its linear ubiquitination by the LUBAC complex of ubiquitinating proteins (Chattopadhyay *et al.*, 2016). However one question that remains is whether ubiquitination of IRF3 alone is sufficient to bring about these changes or whether recruitment of additional adapter proteins are required. BH3-only proteins such as Bid and Bim have recently been reported to bind sequentially to two sites on Bax, the α1/α6 helicies and a canonical groove, that are important for outer membrane translocation and oligomerisation, respectively (see 1.3.1.1, figure 1.9) (Dengler *et al.*, 2019). Due to its homology with human IRF3 and porcine BH3-only proteins, porcine IRF3 may behave in a similar manner when bound to Bax, if indeed they interact.

Future work should seek to further confirm porcine IRF3's role in Bax relocalisation through subcellular fractionation, immunofluorescence co-localisation experiments and the generation of $Bax^{-/-}$ cells. Isolation of pure mitochondrial, cytosolic and nuclear cell fractions would help establish whether the reported mitochondrial relocalisation of IRF3 coincides with induction of Bax relocalisation and apoptosis. With regards to Bax, it has been suggested that knockout is insuffient to prevent MOMP induced by various stimuli and that double knockout of both Bax and Bak is required due to reported functional redundancy (Lindsten *et al.*, 2000, Wei *et al.*, 2001, Zong *et al.*, 2001). It will be interesting to see whether this holds true in porcine cells

treated with poly(I:C) and SeV; indeed, knockout of Bax alone has been associated with a signficant antagonism of IRF3-mediated apoptosis (Chattopadhyay *et al.*, 2010). Additionally, members of the linear ubiquitinating complex (LUBAC) such as SHARPIN, HOIP and HOIL-1 could be deleted to confirm the role of IRF3's ubiquitination in induction of apoptosis as demonstrated with human IRF3 (Chattopadhyay *et al.*, 2016). The ubuquitination sites required for IRF3's apoptotic functions (Chattopadhyay *et al.*, 2016) could also be mutated, further supporting a non-transcriptional, uniquitin-dependent function of IRF3 in the induction of apoptosis.

While rCSFV Alfort was unable to effectively antagonise SeV-mediated mitochondrial relocalisation of endogenous Bax and caspase-3 cleavage in SK6 cells, wild-type CSFV Alfort and Brescia strains offered improved antagonism in PK-15 cells. This was likely due to the fact that N^{pro} was expressed at much higher levels in cells infected with these wild-type strains. SK6 cells were used because ΔN^{pro} rCSFV cannot efficiently replicate in IFN-competent PK-15 cells due to the lost capacity of the virus to antagonise innate responses. Indeed, an increase in virus yields was observed when ΔN^{pro} rCSFV was grown in PK-15 $IRF3^{-/-}$ cells in comparison to wild type PK-15 (data not shown). Unexpectedly, ΔN^{pro} rCSFV was also found to partially antagonise poly(I:C)-mediated endogenous Bax relocalisation and caspase-3 cleavage in SK6 cells. ΔN^{pro} rCSFV still encodes the soluble and secretable endoribonuclease E^{rns} thought to act as a scavenger receptor for dsRNA and poly(I:C), likely explaining these observations (Hausmann *et al.*, 2004, Lussi *et al.*, 2018).

Importantly, mitochondrial relocalisation of endogenous Bax occurred in a manner independent of Bax expression levels, lending credence to the idea that the observed phenotype is due to IFN-independent IRF3/Bax activity. If Bax were an ISG and its upregulation required for induction of apoptosis, mitochondrial relocalisation would be absent in cells devoid of IRF3 or treated with either RXT or SeV, both antagonists of the type I IFN signalling

response (Garcin *et al.*, 2002). Indeed, overexpression of Bax has previously been linked with induction of or sensitisation toward apoptosis (Pastorino *et al.*, 1998, Lin *et al.*, 2005). While RXT was found to partially antagonise poly(I:C)-mediated Bax relocalisation, SeV-mediated relocalisation remained unaffected. Despite this, Bax expression levels remained unchanged following RXT treatment. As discussed in 3.6, several proteins in the TLR3-IRF3 signalling axis are ISGs, providing one possible explanation for this phenomenon. In addition, Bax protein expression levels were unaffected by expression of N^{pro}, further supporting the idea that the observed IRF3/Bax-mediated pathway of apoptosis is antagonised by N^{pro}'s interaction with IRF3. The reported transcriptionally inert S1 mutant of porcine IRF3 (see 6.6 and appendix D) and inhibitors of transcription and translation such as actinomycin D and cycloheximide will prove valuable in confirming the transcription-independent nature of this pathway in porcine cells.

EGFP-Bax fusion protein should be avoided in future studies due to its unexpected behaviour in both wild-type and $IRF3^{-/-}$ PK-15 cells. EGFP-Bax was found to translocate to the mitochondria and visibly oligomerise to form larger strucutres following treatment with poly(I:C), far larger than those observed with endogenous Bax which were distinctly more punctate. Mitochondria also appeared reorganised and homogenous, and surprisingly EGFP-Bax translocated even in the absence of IRF3. The size of the EGFP tag (27 kDa) compared to Bax (22 kDa) as well as EGFP's predisposition to oligomerise at membranes (Snapp *et al.*, 2003, Costantini *et al.*, 2012) might be responsible as may its overexpression. Indeed, overexpression of a protein already expressed within a cell can complicate interpretation of results. Even more surpising was the fact that relocalisation of Bax did not appear to be associated with induction of caspase-3 cleavage in $IRF3^{-/-}$. One possibility is that these oligomeric structures are non-functional and do not facilitate MOMP (Todt *et al.*, 2013), while another is that the PK-15 transfection efficiency was simply too low to be able to detect increases in cleaved caspase-3 levels. Ulimately, studying endogenous protein or utilising a smaller or strictly monomeric GFP

(mGFP) tag would potentially eliminate many of these issues. In addition, future studies should also consider either ommiting Z-VAD(OMe)-FMK or utilising lower concentrations as this compound has been reported to display toxicity by inducing autophagy and necrosis (Lemaire *et al.*, 1998, Chen *et al.*, 2011), potentially explaining the punctate appearance of mitochondria in this experiment and others detailed throughout the chapter.

6.7.2. IRF3 interactions

Identifying an interaction between porcine IRF3 and porcine Bax would explain the findings reported so far, as interaction between their human counterparts proved to be essential in facilitating IRF3-mediated mitochondrial apoptosis (Chattopadhyay *et al.*, 2010). IRF3 is highly conserved in mammals and the putative BH3 domain which facilitates interaction between Bax and human IRF3 might also be present in the porcine IRF3 protein (figure 6.13), suggesting the possibility of interaction. While not antagonising its activity through modulation of expression levels, N^{pro} may still interact with Bax. While a yeast two-hybrid screen confirmed the interaction between porcine IRF3 and N^{pro}, it did not identify interactions between porcine IRF3 and Bax or Bax and N^{pro}. Subsequent reviews of past literature provided evidence that Bax toxicity might have influenced the observed yeast two-hybrid results; indeed, toxicity of mammalian Bax expression in yeast has been reported (Sato *et al.*, 1994, Ligr *et al.*, 1998). In addition, yeast two-hybrid screens rely upon direct protein-protein interactions meaning that a potential interaction between two proteins could go undetected if it were indirect and required a 3rd protein. To avoid such issues such as these, future studies should instead utilise confocal co-localisation or co-immunoprecipitation in mammalian cells, enabling the detection of both direct and indirect interactions.

IRF3 may not be the only protein N^{pro} interacts with in order for it to exert its anti-apoptotic activity. As discussed previously (see 1.3.3.3), an interaction with TID1 has also been identified by yeast two-hybrid (unpublished data). Through a function of its co-chaperone DnaJ domain,

TID1 has been reported to interact with and target p53 to the mitochondrial membrane (Ahn *et al.*, 2010, Trinh *et al.*, 2010), facilitating the activation of Bax via either an interaction in the cytosol or at the MOM (Chipuk *et al.*, 2004, Wolff *et al.*, 2008). How exactly IRF3 and Bax are targeted to the mitochondria remains to be determined, however one possibility is that, as with p53, TID1 directs each protein to the MOM either alone or in complex with p53 to bring about permeabilisation and apoptosis. Another possibility is that p53/TID1-mediated apoptosis occurs parallel to IRF3/Bax-mediated apoptosis, acting synergistically to bring about MOMP. How activation of p53 would occur in the latter scenario is uncertain – p53 has classically been associated with responses to genotoxic stress (Hafner *et al.*, 2019) and more recently with mitochondrial apoptosis through interactions with Bcl-2-family member proteins such as the anti-apoptotic Bcl-xL (Mihara *et al.*, 2003) and the pro-apoptotic Bak (Leu *et al.*, 2004) and Bad (Jiang *et al.*, 2006). In short, TID1$^{-/-}$, p53$^{-/-}$ and Bax$^{-/-}$ PK-15 cells would prove invaluable in testing each of these theories as would co-immunoprecipitation and mass spectrometry studies which could confirm the discussed interactions.

6.7.3. MOMP and cytochrome c release

With regards to mitochondrial outer membrane permeabilization (MOMP), CSFV has been shown to antagonise cytochrome c release and caspase-9 cleavage (Johns *et al.*, 2010a). This fits with the observations made in the present work which identified a clear antagonism of Bax mitochondrial relocalisation by N^{pro} and IRF3 knockout, further increasing the probability that N^{pro} antagonises a distinctly mitochondrial pathway of apoptosis such as RIPA. Multiple attempts were made to study the release of cytochrome c as an additional readout for mitochondrial apoptosis and its antagonism by N^{pro}. Poor homology between porcine cytochrome c and its rat counterpart was likely responsible for the lack of reactivity when screened by immunofluorescence confocal microscopy (appendix E, figure E.1). GFP-tagged cytochrome c offered no improvement as protein tagged at both its N and C termini did not

localise correctly (appendix E, figure E.2). Future studies looking to assess IRF3's capacity to trigger MOMP and release of cytochrome c and their antagonism by N^{pro} should instead utilise available assays that measure caspase-9 cleavage.

6.7.4. N^{pro} and IRF3-mediated apoptosis: the big picture

A past study by Jefferson *et al*. observed that transfected CSFV N^{pro} and the related Pestivirus BVDV antagonised sodium arsenate-mediated mitochondrial Bax relocalisation (Jefferson *et al.*, 2014). However, this agonist is thought to trigger apoptosis by upregulating Bax expression in a c-Jun N-terminal kinase (JNK)-dependent manner (Lau *et al.*, 2004). In the present work, Bax relocalisation has been explored in the context of stably-expressed N^{pro} and CSFV infection utilising authentic agonists of dsRNA signalling pathways. We have demonstrated both poly(I:C) and SeV to be relevant and authentic agonists of TLR3 and RIG-I signalling pathways that converge on IRF3 in their induction of apoptosis. The significance of TLR3 and RIG-I mediated responses during CSFV infection was discussed in 5.5.1 and 5.5.2 and their relevance highlighted by Hüsser *et al*. using shRNA knockdown to target each (Hüsser *et al.*, 2011).

Taken together, these results suggest that N^{pro}'s interaction with IRF3 is not only responsible for antagonising the induction of type I IFN but also the induction of IFN-independent IRF3/Bax-mediated caspase-3 cleavage and apoptosis. Ultimately, N^{pro}'s antagonism of TLR3, RIG-I and IRF3-mediated apoptotic responses might serve as another mechanism of CSFV immune evasion, potentially contributing to the establishment of infection and host persistence.

7. Final discussion and future work

7.1. Discussion

Generated as a replication intermediate of the RNA virus genome, dsRNA triggers the induction of innate responses such as type I IFN and apoptosis. The apoptosis triggered by dsRNA as a consequence of infection is thought to have a protective role, serving to limit further virus dissemination within the host (Jorgensen *et al.*, 2017). Thus, many viruses have evolved proteins which function to counter the response (Benedict *et al.*, 2002). ASFV A179L binds tBid and Bax, antagonising their activity (Galindo *et al.*, 2008, Banjara *et al.*, 2017) while γ-herpesviruses encode a homolog of FLIP, preventing activation of caspase-8 by DISC signalling (Glykofrydes *et al.*, 2000). When expressed stably and during infection, CSFV N^{pro} has been shown to antagonise not only induction of type I IFN, but also apoptosis (Ruggli *et al.*, 2003, Ruggli *et al.*, 2005, Bauhofer *et al.*, 2007, Seago *et al.*, 2007, Johns *et al.*, 2010a).

While N^{pro}'s putative interaction with IRF3 has been identified as the source of IFN antagonism, the mechanism by which N^{pro} antagonises the induction of dsRNA-meditated apoptosis has yet to be identified. Identification of this mechanism will provide further insights into CSFV pathology and potentially help facilitate the development of future, rationally designed vaccines and antivirals to counter infection. Using a combination of CRISPR-Cas9 gene-editing technology and confocal microscopy, it is reported herein that in porcine kidney endothelial cells IRF3 coordinates the induction of RIG-I and TLR3-mediated apoptosis in an IRF3-dependent IFN-independent manner, cumulating in the relocalisation of pro-apoptotic Bax to the mitochondrial membrane and induction of caspase-3 cleavage, key hallmarks of apoptosis. Based on these findings, a provisional model for antagonism of RIG-I and TLR3-mediated apoptosis by CSFV N^{pro} in PK-15 cells is proposed (figure 7.1).

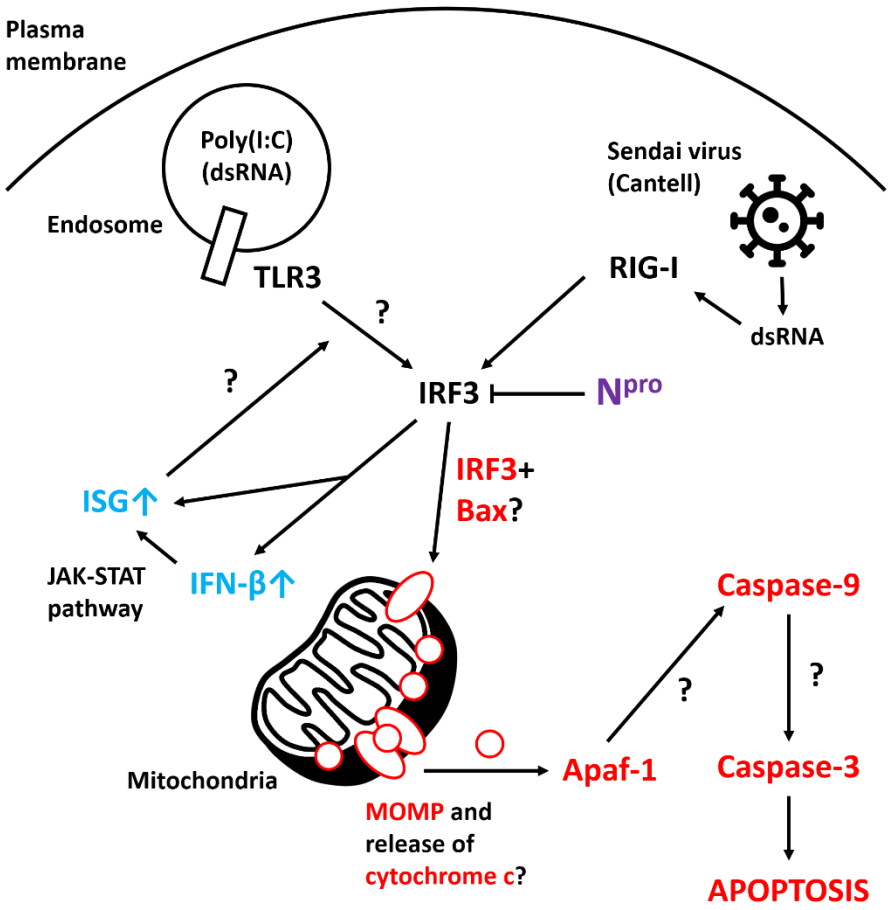

Figure 7.1: Model of TLR3 and RIG-I-mediated apoptosis and its antagonism by CSFV N^{pro} in PK-15 cells. Upon stimulation with poly(I:C) and SeV, TLR3 and RIG-I initiate apoptosis in an IRF3-dependent manner characterised by mitochondrial relocalisation of Bax and activation of caspase-3. IRF3 also triggers induction of IFN-β and IFN-dependent and independent upregulation of ISGs which might amplify the TLR3/IRF3 signalling axis. CSFV N^{pro} (purple), apoptotic signalling (red), IFN signalling (blue) and uncertain or inferred pathways (?) are indicated.

RIG-I activation results in the activation of MAVS which likely assembles two complexes of proteins: (1) IRF3, TRAF3, TBK1 and (2) IRF3, TRAF2, TRAF3, TRAF6, TBK1 and the LUBAC complex (discussed in 1.3.3.2) as previously reported (Chattopadhyay *et al.*, 2010, Chattopadhyay *et al.*, 2016). Assembly of the first complex phosphorylates IRF3, resulting in induction of IFN and subsequent upregulation of IFN-dependent and independent ISGs. Assembly of the second complex termed RIPA facilitates the linear polyubiquitination of IRF3, enabling an interaction with Bax and subsequent induction of apoptosis triggered by MOMP. Due to the shared nature of the induction of these pathways, it is therefore conceivable that

the well characterised turnover of IRF3 following interaction with CSFV N^{pro} (Bauhofer *et al.*, 2007, Seago *et al.*, 2007) is also responsible for the observed antagonism of RIG-I-mediated apoptosis.

It is likely that TLR3 initiates apoptosis in a similar manner to RIG-I However, TLR3-mediated apoptosis is less well characterised and has not been reported to require MAVS (Chattopadhyay *et al.*, 2010, Chattopadhyay *et al.*, 2016). Indeed, stimulation of both TLR3 and RIG-I triggers activation of caspase-3 in an IRF3 dependent manner potentially requiring Bax (figure 7.1). These findings would explain why CSFV N^{pro} is able to antagonise TLR3-mediated apoptosis. Unlike RIG-I activation which uses the adaptor MAVS, TLR3 uses TRIF to initiate production of type I IFN (discussed in 1.2.1.2) (Yamamoto *et al.*, 2003). Recruitment of TRIF to TLR3 upon activation might facilitate pro-apoptotic polyubiquitination of IRF3 in the same way MAVS does upon RIG-I activation. Indeed, components of the RIPA pathway such as LUBAC and TRAF6 have been identified in TLR3 signalling complexes (Zinngrebe *et al.*, 2016), as has TRAF2 (Sasai *et al.*, 2010), while TRAF3 deficiency is associated with impaired induction of type I and III IFN by TLR3 (Pérez de Diego *et al.*, 2010). In contrast to its reported involvement in RIPA induction when associated with MAVS (Chattopadhyay *et al.*, 2016), LUBAC was reported to have an anti-apoptotic effect following poly(I:C) treatment of mice (Zinngrebe *et al.*, 2016). Therefore, the exact mechanism by which TLR3/IRF3-mediated apoptosis occurs remains to be fully elucidated.

While not responsible for induction of TLR3 or RIG-I-mediated apoptosis, type I IFN appears to amplify TLR3-mediated apoptosis. Inhibition of the type I IFN signalling response by RXT (a JAK inhibitor) reduced poly(I:C) mediated apoptosis, suggesting downstream events are responsible for the observed amplification – whether these are pre or post ISG induction remains to be elucidated. It is feasible that ISG products could be responsible, indeed, at least 15 pro-apoptotic ISGs have been identified (Chawla-Sarkar *et al.*, 2003) and porcine TLR3 is

itself upregulated 3.2-fold in *ex vivo* porcine fibroblasts treated with IFN-α (Shaw *et al.*, 2017). Importantly, Bax clearly relocalised to the mitochondria upon stimulation of TLR3 with poly(I:C) in the presence of caspase inhibitor – a phenotype not observed in TLR3$^{-/-}$ cells. If TLR3-mediated apoptosis did not rely on the direct action of IRF3 and instead required DISC/caspase-8 signalling, Bax relocalisation would not have been observed.

IRF3-mediated apoptosis protects multiple human cell lines from persistent infection with SeV (Peters *et al.*, 2008, Chattopadhyay *et al.*, 2013) and CSFV infection *in vitro* is non-cytopathic (Moennig and Plagemann, 1992). CSFV infection is detected *in vitro* by both TLR3 and RIG-I (Hüsser *et al.*, 2011) and it is possible that N^{pro}'s antagonism of the apoptosis mediated by each is required for infection *in vivo*. Tamura demonstrated the importance of CSFV N^{pro} in antagonising type I IFN as a means of maximising localised dissemination and it is possible that antagonism of apoptosis complements this effect (Tamura *et al.*, 2014). Mutation of N^{pro} and E^{rns} prevents persistent foetal infection with BVDV and it is conceivable such mutations might have a similar effect if introduced into CSFV (Meyers *et al.*, 2007).

Collectively, these results suggest that N^{pro}'s interaction with IRF3 is not only responsible for antagonising the induction of type I IFN but also the induction of IFN-independent IRF3/Bax-mediated caspase-3 cleavage and apoptosis. The model presented here is largely in agreement with past findings made by Chattopadhyay *et al.* (Chattopadhyay *et al.*, 2010, Chattopadhyay *et al.*, 2016), TLR3-mediated apoptosis being an exception that requires further investigation. Ultimately, N^{pro}'s antagonism of TLR3, RIG-I and IRF3-mediated apoptotic responses might serve as another mechanism of CSFV immune evasion, contributing to the establishment of infection and host persistence.

7.2. Future work

While the present work has shed light on TLR3 and RIG-I-mediated apoptosis in porcine cell lines and the significance of IRF3 antagonism by CSFV N^{pro}, key questions remain to be addressed.

Complementation experiments with wild-type and S1 mutant porcine IRF3 constructs into $IRF3^{-/-}$ PK-15 cell lines should confirm the observed apoptosis to be independent of IRF3's transcriptional function. If the hypothesis in the present work holds true, then both constructs will display restored sensitivity to these agonists even in the absence of ISG upregulation by the S1 mutant. The mutated residues present in S1 (S396A and S398A) might be insufficient to block IRF3's transcriptional activity and additional mutations might be required (e.g. S386A) (Mori *et al.*, 2004, Chen *et al.*, 2008, Bergstroem *et al.*, 2010). Alternately, inhibitors of transcription and translation actinomycin D (ActD) and cycloheximide (CHX) could be employed to answer the same question by preventing total protein upregulation upon induction of apoptosis.

There are numerous means by which the mitochondrial nature of the apoptosis antagonised by N^{pro} can be determined. As discussed in 6.7.1, Bax knockout cells would prove invaluable as they would confirm the significance of Bax relocalisation observed following treatment with poly(I:C) and SeV. Additionally, Western blot analysis of mitochondrial and cytosolic fractions could be assessed for cytochrome c and Bax expression while luminescence assays could quantify the extent of caspase-9 activation, key hallmarks of mitochondrial apoptosis.

Much of the data presented here fits with the RIPA model of RIG-I and IRF3-mediated apoptosis put forward by Chattopadhyay *et al.* (Chattopadhyay *et al.*, 2010, Chattopadhyay *et al.*, 2016). However, assembly of the MAVS-associated complex implicated in IRF3's apoptotic activity remains to be determined in porcine cells *in vitro*. Knockout of TRAF and LUBAC complex proteins, co-immunoprecipitation (Co-IP) and mutation of the IRF3 residues

implicated in its polyubiquitination would confirm the existence and significance of such a complex. It is unclear whether this pathway is exclusive to MAVS or whether TRIF, the adaptor protein of TLR3, also has IRF3-dependent apoptotic potential. Therefore, additional knockout of TRIF would shed light on the nature of TLR3-mediated apoptosis. Yeast two-hybrid was unable to identify an interaction between IRF3 and Bax, which would have confirmed previous reports and elucidate the mechanism of Bax relocalisation to the mitochondria in PK-15 cells. Alternative techniques such as Co-IP and colocalization could be employed to explore this potential interaction.

Past yeast two-hybrid screens have identified additional interactions with proteins such as TID1 (unpublished) and HX-1 (Johns *et al.*, 2010b) (discussed in 1.3.3.3 and 1.3.3.4). Recently N^{pro} and us10, a ribosomal protein implicated in regulation of TLR3 expression, were found to interact (Lv *et al.*, 2017b). It is unclear how modulation of any of these proteins would affect TLR3 and RIG-I-mediated apoptosis in porcine cells such as PK-15 considering how it is clearly IRF3-mediated. Knockout of the genes encoding each would help determine their involvement in apoptosis mediated by each PRR. Their functions might be accessory to the IRF3/Bax-mediated pathway of apoptosis discussed in the present work or may modulate cellular responses to infection with CSFV. Due to time constraints knockouts of TID1, HAX-1 and us10 were not generated, however they would provide an interesting avenue of study to pursue.

The data presented here demonstrates that clear progress in elucidating the core mechanisms of RIG-I, TLR3 and IRF3-mediated apoptosis and the likely mechanism by which N^{pro} antagonises these pathways *in vitro*. However, there is still a significant body of work which needs to be completed before we can fully appreciate the significance of apoptosis antagonism *in vivo*. Progress made in our understanding of this process, as well as the molecular tools generated over the course of the project, should together facilitate future

studies which might one day inform the development of vaccines and antivirals which may target N^{pro}'s function as an antagonist of TLR3 and RIG-I-mediated apoptosis.

References

ABDELWAHID, E., LI, H., WU, J., IRIODA, A. C., DE CARVALHO, K. A. & LUO, X. 2016. Endoplasmic reticulum (ER) stress triggers Hax1-dependent mitochondrial apoptotic events in cardiac cells. *Apoptosis,* 21**,** 1227-1239.

ADER, N. R., HOFFMANN, P. C., GANEVA, I., BORGEAUD, A. C., WANG, C., YOULE, R. J. & KUKULSKI, W. 2019. Molecular and topological reorganizations in mitochondrial architecture interplay during Bax-mediated steps of apoptosis. *Elife,* 8.

AGALIOTI, T., LOMVARDAS, S., PAREKH, B., YIE, J., MANIATIS, T. & THANOS, D. 2000. Ordered recruitment of chromatin modifying and general transcription factors to the IFN-beta promoter. *Cell,* 103**,** 667-78.

AGAPOV, E. V., MURRAY, C. L., FROLOV, I., QU, L., MYERS, T. M. & RICE, C. M. 2004. Uncleaved NS2-3 is required for production of infectious bovine viral diarrhea virus. *J Virol,* 78**,** 2414-25.

AHN, B. Y., TRINH, D. L., ZAJCHOWSKI, L. D., LEE, B., ELWI, A. N. & KIM, S. W. 2010. Tid1 is a new regulator of p53 mitochondrial translocation and apoptosis in cancer. *Oncogene,* 29**,** 1155-66.

ALEXOPOULOU, L., HOLT, A. C., MEDZHITOV, R. & FLAVELL, R. A. 2001. Recognition of double-stranded RNA and activation of NF-κB by Toll-like receptor 3. *Nature,* 413**,** 732-738.

ALKURDI, L., VIRARD, F., VANBERVLIET, B., WEBER, K., TOSCANO, F., BONNIN, M., LE STANG, N., LANTUEJOUL, S., MICHEAU, O., RENNO, T., LEBECQUE, S. & ESTORNES, Y. 2018. Release of c-FLIP brake selectively sensitizes human cancer cells to TLR3-mediated apoptosis. *Cell Death & Disease,* 9**,** 874.

ALNEMRI, E. S., LIVINGSTON, D. J., NICHOLSON, D. W., SALVESEN, G., THORNBERRY, N. A., WONG, W. W. & YUAN, J. 1996. Human ICE/CED-3 Protease Nomenclature. *Cell,* 87**,** 171.

ALTSCHUL, S. F., GISH, W., MILLER, W., MYERS, E. W. & LIPMAN, D. J. 1990. Basic local alignment search tool. *J Mol Biol,* 215**,** 403-10.

ARZT, J., WHITE, W. R., THOMSEN, B. V. & BROWN, C. C. 2010. Agricultural diseases on the move early in the third millennium. *Vet Pathol,* 47**,** 15-27.

ASHKENAZI, A. & DIXIT, V. M. 1998. Death receptors: signaling and modulation. *Science,* 281**,** 1305-8.

ASHLEY, C. L., ABENDROTH, A., MCSHARRY, B. P. & SLOBEDMAN, B. 2019. Interferon-Independent Upregulation of Interferon-Stimulated Genes during Human Cytomegalovirus Infection is Dependent on IRF3 Expression. *Viruses,* 11**,** 246.

BAILEY, C. C., ZHONG, G., HUANG, I. C. & FARZAN, M. 2014. IFITM-Family Proteins: The Cell's First Line of Antiviral Defense. *Annu Rev Virol,* 1**,** 261-283.

BANERJEE, A., SAITO, K., MEYER, K., BANERJEE, S., AIT-GOUGHOULTE, M., RAY, R. B. & RAY, R. 2009. Hepatitis C virus core protein and cellular protein HAX-1 promote 5-fluorouracil-mediated hepatocyte growth inhibition. *Journal of virology,* 83**,** 9663-9671.

BANJARA, S., CARIA, S., DIXON, L. K., HINDS, M. G. & KVANSAKUL, M. 2017. Structural Insight into African Swine Fever Virus A179L-Mediated Inhibition of Apoptosis. *Journal of virology,* 91**,** e02228-16.

BANNINGER, G. & REICH, N. C. 2004. STAT2 nuclear trafficking. *J Biol Chem,* 279**,** 39199-206.

BARRANGOU, R., FREMAUX, C., DEVEAU, H., RICHARDS, M., BOYAVAL, P., MOINEAU, S., ROMERO, D. A. & HORVATH, P. 2007. CRISPR Provides Acquired Resistance Against Viruses in Prokaryotes. 315**,** 1709-1712.

BARTEL, P., CHIEN, C. T., STERNGLANZ, R. & FIELDS, S. 1993. Elimination of false positives that arise in using the two-hybrid system. *Biotechniques,* 14**,** 920-4.

BAUHOFER, O., SUMMERFIELD, A., MCCULLOUGH, K. C. & RUGGLI, N. 2005. Role of double-stranded RNA and Npro of classical swine fever virus in the activation of monocyte-derived dendritic cells. *Virology,* 343**,** 93-105.

BAUHOFER, O., SUMMERFIELD, A., SAKODA, Y., TRATSCHIN, J.-D., HOFMANN, M. A. & RUGGLI, N. 2007. Classical Swine Fever Virus N(pro) Interacts with Interferon Regulatory Factor 3 and Induces Its Proteasomal Degradation. *Journal of Virology,* 81**,** 3087-3096.

BAUM, A., SACHIDANANDAM, R. & GARCÍA-SASTRE, A. 2010. Preference of RIG-I for short viral RNA molecules in infected cells revealed by next-generation sequencing. *Proceedings of the National Academy of Sciences of the United States of America,* 107**,** 16303-16308.

BEG, A. A., RUBEN, S. M., SCHEINMAN, R. I., HASKILL, S., ROSEN, C. A. & BALDWIN, A. S., JR. 1992. I kappa B interacts with the nuclear localization sequences of the subunits of NF-kappa B: a mechanism for cytoplasmic retention. *Genes Dev,* 6**,** 1899-913.

BELMOKHTAR, C. A., HILLION, J. & SEGAL-BENDIRDJIAN, E. 2001. Staurosporine induces apoptosis through both caspase-dependent and caspase-independent mechanisms. *Oncogene,* 20**,** 3354-62.

BENEDICT, C. A., NORRIS, P. S. & WARE, C. F. 2002. To kill or be killed: viral evasion of apoptosis. *Nature Immunology,* 3**,** 1013-1018.

BENSAUDE, E., TURNER, J. L., WAKELEY, P. R., SWEETMAN, D. A., PARDIEU, C., DREW, T. W., WILEMAN, T. & POWELL, P. P. 2004. Classical swine fever virus induces proinflammatory cytokines and tissue factor expression and inhibits apoptosis and interferon synthesis during the establishment of long-term infection of porcine vascular endothelial cells. *J Gen Virol,* 85**,** 1029-37.

BERGSTROEM, B., JOHNSEN, I. B., NGUYEN, T. T., HAGEN, L., SLUPPHAUG, G., THOMMESEN, L. & ANTHONSEN, M. W. 2010. Identification of a novel in vivo virus-targeted phosphorylation site in interferon regulatory factor-3 (IRF3). *The Journal of biological chemistry,* 285**,** 24904-24914.

BLEICKEN, S., LANDETA, O., LANDAJUELA, A., BASANEZ, G. & GARCIA-SAEZ, A. J. 2013. Proapoptotic Bax and Bak proteins form stable protein-permeable pores of tunable size. *J Biol Chem,* 288**,** 33241-52.

BLOME, S., AEBISCHER, A., LANGE, E., HOFMANN, M., LEIFER, I., LOEFFEN, W., KOENEN, F. & BEER, M. 2012. Comparative evaluation of live marker vaccine candidates “CP7_E2alf” and “flc11” along with C-strain “Riems” after oral vaccination. *Veterinary Microbiology,* 158**,** 42-59.

BLOME, S., GABRIEL, C., SCHMEISER, S., MEYER, D., MEINDL-BÖHMER, A., KOENEN, F. & BEER, M. 2014. Efficacy of marker vaccine candidate CP7_E2alf against challenge with classical swine fever virus isolates of different genotypes. *Veterinary Microbiology,* 169**,** 8-17.

BLOME, S., WERNIKE, K., REIMANN, I., KÖNIG, P., MOß, C. & BEER, M. 2017. A decade of research into classical swine fever marker vaccine CP7_E2alf (Suvaxyn® CSF Marker): a review of vaccine properties. *Veterinary Research,* 48**,** 51.

BOATRIGHT, K. M., RENATUS, M., SCOTT, F. L., SPERANDIO, S., SHIN, H., PEDERSEN, I. M., RICCI, J.-E., EDRIS, W. A., SUTHERLIN, D. P., GREEN, D. R. & SALVESEN, G. S. 2003. A Unified Model for Apical Caspase Activation. *Molecular Cell,* 11**,** 529-541.

BOATRIGHT, K. M. & SALVESEN, G. S. 2003. Mechanisms of caspase activation. *Current Opinion in Cell Biology,* 15**,** 725-731.

BOLDIN, M. P., GONCHAROV, T. M., GOLTSEV, Y. V. & WALLACH, D. 1996. Involvement of MACH, a novel MORT1/FADD-interacting protease, in Fas/APO-1- and TNF receptor-induced cell death. *Cell,* 85**,** 803-15.

BOUMA, A., DE SMIT, A. J., DE JONG, M. C. M., DE KLUIJVER, E. P. & MOORMANN, R. J. M. 2000. Determination of the onset of the herd-immunity induced by the E2 sub-unit vaccine against classical swine fever virus. *Vaccine,* 18**,** 1374-1381.

BRIDGE, A. J., PEBERNARD, S., DUCRAUX, A., NICOULAZ, A. L. & IGGO, R. 2003. Induction of an interferon response by RNAi vectors in mammalian cells. *Nat Genet,* 34**,** 263-4.

BROWN, N. P., LEROY, C. & SANDER, C. 1998. MView: a web-compatible database search or multiple alignment viewer. *Bioinformatics,* 14**,** 380-381.

BROWN, V. R. & BEVINS, S. N. 2018. A Review of Classical Swine Fever Virus and Routes of Introduction into the United States and the Potential for Virus Establishment. *Frontiers in veterinary science,* 5**,** 31-31.

BURKARD, C., OPRIESSNIG, T., MILEHAM, A. J., STADEJEK, T., AIT-ALI, T., LILLICO, S. G., WHITELAW, C. B. A. & ARCHIBALD, A. L. 2018. Pigs Lacking the Scavenger Receptor Cysteine-Rich Domain 5 of CD163 Are Resistant to Porcine Reproductive and Respiratory Syndrome Virus 1 Infection. *Journal of Virology,* 92**,** e00415-18.

CABEZON, O., COLOM-CADENA, A., MUNOZ-GONZALEZ, S., PEREZ-SIMO, M., BOHORQUEZ, J. A., ROSELL, R., MARCO, I., DOMINGO, M., LAVIN, S. & GANGES, L. 2015. Post-Natal Persistent Infection With Classical Swine Fever Virus in Wild Boar: A Strategy for Viral Maintenance? *Transbound Emerg Dis*.

CHARLESTON, B., FRAY, M. D., BAIGENT, S., CARR, B. V. & MORRISON, W. I. 2001. Establishment of persistent infection with non-cytopathic bovine viral diarrhoea virus in cattle is associated with a failure to induce type I interferon. *J Gen Virol,* 82**,** 1893-7.

CHATTOPADHYAY, S., FENSTERL, V., ZHANG, Y., VELEEPARAMBIL, M., YAMASHITA, M. & SEN, G. C. 2013. Role of interferon regulatory factor 3-mediated apoptosis in the establishment and maintenance of persistent infection by Sendai virus. *J Virol,* 87**,** 16-24.

CHATTOPADHYAY, S., KUZMANOVIC, T., ZHANG, Y., WETZEL, J. L. & SEN, G. C. 2016. Ubiquitination of the Transcription Factor IRF-3 Activates RIPA, the Apoptotic Pathway that Protects Mice from Viral Pathogenesis. *Immunity,* 44**,** 1151-61.

CHATTOPADHYAY, S., MARQUES, J. T., YAMASHITA, M., PETERS, K. L., SMITH, K., DESAI, A., WILLIAMS, B. R. G. & SEN, G. C. 2010. Viral apoptosis is induced by IRF-3-mediated activation of Bax. *The EMBO Journal,* 29**,** 1762-1773.

CHATTOPADHYAY, S. & SEN, G. C. 2014. dsRNA-activation of TLR3 and RLR signaling: gene induction-dependent and independent effects. *Journal of interferon & cytokine research : the official journal of the International Society for Interferon and Cytokine Research,* 34**,** 427-436.

CHATTOPADHYAY, S., YAMASHITA, M., ZHANG, Y. & SEN, G. C. 2011. The IRF-3/Bax-mediated apoptotic pathway, activated by viral cytoplasmic RNA and DNA, inhibits virus replication. *J Virol,* 85**,** 3708-16.

CHAWLA-SARKAR, M., LINDNER, D. J., LIU, Y.-F., WILLIAMS, B. R., SEN, G. C., SILVERMAN, R. H. & BORDEN, E. C. 2003. Apoptosis and interferons: Role of interferon-stimulated genes as mediators of apoptosis. *Apoptosis,* 8**,** 237-249.

CHEN, J., HE, W. R., SHEN, L., DONG, H., YU, J., WANG, X., YU, S., LI, Y., LI, S., LUO, Y., SUN, Y. & QIU, H. J. 2015. The laminin receptor is a cellular attachment receptor for classical Swine Fever virus. *J Virol,* 89**,** 4894-906.

CHEN, L., WILLIS, S. N., WEI, A., SMITH, B. J., FLETCHER, J. I., HINDS, M. G., COLMAN, P. M., DAY, C. L., ADAMS, J. M. & HUANG, D. C. S. 2005. Differential Targeting of Prosurvival Bcl-2 Proteins by Their BH3-Only Ligands Allows Complementary Apoptotic Function. *Molecular Cell,* 17**,** 393-403.

CHEN, S. Y., CHIU, L. Y., MAA, M. C., WANG, J. S., CHIEN, C. L. & LIN, W. W. 2011. zVAD-induced autophagic cell death requires c-Src-dependent ERK and JNK activation and reactive oxygen species generation. *Autophagy,* 7**,** 217-28.

CHEN, W., SRINATH, H., LAM, S. S., SCHIFFER, C. A., ROYER, W. E., JR. & LIN, K. 2008. Contribution of Ser386 and Ser396 to activation of interferon regulatory factor 3. *Journal of molecular biology,* 379**,** 251-260.

CHEN, Z., RIJNBRAND, R., JANGRA, R. K., DEVARAJ, S. G., QU, L., MA, Y., LEMON, S. M. & LI, K. 2007. Ubiquitination and proteasomal degradation of interferon regulatory factor-3 induced by Npro from a cytopathic bovine viral diarrhea virus. *Virology,* 366**,** 277-292.

CHIEN, C. T., BARTEL, P. L., STERNGLANZ, R. & FIELDS, S. 1991. The two-hybrid system: a method to identify and clone genes for proteins that interact with a protein of interest. *Proc Natl Acad Sci U S A,* 88**,** 9578-82.

CHINNAIYAN, A. M., O'ROURKE, K., TEWARI, M. & DIXIT, V. M. 1995. FADD, a novel death domain-containing protein, interacts with the death domain of fas and initiates apoptosis. *Cell,* 81**,** 505-512.

CHIPUK, J. E., FISHER, J. C., DILLON, C. P., KRIWACKI, R. W., KUWANA, T. & GREEN, D. R. 2008. Mechanism of apoptosis induction by inhibition of the anti-apoptotic BCL-2 proteins. *Proceedings of the National Academy of Sciences,* 105**,** 20327-20332.

CHIPUK, J. E., KUWANA, T., BOUCHIER-HAYES, L., DROIN, N. M., NEWMEYER, D. D., SCHULER, M. & GREEN, D. R. 2004. Direct activation of Bax by p53 mediates mitochondrial membrane permeabilization and apoptosis. *Science,* 303**,** 1010-4.

CHOI, C., HWANG, K. K. & CHAE, C. 2004. Classical swine fever virus induces tumor necrosis factor-alpha and lymphocyte apoptosis. *Arch Virol,* 149**,** 875-89.

CLAPHAM, D. E. 2007. Calcium Signaling. *Cell,* 131**,** 1047-1058.

CLARK, K., PEGGIE, M., PLATER, L., SORCEK, RONALD J., YOUNG, ERICK R. R., MADWED, JEFFREY B., HOUGH, J., MCIVER, EDWARD G. & COHEN, P. 2011. Novel cross-talk within the IKK family controls innate immunity. *Biochemical Journal,* 434**,** 93-104.

COLEMAN, M. L., SAHAI, E. A., YEO, M., BOSCH, M., DEWAR, A. & OLSON, M. F. 2001. Membrane blebbing during apoptosis results from caspase-mediated activation of ROCK I. *Nat Cell Biol,* 3**,** 339-45.

CONG, L., RAN, F. A., COX, D., LIN, S., BARRETTO, R., HABIB, N., HSU, P. D., WU, X., JIANG, W., MARRAFFINI, L. A. & ZHANG, F. 2013. Multiplex genome engineering using CRISPR/Cas systems. *Science,* 339**,** 819-23.

COSENTINO, K. & GARCÍA-SÁEZ, A. J. 2017. Bax and Bak Pores: Are We Closing the Circle? *Trends in cell biology,* 27**,** 266-275.

COSTANTINI, L. M., FOSSATI, M., FRANCOLINI, M. & SNAPP, E. L. 2012. Assessing the tendency of fluorescent proteins to oligomerize under physiologic conditions. *Traffic (Copenhagen, Denmark),* 13**,** 643-649.

CRAWFORD, E. D., SEAMAN, J. E., AGARD, N., HSU, G. W., JULIEN, O., MAHRUS, S., NGUYEN, H., SHIMBO, K., YOSHIHARA, H. A., ZHUANG, M., CHALKLEY, R. J. & WELLS, J. A. 2013. The DegraBase: a database of proteolysis in healthy and apoptotic human cells. *Mol Cell Proteomics,* 12**,** 813-24.

CUI, S., EISENACHER, K., KIRCHHOFER, A., BRZOZKA, K., LAMMENS, A., LAMMENS, K., FUJITA, T., CONZELMANN, K. K., KRUG, A. & HOPFNER, K. P. 2008. The C-terminal regulatory domain is the RNA 5'-triphosphate sensor of RIG-I. *Mol Cell,* 29**,** 169-79.

CZABOTAR, P. E., LESSENE, G., STRASSER, A. & ADAMS, J. M. 2014. Control of apoptosis by the BCL-2 protein family: implications for physiology and therapy. *Nat Rev Mol Cell Biol,* 15**,** 49-63.

CZABOTAR, P. E., WESTPHAL, D., DEWSON, G., MA, S., HOCKINGS, C., FAIRLIE, W. D., LEE, E. F., YAO, S., ROBIN, A. Y., SMITH, B. J., HUANG, D. C., KLUCK, R. M., ADAMS, J. M. & COLMAN, P. M. 2013. Bax crystal structures reveal how BH3 domains activate Bax and nucleate its oligomerization to induce apoptosis. *Cell,* 152**,** 519-31.

DARNELL, J. E., JR., KERR, I. M. & STARK, G. R. 1994. Jak-STAT pathways and transcriptional activation in response to IFNs and other extracellular signaling proteins. *Science,* 264**,** 1415-21.

DAY, C. L., SMITS, C., FAN, F. C., LEE, E. F., FAIRLIE, W. D. & HINDS, M. G. 2008. Structure of the BH3 domains from the p53-inducible BH3-only proteins Noxa and Puma in complex with Mcl-1. *J Mol Biol,* 380**,** 958-71.

DE SMIT, A. J., BOUMA, A., DE KLUIJVER, E. P., TERPSTRA, C. & MOORMANN, R. J. M. 2001. Duration of the protection of an E2 subunit marker vaccine against classical swine fever after a single vaccination. *Veterinary Microbiology,* 78**,** 307-317.

DECLERCQ, W., VANDEN BERGHE, T. & VANDENABEELE, P. 2009. RIP Kinases at the Crossroads of Cell Death and Survival. *Cell,* 138**,** 229-232.

DENG, X., SONG, L., ZHAO, W., WEI, Y. & GUO, X.-B. 2017. HAX-1 Protects Glioblastoma Cells from Apoptosis through the Akt1 Pathway. 11.

DENGLER, M. A., ROBIN, A. Y., GIBSON, L., LI, M. X., SANDOW, J. J., IYER, S., WEBB, A. I., WESTPHAL, D., DEWSON, G. & ADAMS, J. M. 2019. BAX Activation: Mutations Near Its Proposed Non-canonical BH3 Binding Site Reveal Allosteric Changes Controlling Mitochondrial Association. *Cell Reports,* 27**,** 359-373.e6.

DEWSON, G., KRATINA, T., SIM, H. W., PUTHALAKATH, H., ADAMS, J. M., COLMAN, P. M. & KLUCK, R. M. 2008. To Trigger Apoptosis, Bak Exposes Its BH3 Domain and Homodimerizes via BH3:Groove Interactions. *Molecular Cell,* 30**,** 369-380.

DEWULF, J., KOENEN, F., MINTIENS, K., DENIS, P., RIBBENS, S. & DE KRUIF, A. 2004. Analytical performance of several classical swine fever laboratory diagnostic techniques on live animals for detection of infection. *Journal of Virological Methods,* 119**,** 137-143.

DEWULF, J., LAEVENS, H., KOENEN, F., VANDERHALLEN, H., MINTIENS, K., DELUYKER, H. & DE KRUIF, A. 2000. An experimental infection with classical swine fever in E2 sub-unit marker-vaccine vaccinated and in non-vaccinated pigs. *Vaccine,* 19**,** 475-482.

DIANOV, G. L. & HÜBSCHER, U. 2013. Mammalian base excision repair: the forgotten archangel. *Nucleic acids research,* 41**,** 3483-3490.

DIEBOLD, S. S., KAISHO, T., HEMMI, H., AKIRA, S. & REIS E SOUSA, C. 2004. Innate antiviral responses by means of TLR7-mediated recognition of single-stranded RNA. *Science,* 303**,** 1529-31.

DOCEUL, V., CHARLESTON, B., CROOKE, H., REID, E., POWELL, P. P. & SEAGO, J. 2008. The Npro product of classical swine fever virus interacts with IkappaBalpha, the NF-kappaB inhibitor. *J Gen Virol,* 89**,** 1881-9.

DOYLE, T. M. 1933. The viability of the virus of swine fever in bone marrow, muscle and skin of preserved carcases. *Journal of Comparative Pathology and Therapeutics,* 46**,** 25-37.

DRAGAN, A. I., HARGREAVES, V. V., MAKEYEVA, E. N. & PRIVALOV, P. L. 2007. Mechanisms of activation of interferon regulator factor 3: the role of C-terminal domain phosphorylation in IRF-3 dimerization and DNA binding. *Nucleic Acids Res,* 35**,** 3525-34.

DRÄGER, C., BEER, M. & BLOME, S. 2015. Porcine complement regulatory protein CD46 and heparan sulfates are the major factors for classical swine fever virus attachment in vitro. *Archives of Virology,* 160**,** 739-746.

DU, C., FANG, M., LI, Y., LI, L. & WANG, X. 2000. Smac, a mitochondrial protein that promotes cytochrome c-dependent caspase activation by eliminating IAP inhibition. *Cell,* 102**,** 33-42.

DULL, T., ZUFFEREY, R., KELLY, M., MANDEL, R. J., NGUYEN, M., TRONO, D. & NALDINI, L. 1998. A third-generation lentivirus vector with a conditional packaging system. *Journal of virology,* 72**,** 8463-8471.

DZIMIANSKI, J. V., SCHOLTE, F. E. M., BERGERON, É. & PEGAN, S. D. 2019. ISG15: It's Complicated. *Journal of Molecular Biology*.

EC 1982. Council Directive 82/894/EEC of 21 December 1982 on the notification of animal diseases within the Community. *Off. J. Eur. Union,* 378**,** 0058-0062.
EC 2001. Council Directive 2001/89/EC on Community measures for the control of classical swine fever. *Off. J. Eur. Union,* 316**,** 5-35.
EDGAR, G. 1949. *Studies on the viability of the virus of swine fever*.
EGGER, D., WOLK, B., GOSERT, R., BIANCHI, L., BLUM, H. E., MORADPOUR, D. & BIENZ, K. 2002. Expression of hepatitis C virus proteins induces distinct membrane alterations including a candidate viral replication complex. *J Virol,* 76**,** 5974-84.
EITZ FERRER, P., POTTHOFF, S., KIRSCHNEK, S., GASTEIGER, G., KASTENMÜLLER, W., LUDWIG, H., PASCHEN, S. A., VILLUNGER, A., SUTTER, G., DREXLER, I. & HÄCKER, G. 2011. Induction of Noxa-Mediated Apoptosis by Modified Vaccinia Virus Ankara Depends on Viral Recognition by Cytosolic Helicases, Leading to IRF-3/IFN-β-Dependent Induction of Pro-Apoptotic Noxa. *PLOS Pathogens,* 7**,** e1002083.
EL OMARI, K., IOURIN, O., HARLOS, K., GRIMES, J. M. & STUART, D. I. 2013. Structure of a pestivirus envelope glycoprotein E2 clarifies its role in cell entry. *Cell reports,* 3**,** 30-35.
ELBER, A. R., STEGEMAN, A., MOSER, H., EKKER, H. M., SMAK, J. A. & PLUIMERS, F. H. 1999. The classical swine fever epidemic 1997-1998 in The Netherlands: descriptive epidemiology. *Prev Vet Med,* 42**,** 157-84.
ELBERS, K., TAUTZ, N., BECHER, P., STOLL, D., RÜMENAPF, T. & THIEL, H. J. 1996. Processing in the pestivirus E2-NS2 region: identification of proteins p7 and E2p7. *Journal of virology,* 70**,** 4131-4135.
ENARI, M., SAKAHIRA, H., YOKOYAMA, H., OKAWA, K., IWAMATSU, A. & NAGATA, S. 1998. A caspase-activated DNase that degrades DNA during apoptosis, and its inhibitor ICAD. *Nature,* 391**,** 43-50.
ETTEMA, T. J., HUYNEN, M. A., DE VOS, W. M. & VAN DER OOST, J. 2003. TRASH: a novel metal-binding domain predicted to be involved in heavy-metal sensing, trafficking and resistance. *Trends Biochem Sci,* 28**,** 170-3.
FADOK, V. A., VOELKER, D. R., CAMPBELL, P. A., COHEN, J. J., BRATTON, D. L. & HENSON, P. M. 1992. Exposure of phosphatidylserine on the surface of apoptotic lymphocytes triggers specific recognition and removal by macrophages. *J Immunol,* 148**,** 2207-16.
FANG, R., JIANG, Q., ZHOU, X., WANG, C., GUAN, Y., TAO, J., XI, J., FENG, J.-M. & JIANG, Z. 2017. MAVS activates TBK1 and IKKε through TRAFs in NEMO dependent and independent manner. *PLOS Pathogens,* 13**,** e1006720.
FEOKTISTOVA, M., GESERICK, P., KELLERT, B., DIMITROVA, DIANA P., LANGLAIS, C., HUPE, M., CAIN, K., MACFARLANE, M., HÄCKER, G. & LEVERKUS, M. 2011. cIAPs Block Ripoptosome Formation, a RIP1/Caspase-8 Containing Intracellular Cell Death Complex Differentially Regulated by cFLIP Isoforms. *Molecular Cell,* 43**,** 449-463.
FERNANDEZ-SAINZ, I., GLADUE, D. P., HOLINKA, L. G., O'DONNELL, V., GUDMUNDSDOTTIR, I., PRARAT, M. V., PATCH, J. R., GOLDE, W. T., LU, Z., ZHU, J., CARRILLO, C., RISATTI, G. R. & BORCA, M. V. 2010. Mutations in classical swine fever virus NS4B affect virulence in swine. *Journal of virology,* 84**,** 1536-1549.
FIEBACH, A. R., GUZYLACK-PIRIOU, L., PYTHON, S., SUMMERFIELD, A. & RUGGLI, N. 2011. Classical swine fever virus N(pro) limits type I interferon induction in plasmacytoid dendritic cells by interacting with interferon regulatory factor 7. *J Virol,* 85**,** 8002-11.
FIELDS, S. & SONG, O. 1989. A novel genetic system to detect protein-protein interactions. *Nature,* 340**,** 245-6.
FITZGERALD, K. A., MCWHIRTER, S. M., FAIA, K. L., ROWE, D. C., LATZ, E., GOLENBOCK, D. T., COYLE, A. J., LIAO, S. M. & MANIATIS, T. 2003. IKKepsilon and TBK1 are essential components of the IRF3 signaling pathway. *Nat Immunol,* 4**,** 491-6.

FLOEGEL-NIESMANN, G., BUNZENTHAL, C., FISCHER, S. & MOENNIG, V. 2003. Virulence of recent and former classical swine fever virus isolates evaluated by their clinical and pathological signs. *J Vet Med B Infect Dis Vet Public Health,* 50**,** 214-20.

FRAHM, T., HAUSER, H. & KÖSTER, M. 2006. IFN-type-I-mediated signaling is regulated by modulation of STAT2 nuclear export. *Journal of Cell Science,* 119**,** 1092-1104.

FRANCHI, L., EIGENBROD, T., MUNOZ-PLANILLO, R. & NUNEZ, G. 2009. The inflammasome: a caspase-1-activation platform that regulates immune responses and disease pathogenesis. *Nat Immunol,* 10**,** 241-7.

FRIEDMAN, R. L. & STARK, G. R. 1985. α-Interferon-induced transcription of HLA and metallothionein genes containing homologous upstream sequences. *Nature,* 314**,** 637-639.

FU, Y., FODEN, J. A., KHAYTER, C., MAEDER, M. L., REYON, D., JOUNG, J. K. & SANDER, J. D. 2013. High-frequency off-target mutagenesis induced by CRISPR-Cas nucleases in human cells. *Nat Biotechnol,* 31**,** 822-6.

GABRIEL, C., BLOME, S., URNIZA, A., JUANOLA, S., KOENEN, F. & BEER, M. 2012. Towards licensing of CP7_E2alf as marker vaccine against classical swine fever—Duration of immunity. *Vaccine,* 30**,** 2928-2936.

GALINDO, I., HERNAEZ, B., DIAZ-GIL, G., ESCRIBANO, J. M. & ALONSO, C. 2008. A179L, a viral Bcl-2 homologue, targets the core Bcl-2 apoptotic machinery and its upstream BH3 activators with selective binding restrictions for Bid and Noxa. *Virology,* 375**,** 561-72.

GALLEI, A., BLOME, S., GILGENBACH, S., TAUTZ, N., MOENNIG, V. & BECHER, P. 2008. Cytopathogenicity of classical Swine Fever virus correlates with attenuation in the natural host. *J Virol,* 82**,** 9717-29.

GARCIN, D., MARQ, J. B., STRAHLE, L., LE MERCIER, P. & KOLAKOFSKY, D. 2002. All four Sendai Virus C proteins bind Stat1, but only the larger forms also induce its mono-ubiquitination and degradation. *Virology,* 295**,** 256-65.

GARNER, THOMAS P., REYNA, DENIS E., PRIYADARSHI, A., CHEN, H.-C., LI, S., WU, Y., GANESAN, YOGESH T., MALASHKEVICH, VLADIMIR N., CHENG, EMILY H. & GAVATHIOTIS, E. 2016. An Autoinhibited Dimeric Form of BAX Regulates the BAX Activation Pathway. *Molecular Cell,* 63**,** 485-497.

GAVATHIOTIS, E., REYNA, D. E., DAVIS, M. L., BIRD, G. H. & WALENSKY, L. D. 2010. BH3-Triggered Structural Reorganization Drives the Activation of Proapoptotic BAX. *Molecular Cell,* 40**,** 481-492.

GLADUE, D. P., GAVRILOV, B. K., HOLINKA, L. G., FERNANDEZ-SAINZ, I. J., VEPKHVADZE, N. G., ROGERS, K., O'DONNELL, V., RISATTI, G. R. & BORCA, M. V. 2011. Identification of an NTPase motif in classical swine fever virus NS4B protein. *Virology,* 411**,** 41-9.

GLADUE, D. P., HOLINKA, L. G., LARGO, E., FERNANDEZ SAINZ, I., CARRILLO, C., O'DONNELL, V., BAKER-BRANSTETTER, R., LU, Z., AMBROGGIO, X., RISATTI, G. R., NIEVA, J. L. & BORCA, M. V. 2012. Classical swine fever virus p7 protein is a viroporin involved in virulence in swine. *J Virol,* 86**,** 6778-91.

GLADUE, D. P., LARGO, E., HOLINKA, L. G., RAMIREZ-MEDINA, E., VUONO, E. A., BERGGREN, K. A., RISATTI, G. R., NIEVA, J. L. & BORCA, M. V. 2018. Classical Swine Fever Virus p7 Protein Interacts with Host Protein CAMLG and Regulates Calcium Permeability at the Endoplasmic Reticulum. *Viruses,* 10.

GLYKOFRYDES, D., NIPHUIS, H., KUHN, E. M., ROSENWIRTH, B., HEENEY, J. L., BRUDER, J., NIEDOBITEK, G., MÜLLER-FLECKENSTEIN, I., FLECKENSTEIN, B. & ENSSER, A. 2000. Herpesvirus saimiri vFLIP provides an antiapoptotic function but is not essential for viral replication, transformation, or pathogenicity. *Journal of virology,* 74**,** 11919-11927.

GOLDSTEIN, J. C., WATERHOUSE, N. J., JUIN, P., EVAN, G. I. & GREEN, D. R. 2000. The coordinate release of cytochrome c during apoptosis is rapid, complete and kinetically invariant. *Nat Cell Biol,* 2**,** 156-62.

GOTTIPATI, K., ACHOLI, S., RUGGLI, N. & CHOI, K. H. 2014. Autocatalytic activity and substrate specificity of the pestivirus N-terminal protease Npro. *Virology,* 452–453**,** 303-309.

GOTTIPATI, K., HOLTHAUZEN, L. M., RUGGLI, N. & CHOI, K. H. 2016. Pestivirus Npro directly interacts with interferon regulatory factor 3 (IRF3) monomer and dimer. *J Virol*.

GRAHAM, S. P., EVERETT, H. E., HAINES, F. J., JOHNS, H. L., SOSAN, O. A., SALGUERO, F. J., CLIFFORD, D. J., STEINBACH, F., DREW, T. W. & CROOKE, H. R. 2012. Challenge of Pigs with Classical Swine Fever Viruses after C-Strain Vaccination Reveals Remarkably Rapid Protection and Insights into Early Immunity. *PLOS ONE,* 7**,** e29310.

GRANDVAUX, N., SERVANT, M. J., TENOEVER, B., SEN, G. C., BALACHANDRAN, S., BARBER, G. N., LIN, R. & HISCOTT, J. 2002. Transcriptional profiling of interferon regulatory factor 3 target genes: direct involvement in the regulation of interferon-stimulated genes. *Journal of virology,* 76**,** 5532-5539.

GRAY, E. W. & NETTLETON, P. F. 1987. The ultrastructure of cell cultures infected with border disease and bovine virus diarrhoea viruses. *J Gen Virol,* 68 (Pt 9)**,** 2339-46.

GREISER-WILKE, I., BLOME, S. & MOENNIG, V. 2007. Diagnostic methods for detection of Classical swine fever virus--status quo and new developments. *Vaccine,* 25**,** 5524-30.

HABJAN, M., ANDERSSON, I., KLINGSTRÖM, J., SCHÜMANN, M., MARTIN, A., ZIMMERMANN, P., WAGNER, V., PICHLMAIR, A., SCHNEIDER, U., MÜHLBERGER, E., MIRAZIMI, A. & WEBER, F. 2008. Processing of Genome 5' Termini as a Strategy of Negative-Strand RNA Viruses to Avoid RIG-I-Dependent Interferon Induction. *PLoS ONE,* 3**,** e2032.

HACKER, H., REDECKE, V., BLAGOEV, B., KRATCHMAROVA, I., HSU, L. C., WANG, G. G., KAMPS, M. P., RAZ, E., WAGNER, H., HACKER, G., MANN, M. & KARIN, M. 2006. Specificity in Toll-like receptor signalling through distinct effector functions of TRAF3 and TRAF6. *Nature,* 439**,** 204-7.

HAFNER, A., BULYK, M. L., JAMBHEKAR, A. & LAHAV, G. 2019. The multiple mechanisms that regulate p53 activity and cell fate. *Nature Reviews Molecular Cell Biology,* 20**,** 199-210.

HANDEL, K., KEHLER, H., HILLS, K. & PASICK, J. 2004. Comparison of Reverse Transcriptase–Polymerase Chain Reaction, Virus Isolation, and Immunoperoxidase Assays for Detecting Pigs Infected with Low, Moderate, and High Virulent Strains of Classical Swine Fever Virus. *Journal of Veterinary Diagnostic Investigation,* 16**,** 132-138.

HARADA, H., QUEARRY, B., RUIZ-VELA, A. & KORSMEYER, S. J. 2004. Survival factor-induced extracellular signal-regulated kinase phosphorylates BIM, inhibiting its association with BAX and proapoptotic activity. *Proc Natl Acad Sci U S A,* 101**,** 15313-7.

HAUSMANN, Y., ROMAN-SOSA, G., THIEL, H.-J. & RÜMENAPF, T. 2004. Classical swine fever virus glycoprotein E rns is an endoribonuclease with an unusual base specificity. *Journal of virology,* 78**,** 5507-5512.

HELWIG, D. M. & KEAST, J. C. 1966. VIABILITY OF VIRULENT SWINE FEVER VIRUS IN COOKED AND UNCOOKED HAM AND SAUSAGE CASINGS. *Australian Veterinary Journal,* 42**,** 131-135.

HILTON, L., MOGANERADJ, K., ZHANG, G., CHEN, Y.-H., RANDALL, R. E., MCCAULEY, J. W. & GOODBOURN, S. 2006. The NPro Product of Bovine Viral Diarrhea Virus Inhibits DNA Binding by Interferon Regulatory Factor 3 and Targets It for Proteasomal Degradation. *Journal of Virology,* 80**,** 11723-11732.

HINDS, M. G. & DAY, C. L. 2005. Regulation of apoptosis: uncovering the binding determinants. *Current Opinion in Structural Biology,* 15**,** 690-699.

HONDA, K., YANAI, H., MIZUTANI, T., NEGISHI, H., SHIMADA, N., SUZUKI, N., OHBA, Y., TAKAOKA, A., YEH, W. C. & TANIGUCHI, T. 2004. Role of a transductional-

transcriptional processor complex involving MyD88 and IRF-7 in Toll-like receptor signaling. *Proc Natl Acad Sci U S A,* 101**,** 15416-21.
HOUDEBINE, L.-M. 2014. Impacts of genetically modified animals on the ecosystem and human activities. *Global Bioethics,* 25**,** 3-18.
HSU, P. D., SCOTT, D. A., WEINSTEIN, J. A., RAN, F. A., KONERMANN, S., AGARWALA, V., LI, Y., FINE, E. J., WU, X., SHALEM, O., CRADICK, T. J., MARRAFFINI, L. A., BAO, G. & ZHANG, F. 2013. DNA targeting specificity of RNA-guided Cas9 nucleases. *Nat Biotechnol,* 31**,** 827-32.
HU, Y., BENEDICT, M. A., DING, L. & NÚÑEZ, G. 1999. Role of cytochrome c and dATP/ATP hydrolysis in Apaf-1-mediated caspase-9 activation and apoptosis. *The EMBO journal,* 18**,** 3586-3595.
HULST, M. M. & MOORMANN, R. J. 1997. Inhibition of pestivirus infection in cell culture by envelope proteins E(rns) and E2 of classical swine fever virus: E(rns) and E2 interact with different receptors. *J Gen Virol,* 78 (Pt 11)**,** 2779-87.
HULST, M. M., VAN GENNIP, H. G. & MOORMANN, R. J. 2000. Passage of classical swine fever virus in cultured swine kidney cells selects virus variants that bind to heparan sulfate due to a single amino acid change in envelope protein E(rns). *Journal of virology,* 74**,** 9553-9561.
HULST, M. M., VAN GENNIP, H. G. P., VLOT, A. C., SCHOOTEN, E., DE SMIT, A. J. & MOORMANN, R. J. M. 2001. Interaction of Classical Swine Fever Virus with Membrane-Associated Heparan Sulfate: Role for Virus Replication In Vivo and Virulence. *Journal of Virology,* 75**,** 9585-9595.
HULST, M. M., WESTRA, D. F., WENSVOORT, G. & MOORMANN, R. J. 1993. Glycoprotein E1 of hog cholera virus expressed in insect cells protects swine from hog cholera. *Journal of virology,* 67**,** 5435-5442.
HÜSSER, L., ALVES, M. P., RUGGLI, N. & SUMMERFIELD, A. 2011. Identification of the role of RIG-I, MDA-5 and TLR3 in sensing RNA viruses in porcine epithelial cells using lentivirus-driven RNA interference. *Virus Research,* 159**,** 9-16.
HUSSER, L., RUGGLI, N. & SUMMERFIELD, A. 2012. N(pro) of classical swine fever virus prevents type I interferon-mediated priming of conventional dendritic cells for enhanced interferon-alpha response. *J Interferon Cytokine Res,* 32**,** 221-9.
HUXFORD, T., HUANG, D. B., MALEK, S. & GHOSH, G. 1998. The crystal structure of the IkappaBalpha/NF-kappaB complex reveals mechanisms of NF-kappaB inactivation. *Cell,* 95**,** 759-70.
ICHIM, G. & TAIT, S. W. G. 2016. A fate worse than death: apoptosis as an oncogenic process. *Nature Reviews Cancer,* 16**,** 539.
ICTV. 2019. *Genus: Pestivirus* [Online]. [Accessed 15/09/2019].
IRMLER, M., THOME, M., HAHNE, M., SCHNEIDER, P., HOFMANN, K., STEINER, V., BODMER, J.-L., SCHRÖTER, M., BURNS, K., MATTMANN, C., RIMOLDI, D., FRENCH, L. E. & TSCHOPP, J. 1997. Inhibition of death receptor signals by cellular FLIP. *Nature,* 388**,** 190-195.
ISKEN, O., POSTEL, A., BRUHN, B., LATTWEIN, E., BECHER, P. & TAUTZ, N. 2019. CRISPR/Cas9-Mediated Knockout of DNAJC14 Verifies This Chaperone as a Pivotal Host Factor for RNA Replication of Pestiviruses. *J Virol,* 93.
IWABUCHI, K., LI, B., BARTEL, P. & FIELDS, S. 1993. Use of the two-hybrid system to identify the domain of p53 involved in oligomerization. *Oncogene,* 8**,** 1693-6.
JACOBS, M. D. & HARRISON, S. C. 1998. Structure of an IkappaBalpha/NF-kappaB complex. *Cell,* 95**,** 749-58.
JAMIN, A., GORIN, S., CARIOLET, R., LE POTIER, M. F. & KUNTZ-SIMON, G. 2008. Classical swine fever virus induces activation of plasmacytoid and conventional dendritic cells in tonsil, blood, and spleen of infected pigs. *Vet Res,* 39**,** 7.

JEFFERSON, M., WHELBAND, M., MOHORIANU, I. & POWELL, P. P. 2014. The pestivirus N terminal protease N(pro) redistributes to mitochondria and peroxisomes suggesting new sites for regulation of IRF3 by N(pro.). *PLoS One,* 9**,** e88838.

JENG, P. S., INOUE-YAMAUCHI, A., HSIEH, J. J. & CHENG, E. H. 2018. BH3-dependent and independent activation of BAX and BAK in mitochondrial apoptosis. *Current Opinion in Physiology,* 3**,** 71-81.

JIANG, P., DU, W., HEESE, K. & WU, M. 2006. The Bad Guy Cooperates with Good Cop p53: Bad Is Transcriptionally Up-Regulated by p53 and Forms a Bad/p53 Complex at the Mitochondria To Induce Apoptosis. *Molecular and Cellular Biology,* 26**,** 9071-9082.

JOHNS, H. L., BENSAUDE, E., LA ROCCA, S. A., SEAGO, J., CHARLESTON, B., STEINBACH, F., DREW, T. W., CROOKE, H. & EVERETT, H. 2010a. Classical swine fever virus infection protects aortic endothelial cells from pIpC-mediated apoptosis. *J Gen Virol,* 91**,** 1038-46.

JOHNS, H. L., DOCEUL, V., EVERETT, H., CROOKE, H., CHARLESTON, B. & SEAGO, J. 2010b. The classical swine fever virus N-terminal protease Npro binds to cellular HAX-1. 91**,** 2677-2686.

JORGENSEN, I., RAYAMAJHI, M. & MIAO, E. A. 2017. Programmed cell death as a defence against infection. *Nature reviews. Immunology,* 17**,** 151-164.

JULIEN, O., ZHUANG, M., WIITA, A. P., O'DONOGHUE, A. J., KNUDSEN, G. M., CRAIK, C. S. & WELLS, J. A. 2016. Quantitative MS-based enzymology of caspases reveals distinct protein substrate specificities, hierarchies, and cellular roles. *Proc Natl Acad Sci U S A,* 113**,** E2001-10.

KAISER, W. J., KAUFMAN, J. L. & OFFERMANN, M. K. 2004. IFN-alpha sensitizes human umbilical vein endothelial cells to apoptosis induced by double-stranded RNA. *J Immunol,* 172**,** 1699-710.

KALE, J., KUTUK, O., BRITO, G. C., ANDREWS, T. S., LEBER, B., LETAI, A. & ANDREWS, D. W. 2018. Phosphorylation switches Bax from promoting to inhibiting apoptosis thereby increasing drug resistance. *EMBO Rep,* 19.

KANG, D.-C., GOPALKRISHNAN, R. V., WU, Q., JANKOWSKY, E., PYLE, A. M. & FISHER, P. B. 2002. mda-5: An interferon-inducible putative RNA helicase with double-stranded RNA-dependent ATPase activity and melanoma growth-suppressive properties. 99**,** 637-642.

KARIN, M. & BEN-NERIAH, Y. 2000. Phosphorylation Meets Ubiquitination: The Control of NF-κB Activity. *Annual Review of Immunology,* 18**,** 621-663.

KATO, H., TAKAHASI, K. & FUJITA, T. 2011. RIG-I-like receptors: cytoplasmic sensors for non-self RNA. *Immunol Rev,* 243**,** 91-8.

KATO, H., TAKEUCHI, O., MIKAMO-SATOH, E., HIRAI, R., KAWAI, T., MATSUSHITA, K., HIIRAGI, A., DERMODY, T. S., FUJITA, T. & AKIRA, S. 2008. Length-dependent recognition of double-stranded ribonucleic acids by retinoic acid–inducible gene-I and melanoma differentiation–associated gene 5. *The Journal of Experimental Medicine,* 205**,** 1601-1610.

KATO, H., TAKEUCHI, O., SATO, S., YONEYAMA, M., YAMAMOTO, M., MATSUI, K., UEMATSU, S., JUNG, A., KAWAI, T., ISHII, K. J., YAMAGUCHI, O., OTSU, K., TSUJIMURA, T., KOH, C. S., REIS E SOUSA, C., MATSUURA, Y., FUJITA, T. & AKIRA, S. 2006. Differential roles of MDA5 and RIG-I helicases in the recognition of RNA viruses. *Nature,* 441**,** 101-5.

KAWAI, T., SATO, S., ISHII, K. J., COBAN, C., HEMMI, H., YAMAMOTO, M., TERAI, K., MATSUDA, M., INOUE, J.-I., UEMATSU, S., TAKEUCHI, O. & AKIRA, S. 2004. Interferon-α induction through Toll-like receptors involves a direct interaction of IRF7 with MyD88 and TRAF6. *Nature Immunology,* 5**,** 1061-1068.

KERR, J. F., WYLLIE, A. H. & CURRIE, A. R. 1972. Apoptosis: a basic biological phenomenon with wide-ranging implications in tissue kinetics. *Br J Cancer,* 26**,** 239-57.

KIM, H.-E., DU, F., FANG, M. & WANG, X. 2005. Formation of apoptosome is initiated by cytochrome c-induced dATP hydrolysis and subsequent nucleotide exchange on Apaf-1. *Proceedings of the National Academy of Sciences of the United States of America,* 102**,** 17545-17550.

KIM, T. K. & MANIATIS, T. 1997. The mechanism of transcriptional synergy of an in vitro assembled interferon-beta enhanceosome. *Mol Cell,* 1**,** 119-29.

KIRSHNER, J. R., KARPOVA, A. Y., KOPS, M. & HOWLEY, P. M. 2005. Identification of TRAIL as an interferon regulatory factor 3 transcriptional target. *Journal of virology,* 79**,** 9320-9324.

KISCHKEL, F. C., HELLBARDT, S., BEHRMANN, I., GERMER, M., PAWLITA, M., KRAMMER, P. H. & PETER, M. E. 1995. Cytotoxicity-dependent APO-1 (Fas/CD95)-associated proteins form a death-inducing signaling complex (DISC) with the receptor. *Embo j,* 14**,** 5579-88.

KISCHKEL, F. C., LAWRENCE, D. A., CHUNTHARAPAI, A., SCHOW, P., KIM, K. J. & ASHKENAZI, A. 2000. Apo2L/TRAIL-dependent recruitment of endogenous FADD and caspase-8 to death receptors 4 and 5. *Immunity,* 12**,** 611-20.

KNOWLTON, J. J., DERMODY, T. S. & HOLM, G. H. 2012. Apoptosis induced by mammalian reovirus is beta interferon (IFN) independent and enhanced by IFN regulatory factor 3- and NF-κB-dependent expression of Noxa. *Journal of virology,* 86**,** 1650-1660.

KOENIG, P., LANGE, E., REIMANN, I. & BEER, M. 2007. CP7_E2alf: A safe and efficient marker vaccine strain for oral immunisation of wild boar against Classical swine fever virus (CSFV). *Vaccine,* 25**,** 3391-3399.

KONIG, M., LENGSFELD, T., PAULY, T., STARK, R. & THIEL, H. J. 1995. Classical swine fever virus: independent induction of protective immunity by two structural glycoproteins. *J Virol,* 69**,** 6479-86.

KREY, T., HIMMELREICH, A., HEIMANN, M., MENGE, C., THIEL, H. J., MAURER, K. & RUMENAPF, T. 2006. Function of bovine CD46 as a cellular receptor for bovine viral diarrhea virus is determined by complement control protein 1. *J Virol,* 80**,** 3912-22.

LA ROCCA, S. A., HERBERT, R. J., CROOKE, H., DREW, T. W., WILEMAN, T. E. & POWELL, P. P. 2005. Loss of interferon regulatory factor 3 in cells infected with classical swine fever virus involves the N-terminal protease, Npro. *J Virol,* 79**,** 7239-47.

LACKNER, T., MÜLLER, A., KÖNIG, M., THIEL, H.-J. & TAUTZ, N. 2005. Persistence of Bovine Viral Diarrhea Virus Is Determined by a Cellular Cofactor of a Viral Autoprotease. *Journal of Virology,* 79**,** 9746-9755.

LACKNER, T., THIEL, H.-J. & TAUTZ, N. 2006. Dissection of a viral autoprotease elucidates a function of a cellular chaperone in proteolysis. *Proceedings of the National Academy of Sciences,* 103**,** 1510-1515.

LAMP, B., RIEDEL, C., ROMAN-SOSA, G., HEIMANN, M., JACOBI, S., BECHER, P., THIEL, H.-J. & RÜMENAPF, T. 2011. Biosynthesis of classical swine fever virus nonstructural proteins. *Journal of virology,* 85**,** 3607-3620.

LARGO, E., VERDIÁ-BÁGUENA, C., AGUILELLA, V. M., NIEVA, J. L. & ALCARAZ, A. 2016. Ion channel activity of the CSFV p7 viroporin in surrogates of the ER lipid bilayer. *Biochimica et Biophysica Acta (BBA) - Biomembranes,* 1858**,** 30-37.

LAU, A. T. Y., LI, M., XIE, R., HE, Q.-Y. & CHIU, J.-F. 2004. Opposed arsenite-induced signaling pathways promote cell proliferation or apoptosis in cultured lung cells. *Carcinogenesis,* 25**,** 21-28.

LECOT, S., BELOUZARD, S., DUBUISSON, J. & ROUILLÉ, Y. 2005. Bovine Viral Diarrhea Virus Entry Is Dependent on Clathrin-Mediated Endocytosis. *Journal of Virology,* 79**,** 10826-10829.

LEE, H. K., LUND, J. M., RAMANATHAN, B., MIZUSHIMA, N. & IWASAKI, A. 2007. Autophagy-Dependent Viral Recognition by Plasmacytoid Dendritic Cells. 315**,** 1398-1401.

LEIFER, I., DEPNER, K., BLOME, S., LE POTIER, M.-F., LE DIMNA, M., BEER, M. & HOFFMANN, B. 2009a. Differentiation of C-strain “Riems” or CP7_E2alf vaccinated animals from

animals infected by classical swine fever virus field strains using real-time RT-PCR. *Journal of Virological Methods,* 158**,** 114-122.

LEIFER, I., HOFFMANN, B., HÖPER, D., BRUUN RASMUSSEN, T., BLOME, S., STREBELOW, G., HÖRETH-BÖNTGEN, D., STAUBACH, C. & BEER, M. 2010. Molecular epidemiology of current classical swine fever virus isolates of wild boar in Germany. *Journal of General Virology,* 91**,** 2687-2697.

LEIFER, I., LANGE, E., REIMANN, I., BLOME, S., JUANOLA, S., DURAN, J. P. & BEER, M. 2009b. Modified live marker vaccine candidate CP7_E2alf provides early onset of protection against lethal challenge infection with classical swine fever virus after both intramuscular and oral immunization. *Vaccine,* 27**,** 6522-6529.

LEMAIRE, C., ANDRÉAU, K., SOUVANNAVONG, V. & ADAM, A. 1998. Inhibition of caspase activity induces a switch from apoptosis to necrosis. *FEBS Letters,* 425**,** 266-270.

LEU, J. I. J., DUMONT, P., HAFEY, M., MURPHY, M. E. & GEORGE, D. L. 2004. Mitochondrial p53 activates Bak and causes disruption of a Bak–Mcl1 complex. *Nature Cell Biology,* 6**,** 443-450.

LEVY, D. E., MARIE, I., SMITH, E. & PRAKASH, A. 2002. Enhancement and diversification of IFN induction by IRF-7-mediated positive feedback. *J Interferon Cytokine Res,* 22**,** 87-93.

LI, B. & FIELDS, S. 1993. Identification of mutations in p53 that affect its binding to SV40 large T antigen by using the yeast two-hybrid system. *Faseb j,* 7**,** 957-63.

LI, J., DAI, Y., LIU, S., GUO, H., WANG, T., OUYANG, H. & TU, C. 2011. In vitro inhibition of CSFV replication by multiple siRNA expression. *Antiviral Res,* 91**,** 209-16.

LI, J., GUO, H., SHI, Z. & TU, C. 2010. In vitro inhibition of CSFV replication by retroviral vector-mediated RNA interference. *J Virol Methods,* 169**,** 316-21.

LI, X., LU, C., STEWART, M., XU, H., STRONG, R. K., IGUMENOVA, T. & LI, P. 2009. Structural basis of double-stranded RNA recognition by the RIG-I like receptor MDA5. *Arch Biochem Biophys,* 488**,** 23-33.

LI, Y., SHEN, L., LI, C., HUANG, J., ZHAO, B., SUN, Y., LI, S., LUO, Y. & QIU, H. J. 2014. Visualization of the Npro protein in living cells using biarsenically labeling tetracysteine-tagged classical swine fever virus. *Virus Res,* 189**,** 67-74.

LIGR, M., MADEO, F., FROHLICH, E., HILT, W., FROHLICH, K. U. & WOLF, D. H. 1998. Mammalian Bax triggers apoptotic changes in yeast. *FEBS Lett,* 438**,** 61-5.

LIN, P. H., PAN, Z., ZHENG, L., LI, N., DANIELPOUR, D. & MA, J. J. 2005. Overexpression of Bax sensitizes prostate cancer cells to TGF-β induced apoptosis. *Cell Research,* 15**,** 160-166.

LIN, R., HEYLBROECK, C., PITHA, P. M. & HISCOTT, J. 1998. Virus-dependent phosphorylation of the IRF-3 transcription factor regulates nuclear translocation, transactivation potential, and proteasome-mediated degradation. *Mol Cell Biol,* 18**,** 2986-96.

LINDENBACH, B., THIEL, H. J. & RICE, C. M. 2007. Flaviviridae: The viruses and their replication. *Fields Virology***,** 1101-1151.

LINDSTEN, T., ROSS, A. J., KING, A., ZONG, W.-X., RATHMELL, J. C., SHIELS, H. A., ULRICH, E., WAYMIRE, K. G., MAHAR, P., FRAUWIRTH, K., CHEN, Y., WEI, M., ENG, V. M., ADELMAN, D. M., SIMON, M. C., MA, A., GOLDEN, J. A., EVAN, G., KORSMEYER, S. J., MACGREGOR, G. R. & THOMPSON, C. B. 2000. The Combined Functions of Proapoptotic Bcl-2 Family Members Bak and Bax Are Essential for Normal Development of Multiple Tissues. *Molecular Cell,* 6**,** 1389-1399.

LIU, L., HOFFMANN, B., BAULE, C., BEER, M., BELÁK, S. & WIDÉN, F. 2009. Two real-time RT-PCR assays of classical swine fever virus, developed for the genetic differentiation of naturally infected from vaccinated wild boars. *Journal of Virological Methods,* 159**,** 131-133.

LIU, S., CAI, X., WU, J., CONG, Q., CHEN, X., LI, T., DU, F., REN, J., WU, Y. T., GRISHIN, N. V. & CHEN, Z. J. 2015. Phosphorylation of innate immune adaptor proteins MAVS, STING, and TRIF induces IRF3 activation. *Science,* 347**,** aaa2630.

LIU, S., CHEN, J., CAI, X., WU, J., CHEN, X., WU, Y.-T., SUN, L. & CHEN, Z. J. 2013. MAVS recruits multiple ubiquitin E3 ligases to activate antiviral signaling cascades. *eLife,* 2**,** e00785.
LLAMBI, F., MOLDOVEANU, T., TAIT, STEPHEN W. G., BOUCHIER-HAYES, L., TEMIROV, J., MCCORMICK, LAURA L., DILLON, CHRISTOPHER P. & GREEN, DOUGLAS R. 2011. A Unified Model of Mammalian BCL-2 Protein Family Interactions at the Mitochondria. *Molecular Cell,* 44**,** 517-531.
LOEFFEN, W. 2005. Evaluation of five commercially available CSF-ELISA kits. *Brussels, Belgium*.
LOO, Y. M., FORNEK, J., CROCHET, N., BAJWA, G., PERWITASARI, O., MARTINEZ-SOBRIDO, L., AKIRA, S., GILL, M. A., GARCIA-SASTRE, A., KATZE, M. G. & GALE, M., JR. 2008. Distinct RIG-I and MDA5 signaling by RNA viruses in innate immunity. *J Virol,* 82**,** 335-45.
LOUBER, J., BRUNEL, J., UCHIKAWA, E., CUSACK, S. & GERLIER, D. 2015. Kinetic discrimination of self/non-self RNA by the ATPase activity of RIG-I and MDA5. *BMC biology,* 13**,** 54-54.
LU, B., GARRIDO, N., SPELBRINK, J. N. & SUZUKI, C. K. 2006. Tid1 isoforms are mitochondrial DnaJ-like chaperones with unique carboxyl termini that determine cytosolic fate. *J Biol Chem,* 281**,** 13150-8.
LUO, Q., ZHANG, L., WEI, F., FANG, Q., BAO, F., MI, S., LI, N., WANG, C., LIU, Y. & TU, C. 2018. mTORC1 Negatively Regulates the Replication of Classical Swine Fever Virus Through Autophagy and IRES-Dependent Translation. *iScience,* 3**,** 87-101.
LUO, Y., JI, S., LEI, J.-L., XIANG, G.-T., LIU, Y., GAO, Y., MENG, X.-Y., ZHENG, G., ZHANG, E.-Y., WANG, Y., DU, M.-L., LI, Y., LI, S., HE, X.-J., SUN, Y. & QIU, H.-J. 2017. Efficacy evaluation of the C-strain-based vaccines against the subgenotype 2.1d classical swine fever virus emerging in China. *Veterinary Microbiology,* 201**,** 154-161.
LUSSI, C., SAUTER, K.-S. & SCHWEIZER, M. 2018. Homodimerisation-independent cleavage of dsRNA by a pestiviral nicking endoribonuclease. *Scientific Reports,* 8**,** 8226.
LUTTICKEN, D., DREXLER, C., VISSER, N. & KADEN, V. 1998. The relevance of CSF marker vaccines for field use. *Proc OIE Sym CSF*.
LV, H., DONG, W., CAO, Z., LI, X., WANG, J., QIAN, G., LV, Q., WANG, C., GUO, K. & ZHANG, Y. 2017a. TRAF6 is a novel NS3-interacting protein that inhibits classical swine fever virus replication. *Scientific Reports,* 7**,** 6737.
LV, H., DONG, W., QIAN, G., WANG, J., LI, X., CAO, Z., LV, Q., WANG, C., GUO, K. & ZHANG, Y. 2017b. uS10, a novel Npro-interacting protein, inhibits classical swine fever virus replication. 98**,** 1679-1692.
MACOVEI, A., ZITZMANN, N., LAZAR, C., DWEK, R. A. & BRANZA-NICHITA, N. 2006. Brefeldin A inhibits pestivirus release from infected cells, without affecting its assembly and infectivity. *Biochem Biophys Res Commun,* 346**,** 1083-90.
MALSY, M., BITZINGER, D., GRAF, B. & BUNDSCHERER, A. 2019. Staurosporine induces apoptosis in pancreatic carcinoma cells PaTu 8988t and Panc-1 via the intrinsic signaling pathway. *European Journal of Medical Research,* 24**,** 5.
MARIÉ, I., DURBIN, J. E. & LEVY, D. E. 1998. Differential viral induction of distinct interferon-alpha genes by positive feedback through interferon regulatory factor-7. *The EMBO journal,* 17**,** 6660-6669.
MAURER, K., KREY, T., MOENNIG, V., THIEL, H. J. & RUMENAPF, T. 2004. CD46 is a cellular receptor for bovine viral diarrhea virus. *J Virol,* 78**,** 1792-9.
MAYER, D., HOFMANN, M. A. & TRATSCHIN, J.-D. 2004. Attenuation of classical swine fever virus by deletion of the viral Npro gene. *Vaccine,* 22**,** 317-328.
MCCARTHY, R. R., EVERETT, H. E., GRAHAM, S. P., STEINBACH, F. & CROOKE, H. R. 2019. Head Start Immunity: Characterizing the Early Protection of C Strain Vaccine Against Subsequent Classical Swine Fever Virus Infection. *Frontiers in Immunology,* 10.
MCILWAIN, D. R., BERGER, T. & MAK, T. W. 2013. Caspase functions in cell death and disease. *Cold Spring Harbor perspectives in biology,* 5**,** a008656-a008656.

MCNAB, F., MAYER-BARBER, K., SHER, A., WACK, A. & O'GARRA, A. 2015. Type I interferons in infectious disease. *Nature Reviews Immunology,* 15**,** 87.
MERRICK, W. C. 2004. Cap-dependent and cap-independent translation in eukaryotic systems. *Gene,* 332**,** 1-11.
MESA, R. A. 2010. Ruxolitinib, a selective JAK1 and JAK2 inhibitor for the treatment of myeloproliferative neoplasms and psoriasis. *IDrugs,* 13**,** 394-403.
MEYERS, G., EGE, A., FETZER, C., VON FREYBURG, M., ELBERS, K., CARR, V., PRENTICE, H., CHARLESTON, B. & SCHURMANN, E. M. 2007. Bovine viral diarrhea virus: prevention of persistent fetal infection by a combination of two mutations affecting Erns RNase and Npro protease. *J Virol,* 81**,** 3327-38.
MICHEAU, O., LENS, S., GAIDE, O., ALEVIZOPOULOS, K. & TSCHOPP, J. 2001. NF-kappaB signals induce the expression of c-FLIP. *Molecular and cellular biology,* 21**,** 5299-5305.
MIHARA, M., ERSTER, S., ZAIKA, A., PETRENKO, O., CHITTENDEN, T., PANCOSKA, P. & MOLL, U. M. 2003. p53 Has a Direct Apoptogenic Role at the Mitochondria. *Molecular Cell,* 11**,** 577-590.
MITTELHOLZER, C., MOSER, C., TRATSCHIN, J.-D. & HOFMANN, M. A. 2000. Analysis of classical swine fever virus replication kinetics allows differentiation of highly virulent from avirulent strains. *Veterinary Microbiology,* 74**,** 293-308.
MOENNIG, V. 2015. The control of classical swine fever in wild boar. *Frontiers in microbiology,* 6**,** 1211-1211.
MOENNIG, V., FLOEGEL-NIESMANN, G. & GREISER-WILKE, I. 2003a. Clinical Signs and Epidemiology of Classical Swine Fever: A Review of New Knowledge. *The Veterinary Journal,* 165**,** 11-20.
MOENNIG, V., FLOEGEL-NIESMANN, G. & GREISER-WILKE, I. 2003b. Clinical signs and epidemiology of classical swine fever: a review of new knowledge. *Vet J,* 165**,** 11-20.
MOENNIG, V. & PLAGEMANN, P. G. W. 1992. The Pestiviruses. *In:* MARAMOROSCH, K., MURPHY, F. A. & SHATKIN, A. J. (eds.) *Advances in Virus Research.* Academic Press.
MOJICA, F. J. M., DÍEZ-VILLASEÑOR, C. S., GARCÍA-MARTÍNEZ, J. & SORIA, E. J. J. O. M. E. 2005. Intervening Sequences of Regularly Spaced Prokaryotic Repeats Derive from Foreign Genetic Elements. 60**,** 174-182.
MOORMANN, R. J. M., BOUMA, A., KRAMPS, J. A., TERPSTRA, C. & DE SMIT, H. J. 2000. Development of a classical swine fever subunit marker vaccine and companion diagnostic test. *Veterinary Microbiology,* 73**,** 209-219.
MORI, M., YONEYAMA, M., ITO, T., TAKAHASHI, K., INAGAKI, F. & FUJITA, T. 2004. Identification of Ser-386 of interferon regulatory factor 3 as critical target for inducible phosphorylation that determines activation. *J Biol Chem,* 279**,** 9698-702.
MOSER, C., RUGGLI, N., TRATSCHIN, J. D. & HOFMANN, M. A. 1996. Detection of antibodies against classical swine fever virus in swine sera by indirect ELISA using recombinant envelope glycoprotein E2. *Veterinary Microbiology,* 51**,** 41-53.
MOULIN, H. R., SEUBERLICH, T., BAUHOFER, O., BENNETT, L. C., TRATSCHIN, J.-D., HOFMANN, M. A. & RUGGLI, N. 2007. Nonstructural proteins NS2-3 and NS4A of classical swine fever virus: Essential features for infectious particle formation. *Virology,* 365**,** 376-389.
MULLER, M., BRISCOE, J., LAXTON, C., GUSCHIN, D., ZIEMIECKI, A., SILVENNOINEN, O., HARPUR, A. G., BARBIERI, G., WITTHUHN, B. A., SCHINDLER, C. & ET AL. 1993. The protein tyrosine kinase JAK1 complements defects in interferon-alpha/beta and -gamma signal transduction. *Nature,* 366**,** 129-35.
MULLER, T., TEUFFERT, J., STAUBACH, C., SELHORST, T. & DEPNER, K. R. 2005. Long-term studies on maternal immunity for Aujeszky's disease and classical swine fever in wild boar piglets. *J Vet Med B Infect Dis Vet Public Health,* 52**,** 432-6.
MUNOZ-GONZALEZ, S., RUGGLI, N., ROSELL, R., PEREZ, L. J., FRIAS-LEUPOREAU, M. T., FRAILE, L., MONTOYA, M., CORDOBA, L., DOMINGO, M., EHRENSPERGER, F., SUMMERFIELD, A.

& GANGES, L. 2015. Postnatal persistent infection with classical Swine Fever virus and its immunological implications. *PLoS One,* 10**,** e0125692.
MURPHY, K. M., STREIPS, U. N. & LOCK, R. B. 2000. Bcl-2 inhibits a Fas-induced conformational change in the Bax N terminus and Bax mitochondrial translocation. *J Biol Chem,* 275**,** 17225-8.
NAGATA, S. 2018. Apoptosis and Clearance of Apoptotic Cells. 36**,** 489-517.
NECHUSHTAN, A., SMITH, C. L., HSU, Y. T. & YOULE, R. J. 1999. Conformation of the Bax C-terminus regulates subcellular location and cell death. *Embo j,* 18**,** 2330-41.
NG, A. C., BAIRD, S. D. & SCREATON, R. A. 2014. Essential role of TID1 in maintaining mitochondrial membrane potential homogeneity and mitochondrial DNA integrity. *Mol Cell Biol,* 34**,** 1427-37.
NING, S., PAGANO, J. S. & BARBER, G. N. 2011. IRF7: activation, regulation, modification and function. *Genes and immunity,* 12**,** 399-414.
NISHI, T., KAMEYAMA, K.-I., KATO, T. & FUKAI, K. 2019. Genome Sequence of a Classical Swine Fever Virus of Subgenotype 2.1, Isolated from a Pig in Japan in 2018. *Microbiology resource announcements,* 8**,** e01362-18.
NOVICK, D., COHEN, B. & RUBINSTEIN, M. 1994. The human interferon alpha/beta receptor: characterization and molecular cloning. *Cell,* 77**,** 391-400.
O'DOHERTY, U., SWIGGARD, W. J. & MALIM, M. H. 2000. Human immunodeficiency virus type 1 spinoculation enhances infection through virus binding. *J Virol,* 74**,** 10074-80.
O'NEILL, L. A. J., GOLENBOCK, D. & BOWIE, A. G. 2013. The history of Toll-like receptors [mdash] redefining innate immunity. *Nat Rev Immunol,* 13**,** 453-460.
OBERST, A., POP, C., TREMBLAY, A. G., BLAIS, V., DENAULT, J. B., SALVESEN, G. S. & GREEN, D. R. 2010. Inducible dimerization and inducible cleavage reveal a requirement for both processes in caspase-8 activation. *J Biol Chem,* 285**,** 16632-42.
OGANESYAN, G., SAHA, S. K., GUO, B., HE, J. Q., SHAHANGIAN, A., ZARNEGAR, B., PERRY, A. & CHENG, G. 2006. Critical role of TRAF3 in the Toll-like receptor-dependent and -independent antiviral response. *Nature,* 439**,** 208-11.
OIE. 2019a. *Information received on 18/08/2019 from Dr Norio Kumagai, Director, Chief Veterinary Officer, Animal Health Division, Food Safety and Consumer Affairs Bureau, Ministry of Agriculture, Forestry and Fisheries, Tokyo, Japan; Follow-up report No. 34* [Online]. OIE. Available: https://www.oie.int/wahis_2/public/wahid.php/Reviewreport/Review?page_refer=MapFullEventReport&reportid=31405 [Accessed 15/09/2019].
OIE. 2019b. *OIE-Listed diseases, infections and infestations in force in 2019* [Online]. Available: https://www.oie.int/animal-health-in-the-world/oie-listed-diseases-2019/ [Accessed 15/09/2019].
PANNE, D., MCWHIRTER, S. M., MANIATIS, T. & HARRISON, S. C. 2007. Interferon regulatory factor 3 is regulated by a dual phosphorylation-dependent switch. *J Biol Chem,* 282**,** 22816-22.
PASTORINO, J. G., CHEN, S. T., TAFANI, M., SNYDER, J. W. & FARBER, J. L. 1998. The overexpression of Bax produces cell death upon induction of the mitochondrial permeability transition. *J Biol Chem,* 273**,** 7770-5.
PATON, D. J. & GREISER-WILKE, I. 2003. Classical swine fever – an update. *Research in Veterinary Science,* 75**,** 169-178.
PAZ, S., VILASCO, M., WERDEN, S. J., ARGUELLO, M., JOSEPH-PILLAI, D., ZHAO, T., NGUYEN, T. L.-A., SUN, Q., MEURS, E. F., LIN, R. & HISCOTT, J. 2011. A functional C-terminal TRAF3-binding site in MAVS participates in positive and negative regulation of the IFN antiviral response. *Cell Research,* 21**,** 895-910.

PEI, J., ZHAO, M., YE, Z., GOU, H., WANG, J., YI, L., DONG, X., LIU, W., LUO, Y., LIAO, M. & CHEN, J. 2014. Autophagy enhances the replication of classical swine fever virus in vitro. *Autophagy,* 10**,** 93-110.

PERALES-LINARES, R. & NAVAS-MARTIN, S. 2013. Toll-like receptor 3 in viral pathogenesis: friend or foe? *Immunology,* 140**,** 153-67.

PÉREZ DE DIEGO, R., SANCHO-SHIMIZU, V., LORENZO, L., PUEL, A., PLANCOULAINE, S., PICARD, C., HERMAN, M., CARDON, A., DURANDY, A., BUSTAMANTE, J., VALLABHAPURAPU, S., BRAVO, J., WARNATZ, K., CHAIX, Y., CASCARRIGNY, F., LEBON, P., ROZENBERG, F., KARIN, M., TARDIEU, M., AL-MUHSEN, S., JOUANGUY, E., ZHANG, S.-Y., ABEL, L. & CASANOVA, J.-L. 2010. Human TRAF3 Adaptor Molecule Deficiency Leads to Impaired Toll-like Receptor 3 Response and Susceptibility to Herpes Simplex Encephalitis. *Immunity,* 33**,** 400-411.

PESTKA, S., KRAUSE, C. D. & WALTER, M. R. 2004. Interferons, interferon-like cytokines, and their receptors. *Immunol Rev,* 202**,** 8-32.

PETER, M. E. & KRAMMER, P. H. 1998. Mechanisms of CD95 (APO-1/Fas)-mediated apoptosis. *Current Opinion in Immunology,* 10**,** 545-551.

PETERHANS, E., BACHOFEN, C., STALDER, H. & SCHWEIZER, M. 2010. Cytopathic bovine viral diarrhea viruses (BVDV): emerging pestiviruses doomed to extinction. *Veterinary research,* 41**,** 44-44.

PETERS, K., CHATTOPADHYAY, S. & SEN, G. C. 2008. IRF-3 activation by Sendai virus infection is required for cellular apoptosis and avoidance of persistence. *J Virol,* 82**,** 3500-8.

PETRASEK, J., IRACHETA-VELLVE, A., CSAK, T., SATISHCHANDRAN, A., KODYS, K., KURT-JONES, E. A., FITZGERALD, K. A. & SZABO, G. 2013. STING-IRF3 pathway links endoplasmic reticulum stress with hepatocyte apoptosis in early alcoholic liver disease. 110**,** 16544-16549.

PINTON, P., GIORGI, C., SIVIERO, R., ZECCHINI, E. & RIZZUTO, R. 2008. Calcium and apoptosis: ER-mitochondria Ca2+ transfer in the control of apoptosis. *Oncogene,* 27**,** 6407.

POPP, M. W. & MAQUAT, L. E. 2016. Leveraging Rules of Nonsense-Mediated mRNA Decay for Genome Engineering and Personalized Medicine. *Cell,* 165**,** 1319-1322.

PORTER, A. C., CHERNAJOVSKY, Y., DALE, T. C., GILBERT, C. S., STARK, G. R. & KERR, I. M. 1988. Interferon response element of the human gene 6-16. *Embo j,* 7**,** 85-92.

POSTEL, A., MOENNIG, V. & BECHER, P. 2013a. Classical swine fever in Europe--the current situation. *Berl Munch Tierarztl Wochenschr,* 126**,** 468-75.

POSTEL, A., NISHI, T., KAMEYAMA, K.-I., MEYER, D., SUCKSTORFF, O., FUKAI, K. & BECHER, P. 2019. Reemergence of Classical Swine Fever, Japan, 2018. *Emerging infectious diseases,* 25**,** 1228-1231.

POSTEL, A., SCHMEISER, S., PERERA, C. L., RODRIGUEZ, L. J., FRIAS-LEPOUREAU, M. T. & BECHER, P. 2013b. Classical swine fever virus isolates from Cuba form a new subgenotype 1.4. *Vet Microbiol,* 161**,** 334-8.

POTHLICHET, J., BURTEY, A., KUBARENKO, A. V., CAIGNARD, G., SOLHONNE, B., TANGY, F., BEN-ALI, M., QUINTANA-MURCI, L., HEINZMANN, A., CHICHE, J.-D., VIDALAIN, P.-O., WEBER, A. N. R., CHIGNARD, M. & SI-TAHAR, M. 2009. Study of Human RIG-I Polymorphisms Identifies Two Variants with an Opposite Impact on the Antiviral Immune Response. *PLOS ONE,* 4**,** e7582.

PYTHON, S., GERBER, M., SUTER, R., RUGGLI, N. & SUMMERFIELD, A. 2013. Efficient sensing of infected cells in absence of virus particles by plasmacytoid dendritic cells is blocked by the viral ribonuclease E(rns.). *PLoS pathogens,* 9**,** e1003412-e1003412.

QIAO, J. T., CUI, C., QING, L., WANG, L. S., HE, T. Y., YAN, F., LIU, F. Q., SHEN, Y. H., HOU, X. G. & CHEN, L. 2018. Activation of the STING-IRF3 pathway promotes hepatocyte inflammation, apoptosis and induces metabolic disorders in nonalcoholic fatty liver disease. *Metabolism - Clinical and Experimental,* 81**,** 13-24.

QIN, B. Y., LIU, C., LAM, S. S., SRINATH, H., DELSTON, R., CORREIA, J. J., DERYNCK, R. & LIN, K. 2003. Crystal structure of IRF-3 reveals mechanism of autoinhibition and virus-induced phosphoactivation. *Nature Structural & Molecular Biology,* 10**,** 913-921.

RAN, F. A., HSU, P. D., LIN, C.-Y., GOOTENBERG, J. S., KONERMANN, S., TREVINO, A., SCOTT, D. A., INOUE, A., MATOBA, S., ZHANG, Y. & ZHANG, F. 2013a. Double nicking by RNA-guided CRISPR Cas9 for enhanced genome editing specificity. *Cell,* 154**,** 1380-1389.

RAN, F. A., HSU, P. D., WRIGHT, J., AGARWALA, V., SCOTT, D. A. & ZHANG, F. 2013b. Genome engineering using the CRISPR-Cas9 system. *Nature Protocols,* 8**,** 2281.

RANDALL, R. E. & GOODBOURN, S. 2008. Interferons and viruses: an interplay between induction, signalling, antiviral responses and virus countermeasures. *Journal of General Virology,* 89**,** 1-47.

RAWLINGS, N. D., BARRETT, A. J. & BATEMAN, A. 2012. MEROPS: the database of proteolytic enzymes, their substrates and inhibitors. *Nucleic Acids Res,* 40**,** D343-50.

REED, L. J. & MUENCH, H. 1938. A simple method of estimating fifty per cent endpoints. *American journal of epidemiology,* 27**,** 493-497.

RENSON, P., BLANCHARD, Y., LE DIMNA, M., FELIX, H., CARIOLET, R., JESTIN, A. & LE POTIER, M.-F. J. V. R. 2010. Acute induction of cell death-related IFN stimulated genes (ISG) differentiates highly from moderately virulent CSFV strains. 41**,** 07.

RENSON, P., LE DIMNA, M., GABRIEL, C., LEVAI, R., BLOME, S., KULCSAR, G., KOENEN, F. & LE POTIER, M. F. 2014. Cytokine and immunoglobulin isotype profiles during CP7_E2alf vaccination against a challenge with the highly virulent Koslov strain of classical swine fever virus. *Research in Veterinary Science,* 96**,** 389-395.

RENSON, P., LE DIMNA, M., KERANFLECH, A., CARIOLET, R., KOENEN, F. & LE POTIER, M.-F. 2013. CP7_E2alf oral vaccination confers partial protection against early classical swine fever virus challenge and interferes with pathogeny-related cytokine responses. *Veterinary Research,* 44**,** 9.

RIBBENS, S., DEWULF, J., KOENEN, F., LAEVENS, H. & KRUIF, A. 2005. Transmission of classical swine fever. A review. *The Veterinary quarterly,* 26**,** 146-55.

RIEDEL, C., LAMP, B., HAGEN, B., INDIK, S. & RUMENAPF, T. 2017. The core protein of a pestivirus protects the incoming virus against IFN-induced effectors. *Sci Rep,* 7**,** 44459.

RIEDL, S. J. & SALVESEN, G. S. 2007. The apoptosome: signalling platform of cell death. *Nat Rev Mol Cell Biol,* 8**,** 405-13.

RIJNBRAND, R., VAN DER STRAATEN, T., VAN RIJN, P. A., SPAAN, W. J. & BREDENBEEK, P. J. 1997. Internal entry of ribosomes is directed by the 5' noncoding region of classical swine fever virus and is dependent on the presence of an RNA pseudoknot upstream of the initiation codon. *J Virol,* 71**,** 451-7.

RINCK, G., BIRGHAN, C., HARADA, T., MEYERS, G., THIEL, H. J. & TAUTZ, N. 2001. A cellular J-domain protein modulates polyprotein processing and cytopathogenicity of a pestivirus. *J Virol,* 75**,** 9470-82.

RIOS, L., NUNEZ, J. I., DIAZ DE ARCE, H., GANGES, L. & PEREZ, L. J. 2018. Revisiting the genetic diversity of classical swine fever virus: A proposal for new genotyping and subgenotyping schemes of classification. *Transbound Emerg Dis,* 65**,** 963-971.

RISAGER, P. C., FAHNOE, U., GULLBERG, M., RASMUSSEN, T. B. & BELSHAM, G. J. 2013. Analysis of classical swine fever virus RNA replication determinants using replicons. *J Gen Virol,* 94**,** 1739-48.

ROBERTS, M. Evaluation of optimal size of restriction zones in disease control with particular reference to classical swine fever. Proceedings of a meeting held at the... on the, 1995.

ROBIN, A. Y., IYER, S., BIRKINSHAW, R. W., SANDOW, J., WARDAK, A., LUO, C. S., SHI, M., WEBB, A. I., CZABOTAR, P. E., KLUCK, R. M. & COLMAN, P. M. 2018. Ensemble Properties of Bax Determine Its Function. *Structure,* 26**,** 1346-1359.e5.

RODRIGUEZ, J. & LAZEBNIK, Y. 1999. Caspase-9 and APAF-1 form an active holoenzyme. *Genes & development,* 13**,** 3179-3184.

RUDD, A. K. & DEVARAJ, N. K. 2018. Traceless synthesis of ceramides in living cells reveals saturation-dependent apoptotic effects. *Proc Natl Acad Sci U S A,* 115**,** 7485-7490.

RUGGLI, N., BIRD, B. H., LIU, L., BAUHOFER, O., TRATSCHIN, J.-D. & HOFMANN, M. A. 2005. Npro of classical swine fever virus is an antagonist of double-stranded RNA-mediated apoptosis and IFN-α/β induction. *Virology,* 340**,** 265-276.

RUGGLI, N., SUMMERFIELD, A., FIEBACH, A. R., GUZYLACK-PIRIOU, L., BAUHOFER, O., LAMM, C. G., WALTERSPERGER, S., MATSUNO, K., LIU, L., GERBER, M., CHOI, K. H., HOFMANN, M. A., SAKODA, Y. & TRATSCHIN, J.-D. 2009. Classical swine fever virus can remain virulent after specific elimination of the interferon regulatory factor 3-degrading function of Npro. *Journal of virology,* 83**,** 817-829.

RUGGLI, N., TRATSCHIN, J. D., SCHWEIZER, M., MCCULLOUGH, K. C., HOFMANN, M. A. & SUMMERFIELD, A. 2003. Classical swine fever virus interferes with cellular antiviral defense: evidence for a novel function of N(pro). *J Virol,* 77**,** 7645-54.

RUMENAPF, T., STARK, R., HEIMANN, M. & THIEL, H. J. 1998. N-terminal protease of pestiviruses: identification of putative catalytic residues by site-directed mutagenesis. *J Virol,* 72**,** 2544-7.

RÜMENAPF, T., UNGER, G., STRAUSS, J. H. & THIEL, H. J. 1993. Processing of the envelope glycoproteins of pestiviruses. *Journal of Virology,* 67**,** 3288.

SAHA, S. K., PIETRAS, E. M., HE, J. Q., KANG, J. R., LIU, S.-Y., OGANESYAN, G., SHAHANGIAN, A., ZARNEGAR, B., SHIBA, T. L., WANG, Y. & CHENG, G. 2006. Regulation of antiviral responses by a direct and specific interaction between TRAF3 and Cardif. *The EMBO Journal,* 25**,** 3257-3263.

SALAUN, B., COSTE, I., RISSOAN, M.-C., LEBECQUE, S. J. & RENNO, T. 2006. TLR3 Can Directly Trigger Apoptosis in Human Cancer Cells. 176**,** 4894-4901.

SALVESEN, G. S. & DUCKETT, C. S. 2002. IAP proteins: blocking the road to death's door. *Nature Reviews Molecular Cell Biology,* 3**,** 401-410.

SANCAK, Y., PETERSON, T. R., SHAUL, Y. D., LINDQUIST, R. A., THOREEN, C. C., BAR-PELED, L. & SABATINI, D. M. 2008. The Rag GTPases bind raptor and mediate amino acid signaling to mTORC1. *Science,* 320**,** 1496-501.

SANCHEZ-CORDON, P. J., ROMANINI, S., SALGUERO, F. J., NUNEZ, A., BAUTISTA, M. J., JOVER, A. & GOMEZ-VILLAMOS, J. C. 2002. Apoptosis of thymocytes related to cytokine expression in experimental classical swine fever. *J Comp Pathol,* 127**,** 239-48.

SARASTE, A. & PULKKI, K. 2000. Morphologic and biochemical hallmarks of apoptosis. *Cardiovascular Research,* 45**,** 528-537.

SASAI, M., TATEMATSU, M., OSHIUMI, H., FUNAMI, K., MATSUMOTO, M., HATAKEYAMA, S. & SEYA, T. 2010. Direct binding of TRAF2 and TRAF6 to TICAM-1/TRIF adaptor participates in activation of the Toll-like receptor 3/4 pathway. *Mol Immunol,* 47**,** 1283-91.

SATO, M., HATA, N., ASAGIRI, M., NAKAYA, T., TANIGUCHI, T. & TANAKA, N. 1998. Positive feedback regulation of type I IFN genes by the IFN-inducible transcription factor IRF-7. *FEBS Lett,* 441**,** 106-10.

SATO, T., HANADA, M., BODRUG, S., IRIE, S., IWAMA, N., BOISE, L. H., THOMPSON, C. B., GOLEMIS, E., FONG, L. & WANG, H. G. 1994. Interactions among members of the Bcl-2 protein family analyzed with a yeast two-hybrid system. *Proceedings of the National Academy of Sciences of the United States of America,* 91**,** 9238-9242.

SAUBUSSE, T., MASSON, J.-D., LE DIMMA, M., ABRIAL, D., MARCÉ, C., MARTIN-SCHALLER, R., DUPIRE, A., LE POTIER, M.-F. & ROSSI, S. 2016. How to survey classical swine fever in wild boar (Sus scrofa) after the completion of oral vaccination? Chasing away the ghost of infection at different spatial scales. *Veterinary Research,* 47**,** 21.

SCHAFER, S. L., LIN, R., MOORE, P. A., HISCOTT, J. & PITHA, P. M. 1998. Regulation of type I interferon gene expression by interferon regulatory factor-3. *J Biol Chem,* 273**,** 2714-20.

SCHMEISER, S., MAST, J., THIEL, H. J. & KONIG, M. 2014. Morphogenesis of pestiviruses: new insights from ultrastructural studies of strain Giraffe-1. *J Virol,* 88**,** 2717-24.

SCHNEIDER, C. A., RASBAND, W. S. & ELICEIRI, K. W. 2012. NIH Image to ImageJ: 25 years of image analysis. *Nature Methods,* 9**,** 671-675.

SCHOGGINS, J. W. 2019. Interferon-Stimulated Genes: What Do They All Do? *Annu Rev Virol*.

SCHOGGINS, J. W., WILSON, S. J., PANIS, M., MURPHY, M. Y., JONES, C. T., BIENIASZ, P. & RICE, C. M. 2011. A diverse range of gene products are effectors of the type I interferon antiviral response. *Nature,* 472**,** 481-5.

SCHWEIZER, M. & PETERHANS, E. 2001. Noncytopathic Bovine Viral Diarrhea Virus Inhibits Double-Stranded RNA-Induced Apoptosis and Interferon Synthesis. *Journal of Virology,* 75**,** 4692-4698.

SEAGO, J., GOODBOURN, S. & CHARLESTON, B. 2010. The classical swine fever virus Npro product is degraded by cellular proteasomes in a manner that does not require interaction with interferon regulatory factor 3. *J Gen Virol,* 91**,** 721-6.

SEAGO, J., HILTON, L., REID, E., DOCEUL, V., JEYATHEESAN, J., MOGANERADJ, K., MCCAULEY, J., CHARLESTON, B. & GOODBOURN, S. 2007. The Npro product of classical swine fever virus and bovine viral diarrhea virus uses a conserved mechanism to target interferon regulatory factor-3. *J Gen Virol,* 88**,** 3002-6.

SEGAWA, K., KURATA, S., YANAGIHASHI, Y., BRUMMELKAMP, T. R., MATSUDA, F. & NAGATA, S. 2014. Caspase-mediated cleavage of phospholipid flippase for apoptotic phosphatidylserine exposure. *Science,* 344**,** 1164-8.

SERVANT, M. J., GRANDVAUX, N., TENOEVER, B. R., DUGUAY, D., LIN, R. & HISCOTT, J. 2003. Identification of the minimal phosphoacceptor site required for in vivo activation of interferon regulatory factor 3 in response to virus and double-stranded RNA. *J Biol Chem,* 278**,** 9441-7.

SHAMAS-DIN, A., BRAHMBHATT, H., LEBER, B. & ANDREWS, D. W. 2011. BH3-only proteins: Orchestrators of apoptosis. *Biochimica et Biophysica Acta (BBA) - Molecular Cell Research,* 1813**,** 508-520.

SHAW, A. E., HUGHES, J., GU, Q., BEHDENNA, A., SINGER, J. B., DENNIS, T., ORTON, R. J., VARELA, M., GIFFORD, R. J., WILSON, S. J. & PALMARINI, M. 2017. Fundamental properties of the mammalian innate immune system revealed by multispecies comparison of type I interferon responses. *PLOS Biology,* 15**,** e2004086.

SHENG, C., XIAO, M., GENG, X., LIU, J., WANG, Y. & GU, F. 2007. Characterization of interaction of classical swine fever virus NS3 helicase with 3' untranslated region. *Virus Research,* 129**,** 43-53.

SHI, B. J., LIU, C. C., ZHOU, J., WANG, S. Q., GAO, Z. C., ZHANG, X. M., ZHOU, B. & CHEN, P. Y. 2016. Entry of Classical Swine Fever Virus into PK-15 cells via a pH-, dynamin- and cholesterol-dependent, clathrin-mediated endocytic pathway that requires Rab5 and Rab7. *J Virol*.

SHI, Y. 2004. Caspase Activation: Revisiting the Induced Proximity Model. *Cell,* 117**,** 855-858.

SHIGEMOTO, T., KAGEYAMA, M., HIRAI, R., ZHENG, J., YONEYAMA, M. & FUJITA, T. 2009. Identification of loss of function mutations in human genes encoding RIG-I and MDA5: implications for resistance to type I diabetes. *The Journal of biological chemistry,* 284**,** 13348-13354.

SNAPP, E. L., HEGDE, R. S., FRANCOLINI, M., LOMBARDO, F., COLOMBO, S., PEDRAZZINI, E., BORGESE, N. & LIPPINCOTT-SCHWARTZ, J. 2003. Formation of stacked ER cisternae by low affinity protein interactions. *J Cell Biol,* 163**,** 257-69.

SOOS, P., MOJZIS, M., POLLNER, A. & SUMEGHY, L. 2001. Evaluation of vaccine-induced maternal immunity against classical swine fever. *Acta Vet Hung,* 49**,** 17-24.
SPENCE, J. S., HE, R., HOFFMANN, H.-H., DAS, T., THINON, E., RICE, C. M., PENG, T., CHANDRAN, K. & HANG, H. C. 2019. IFITM3 directly engages and shuttles incoming virus particles to lysosomes. *Nature Chemical Biology,* 15**,** 259-268.
SPRICK, M. R., WEIGAND, M. A., RIESER, E., RAUCH, C. T., JUO, P., BLENIS, J., KRAMMER, P. H. & WALCZAK, H. 2000. FADD/MORT1 and caspase-8 are recruited to TRAIL receptors 1 and 2 and are essential for apoptosis mediated by TRAIL receptor 2. *Immunity,* 12**,** 599-609.
STANCATO, L. F., DAVID, M., CARTER-SU, C., LARNER, A. C. & PRATT, W. B. 1996. Preassociation of STAT1 with STAT2 and STAT3 in separate signalling complexes prior to cytokine stimulation. *J Biol Chem,* 271**,** 4134-7.
STARK, R., MEYERS, G., RÜMENAPF, T. & THIEL, H. J. 1993. Processing of pestivirus polyprotein: cleavage site between autoprotease and nucleocapsid protein of classical swine fever virus. *Journal of Virology,* 67**,** 7088-7095.
STEAR, M. 2005. OIE Manual of Diagnostic Tests and Vaccines for Terrestrial Animals (Mammals, Birds and Bees) 5th Edn. Volumes 1 & 2. World Organization for Animal Health 2004. ISBN 92 9044 622 6. €140. *Parasitology,* 130**,** 727-727.
STEFFENS , S., THIEL , H.-J. & BEHRENS, S.-E. 1999. The RNA-dependent RNA polymerases of different members of the family Flaviviridae exhibit similar properties in vitro. *Journal of General Virology,* 80**,** 2583-2590.
STENNICKE, H., DEVERAUX, Q., HUMKE, E., REED, J., DIXIT, V. & SALVESEN, G. 1999. Caspase-9 Can Be Activated without Proteolytic Processing. *The Journal of biological chemistry,* 274**,** 8359-62.
STRAHLE, L., GARCIN, D. & KOLAKOFSKY, D. 2006. Sendai virus defective-interfering genomes and the activation of interferon-beta. *Virology,* 351**,** 101-11.
STRASSER, A., JOST, P. J. & NAGATA, S. 2009. The many roles of FAS receptor signaling in the immune system. *Immunity,* 30**,** 180-92.
SUBBURAJ, Y., COSENTINO, K., AXMANN, M., PEDRUEZA-VILLALMANZO, E., HERMANN, E., BLEICKEN, S., SPATZ, J. & GARCIA-SAEZ, A. J. 2015. Bax monomers form dimer units in the membrane that further self-assemble into multiple oligomeric species. *Nat Commun,* 6**,** 8042.
SULLIVAN, C. S. & PIPAS, J. M. 2001. The Virus–Chaperone Connection. *Virology,* 287**,** 1-8.
SUMMERFIELD, A. 2012. Viewpoint: factors involved in type I interferon responses during porcine virus infections. *Vet Immunol Immunopathol,* 148**,** 168-71.
SUMMERFIELD, A., ALVES, M., RUGGLI, N., DE BRUIN, M. G. & MCCULLOUGH, K. C. 2006. High IFN-alpha responses associated with depletion of lymphocytes and natural IFN-producing cells during classical swine fever. *J Interferon Cytokine Res,* 26**,** 248-55.
SUMMERFIELD, A., HOFMANN, M. A. & MCCULLOUGH, K. C. 1998. Low density blood granulocytic cells induced during classical swine fever are targets for virus infection. *Vet Immunol Immunopathol,* 63**,** 289-301.
SUMMERFIELD, A., KNOETIG, S. M., TSCHUDIN, R. & MCCULLOUGH, K. C. 2000. Pathogenesis of Granulocytopenia and Bone Marrow Atrophy during Classical Swine Fever Involves Apoptosis and Necrosis of Uninfected Cells. *Virology,* 272**,** 50-60.
SUMMERFIELD, A. & RUGGLI, N. 2015. Immune responses against classical swine fever virus: between ignorance and lunacy. *Frontiers in Veterinary Science,* 2.
SUZUKI, J., DENNING, D. P., IMANISHI, E., HORVITZ, H. R. & NAGATA, S. 2013. Xk-related protein 8 and CED-8 promote phosphatidylserine exposure in apoptotic cells. *Science,* 341**,** 403-6.

SUZUKI, Y., TAKAHASHI-NIKI, K., AKAGI, T., HASHIKAWA, T. & TAKAHASHI, R. 2004. Mitochondrial protease Omi/HtrA2 enhances caspase activation through multiple pathways. *Cell Death & Differentiation,* 11**,** 208-216.

SYKEN, J., DE-MEDINA, T. & MÜNGER, K. 1999. TID1, a human homolog of the Drosophila tumor suppressor l(2)tid, encodes two mitochondrial modulators of apoptosis with opposing functions. *Proceedings of the National Academy of Sciences of the United States of America,* 96**,** 8499-8504.

SZYMANSKA, J., SMOLEWSKI, P., MAJCHRZAK, A., CEBULA-OBRZUT, B., CHOJNOWSKI, K. & TRELINSKI, J. 2015. Pro-Apoptotic Activity of Ruxolitinib Alone and in Combination with Hydroxyurea, Busulphan, and PI3K/mTOR Inhibitors in JAK2-Positive Human Cell Lines. *Adv Clin Exp Med,* 24**,** 195-202.

SZYMANSKI, M. R., FIEBACH, A. R., TRATSCHIN, J. D., GUT, M., RAMANUJAM, V. M., GOTTIPATI, K., PATEL, P., YE, M., RUGGLI, N. & CHOI, K. H. 2009. Zinc binding in pestivirus N(pro) is required for interferon regulatory factor 3 interaction and degradation. *J Mol Biol,* 391**,** 438-49.

TAIT, S. W. G. & GREEN, D. R. 2010. Mitochondria and cell death: outer membrane permeabilization and beyond. *Nature Reviews Molecular Cell Biology,* 11**,** 621.

TAIT, S. W. G. & GREEN, D. R. 2013. Mitochondrial regulation of cell death. *Cold Spring Harbor perspectives in biology,* 5**,** a008706.

TAKEUCHI, K., KOMATSU, T., KITAGAWA, Y., SADA, K. & GOTOH, B. 2008. Sendai virus C protein plays a role in restricting PKR activation by limiting the generation of intracellular double-stranded RNA. *J Virol,* 82**,** 10102-10.

TAKEUCHI, O. & AKIRA, S. 2008. MDA5/RIG-I and virus recognition. *Current Opinion in Immunology,* 20**,** 17-22.

TAKEUCHI, O. & AKIRA, S. 2010. Pattern Recognition Receptors and Inflammation. *Cell,* 140**,** 805-820.

TAMURA, T., NAGASHIMA, N., RUGGLI, N., SUMMERFIELD, A., KIDA, H. & SAKODA, Y. 2014. Npro of classical swine fever virus contributes to pathogenicity in pigs by preventing type I interferon induction at local replication sites. *Vet Res,* 45**,** 47.

TANG, Q.-H., ZHANG, Y.-M., FAN, L., TONG, G., HE, L. & DAI, C. 2010. Classic swine fever virus NS2 protein leads to the induction of cell cycle arrest at S-phase and endoplasmic reticulum stress. *Virology journal,* 7**,** 4-4.

TARRADAS, J., DE LA TORRE, M. E., ROSELL, R., PEREZ, L. J., PUJOLS, J., MUNOZ, M., MUNOZ, I., MUNOZ, S., ABAD, X., DOMINGO, M., FRAILE, L. & GANGES, L. 2014. The impact of CSFV on the immune response to control infection. *Virus Res,* 185**,** 82-91.

TAUTZ, N., KAISER, A. & THIEL, H.-J. 2000. NS3 Serine Protease of Bovine Viral Diarrhea Virus: Characterization of Active Site Residues, NS4A Cofactor Domain, and Protease–Cofactor Interactions. *Virology,* 273**,** 351-363.

TENEV, T., BIANCHI, K., DARDING, M., BROEMER, M., LANGLAIS, C., WALLBERG, F., ZACHARIOU, A., LOPEZ, J., MACFARLANE, M., CAIN, K. & MEIER, P. 2011. The Ripoptosome, a Signaling Platform that Assembles in Response to Genotoxic Stress and Loss of IAPs. *Molecular Cell,* 43**,** 432-448.

TERPSTRA, C. 1988. Epizootiology of hog cholera. En, Classical Swine Fever and related viral infections. Ed. B. Liess. Martinus Nijhoff Publishing, Boston.

TERPSTRA, C., WOORTMEYER, R. & BARTELING, S. J. 1990. Development and properties of a cell culture produced vaccine for hog cholera based on the Chinese strain. *Dtsch Tierarztl Wochenschr,* 97**,** 77-9.

THIEL, H. J., STARK, R., WEILAND, E., RÜMENAPF, T. & MEYERS, G. 1991. Hog cholera virus: molecular composition of virions from a pestivirus. *Journal of virology,* 65**,** 4705-4712.

TODT, F., CAKIR, Z., REICHENBACH, F., YOULE, R. J. & EDLICH, F. 2013. The C-terminal helix of Bcl-x(L) mediates Bax retrotranslocation from the mitochondria. *Cell death and differentiation,* 20**,** 333-342.

TRATSCHIN, J. D., MOSER, C., RUGGLI, N. & HOFMANN, M. A. 1998. Classical swine fever virus leader proteinase Npro is not required for viral replication in cell culture. *J Virol,* 72**,** 7681-4.

TRINH, D. L., ELWI, A. N. & KIM, S. W. 2010. Direct interaction between p53 and Tid1 proteins affects p53 mitochondrial localization and apoptosis. *Oncotarget,* 1**,** 396-404.

UTTENTHAL, Å., LE POTIER, M.-F., ROMERO, L., DE MIA, G. M. & FLOEGEL-NIESMANN, G. 2001. Classical swine fever (CSF) marker vaccine: Trial I. Challenge studies in weaner pigs. *Veterinary Microbiology,* 83**,** 85-106.

VAFIADAKI, E., ARVANITIS, D. A., PAGAKIS, S. N., PAPALOUKA, V., SANOUDOU, D., KONTROGIANNI-KONSTANTOPOULOS, A. & KRANIAS, E. G. 2009. The anti-apoptotic protein HAX-1 interacts with SERCA2 and regulates its protein levels to promote cell survival. *Mol Biol Cell,* 20**,** 306-18.

VAN OIRSCHOT, J. T. 2003a. Emergency vaccination against classical swine fever. *Dev Biol (Basel),* 114**,** 259-67.

VAN OIRSCHOT, J. T. 2003b. Vaccinology of classical swine fever: from lab to field. *Veterinary Microbiology,* 96**,** 367-384.

VAN RIJN, P. A., BOSSERS, A., WENSVOORT, G. & MOORMANN, R. J. 1996. Classical swine fever virus (CSFV) envelope glycoprotein E2 containing one structural antigenic unit protects pigs from lethal CSFV challenge. *J Gen Virol,* 77 (Pt 11)**,** 2737-45.

VAN ZIJL, M., WENSVOORT, G., DE KLUYVER, E., HULST, M., VAN DER GULDEN, H., GIELKENS, A., BERNS, A. & MOORMANN, R. 1991. Live attenuated pseudorabies virus expressing envelope glycoprotein E1 of hog cholera virus protects swine against both pseudorabies and hog cholera. *Journal of virology,* 65**,** 2761-2765.

VANDERHALLEN, H., MITTELHOLZER, C., HOFMANN, M. A. & KOENEN, F. 1999. Classical swine fever virus is genetically stable in vitro and in vivo. *Archives of Virology,* 144**,** 1669-1677.

VELAZQUEZ, L., FELLOUS, M., STARK, G. R. & PELLEGRINI, S. 1992. A protein tyrosine kinase in the interferon alpha/beta signaling pathway. *Cell,* 70**,** 313-22.

VERCAMMEN, E., STAAL, J. & BEYAERT, R. 2008. Sensing of Viral Infection and Activation of Innate Immunity by Toll-Like Receptor 3. *Clinical Microbiology Reviews,* 21**,** 13-25.

VIRALZONE. 2010. Available: https://viralzone.expasy.org/39?outline=all_by_species [Accessed 16/09/2019].

WALCZAK, H. 2013. Death receptor-ligand systems in cancer, cell death, and inflammation. *Cold Spring Harbor perspectives in biology,* 5**,** a008698-a008698.

WALCZAK, H., DEGLI-ESPOSTI, M. A., JOHNSON, R. S., SMOLAK, P. J., WAUGH, J. Y., BOIANI, N., TIMOUR, M. S., GERHART, M. J., SCHOOLEY, K. A., SMITH, C. A., GOODWIN, R. G. & RAUCH, C. T. 1997. TRAIL-R2: a novel apoptosis-mediating receptor for TRAIL. *Embo j,* 16**,** 5386-97.

WALENSKY, L. D. 2019. Targeting BAX to drug death directly. *Nature Chemical Biology,* 15**,** 657-665.

WANG, J., LIU, B., WANG, N., LEE, Y.-M., LIU, C. & LI, K. 2011. TRIM56 is a virus- and interferon-inducible E3 ubiquitin ligase that restricts pestivirus infection. *Journal of virology,* 85**,** 3733-3745.

WANG, K., YIN, X. M., CHAO, D. T., MILLIMAN, C. L. & KORSMEYER, S. J. 1996. BID: a novel BH3 domain-only death agonist. *Genes Dev,* 10**,** 2859-69.

WANG, L., DU, F. & WANG, X. 2008. TNF-α Induces Two Distinct Caspase-8 Activation Pathways. *Cell,* 133**,** 693-703.

WANG, Z., NIE, Y., WANG, P., DING, M. & DENG, H. 2004. Characterization of classical swine fever virus entry by using pseudotyped viruses: E1 and E2 are sufficient to mediate viral entry. *Virology,* 330**,** 332-341.

WEI, M. C., ZONG, W. X., CHENG, E. H., LINDSTEN, T., PANOUTSAKOPOULOU, V., ROSS, A. J., ROTH, K. A., MACGREGOR, G. R., THOMPSON, C. B. & KORSMEYER, S. J. 2001. Proapoptotic BAX and BAK: a requisite gateway to mitochondrial dysfunction and death. *Science,* 292**,** 727-30.

WENSVOORT, G., BLOEMRAAD, M. & TERPSTRA, C. 1988. An enzyme immunoassay employing monoclonal antibodies and detecting specifically antibodies to classical swine fever virus. *Veterinary Microbiology,* 17**,** 129-140.

WESTPHAL, D., KLUCK, R. M. & DEWSON, G. 2014. Building blocks of the apoptotic pore: how Bax and Bak are activated and oligomerize during apoptosis. *Cell Death & Differentiation,* 21**,** 196-205.

WHITWORTH, K. M., ROWLAND, R. R. R., PETROVAN, V., SHEAHAN, M., CINO-OZUNA, A. G., FANG, Y., HESSE, R., MILEHAM, A., SAMUEL, M. S., WELLS, K. D. & PRATHER, R. S. 2019. Resistance to coronavirus infection in amino peptidase N-deficient pigs. *Transgenic Research,* 28**,** 21-32.

WISKERCHEN, M., BELZER, S. K. & COLLETT, M. S. 1991. Pestivirus gene expression: the first protein product of the bovine viral diarrhea virus large open reading frame, p20, possesses proteolytic activity. *J Virol,* 65**,** 4508-14.

WOLFF, S., ERSTER, S., PALACIOS, G. & MOLL, U. M. 2008. p53's mitochondrial translocation and MOMP action is independent of Puma and Bax and severely disrupts mitochondrial membrane integrity. *Cell Res,* 18**,** 733-44.

WU, B. & HUR, S. 2015. How RIG-I like receptors activate MAVS. *Current Opinion in Virology,* 12**,** 91-98.

XIAO, M., CHEN, J. & LI, B. 2003. RNA-dependent RNA polymerase activity of Classical swine fever virus NS5B protein expressed in natural host cells. *Acta Virol,* 47**,** 79-85.

XIAO, M., GAO, J., WANG, W., WANG, Y., CHEN, J., CHEN, J. & LI, B. 2004. Specific interaction between the classical swine fever virus NS5B protein and the viral genome. *European Journal of Biochemistry,* 271**,** 3888-3896.

XIE, Z., PANG, D., YUAN, H., JIAO, H., LU, C., WANG, K., YANG, Q., LI, M., CHEN, X., YU, T., CHEN, X., DAI, Z., PENG, Y., TANG, X., LI, Z., WANG, T., GUO, H., LI, L., TU, C., LAI, L. & OUYANG, H. 2018. Genetically modified pigs are protected from classical swine fever virus. *PLOS Pathogens,* 14**,** e1007193.

XU, X., GUO, H., XIAO, C., ZHA, Y., SHI, Z., XIA, X. & TU, C. 2008. In vitro inhibition of classical swine fever virus replication by siRNAs targeting Npro and NS5B genes. *Antiviral Res,* 78**,** 188-93.

XU, X. P., ZHAI, D., KIM, E., SWIFT, M., REED, J. C., VOLKMANN, N. & HANEIN, D. 2013. Three-dimensional structure of Bax-mediated pores in membrane bilayers. *Cell Death Dis,* 4**,** e683.

YAMAMOTO, M., SATO, S., HEMMI, H., HOSHINO, K., KAISHO, T., SANJO, H., TAKEUCHI, O., SUGIYAMA, M., OKABE, M., TAKEDA, K. & AKIRA, S. 2003. Role of adaptor TRIF in the MyD88-independent toll-like receptor signaling pathway. *Science,* 301**,** 640-3.

YE, Q. & WORMAN, H. J. 1995. Protein-protein interactions between human nuclear lamins expressed in yeast. *Exp Cell Res,* 219**,** 292-8.

YONEYAMA, M. & FUJITA, T. 2008. Structural Mechanism of RNA Recognition by the RIG-I-like Receptors. *Immunity,* 29**,** 178-181.

YONEYAMA, M., KIKUCHI, M., NATSUKAWA, T., SHINOBU, N., IMAIZUMI, T., MIYAGISHI, M., TAIRA, K., AKIRA, S. & FUJITA, T. 2004. The RNA helicase RIG-I has an essential function in double-stranded RNA-induced innate antiviral responses. *Nat Immunol,* 5**,** 730-7.

YONEYAMA, M., SUHARA, W., FUKUHARA, Y., FUKUDA, M., NISHIDA, E. & FUJITA, T. 1998. Direct triggering of the type I interferon system by virus infection: activation of a transcription factor complex containing IRF-3 and CBP/p300. 17**,** 1087-1095.

YUAN, S. & AKEY, CHRISTOPHER W. 2013. Apoptosome Structure, Assembly, and Procaspase Activation. *Structure,* 21**,** 501-515.

ZHANG, C., KANG, K., NING, P., PENG, Y., LIN, Z., CUI, H., CAO, Z., WANG, J. & ZHANG, Y. 2015. Heat shock protein 70 is associated with CSFV NS5A protein and enhances viral RNA replication. *Virology,* 482**,** 9-18.

ZHANG, J., HUANG, K., O'NEILL, K. L., PANG, X. & LUO, X. 2016. Bax/Bak activation in the absence of Bid, Bim, Puma, and p53. *Cell Death & Disease,* 7**,** e2266-e2266.

ZHANG, M., ZHENG, J., NUSSINOV, R. & MA, B. 2017. Release of Cytochrome C from Bax Pores at the Mitochondrial Membrane. *Scientific Reports,* 7**,** 2635.

ZHANG, X. D., GILLESPIE, S. K. & HERSEY, P. 2004. Staurosporine induces apoptosis of melanoma by both caspase-dependent and -independent apoptotic pathways. *Molecular Cancer Therapeutics,* 3**,** 187-197.

ZHANG, Y.-N., LIU, Y.-Y., XIAO, F.-C., LIU, C.-C., LIANG, X.-D., CHEN, J., ZHOU, J., BALOCH, A. S., KAN, L., ZHOU, B. & QIU, H.-J. 2018. Rab5, Rab7, and Rab11 Are Required for Caveola-Dependent Endocytosis of Classical Swine Fever Virus in Porcine Alveolar Macrophages. *Journal of Virology,* 92**,** e00797-18.

ZHAO, C., SHEN, X., WU, R., LI, L. & PAN, Z. 2017. Classical swine fever virus nonstructural protein p7 modulates infectious virus production. *Scientific Reports,* 7**,** 12995.

ZHAO, T., YANG, L., SUN, Q., ARGUELLO, M., BALLARD, D. W., HISCOTT, J. & LIN, R. 2007. The NEMO adaptor bridges the nuclear factor-κB and interferon regulatory factor signaling pathways. *Nature Immunology,* 8**,** 592.

ZHEN, Y. & STENMARK, H. 2015. Cellular functions of Rab GTPases at a glance. *Journal of Cell Science,* 128**,** 3171-3176.

ZHENG, N. & SHABEK, N. 2017. Ubiquitin Ligases: Structure, Function, and Regulation. *Annual Review of Biochemistry,* 86**,** 129-157.

ZHOU, L. & CHANG, D. C. 2008. Dynamics and structure of the Bax-Bak complex responsible for releasing mitochondrial proteins during apoptosis. 121**,** 2186-2196.

ZIEGLER, U. & KADEN, V. 2002. [Vaccination of weaner pigs against classical swine fever with the subunit vaccine "Porcilis Pesti": influence of different immunization plans on excretion and transmission of challenge virus]. *Berl Munch Tierarztl Wochenschr,* 115**,** 267-73.

ZINNGREBE, J., RIESER, E., TARABORRELLI, L., PELTZER, N., HARTWIG, T., REN, H., KOVÁCS, I., ENDRES, C., DRABER, P., DARDING, M., VON KARSTEDT, S., LEMKE, J., DOME, B., BERGMANN, M., FERGUSON, B. J. & WALCZAK, H. 2016. --LUBAC deficiency perturbs TLR3 signaling to cause immunodeficiency and autoinflammation. *The Journal of Experimental Medicine,* 213**,** 2671-2689.

ZONG, W. X., LINDSTEN, T., ROSS, A. J., MACGREGOR, G. R. & THOMPSON, C. B. 2001. BH3-only proteins that bind pro-survival Bcl-2 family members fail to induce apoptosis in the absence of Bax and Bak. *Genes & development,* 15**,** 1481-1486.

ZOU, H., LI, Y., LIU, X. & WANG, X. 1999. An APAF-1.cytochrome c multimeric complex is a functional apoptosome that activates procaspase-9. *J Biol Chem,* 274**,** 11549-56.

ZURCHER, C., SAUTER, K. S., MATHYS, V., WYSS, F. & SCHWEIZER, M. 2014a. Prolonged activity of the pestiviral RNase Erns as an interferon antagonist after uptake by clathrin-mediated endocytosis. *J Virol,* 88**,** 7235-43.

ZURCHER, C., SAUTER, K. S. & SCHWEIZER, M. 2014b. Pestiviral E(rns) blocks TLR-3-dependent IFN synthesis by LL37 complexed RNA. *Vet Microbiol,* 174**,** 399-408.

Appendix A

Cloning of EGFP-N^{pro}-expressing 3rd-generation lentivirus

Briefly, an N^{pro} sequence (Brescia strain) was PCR amplified (Npro-EcoRI-fw, Npro-EcoRI-rev; table 2.20) from an existing plasmid and ligated into a lentiviral EGFP-expressing 3rd-generation transfer plasmid (pLJM1-EGFP, AddGene #19319). Sequence was ligated downstream of N^{pro} resulting in an N-terminal tag since a C-terminal tag would be post-translationally cleaved as a consequence of N^{pro}'s own autoprotease activity (Stark *et al.*, 1993, Rumenapf *et al.*, 1998). Bacterial transformations with each ligation product were carried out as described in 2.4.1. In total, 40 colonies were screened by whole-colony PCR (see 2.8.2) utilising primers spanning the vector-insert boundary (EGFP_F1_c, Npro-EcoRI-rev; table 2.20), identifying a single colony containing a plasmid with the N^{pro} insert in the correct orientation. Subsequent restriction digestion analysis and Sanger sequencing of the plasmid cDNA (see 2.6.1 and 2.8.3) confirmed it to be correct. EGFP and EGFP-N^{pro}-expressing lentiviruses were then generated in HEK 293T cells as detailed in 2.12.

Appendix B

Generation of MDA5 knockout cell lines

Identification of MDA5 knockout cell lines by Western blot

Prior to the screening of isolated colonies of possible MDA5 knockout PK-15 cells, an antibody reactive against porcine MDA5 first had to be identified. Due to the high level of homology between the immunising peptide from human MDA5 and the corresponding sequence of porcine MDA5, ab126630 (Abcam) was chosen for screening. PK-15 and HEK 293T cells were treated with 1000 IU/ml of IFN-α for 24 hours; whole cell lysates were then harvested and subjected to Western blot analysis, using the antibody at a concentration of 1/1000 (figure B.1, left panel). Untreated PK-15 cells gave a faint 125 kDa band which increased in intensity considerably when treated with IFN-α. Following IFN-α treatment, a number of smaller bands

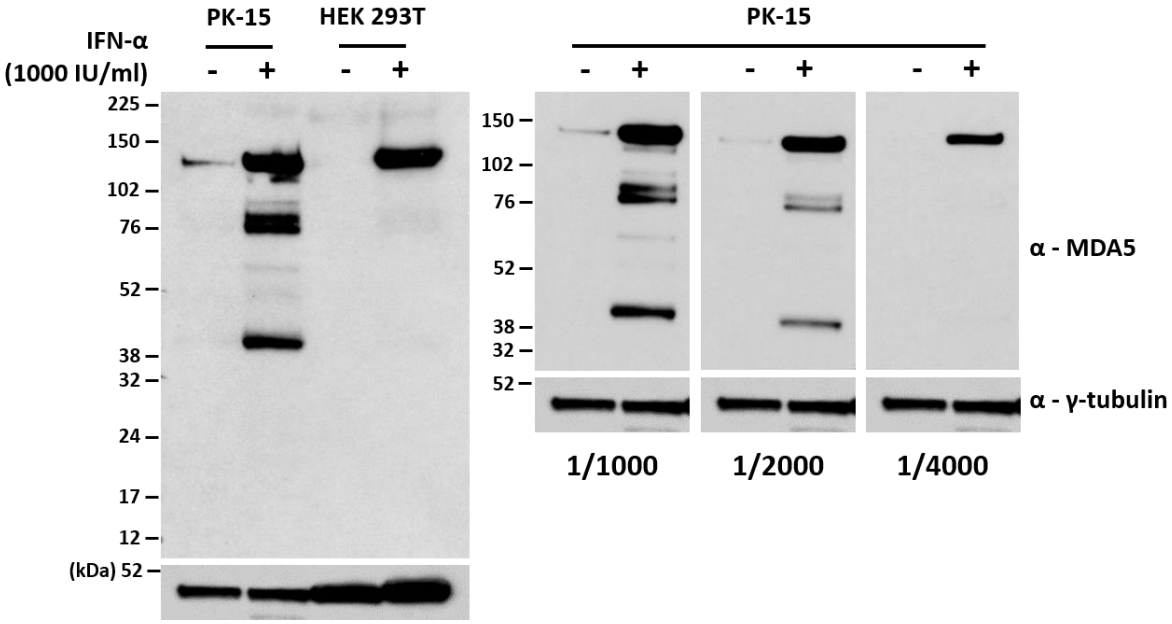

Figure B.1: Identification and optimisation of antibody for detection of porcine MDA5 by Western blot. PK-15 or HEK 293T (control) cells were seeded in 12-well plates and treated with IFN-α at the indicated concentration. 18 hours post-treatment, whole cell lysates were prepared and analysed by Western blotting using a mAb that recognises human MDA5 (ab126630) as indicated. Western blots were performed to determine antibody reactivity at a 1/1000 dilution (left-panel) and to optimise detection and clarity (right-panel). A mAb recognising γ-tubulin was used to determine relative protein concentrations.

were also detected at approximately 40, 76 and 105 kDa. HEK 293T cells were used as a positive control and following IFN-α treatment an intense band was detected at 125 kDa, close to the predicted molecular weight (117 kDa) of human MDA5. As the large 125 kDa band present in the treated PK-15 lane runs at the same size as the corresponding band in the HEK

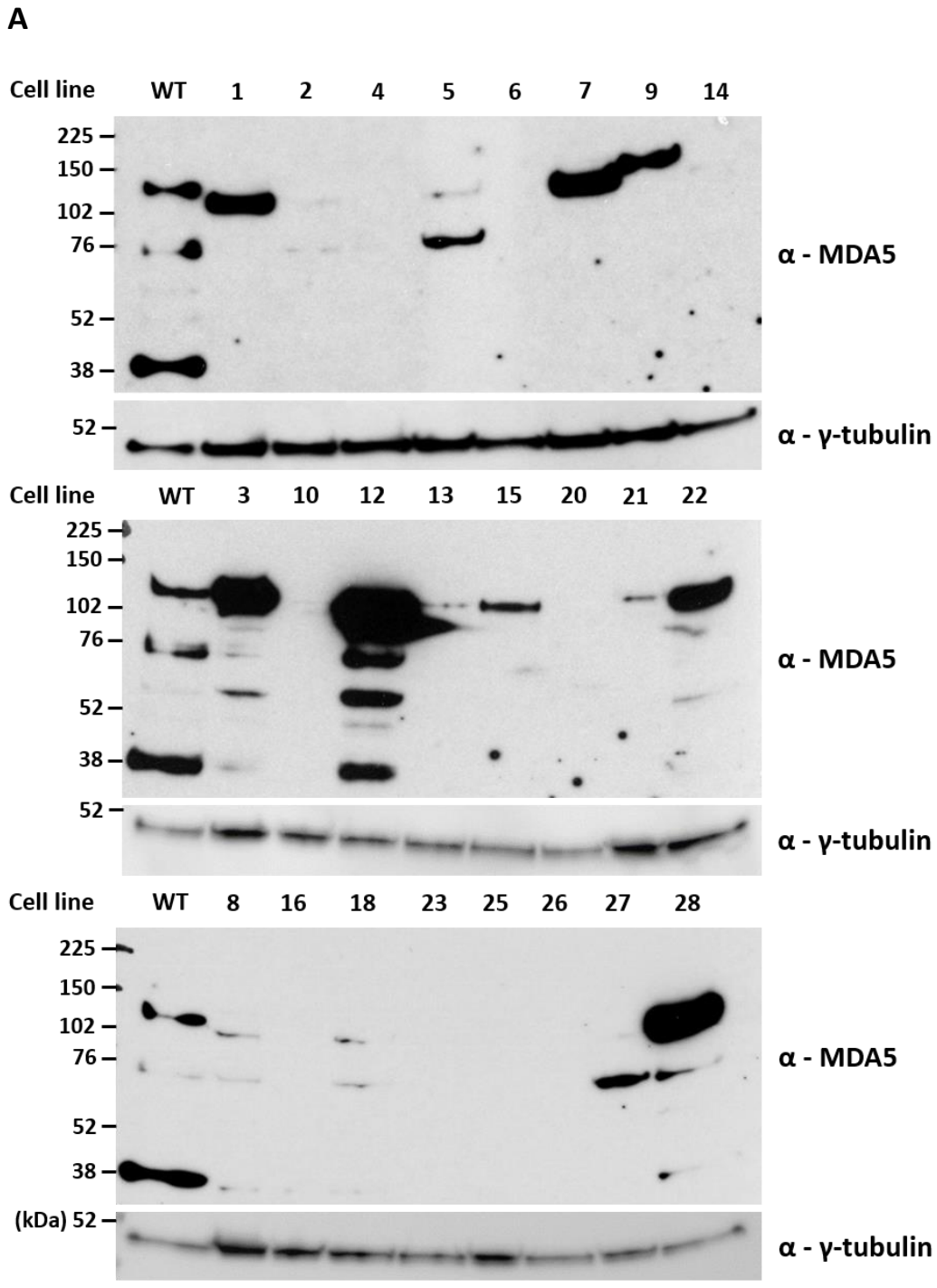

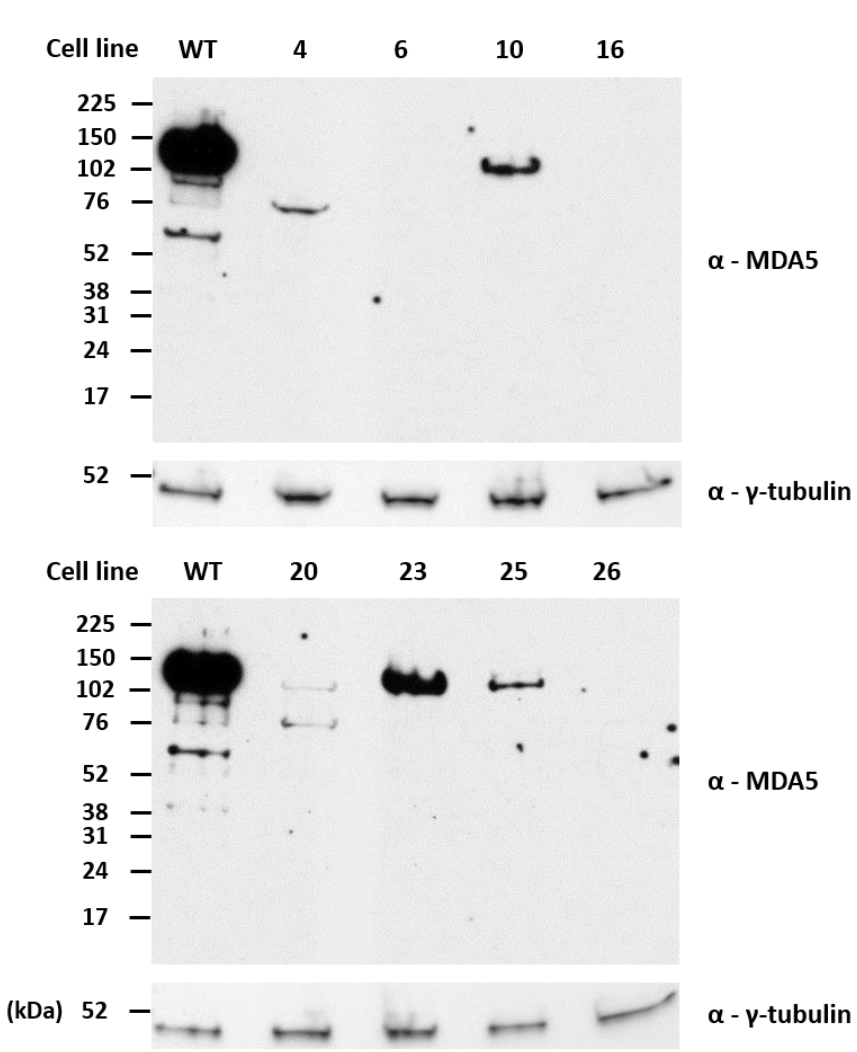

Figure B.2: Identification of putative MDA5 knockout cell lines by Western blot. (A) Putative MDA5 knockout PK-15 cell lines were seeded in 12-well plates and treated with IFN-α (1000 IU/ml). 18 hours post-treatment, whole cell lysates were prepared and analysed by Western blotting using a mAb (ab126630, Abcam) recognising MDA5. A mAb recognising γ-tubulin was used to determine relative protein concentrations. (B) Whole cell lysates from putative MDA5 knockout PK-15 cell lines were independently re-analysed by Western blotting as described in (A).

293T lane (positive control), it likely corresponds to porcine MDA5. These observations are in agreement with past literature which identified MDA5 to be an ISG (Kang *et al.*, 2002). Replicate membranes were probed with the same anti-MDA5 antibody at dilutions of 1/1000, 1/2000 and 1/4000 (figure B.1, right panel) in order to identify the concentration which would give the clearest bands. Consequently, the 1/2000 dilution was chosen.

Subsequently, whole cell lysates prepared from IFN-α treated MDA5 knockout cell lines were analysed by Western blot alongside whole cell lysates from parental WT PK-15 cells (positive control) (figure B.2, A). A band corresponding to MDA5 was not observed for several cell lines (4, 6, 10, 16, 20, 23, 25, 26), indicating putative knockouts. For some cell lines (1, 7, 12), bands that ran smaller than expected were observed, suggesting the formation of indels that truncated protein either through the introduction of premature stop codons later in the open reading frame (ORF) or through excision of large sections of coding sequence. The lysates from cell lines that gave no bands were re-run on a fresh Western blot to further confirm the absence of protein (figure B.2, B) – only cell lines 6, 16 and 26 were negative for MDA5 protein while cell line 4 revealed a potentially truncated protein. Consequently, cell lines 4, 6, 16 and 26 were selected for further screening.

Identification of MDA5 knockout cell lines by PCR and Sanger sequencing

To confirm the MDA5 gene of the edited PK-15 cells had been targeted, DNA was extracted, MDA5 sequence amplified by PCR and the resulting products Sanger sequenced (see 2.17, 2.8.1 and 2.8.3). Two primer pairs, each flanking the gRNA target sites within the first coding exon of porcine MDA5, were used (poMDA5 fw.1, poMDA5 rv.1 and poMDA5 fw.2, poMDA5 rv.2; table 2.20). The same, modified PCR program as used in 4.3.2 was used to amplify these fragments. Each reaction was analysed by agarose gel electrophoresis (figure B.3).

As expected, the fragment amplified by each primer pair gave a single band running close to the 500 bp ladder marker (expected: 487 bp) for the DNA extracted from non-edited PK-15 cells (positive control). However, amplification of the same fragment using DNA extracted from MDA5 cell line 6 cells gave a bright band of ~350 bp and a series of larger bands (700 – 1400 bp) that were comparatively less intense. The ~350 bp band indicated an indel in at least one allele of the MDA5 gene, and the total absence of a ~500 bp band suggested that both alleles had been edited (figure B.3, A). The identity of the fainter bands observed in lanes

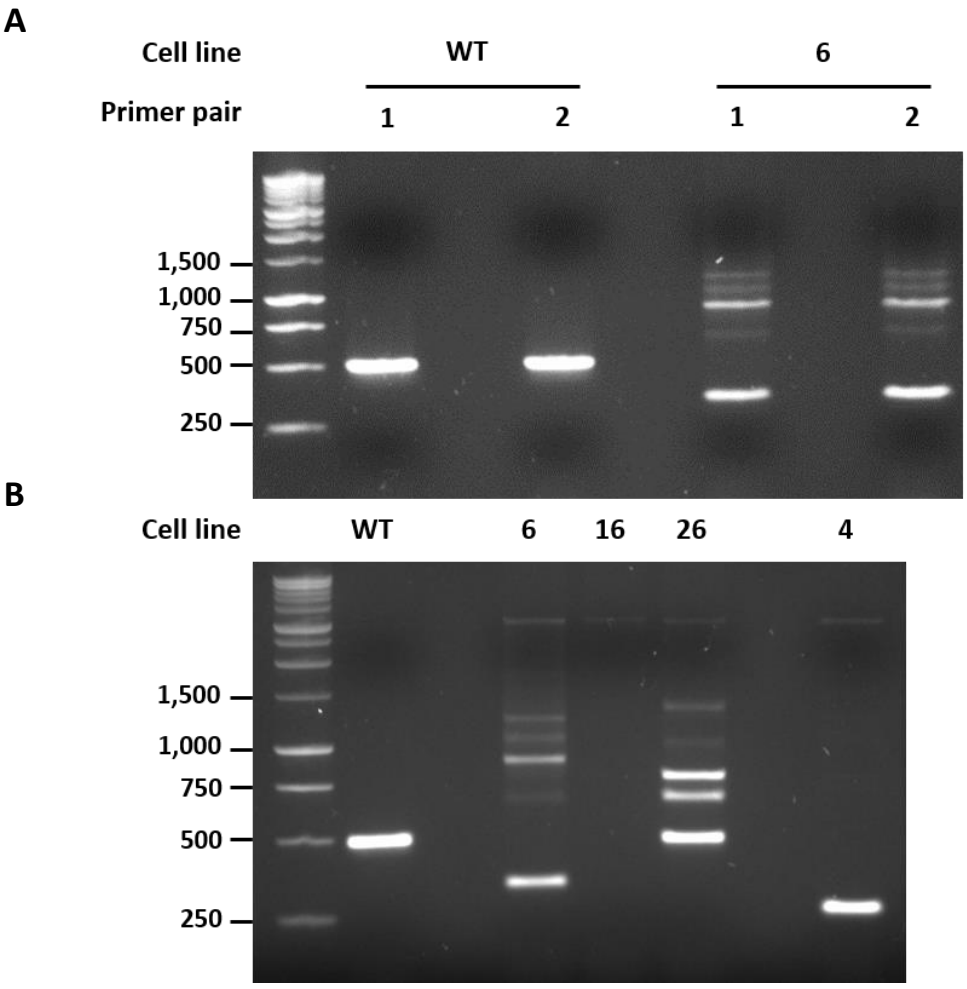

Figure B.3: PCR amplification of MDA5 gene edited cell line reveals putative indels. (A) gDNA was extracted from non-edited PK-15 cells and cell line 6, a PK-15 cell line gene edited for MDA5. Two pairs of primers (1 and 2) were then used to amplify a region (~500 bp) of MDA5 that contained both gRNA target sites. PCR products were analysed by agarose gel electrophoresis. (B) PCR reactions using primer pair 2 were repeated using gDNA extracted from cell lines 4, 16 and 26 and ran alongside PCR products derived from non-edited PK-15 and cell line 6 cells. 1 kb DNA ladder values are indicated in bp.

corresponding to MDA5 cell line 6 cells remains unknown. It is possible they correspond to ssDNA extending off a single primer, suggesting the annealing site for one primer has been destroyed by an indel on one allele.

PCR reactions utilising primer pair 2 were repeated using DNA extracted from cell lines 16, 26 and 4. The resulting products were then analysed by agarose gel electrophoresis alongside the previous WT and cell line 6 products for comparison (figure B.3, B). While no band was

observed for cell line 16, cell line 26 gave a single bright band close to 500 bp as well as two fainter bands at 700 bp and 750 bp. Cell line 4 gave only a single bright band of ~300 bp. Subsequently, the brightest band from each lane was extracted, purified and then sequenced using a BigDye® Terminator v3.1 Cycle Sequencing Kit (ThermoFisher Scientific, #4337454) as detailed in 2.8.3 using forward and reverse primers (poMDA5 fw.2, poMDA5 rv.2; table 2.12) to obtain sequence flanking both gRNA target sites.

Obtained sequences were then aligned with a reference genomic porcine MDA5 sequence (NC_010457.5:68930998-68985145) using MEGA7 software. The resulting alignments were then reformatted using EMBL's MView software (http://www.ebi.ac.uk/Tools/msa/mview/; figure B.4). Deletions of 227 bp, 155 bp and 19 bp were identified in the sequences determined for cell lines 4, 6 and 26 respectively. Each of these indels were within the first coding exon of MDA5, beginning within the target sequence of the first gRNA and ending either within the second target sequence (cell line 26) or significantly downstream of it (cell lines 4 and 6).

Nucleotide sequences from MDA5 cell lines 4, 6 and 26 were then translated as detailed in 4.3.2 and the resulting amino acid sequences aligned against a reference sequence for porcine MDA5 (NP_001093664.1) (figure B.5). Upon translation, truncated amino acid sequences were observed for each of the cell lines compared to WT and reference sequences, indicating the introduction of premature stop codons (figure B.4, red) as a consequence of the frameshifts introduced by each indel. Bioinformatics.org's protein molecular weight prediction tool (https://www.bioinformatics.org/sms/prot_mw.html) found each of these truncated proteins to have predicted molecular weights of approximately 5 kDa (figure B.5, B). These findings and observations are in agreement with those made in figure B.2 and indicate that cell lines 4, 6 and 26 are homozygous MDA5 knockouts.

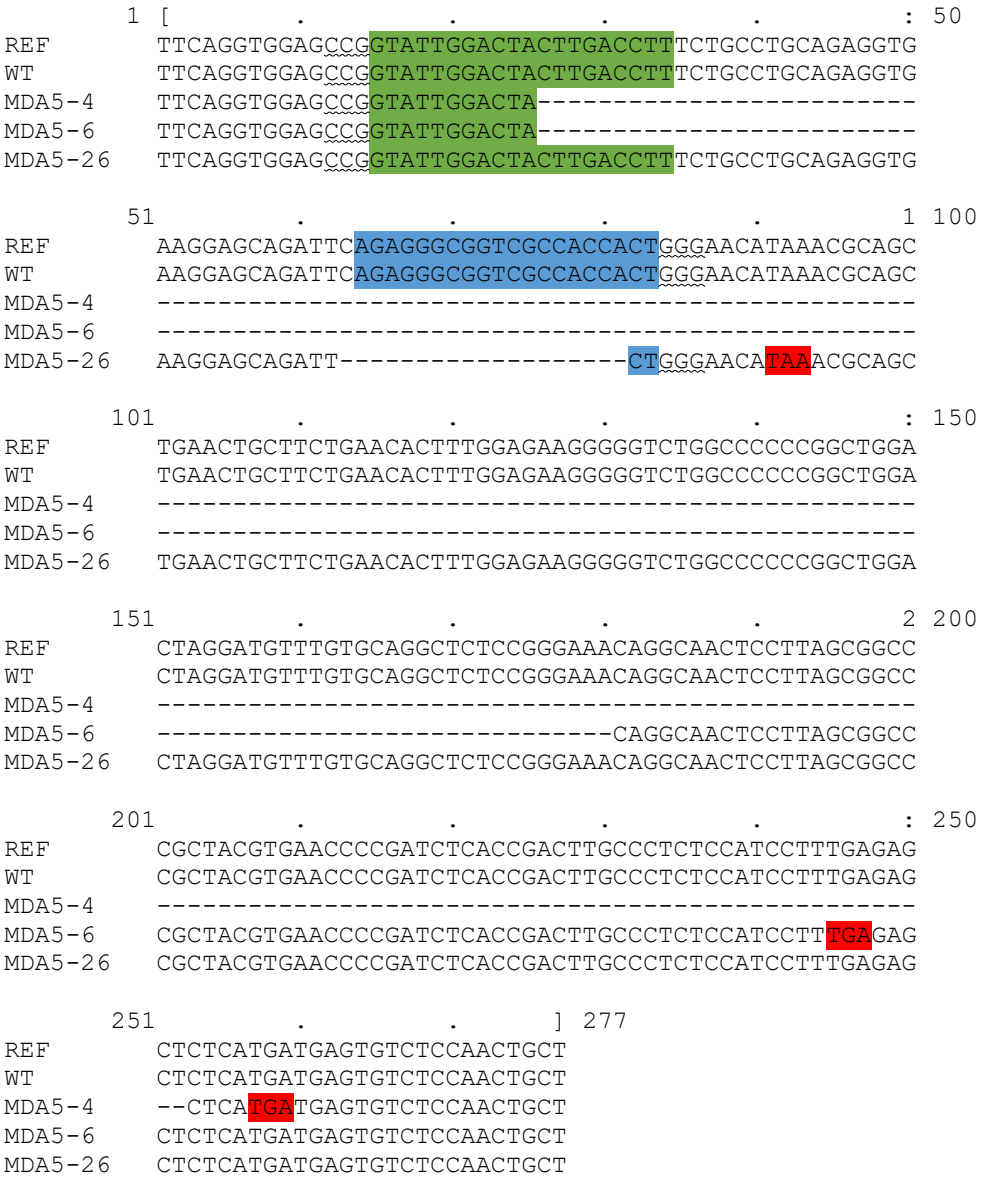

Figure B.4: Alignment of nucleotide sequences reveals MDA5 gene edited cell lines contain indels within the first exon. MDA5 sequences obtained using gDNA extracted from non-edited PK-15 cells (WT) and PK-15 cell lines (4, 6 and 26) gene edited for MDA5 were aligned with the cDNA sequence for porcine MDA5 (NP_001093664.1) using MEGA7 software. Large indels were identified for all gene edited cell lines. PAM sites (waves, underlined) and the sequence of the first (green) and second (blue) gRNA targets are indicated as are premature stop codons (red).

A

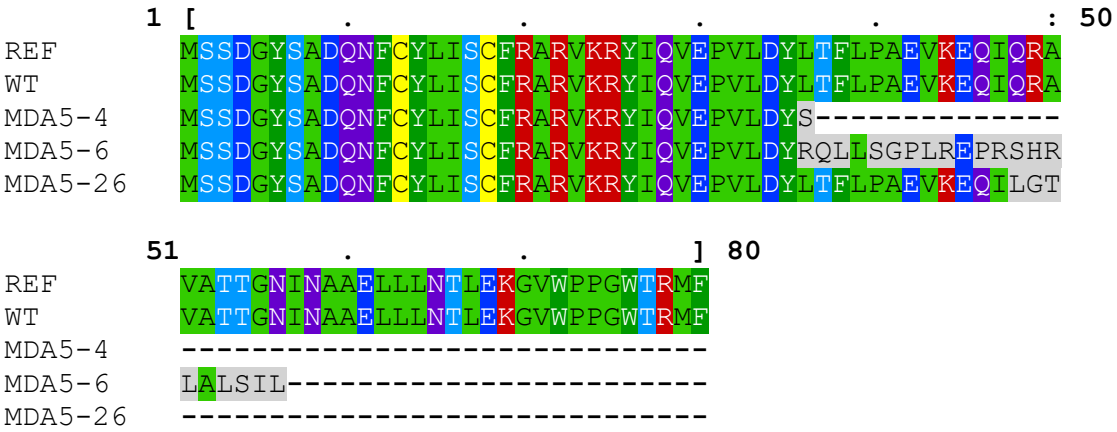

B

Cell line	Amino acid residue count	Predicted molecular weight (kDa)
MDA5-4	36	4.23
MDA5-6	56	6.53
MDA5-26	50	5.78

Figure B.5: Amino acid alignment reveals MDA5 gene edited cell lines contain premature stop codons. (A) The MDA5 sequences shown in Figure *** were translated and then aligned using MEGA7 software. Truncated protein products were identified for all the MDA5 gene edited cell lines (4, 6 and 26). Colours relate to the physiochemical properties of each amino acid while grey indicates inserted or non-homologous sequence. (B) Bioinformatics.org's protein molecular weight prediction tool was used to predict the molecular weights of the translated sequences.

Appendix C

Transfected poly(I:C) triggers no observable apoptosis in TLR3$^{-/-}$ cells

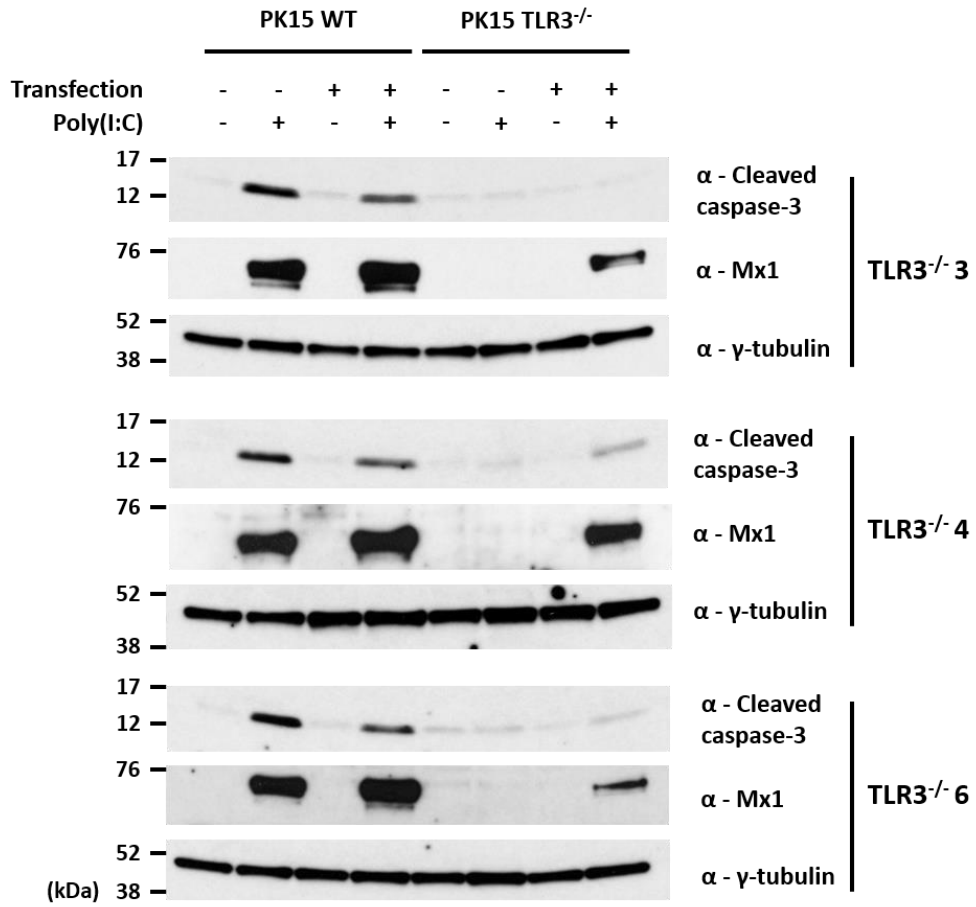

Figure C.1: Transfected poly(I:C) triggers no observable apoptosis in TLR3 knockout PK-15 cells. WT and three CRISPR-Cas9 knockout TLR3$^{-/-}$ PK-15 cell lines were seeded in 12-well plates and treated with 100 µg/ml poly(I:C) in the presence and absence of transfection reagent. 18 hours post-treatment, whole cell lysates were prepared and analysed by Western blot using mAbs recognising cleaved caspase-3 and Mx1. A mAb recognising γ-tubulin was used to determine relative protein concentrations.

Appendix D

Generation of porcine IRF3 mutant to investigate IFN and transcriptional upregulation-independent IRF3-mediated apoptosis

Cloning of EGFP-tagged WT and S1 mutant porcine IRF3 into the pcDNA3.1 expression vector

In the absence of a suitable antibody reactive with porcine IRF3, N-terminus EGFP-tagged WT (poIRF3^{WT}) and poIRF3^{S1} constructs were cloned in the pcDNA3.1 vector (Invitrogen). Briefly, poIRF3^{WT} was PCR amplified from pGADT7-IRF3 (2.8.1) with *Bam*HI/*Not*I overhangs (poIRF3_BamHI_fw, poIRF3_NotI_rev; table 2.20) and ligated into the pcDNA3.1 mammalian expression vector (2.6.2) to generate pcDNA3.1-poIRF3-WT. To introduce an n-terminal tag, EGFP was amplified from pLJM1-EGFP using a forward primer with a 5' *Kpn*I site, a Kozak sequence and a start codon, and a reverse primer that contained 32 nt of the poIRF3^{WT} 3' ORF containing an internal *Eco*RV site (KpnI_Kozak_5'EGFP_FW, 3'EGFP_BamHI_5'poIRF3_REV; table 2.20) and subsequently ligated into pcDNA3.1-poIRF3-WT to generate pcDNA3.1-EGFP-poIRF3-WT. poIRF3^{S1} cDNA was acquired from GeneArt and PCR amplified using a forward primer containing the internal *Eco*RV site and a reverse primer containing a *Not*I site (intEcoRV-poIRF3, poIRF3-NotI; table 2.20), which upon ligation generated the pcDNA3.1-EGFP-poIRF3-S1 plasmid.

Confirmation of EGFP-IRF3 WT and S1 mutant expression and localisation

PK-15 and SK6 cells were transfected (see 2.7.1) with pcDNA3.1-poIRF3-W1 and S1 plasmids in order to confirm expression and correct localisation. Each cell line was also transfected with an EGFP control plasmid[2]. Expression was confirmed by Western blot (figure D.1) and confocal microscopy (figure D.2).

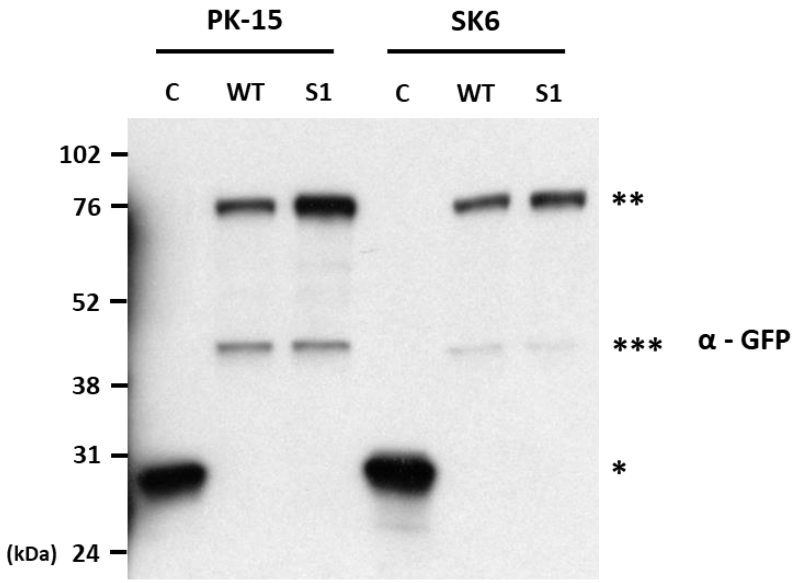

Figure D.1: EGFP-tagged WT and S1 mutant porcine IRF3 resolve at their predicted sizes when analysed by Western following expression in PK-15 and SK6 cells. PK-15 and SK6 cells were prepared 24-well plates and transfected with pcDNA3.1 plasmid encoding either EGFP, EGFP-poIRF3-WT or EGFP-poIRF3-S1. 24 hours post-transfection, whole cell lysates were prepared and analysed by Western blotting using a mAb recognising GFP.

[2] Prepared by annealing two oligos bearing internal stop codons (BamHI-3frameSTOP-NotI_FW, BamHI-3frameSTOP-NotI_REV; table 2.20) and ligating them into pcDNA3.1-EGFP-poIRF3-WT following *Bam*HI/*Not*I digest to remove poIRF3^{S1}.

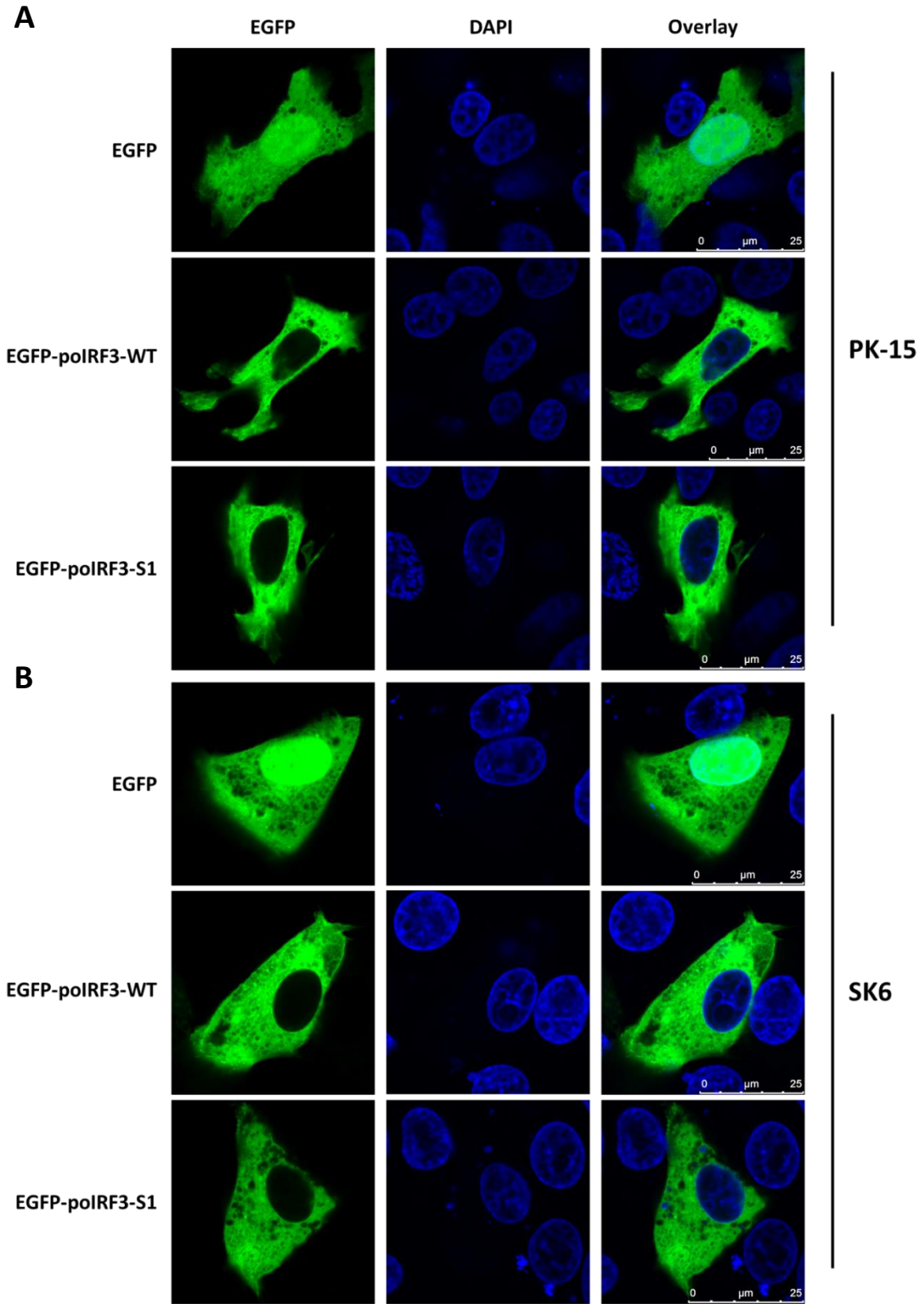

Figure D.2: EGFP-tagged WT and S1 mutant porcine IRF3 is distributed exclusively in the cytosol and is excluded from the nucleus in unstimulated PK-15 and SK6 cells. (A) PK-15 and (B) SK6 cells were seeded onto coverslips in 24-well plates and transfected with pcDNA3.1 plasmid encoding either EGFP, EGFP-poIRF3-WT or EGFP-poIRF3-S1. 24 hours post-transfection, cells were fixed and analysed by confocal microscopy. Nuclei are stained blue with DAPI.

Appendix E

Problematic visualisation of cytochrome c in porcine cell lines

Endogenous cytochrome c was detectable by immunofluorescence in human but not porcine cell lines

The mouse mAb 6H2.B4 (Cell Signalling, #12963), was acquired in order to detect cytochrome c in unstimulated and apoptotic cells by immunofluorescence confocal microscopy. PK-15 cells were prepared alongside two human cell lines (HEK 293T and HeLa), the latter of which acted as positive controls. Once each cell line neared confluency they were stained with MitoTracker Red CMXRos for 30 min after which they were fixed and subjected to immunofluorescent staining to detect cytochrome c. In HEK 293T and HeLa cells, cytochrome c signal was intense and matched the distribution of MitoTracker signal, indicating perfect co-localisation with the mitochondria (figure E.1). While the mitochondria of HeLa cells appeared more elongated than those of HEK 293T cells, cytochrome c still co-localised to the same extent. However, in PK-15 cells the cytochrome c signal appeared punctate throughout the cytosol with no detectable co-localisation with the mitochondria (figure E.1) suggesting that BH2.B4 does not recognise porcine cytochrome c by immunofluorescence.

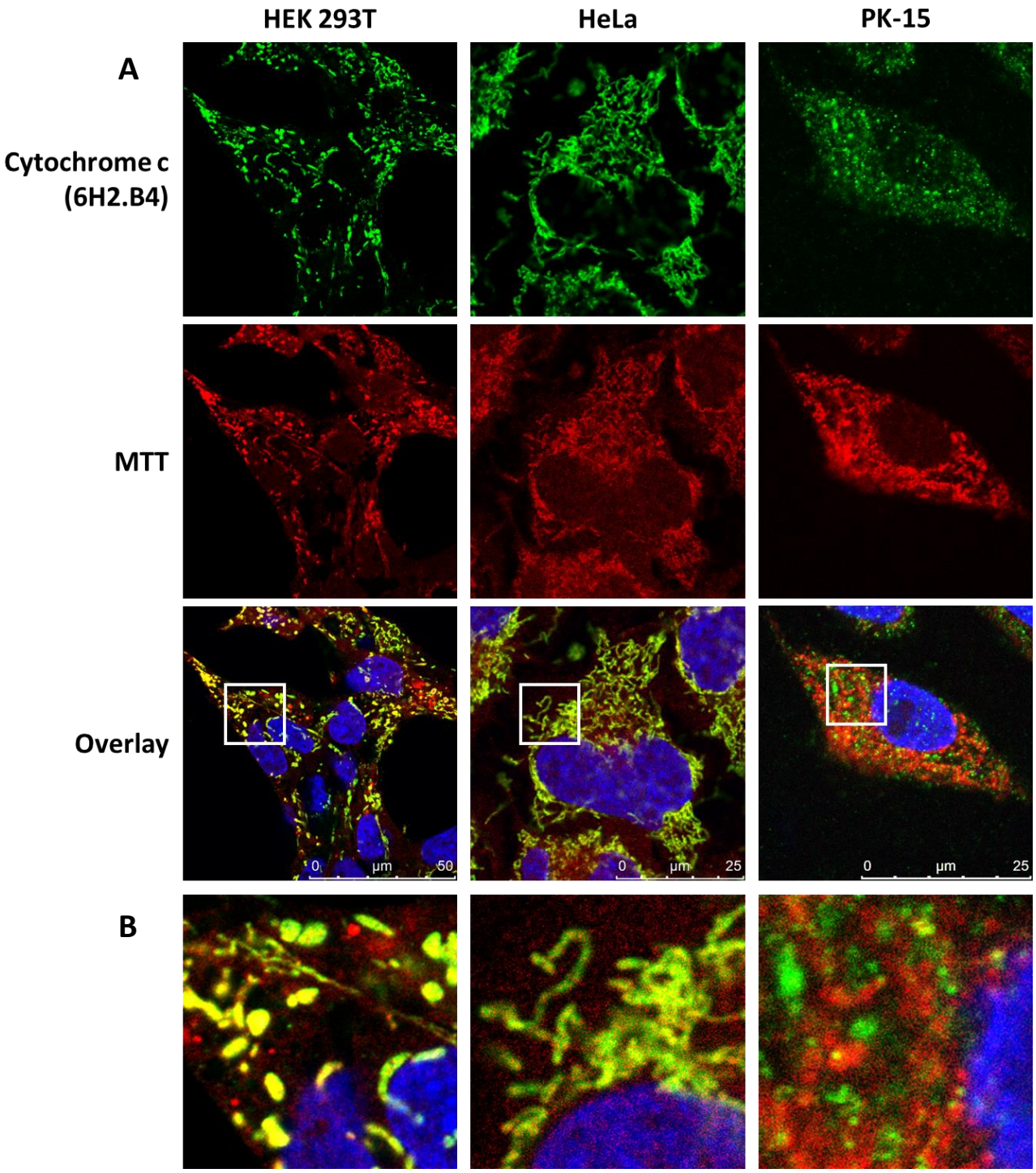

Figure E.1: Endogenous cytochrome c was detectable by immunofluorescence with mAb 6H2.B4 by immunofluorescence in HEK 293T and HeLa cells but not PK-15 cells. HEK 293T, HeLa and PK-15 cells were seeded onto coverslips in 24-well plates. Cells were then treated with MitoTracker (MTT) Red CMXRos (red) for 30 min and fixed with 4% paraformaldehyde. Fixed cells were analysed by immunofluorescence using a mAb (6H2.B4) recognising cytochrome c which was co-stained with Alexa Fluor 488 IgG1 (green). Nuclei are stained blue with DAPI. Cells were visualised at the single-cell level (A); white boxes indicate cropped fields of view (B).

Transfected GFP-cytochrome c localises primarily to the mitochondria and nucleus while cytochrome c-GFP is distributed evenly throughout the cytosol of PK-15 cells

PK-15 cells were prepared on coverslips and initially transfected with pGFP-Cytochrome (Addgene plasmid #41181). Twenty-four hr post-transfection, mitochondria were stained with MitoTracker and the cells were fixed. While GFP-cytochrome c clearly localised to the mitochondria as indicated by its clear co-localisation with the mitochondria, a significant portion was also present in the nucleus (figure E.2, A and B). To a lesser extent, GFP-cytochrome c was also present in the cytosol however this varied from cell to cell – the cytochrome c signal co-localised with mitochondria in all cells, but differences were observed between cells with regards to cytosolic and nuclear distribution (figure E.2, A, middle) than others (figure E.2, A, top and bottom). PK-15 cells were subsequently transfected with pCytochrome C-GFP (Addgene plasmid #41182) to determine whether C-terminal fusion with GFP eliminates unwanted nuclear and cytosolic localisation. However, upon visualisation by confocal microscopy it was clear that cytochrome c-GFP was devoid of any mitochondrial localisation and instead appeared to be distributed throughout all subcellular compartments (figure E.2, C and D). It was decided that neither cytochrome c GFP-fusion would be suitable for apoptotic studies involving N^{pro}.

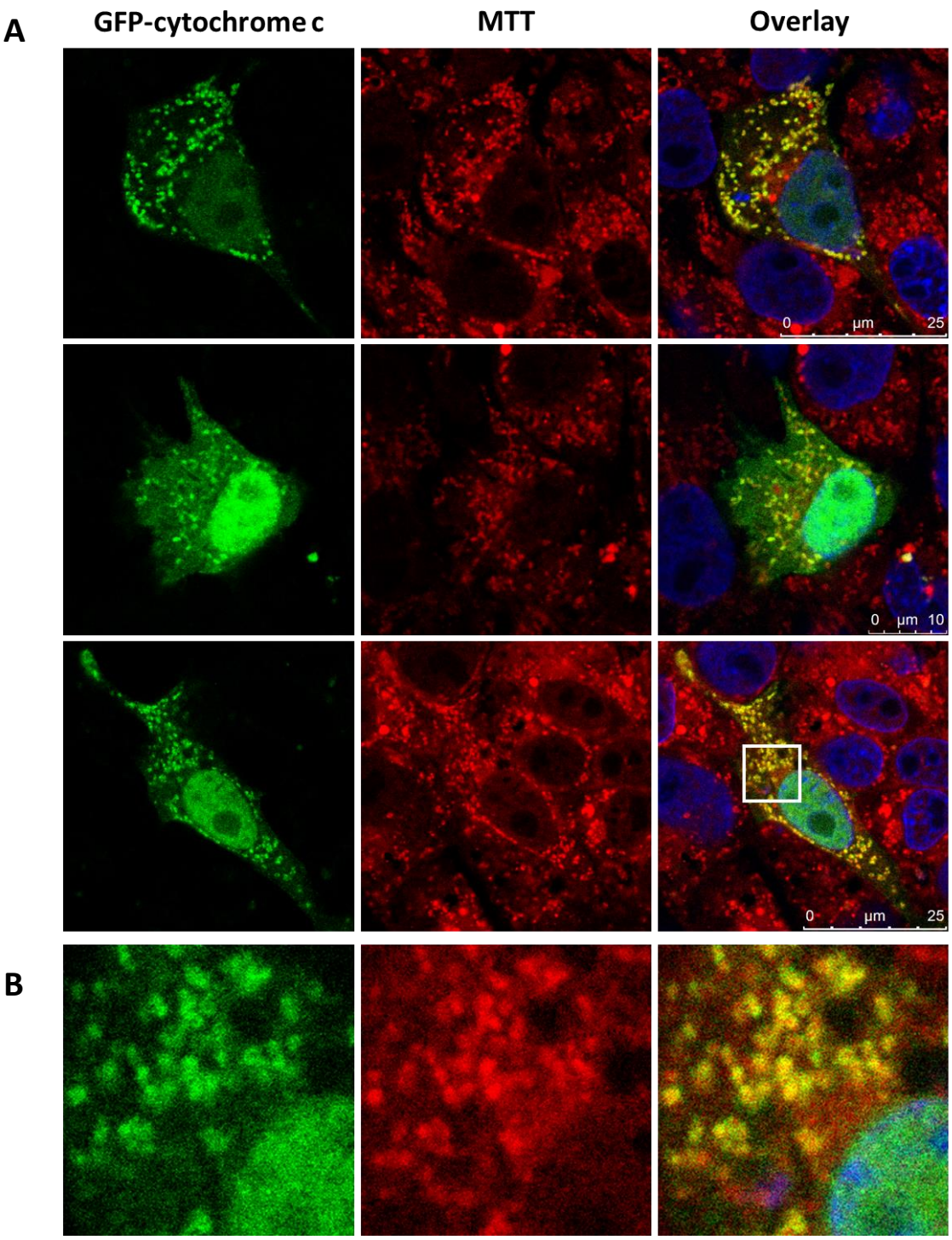
A
GFP-cytochrome c
MTT
Overlay
0 µm 25
0 µm 10
0 µm 25
B

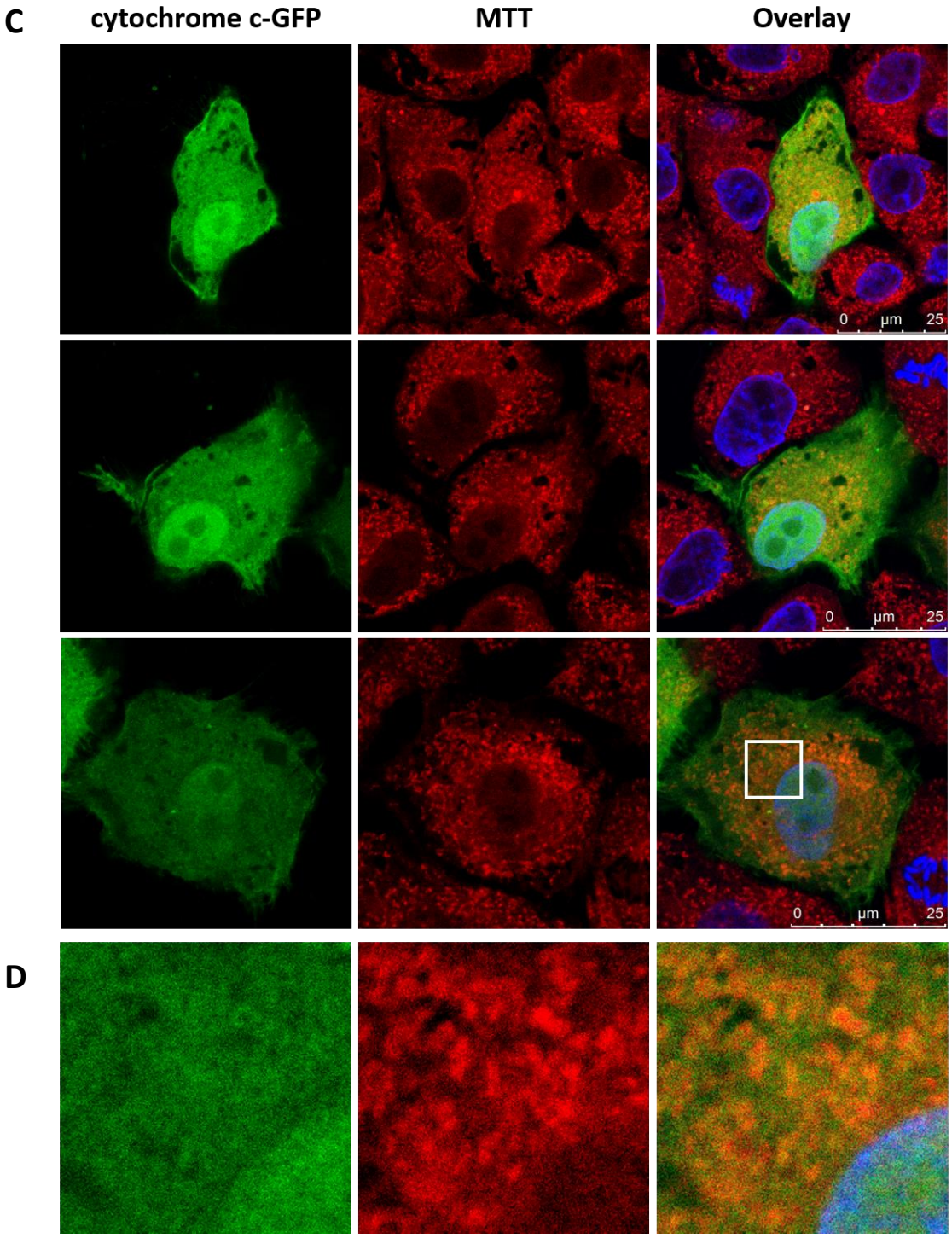

Figure E.2: Transfected GFP-cytochrome c localises primarily to the mitochondria and nucleus while cytochrome c-GFP is distributed evenly throughout the cytosol of PK-15 cells. (A, B, C, D) PK-15 cells were seeded onto coverslips in 24-well plates and transfected with (A, B) pGFP-Cytochrome C (Addgene plasmid #41181) or (C, D) pCytochrome c-GFP (Addgene plasmid #41182). 24 hours post-transfection, cells were treated with MitoTracker (MTT) Red CMXRos (red) for a further 30 min and fixed with 4% paraformaldehyde. Fixed cells were then analysed by confocal microscopy; images of single cells (A, C) were cropped and enlarged (B, D) for clearer visualisation of protein localisation. Nuclei are stained blue with DAPI.